Spectral identification of non linear devices

Armstrong, R

SPECTRAL IDENTIFICATION OF NON LINEAR DEVICES

by

R. ARMSTRONG
B.Sc(Hons), M.Sc., C.Eng., M.I.E.E., A.F.I.M.A.

A thesis submitted to the Faculty of Science,
University of Durham, for the degree of
Doctor of Philosophy

Department of Applied Physics
and Electronics,
University of Durham, U.K.

April 1983

ABSTRACT

A method of non-linear device identification derived from the measured spectral response to a sinusoidal drive is developed. From these considerations the concept of dynamic characteristics is proposed as a generalisation of the static characteristics. An example of the design of a frequency multiplying circuit based on the test spectrum is given. Important parameters such as internal capacitance and characteristic conductance are derived in terms of the components of the test spectrum.

The effect of series resistance on the performance of exponential diodes is fully discussed. Three new diode models are proposed:-

(i) a two-term functional expansion,

(ii) a logarithmic approximation,

(iii) a bi-linear model with exponential correcting cusp.

Model (iii) is used to develop expressions to predict the spectral response to a sinusoidal drive voltage and the importance of the curvature of the diode characteristic is discussed.

The effect of parasitic capacitance on the performance of lattice mixers is examined and the resulting angle of delay in the diode current is predicted.

A new spectrum analyser system is designed and developed which is capable of measuring harmonic amplitudes and phases up to a maximum frequency of 1 GHz.

ACKNOWLEDGEMENTS

I would like to express my thanks and appreciation to my supervisor Dr. B.L.J. Kulesza for his continued guidance and interest throughout this project. I found his lively enthusiasm very stimulating which spurred me on to greater efforts.

I would also like to thank my friends at Newcastle Polytechnic, especially Mr. E. Korolkiewicz and Mr. D.F. Oxford for their help and encouragement. Many thanks are also due to Professor P.H. Roberts (School of Mathematics, University of Newcastle), who first introduced me to perturbation techniques, and to Dr. Robin Johnson who gave considerable assistance with the asymptotic expansions developed in Chapter 5.

My appreciation must also extend to the Directorate of Newcastle Polytechnic, Mr. A. Ritchey, (Head of School of Electronics, Newcastle Polytechnic) and to Professor G.G. Roberts (Department of Applied Physics and Electronics, University of Durham) for placing the facilities of their departments at my disposal and also to Mrs. L. Bateson for typing the thesis.

Finally I wish to thank my wife Angela, and my two children, Jonathan and Jayne, for their encouragement and understanding while I have been involved with this project.

R. Armstrong,
April 1983.

CONTENTS

Page No.

APPENDICES

APPENDIX F

APPENDIX G

LIST OF PRINCIPAL SYMBOLS

Chapter 1

i	Diode current
I_s	Diode reverse saturation current
α	Diode exponential factor
V	Local oscillator voltage
C	Reverse biassed incremental diode capacitance
C_o	Zero volts incremental diode capacitance
V_T	Diode turn-on voltage
γ	Capacitance index
r	Diode series substrate resistance

Chapter 2

$\hat{V}$	Peak value of local oscillator voltage
ω	Angular frequency
t	Time
θ	Angle (radians)
I_n	Peak magnitude of n^{th} harmonic component of diode current
T_n	Chebyshev polynomial of the first kind of order n
U_n	Chebyshev polynomials of the second kind of order n
I_{rn}	Peak magnitude of in-phase component of n^{th} harmonic component
I_{xn}	Peak magnitude of quadrature component at n^{th} harmonic component
E	d.c. bias voltage
$g(t)$	Time varying incremental conductance
g_n	n^{th} harmonic component of time varying conductance
$\hat{V}_T$	Peak value of sinusoidal test voltage
Q_k	Peak value of k^{th} harmonic component of test charge spectrum
Re	Real part of a complex number

Im	Imaginary part of a complex number
j	$\sqrt{-1}$
a	Normalised input voltage of varactor multiplier
b	Normalised output voltage of varactor multiplier
C_1, C_2	Input and output capacitance of varactor multiplier
G_1	Output conductance to varactor multiplier
G_{21}	Test transconductance of varactor
G_0	Characteristic conductance of varactor multiplier
δ	Loss angle of varactor
g_1	Fundamental loss conductance

<u>Chapter 3</u>

x	Normalised diode current
ε	Normalised diode voltage
V_o	First estimate of diode turn-on voltage
V_1	Corrected estimate of diode turn-on voltage
r_m	Modified diode resistance parameter

<u>Chapter 4</u>

V_6	Diode bias voltage
V_2	Effective diode turn-on voltage
K	Effective diode reverse saturation current
Z	Effective exponential diode factor
I_n	Bessel function of the first kind, order n
θ_o	Angular position of diode voltage waveform corresponding to diode turn-on voltage
$\sqrt{\chi}$	Diode overdrive coefficient
β	Diode bias coefficient
a_{n+}	n^{th} harmonic component of positive exponential cusp current
a_{n-}	n^{th} harmonic component of negative exponential cusp current

g_m	Modified diode conductance
g_1	Incremental conductance due to bi-linear diode model
g_+	Incremental conductance due to positive exponential cusp current
g_-	Incremental conductance due to negative exponential cusp current

Chapter 5

I_p	Local oscillator drive current
ω_p	Local oscillator angular frequency
i_s	Signal current
ω_s	Angular frequency of signal current
$S(t)$	Switching Function
C_e	Equivalent capacitance of lattice array of diodes
θ_c	Delayed diode conjunction angle
K	Effective normalised saturation current
ε	Normalised effective capacitance
y	Effective normalised diode current
y_o	Outer solution for diode current
Y_o	Inner solution for diode current

CHAPTER 1

INTRODUCTION

This report is concerned with the analysis, and subsequent experimental verification, of the response of passive non-linear devices to periodic excitations. It is the rule rather than the exception that the variablesdescribing the behaviour of such physical systems are not directly proportional to one another, i.e. they are related in a nonlinear fashion. A vast body of knowledge exists concerning linear systems and in some practical situations the restricted ranges of the variables or a small degree of nonlinearity allows the application of linear theory in the analysis to predict the performance. However, in the field of electrical communication systems the processes of frequency conversion, all forms of modulation and demodulation, the generation of carrier frequencies from a lower frequency, crystal-controlled, oscillator depend for their operation on the nonlinearities of the components. Indeed, it can be said that electronic communication systems as we know them today would be non-existent if only linear devices were available. It is apparent therefore, that the need for a conceptual and quantitative understanding of the nonlinearities and their effects is essential in the study of such systems.

Additional to the intrinsic nonlinearities all solid state devices exhibit parasitic effects such as semiconductor bulk resistance, stray capacitance and inductance. Some of these parasitic effects may be linear, such as diode package capacitance. Other parasitic effects are themselves nonlinear, e.g. diode depletion layer capacitance, which of course adds to the complexity of the overall system. Unlike linear systems, a unified simple nonlinear theory does not exist and thus the nonlinear nature of devices used in frequency converting systems introduces severe mathematical difficulties into the analysis.

Before the onset of readily accessible digital computers the aforementioned mathematical difficulties forced many investigators to introduce severe restrictions into their analyses in order to obtain information regarding frequency conversion processes. The understanding and the accuracy of predictions are related to the degree of approximations made to obtain the analytic solutions. With the advent of high speed computing facilities, more detailed numerical information may now be achieved - these results being invaluable to improve and optimize the design of frequency converting circuits. However, the numerical form of the results does not readily aid in the fundamental understanding of the frequency generating properties and behaviour of nonlinear elements.

There are three main groups of passive nonlinear elements namely:-

(i) resistive elements,

(ii) reactive elements,

(iii) negative resistance elements.

Group (i) includes devices such as Schottky barrier diodes, point contact diodes and backward diodes. The voltage-current characteristics of these devices are of the exponential form

$$i = I_s \exp(\alpha v) - I_s$$

Elements in group (ii) include varactor diodes (abrupt and graded junction). The incremental capacitance of these elements follows a law of the form

$$C = C_o/(1 - V/V_T)^{\gamma}$$

where the index γ lies in the range $1/2 > \gamma > 1/6$ for practical diodes Both groups of elements display a diffusion capacitance due to charge storage effects and this phenomenon has been exploited in the step-recovery diode used to produce high order frequency multiplication. Group (iii) contains elements such as tunnel diodes, gunn effect diodes and impatt diodes. These devices are generally used in a free oscillation mode, i.e. autonomous systems, in which the frequency of oscillation is essentially dictated by the imbedding network. Elements of this kind will not be considered.

The response of exponential diodes to sinusoidal drives has been the subject of many investigations. The simplest approach by Torrey and Whitmer[1] was to assume that the diode junction voltage was sinusoidal, the harmonic components of the current are then given by the well known Bessel function.

In 1963, Kahng[2] showed that the terminal behaviour of the diode deviated from the true exponential form since the voltage drop across the series substrate resistance resulted in a non-sinusoidal diode junction voltage and consequently the diode equation must be modified to

$$i = I_s \exp(\alpha V - \alpha i r) - I_s$$

This equation is implicit in the unknown current, and in order to predict the harmonic content of the current Mill[3] expanded the above equation into a powers series in the applied voltage. The computation of the derivatives of this function to give the Taylor series coefficient is labourious and requires numerical computation if a large number of terms is required. More recently Katib[4] (1976) approached this problem from a similar point of view and showed that the coefficients in the power series expansion could be represented in terms of Stirling numbers of the second kind. However, the resulting series for the harmonic components were found to converge extremely slowly. From the aforegoing remarks it is obvious that at present there is no known analytic solution for the exponential diode which includes the effect of the series resistance.

In view of the extreme analytic difficulties encountered to obtain the large signal behaviour some authors[5, 6] have made the simplifying assumption that the diode with series resistance may be represented by a piece-wise linear model switched between the diode reverse and series resistance levels. This bi-linear approximation considerably simplifies the analysis but clearly ignores the curvature of the diodes characteristic in the neighbourhood of the turn-on voltage.

To improve design and optimize performance many investigators have obtained the large signal solution by numerical means. Indeed in 1972 a numerical investigation by Glover[7] et. al. into a single diode mixer showed that the bi-linear approximation is sufficiently accurate when biased in the mark-space ratios from 0.1 to 0.9. For mark-space ratios less than 0.1, required to realize low loss condition, it was found that the bi-linear approximation is not sufficiently accurate and the diode must be represented by its exponential characteristic with the series resistance.

As the demand to operate mixers at higher frequencies increased it became clear that the effect of depletion layer capacitance must also be taken into account. In 1970, Liechta[8] incorporated the capacitance effect into the numerical analysis in order to investigate the noise performance of mixers. The numerical analysis of Fleri and Cohen[9] in 1973 verified that the diode junction voltage departs significantly from a sinewave. The effect of diode junction capacitance on conversion loss was also examined by Mania and Stracca[10] in 1974 with the assumption that the capacitance was constant; again the large signal solution being obtained by numerical methods.

The depletion layer capacitance which appears as a parasitic in resistive diode circuits has application in its own right in frequency multiplying systems. In such systems the diode is biased so that forward conduction is not allowed and harmonic generation results from the non-linear depletion layer capacitance. Leeson and Weinreb[11] have obtained a small signal analysis for general values of the index γ by expanding the nonlinear q-v characteristic in a power series having a limited number of terms. In 1965, Scanlan and Laybourn[12] presented a large signal analysis taking into account the modification of the diode wave-form due to the harmonic output when the index $\gamma = 1/2$, but mathematical difficulties necessited numerical solutions for general values of γ.

In recent years attention has been focussed on the step-recovery diode used to obtain high order multiplication of frequency. Initially, investigators[13, 14] represented the charge storage capacitance as a perfect capacitor under forward voltage conditions and zero capacitance when the voltage was negative, i.e. a bi-linear capacitance. An alternative approach by Gardiner and Wagiealla[15] was to represent the step-recovery effect as a charge-controlled switch. This allowed the device to be represented as a time-varying element which permitted the application of linear circuit theory.

The aforegoing remarks clearly indicate that the main method of attack to obtain the analytic information has been through piece-wise linearisation and power series expansion. Only in the isolated cases (exponential diode with no parasitics, the varactor diode with $\gamma = 1/2$) is the nonlinear problem solvable directly in closed analytic form. In all cases the analyses have proceeded from a precise mathematical law of the device and it is logical to assume that all the information necessary to predict the behaviour of a nonlinear device must be present in the spectrum produced when it is driven with a sinewave.

In this work it is shown that nonlinear devices may be assessed by their spectral performance and the information is made available in terms of Chebyshev polynomials. The coefficients of the Chebyshev representation are directly related to the spectral response of the device. The concept is analogous to system identification testing and indeed a device or system may be represented in analytic form even though precise mathematical laws are not available. This approach to nonlinear problems also leads to the generalisation of device characteristics in terms of dynamic time-domain portraits. Such portraits contain information relating to resistance, reactance, energy storage and may be of value in selecting high quality devices from large production yields. The technique is regarded as a generalisation of the power series expansion method which has not been used in this context before.

Whilst the Chebyshev expansion procedure appears to be useful, information may often be determined by other forms of analysis. A technique which has had some success in handling nonlinear problems is perturbation theory[16] leading to solutions in terms of asymptotic expansions. Apart from obtaining the small signal behaviour of mixer circuits as a perturbation of the large signal solutions this method has not in general been applied to the devices and systems previously mentioned. The perturbation methods available have greatest utility when the solution required is perturbed from a known solution by the presence of a small parameter and therefore have applicability in determining the effects of parasitics .

A successful application of a perturbation technique, similar in character to the classical method of variation of parameters, is the analysis of the exponential diode with a series resistance. The essential elements of this original analysis have been published by the author et al and the paper is reproduced in Appendix A1.

Another successful application of perturbation methods in the form of matched asymptotic expansions was the prediction of the effect of package capacitance on the switching waveforms of balanced mixers. This analysis has been published by the author et al and is reproduced in Appendix A1.

In Chapter 2 a method of device identification based on the spectral response to a sinusoidal test drive is developed. A frequency multiplying network is studied to demonstrate that spectral information may be of considerable use in predicting the performance of non-linear devices embedded in frequency selective circuits.

Chapter 3 deals with the static characteristic of an exponential diode with series resistance. Three new mathematical models are developed which may be used to predict the diode current in terms of the applied voltage and the device parameters. In addition the proposed models also predict secondary parameters, i.e. diode turn-on voltage and effective diode forward resistance, in terms of the basic diode parameters.

The dynamic response of an exponential diode with series resistance to a sinusoidal voltage drive is examined in Chapter 4. A bi-linear model with exponential correcting terms is used to demonstrate that the current waveshape changes from a gaussian to an offset sinusoidal pulse as the voltage drive is increased. The harmonic components of the diode current are also predicted and their dependence on bias voltage and degree of overdrive beyond the turn-on voltage identified.

Chapter 5 is devoted to an investigation of the effect of parasitic capacitance on the switching performance of a lattice of exponential diodes. The predicted delay in conduction of the diode has considerable effect on the frequency converting properties of balanced mixers.

The development of a computer aided harmonic measuring system is described in Chapter 6. The system described is capable of measuring both magnitude and phase (or real and imaginary parts) of the Fourier decomposition of a periodic wave. The effects of sampling and digitising errors on the accuracy of the system is fully discussed.

Chapter 7 contains descriptions of experimental investigations and summaries of experimental test results for comparison with the theoretical predictions made in preceding chapters.

CHAPTER 2

NON LINEAR SPECTRAL ANALYSIS

2.1 Modelling of non-linear devices from their spectral response

The usual approach in analysing non-linear frequency converting networks is to use as the basis a theoretical equation derived from the physics of the device being used. Such analyses are valid provided the precise law is known. In many instances however, the law is only approximate and intrinsic parasitic effects may not be known accurately. In addition, it may be necessary to introduce severe approximations into the analysis to obtain a closed form solution.

If a non-linear device is driven by a single frequency drive (voltage or current) it is logical to assume that the generated spectrum contains all the necessary information required to model the device. Consequently the spectral response of a large signal dynamic test will contain information on effects which maybe amplitude and/or frequency dependent and may not be present with static testing procedures. The test spectrum will also include information reflecting stray effects.

The technique used is the inverse of a method proposed by Lewis (17) who, showed how to determine the harmonic response to a sinusoidal drive. The method was extended by Douce (18) to include the case of random signals whilst Karybakas (19) applied it to obtain the describing function for use in non-linear control systems.

2.2 The Chebyshev representation

The connection between the device characteristic and its spectral response may be expressed in terms of Chebyshev polynomials. To appreciate this, consider the case of a pure non-linear resistor driven by a sinusoidal voltage.

If the applied voltage is

$$v = \hat{V} \cos \theta, \tag{2.1}$$

where $\theta = \omega t$

then the resulting current may be represented by a Fourier series as

$$i = I_o/2 + \sum_{1}^{\infty} I_n \cos n\theta \tag{2.2}$$

From equation (2.1), the angle θ may be expressed as

$$\theta = \cos^{-1} (v/\hat{V}) \tag{2.3}$$

which when substituted into (2.2) gives

$$i = I_o/2 + \sum_{1}^{\infty} I_n \cos n \left(\cos^{-1} v/\hat{V}\right) \tag{2.4}$$

leading to the Chebyshev expansion since these polynomials may be defined as[20]

$$T_n(\chi) = \cos \left(n \cos^{-1} \chi\right) \tag{2.5}$$

and (2.4) can then be written

$$i = I_o/2 + \sum_{1}^{\infty} I_n T_n (v/\hat{V}) \tag{2.6}$$

The case of a sinusoidal current drive may be treated similarly with a trivial change in notation.

From this analysis it may be concluded that

(a) if the device is driven over its maximum working range and the harmonic spectrum is measured then the characteristic in the i-v plane is given by (2.6).

(b) conversely given the i-v characteristic over the range $-\hat{V}$ to $+\hat{V}$ then the harmonic spectrum to a sinusoidal drive of magnitude $\hat{V}$ may be predicted using the Chebyshev expansions.

It is not possible to obtain a pure resistive element and especially at high frequencies apparently resistive devices will exhibit parasitic reactance. It is therefore appropriate to indicate how the characteristic of a non-linear reactance is related to its spectral response. The q-v characteristic is determined as for the resistive case provided harmonic components of charge (q) are measured. Since it is much easier to measure current it is better to obtain an equivalent i-v characteristic. If the applied voltage is given by (2.1) then for a pure non-linear capacitance the current will be of the form

$$i = \sum_{1}^{\infty} I_n \sin n\theta \tag{2.7}$$

Again using (2.3) the current spectrum may be written as

$$i = \sqrt{1 - (v/\hat{V})^2} \sum_{1}^{\infty} I_n U_{n-1} (v/\hat{V}) \tag{2.8}$$

where the Chebyshev polynomials of the second kind are defined as

$$U_{n-1}(\chi) = \sin (n \cos^{-1} \chi) \Big/ \sqrt{1 - \chi^2} \tag{2.9}$$

The i-v characteristic is double-valued and forms a closed loop in the i-v plane and is symmetrical about the v axis for a purely reactive case.

The general case of a non-linear resistor and non-linear reactance is now easily treated for a sinusoidal voltage drive. In which case the current will have the form

$$i = I_o/2 + \sum_{1}^{\infty} \left[I_{rn} \cos n\theta + I_{xn} \sin n\theta \right] \qquad (2.10)$$

which has the corresponding i-v representation of

$$i = I_o/2 + \sum_{1}^{\infty} \left[I_{rn} T_n (v/\hat{V}) \pm I_{xn} \sqrt{1 - (v/\hat{V})^2}\, U_{n-1} \right] \qquad (2.11)$$

In order to obtain this representation it is necessary to measure the in-phase and quadrature components of the harmonic currents (I_{rn} and I_{xn}). This is indeed possible up to frequencies of the order of 1 GHz using the system outlined in Chapter 6.

2.3 Properties of Chebyshev polynomials

Since Chebyshev polynomials appear to be naturally related to the spectral response of non-linear devices it is important to appreciate some of the salient features of these functions. Proofs of the following statements may be found in Snyder[20]:-

(i) Chebyshev polynomials are orthogonal over a closed interval,

(ii) of all possible orthogonal polynomial approximations to a given characteristic the Chebyshev representation has the least deviation,

(iii) in the class of ultra-spherical polynomials, the Chebyshev polynomials display the strongest possible convergence, (Taylor series displays the weakest),

(iv) the error created in truncating a Chebyshev series is of the order of the first term neglected.

The speed of convergence of Chebyshev polynomials is aptly illustrated by calculating $\exp(\chi)$, $-1 \leq \chi < 1$, to within 1% by Taylor series and Chebyshev polynomials. The former requires five terms of the series whilst the latter only requires a three term expansion. This economisation process has been used by Holt et.al.[21] to approximate the transfer function of distributed RC transmission lines.

2.4 Dynamic portraits

A natural generalisation of a static characteristic is the dynamic characteristic of the device obtained by eliminating time from the equation (2.10) which is the Chebyshev representation of (2.11). Such a characteristic may be termed a dynamic portrait of the device. Such a characteristic can easily be displayed on a cathode ray oscilloscope (C.R.O.). Some typical dynamic portraits are shown in Figure (2.1).

Certain information may be determined by examination of the portrait of a device,

(a) if no reactance is present the portrait is single valued.

(b) if the portrait is a closed loop then reactance is present.

(c) if the loop is symmetrical about the horizontal axis then the device is purely reactive,

(d) the wider the loop the larger the reactance.

2.5 Small signal equations

With the Chebyshev representation established from test it is possible to determine the behaviour of a non linear device for small signals superimposed upon a d.c. bias by expanding (2.6) in a Taylor series about the bias point. To do this let

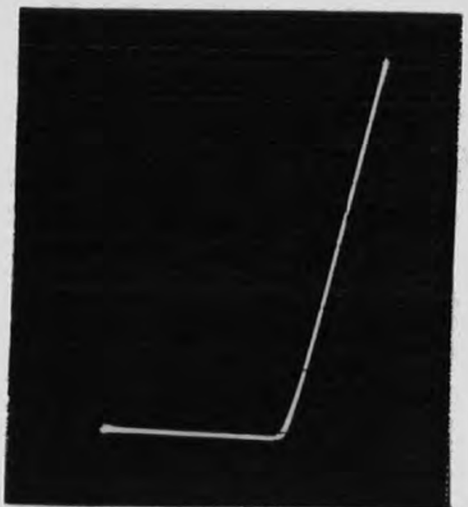

(a) non-linear resistance
(exponential diode)

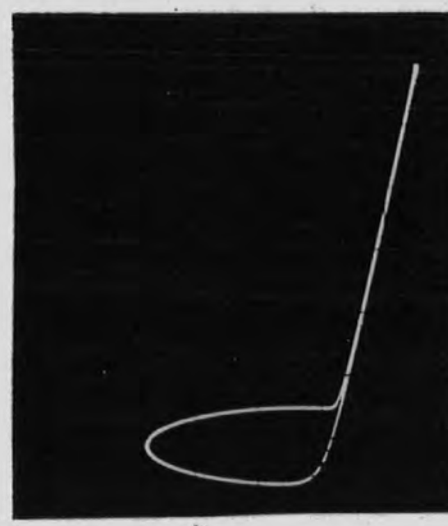

(b) non-linear resistor with
parallel linear capacitance

(c) non-linear capacitance
(reversed biassed diode)

(b) non-linear resistance and
non-linear capacitance
(exponential diode + depletion
layer capacitance + diffusion
capacitance).

Figure 2.1

Typical Time Domain Portraits

Vertical axis-current: Horizontal axis-voltage

$$v = E + v_s \qquad (2.12)$$

where

$$v_s = a \cos \theta, \qquad \theta = \omega t \qquad (2.13)$$

with

$$|E| < \hat{V}$$

then

$$i = \sum_o^\infty I_n T_n \left(\frac{E + v_s}{\hat{V}}\right) \qquad (2.14)$$

and for small v_s the Taylor series approximation is

$$\simeq \sum_o^\infty I_n T_n \left(\frac{E}{\hat{V}}\right) + v_s \frac{d}{dE} \sum_o^\infty T_n \left(\frac{E}{\hat{V}}\right)$$

$$= \sum_o^\infty I_n T_n (E/\hat{V}) + v_s \frac{1}{\hat{V}} \sum_o^\infty n\, U_{n-1} \left(\frac{E}{\hat{V}}\right)$$

$$= \sum_o^\infty I_n T_n (E/\hat{V}) + \frac{v_s}{a} \frac{a}{\hat{V}} \sum_1^\infty n\, U_{n-1} (E/\hat{V})$$

$$= \beta_o + \beta_1 T_1 (v_s/a) \qquad (2.15)$$

where $\beta_o = \sum_o^\infty I_n T_n (E/\hat{V})$

and $\beta_1 = \frac{a}{\hat{V}} \sum_1^\infty n\, U_{n-1} (E/\hat{V}) \qquad (2.16)$

Thus it is possible to deduce small signal behaviour from a large signal dynamic test whilst it is not possible to deduce large signal performance from a single small signal test.

2.6 Time varying parameters

Once the harmonic spectrum of a non-linear device is known it is also possible to predict time varying parameters such as incremental conductance or resistance for use in mixer analysis where the small signal source voltage is superimposed on the large local oscillator voltage.

The incremental conductance is the slope of the i-v characteristic which changes in sympathy with the local oscillator drive thus

$$g(t) = \frac{di}{dv} = \frac{di/d\theta}{dv/d\theta} = \frac{\frac{d}{d\theta}\left(I_o/2 + \sum_1^\infty I_n \cos n\theta\right)}{d/d\theta\ (\hat{V} \cos \omega\theta)\ d\theta}$$

$$= \frac{\sum_1^\infty n\ I_n \sin n\theta}{\hat{V} \sin \theta} \qquad (2.17)$$

Now $g(t)$ is obviously periodic with period 2π and furthermore $g(t)$ is an even function of θ and so the Fourier expansion takes the form

$$g(t) = g_o/2 + \sum_1^\infty g_n \cos n\theta \qquad (2.18)$$

Equating (2.17) to (2.18), cross multiplying by $\hat{V} \sin \theta$, and comparing coefficients yields the following two sequences of equations

$$g_o - g_2 = 2I_1/\hat{V} \quad , \quad g_1 - g_3 = 2I_2/\hat{V}$$

$$g_2 - g_4 = 2I_3/\hat{V} \quad , \quad g_3 - g_5 = 2I_4/\hat{V}$$

$$g_4 - g_6 = 2I_5/\hat{V} \quad , \quad g_5 - g_6 = 2I_6/\hat{V}$$

etc   etc   (2.19)

The solution to the above infinite sets of equations is accomplished by noting that $I_n \rightarrow 0$ as $n \rightarrow \infty$ and therefore $g_n \rightarrow 0$ as $n \rightarrow \infty$. If the set of equations containing the even coefficients of g are now added together then

$$g_o = \frac{2}{\hat{V}} \sum_{k=0}^{\infty} (2k - 1)\, I_{2k - 1} \tag{2.20}$$

and consequently

$$g_{2n} = \frac{2}{\hat{V}} \sum_{k=n}^{\infty} (2k - 1)\, I_{2k - 1} \quad , \quad n = 0, 1, 2 \dots. \tag{2.21}$$

In a similar manner the odd coefficients of g may be shown to be

$$g_{2n + 1} = \frac{2}{\hat{V}} \sum_{k=n + 1}^{\infty} 2k\, I_{2k} \quad , \quad n = 0, 1, 2 \dots. \tag{2.22}$$

Alternatively, the coefficients of the incremental conductance may be found by direct Fourier Analysis. The p th coefficient is given by

$$g_p = \frac{1}{\pi} \int_{o}^{2\pi} \left(\frac{1}{\hat{V} \sin \theta} \sum^{\infty} n\, I_n \sin n\theta\right) \cos p\theta \quad d\theta \tag{2.23}$$

which is readily evaluated by contour integration to give the same results as (2.21) and (2.22).

2.7 The analysis of multiplying circuits using Chebyshev Polynomials

As outlined in section 2.2 the characteristics of a non-linear capacitance (varactor diode) can be derived by measurement of the current spectrum when the device is driven with a single frequency forcing function. Neglecting any resistive effects the current spectrum will be of the form

$$i = - \sum_{k=1}^{\infty} \hat{I}_k \sin k\theta, \qquad \theta = \omega t \tag{2.24}$$

when the applied voltage is

$$v = \hat{V}_T \cos\theta \qquad (2.25)$$

where v is the deviation from the d.c. bias level and $\hat{V}_T$ is the peak value of the test voltage. Integrating (2.24) gives the charge

$$q = Q_0 + \sum_{k=1}^{\infty} Q_k \cos k\theta \qquad (2.26)$$

where Q_0 is the constant of integration, and $Q_k = - I_k/k\omega$

With

$$x = v/\hat{V}_T \qquad (2.27)$$

equation (2.26) becomes

$$q = Q_0 + \sum_{k=1}^{\infty} Q_k T_k(x) \qquad (2.28)$$

which is the algebraic representation of the device characteristic.

Consider now a frequency doubler circuit as shown in Figure (2.2). Higher order multiplication systems may be analysed using an identical procedure. The two tuned circuits are assumed ideal so that the input circuit operates at frequency ω whilst the output circuit operates at frequency 2ω.

The output voltage from the system will therefore be

$$v_2 = \hat{V}_2 \cos(2\theta - \phi) \qquad (2.29)$$

where $\hat{V}_2$ and ϕ have to be determined. The voltage existing across the non-linear capacitor is then given by

$$v = v_1 - v_2 = \hat{V}_1 \cos\theta - \hat{V}_2 \cos(2\theta - \phi) \qquad (2.30)$$

which in terms of the test voltage may be represented as

$$x = a\cos\theta - b\cos(2\theta - \phi) \qquad (2.31)$$

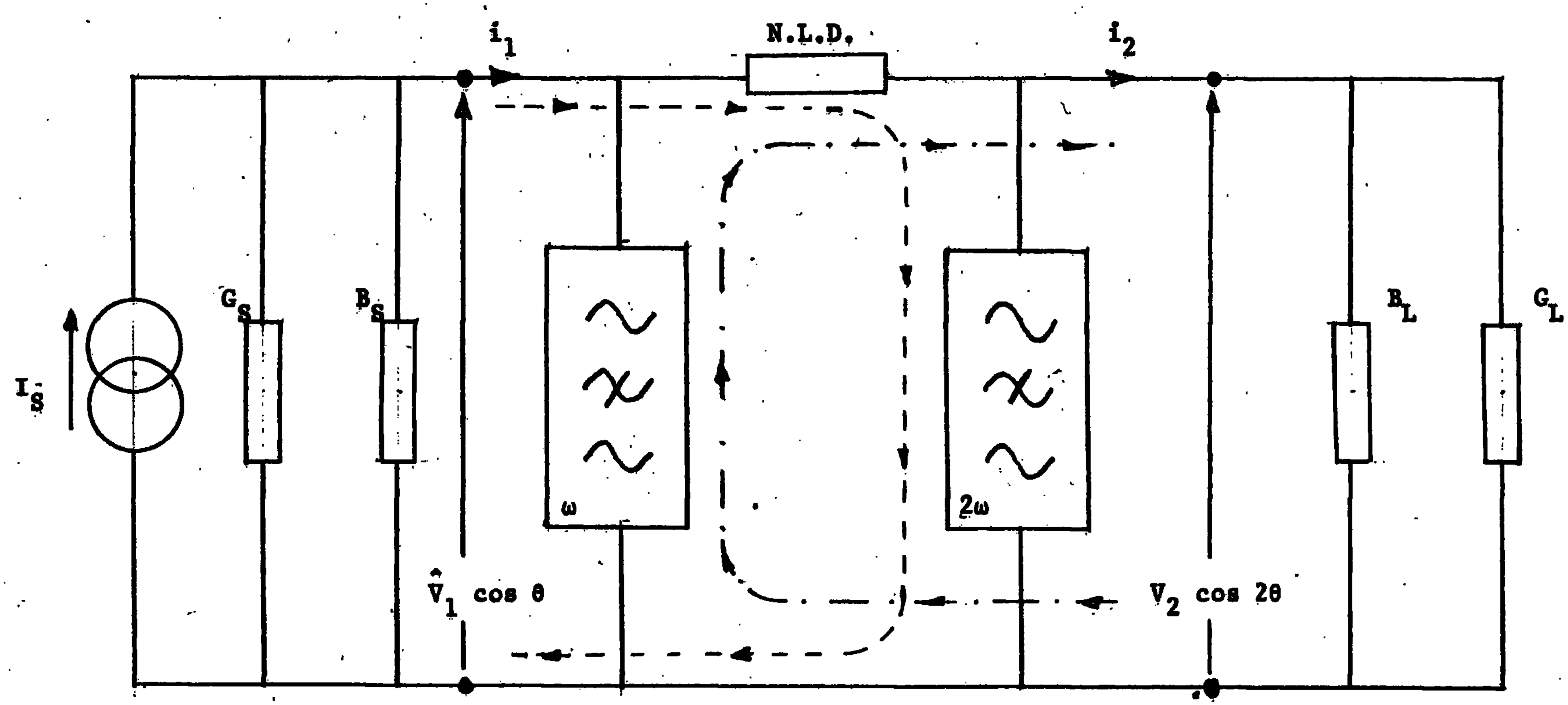

N.L.D. Non linear device

path of fundamental current

path of second harmonic current

Figure 2.2

Basic Circuit of Frequency Doubler

where $a = \hat{V}_1/\hat{V}_T$

$$b = \hat{V}_2/\hat{V}_T \tag{2.32}$$

with $0 < b < a \leq 1$

Equations (2.30) and (2.31) assume that the applied voltage $\hat{V}_1$ will be less than $\hat{V}_T$. This is necessary since the second harmonic voltage developed at the output may enhance the voltage across the non-linear capacitance during a fundamental cycle such that $v_1 - v_2$ may exceed $\hat{V}_T$. If V_T is taken as maximum possible working voltage across the device, then the device could breakdown due to second harmonic "punch through". Thus there is a constraint on v_1 and v_2 such that

$$\max |v_1 - v_2| \leq \hat{V}_T \text{ or } |a\cos\theta - b\cos(2\theta - \phi)| \leq 1 \tag{2.33}$$

The charge spectrum existing on the non-linear capacitor is given from (2.28) and (2.31). Because of the presence of the two tuned circuits it is only necessary to evaluate the fundamental and second harmonic components of these equations, the appropriate expansions of equation (2.28) up to the term involving Q_3 are given in Appendix B1.
The expansion is limited to terms in Q_3 since examination of typical spectra of varactor diodes shows that the harmonics of the current are less than 5% of the fundamental current for harmonic numbers exceeding three. Furthermore, the charge spectrum is related to the current spectrum by

$$Q_k = \frac{-I_k}{k\omega} \tag{2.34}$$

and will consequently diminish more rapidly as $k\omega$ increases.

Using the expansions developed in Appendix B1 the input and output charge spectra are given by

$$q_1 = \left[aQ_1 - 2ab\, Q_2 \cos\phi + 3\, Q_3 a\, (a^2 + 2b^2 - 1)\right] \cos\theta - \left[2ab\, Q_2 \sin\phi\right] \sin\theta \tag{2.35}$$

$$q_2 = \left[- b\, Q_1 \cos\phi + a^2 Q_2 - 3b\, Q_3\, (b^2 + 2a^2 - 1) \cos\phi\right] \cos 2\theta + \left[- b\, Q_1 \sin\phi - 3b\, Q_3\, (b^2 + 2a^2 - 1) \sin\phi\right] \sin 2\theta \tag{2.36}$$

The input and output current spectra may now be obtained by differentiation

$$i_1 = - \left[a\, Q_1 - 2ab\, Q_2 \cos\phi + 3a\, Q_3\, (a^2 + 2b^2 - 1)\right] \omega \sin\theta - \left[2\omega\, ab \sin\phi\, Q_2\right] \cos\theta \tag{2.37}$$

$$i_2 = - 2\omega \left[- b\, Q_1 \cos\phi + a^2 Q_2 - 3b\, Q_3\, (b^2 + 2a^2 - 1) \cos\phi\right] \sin 2\theta + 2\omega \left[- b\, Q_1 \sin\phi - 3b\, Q_3\, (b^2 + 2a^2 - 1) \sin\phi\right] \cos 2\theta \tag{2.38}$$

To interpret the engineering implication of the above two equations, consider first the output current, and define

$$\cos 2\theta = \mathrm{Re} \exp(- j\, 2\theta) \tag{2.39}$$

$$\sin 2\theta = \mathrm{Im} \exp(- j\, 2\theta) \tag{2.40}$$

and consequently i_2 may be written as

$$i_2 = - 2\omega b \sin\phi \left[Q_1 + 3Q_3\, (b^2 + 2a^2 - 1)\right] - j\, 2\omega b \cos\phi \left[Q_1 + 3Q_3\, (b^2 + 2a^2 - 1)\right] + j\omega a^2\, Q_2 \tag{2.41}$$

Equation (2.41) divides the output current into three component currents, as shown in Figure (2.3a). The last component ($j\omega a^2 Q_2$) is independent of the output voltage 'b', depending only on the input voltage 'a', and may therefore be interpreted as the current injected into the output circuit by the voltage applied to the input circuit. The other two components of the output current depend on the output voltage. These two components of current may be related to the output voltage

$$\begin{aligned} V_2 &= \hat{V}_2 \cos(2\theta - \phi) \\ &\longrightarrow \hat{V}_2 \cos\phi - j\hat{V}_2 \sin\phi \end{aligned} \tag{2.42}$$

by an admittance Y (as shown in Figure (2.3b)). Thus,

$$Y = \frac{2\omega b\ (Q_1 + 3Q_2\ (b^2 + 2a^2 - 1))\ (\sin\phi + j\cos\phi)}{\hat{V}_2(\cos\phi - j\sin\phi)} \tag{2.43}$$

which rationalises to

$$Y = \frac{j2\omega}{V_T}\left[Q_1 + 3Q_3\ (b^2 + 2a^2 - 1)\right] \tag{2.44}$$

and is the admittance of a capacitor

$$C_2 = \frac{Q_1 + 3Q_3\ (b^2 + 2a^2 - 1)}{\hat{V}_T} \tag{2.45}$$

The output circuit must be constrained to operate at the second harmonic and the presence of the above capacitance as an internal element of the non-linear device will alter the resonant frequency of the output filter. To obviate this problem it is necessary to connect a shunt susceptance B_L at the load terminals of equal but opposite type to the internal susceptance of the device.

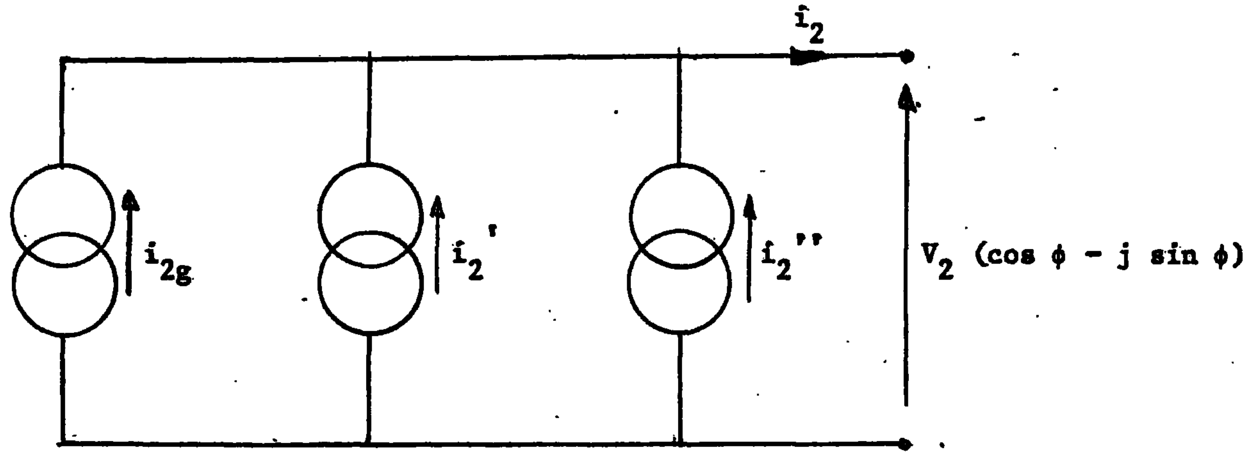

$i_{2g} = j\omega a^2\ Q_2$

$i_2' + i_2'' = j\omega b\ Q_1 + 3Q_3\ (b^2 + 2a^2 - 1)\ (\sin\phi + j\cos\phi)$

Figure 2.3(a)

Current Balance in Output Circuit of Frequency Doubler

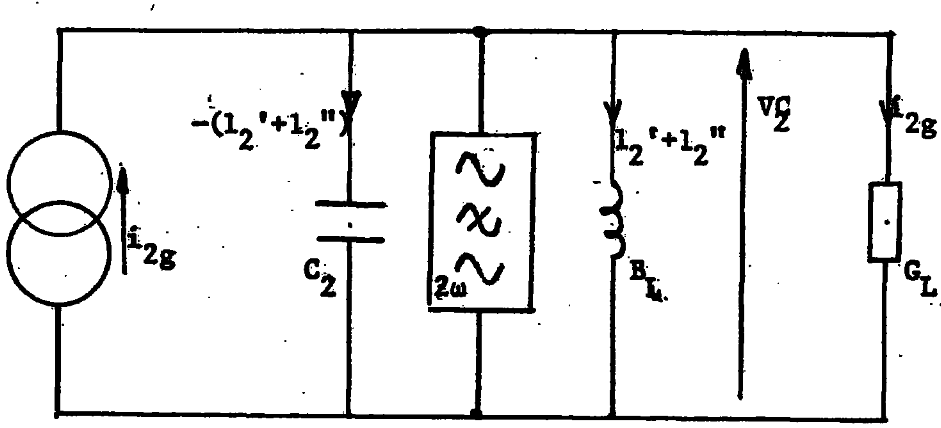

$C_2 = Q_1 + 3Q_3\ (b^2 + 2a^2 - 1)\ /V_T$

B_L cancels C_2

Figure 2.3(b)

Equivalent Circuit of Output of Frequency Doubler

In practice the output tuned circuit will be constructed to resonate above the second harmonic when not connected to the device. When embedded into the circuit the effect of C_2 will be to detune to the required frequency. Trimmer capacitors will also be added for final tuning.

The current which will flow through B_L will be antiphase to the current through the capacitor C_2 leaving the component $(j\omega a^2 Q_2)$ to flow through the load conductance G_L. The output voltage will then be

$$\hat{V}_2 \cos\phi - j\hat{V}_2 \sin\phi = j\omega 2a^2 Q_2/G_L \tag{2.46}$$

which implies that $\phi = \pm \pi/2$,

and consequently

$$\hat{V}_2 = - 2\omega a^2 Q_2/\left[G_L \sin(\pm \pi/2)\right]. \tag{2.47}$$

To make $\hat{V}_2$ positive then

$$\phi = - \pi/2 \tag{2.48}$$

This last result is in agreement with the numerical analysis of Scanlan and Laybourn(12).

Analysis of the input proceeds in an identical manner and is simplified by the condition that $\cos\phi = 0$ and $\sin\phi = -1$. Complex notation is introduced by

$$\begin{aligned} \cos\theta &= \mathrm{Re}\exp(j\theta) \\ \sin\theta &= \mathrm{Im}\exp(-j\theta) \end{aligned} \tag{2.49}$$

and the input voltage is taken as $v_1 = \hat{V}_1 \cos\theta$. The input conductance to the system is easily shown to be

$$G_1 = 2\omega\, \hat{V}_2\, Q_2/V_T^{\,2} \tag{2.50}$$

which by (2.43) may be written as

$$G_1 = 4\omega^2 \hat{V}_1^{\,2} Q_2^{\,2}/V_T^{\,4} G_L \tag{2.51}$$

The second harmonic component of the test spectrum is given by

$$I_2 = -2\omega Q_2 \tag{2.52}$$

and therefore (2.51) becomes

$$G_1 = \hat{V}_1^{\,2} I_2^{\,2}/V_T^{\,4} G_L \tag{2.53}$$

Define the test transconductance by

$$G_{21} = I_2/V_T \tag{2.54}$$

allow (2.53) to be expressed as

$$G_1 G_L = (G_{21})^2 \frac{\hat{V}_1^{\,2}}{\hat{V}_T^{\,2}} \tag{2.55}$$

Since the device is assumed lossless the conductance G_1 is the reflected image of the load conductance G_L. The load G_L is operating at the second harmonic components of frequency whilst the conductance G_1 accepts power at the fundamental frequency.

The input capacitance of the system is readily found to be

$$C_I = \frac{Q_1 + 3Q_3 (a^2 + 2b^2 - 1)}{\hat{V}_T} \tag{2.56}$$

and the input generator circuit must include an inductance to cancel this capacitance to permit operation at the fundamental frequency

Maximum power transfer through the system will be obtained when the source conductance G_S equals the input conductance G_1 and by (2.55) this is given by

$$G_S G_L = (G_{21})^2 \frac{\hat{V}_1^{\,2}}{\hat{V}_T^{\,2}} \tag{2.57}$$

Equation (2.57) defines the impedance transforming property of the multiplying network, in an analogous manner to say a quarter wavelength transformer where $Z_{in} Z_L = Z_0^2$. It is therefore convenient to define a characteristic conductance for the system, as

$$G_0 = G_{21} \hat{V}_1/\hat{V}_T \tag{2.58}$$

and to design the system to work between $G_s = G_L = G_0$. If the actual system conductances between which the multiplier must work differ from G_0 then passive impedance changing network can be added to the input and output as necessary. The complete equivalent circuit for the multiplier is shown in Figure (2.4).

The effect of resistive losses in the non-linear capacitor can be taken into account from a knowledge of the test spectrum. The test spectrum will be of the form

$$i = \sum_1^{\infty} I_{R_k} \cos k\theta - \sum_1^{\infty} I_k \sin k\theta \tag{2.59}$$

where I_{R_k} represents the harmonic amplitudes of the resistive portion of the spectrum and I_k represents the amplitudes due to the capacitance effect of the device. Equation (2.59) segregates the two components of current to represent the device as a parallel combination of a non-linear resistance and a non-linear reactance as shown in Figure (2.5). The same voltage appears across the two non-linear elements and thus the fundamental and second harmonic components of currents flowing in these two elements may be determined as shown previously. The components of currents flowing in the non-linear capacitor will be as given by equations (2.37) and (2.38) and the components in the non-linear resistance will be

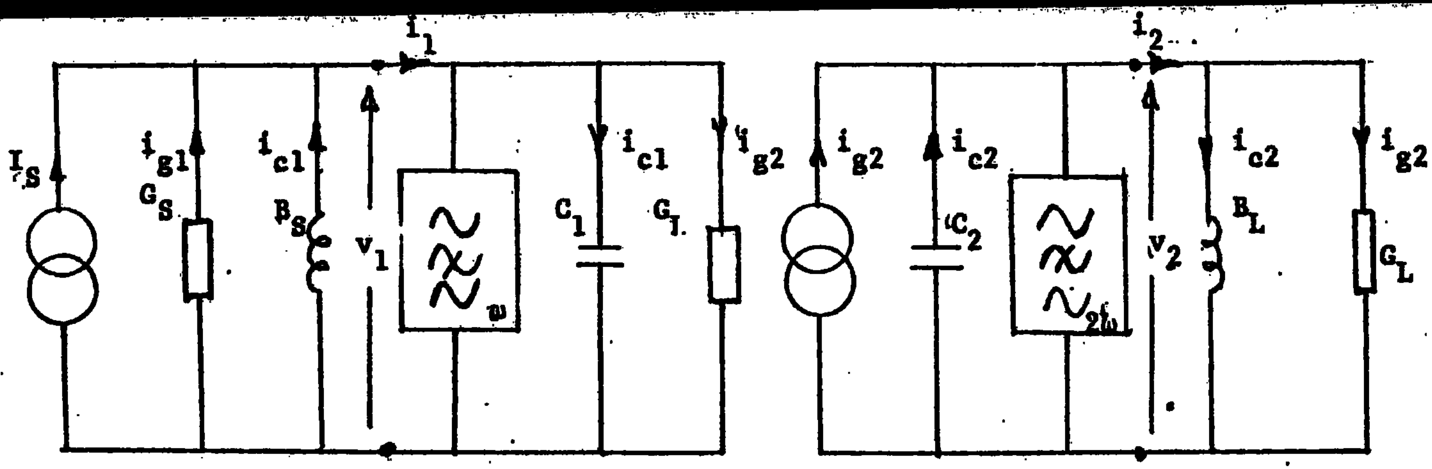

$v_1 = aV_T\ (1 + j0)$ $\qquad$ $v_2 = j2\omega a^2\ Q_2/G_L$

$i_1 = i_{g1} + i_{c1}$ $\qquad$ $i_2 = i_{g2} + i_{c2}$

$\quad = 2\omega ab\ Q_2 + j\omega a\ \ Q_1 + 3Q_3\ (a^2 + 2b^2 - 1)$ $\qquad$ $\quad = j\omega a^2\ Q_2 + 2\omega b\ \ Q_1 + 3Q_3\ (2a^2 + b^2 - 1)$

$B_S = j/\omega C_1$ $\qquad$ $B_L = j/2\omega C_2$

$C_1 = \ Q_1 + 3Q_3\ (a^2 + 2b^2 - 1\ /V_T$ $\qquad$ $C_2 = \ Q_1 + 3Q_3\ (2a^2 + b^2 - 1)\ \ /V_T$

Conductance transformation $G_1\ G_L = (a\ G_{21})^2 = G_0^{\ 2}$, the characteristic conductance

V_T = peak level of cosine test voltage $\qquad a = \hat{V}_1/V_T,\quad b = \ddot{V}_2/V_T,\quad a \cos\theta + b \sin 2\theta \leq 1$

Q_1, Q_2, Q_3: charge coefficients of test spectrum

$G_{21} = 2\omega\ Q_2/V_T = I_2/V_T$: the test transconductance

Figure 2.4

Complete Equivalent Circuit of a Lossfree

Frequency Doubler

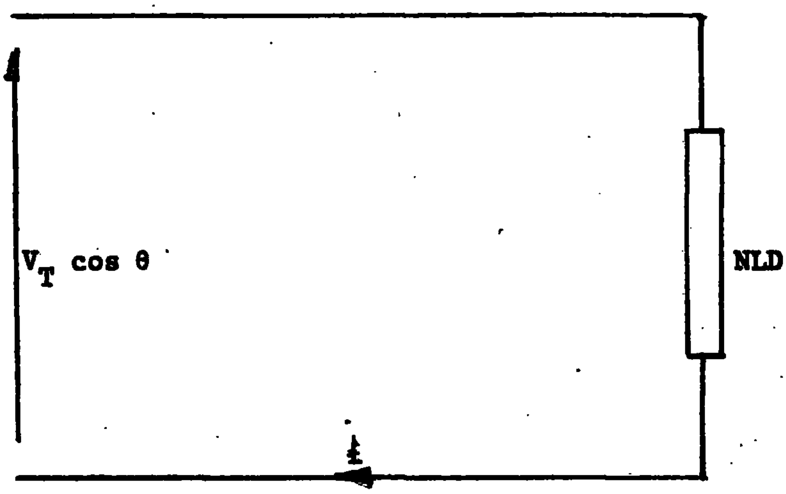

$$i = \sum_{1}^{\infty} (I_{R_k} \cos\theta - I_k \sin\theta)$$

N.L.D. Non-linear device

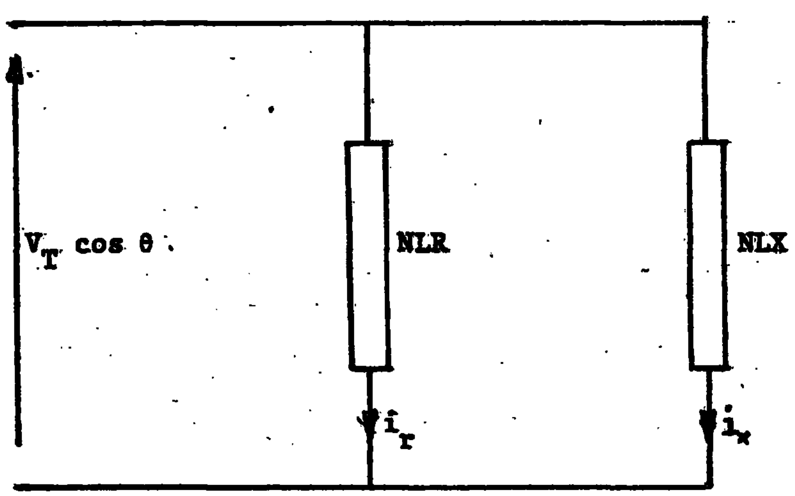

$$i_r = \Sigma\, I_{R_k} \cos\theta$$

$$i_x = -\ \Sigma\, I_k \sin\theta$$

N.L.R. non-linear resistor

N.L.X. non-linear reactance

Figure 2.5

Parallel Representation of a Non Linear Device

$$i_{r_2} = \left[- b\, I_{R_1} \cos\phi + Q^2\, I_{R_2} - 3b\, I_{R_3} (b^2 + 2a^2 - 1) \cos\phi \right] \cos 2\theta$$

$$+ \left[- b\, I_{R_1} \sin\phi - 3b\, I_{R_3} (b^2 + 2a^2 - 1) \sin\phi \right] \sin 2\theta \tag{2.60}$$

$$i_{r_1} = \left[a\, I_{R_1} - 2ab\, I_{R_2} \cos\phi + 3 I_{R_3}{}^{a} (a^2 + 2b^2 - 1) \right] \cos\theta$$

$$- 2ab\, I_{R_2} \sin\phi \sin\theta \tag{2.61}$$

The second harmonic component has terms independent of b, the normalised output voltage, and this represents the current injected into the output circuit by the input. These are,

$$i_g = + a^2\, I_{R_2} + j\, 2\omega a^2\, Q_2 \tag{2.62}$$

where complex notation has been introduced by means of (2.39) and (2.40).

The admittance representation of the remaining second harmonic currents is

$$Y = 2\omega b \frac{\left[Q_1 + 3Q_3 (b^2 + 2a^2 - 1) \right] (\sin\theta + j \cos\phi)}{\hat{V}_2 (\cos\phi + j \sin\phi)}$$

$$+ \frac{b\, I_{R_1} (\cos\phi - j \sin\phi)}{\hat{V}_2 (\cos\phi - j \sin\phi)} + \frac{3b\, I_{R_3} (b^2 + 2a^2 - 1) (\cos\phi - j \sin\phi)}{\hat{V}_2 (\cos\phi - j \sin\phi)}$$

$$= \frac{I_{R_1}}{V^T} \left[1 + \frac{3 I_{R_3}}{I_{R_1}} (b^2 + 2a^2 - 1) \right] + \frac{j 2\omega\, Q_1}{V_T} \left[1 + \frac{3Q_3}{Q_1} (b^2 + 2a^2 - 1) \right]$$

$$= G_2 + j 2\omega\, C_2 \tag{2.63}$$

which represent the internal conductance and capacitance of the device. To constrain operation of the system to the second harmonic the load must include an inductance to cancel the internal capacitance C_2.

The output current now available to develop a voltage across the load is that from the constant current generator, equation (2.62) together with the resistive current through G_2 and therefore

$$G_L \hat{V}_2 (\cos\phi - j\sin\phi) = j\omega 2a^2 Q_2 + a^2 I_{R_2} - \left[bI_{R_1} + 3b\, I_{R_3} (b^2 + 2a^2 - 1)\right] (\cos\phi - j\sin\phi) \tag{2.64}$$

which separates into real and imaginary parts

$$\left\{G_L \hat{V}_2 + \left[bI_{R_1} + 3bI_{R_3} (2a^2 + b^2 - 1)\right]\right\} \cos\phi = a^2 I_{R_2} \tag{2.65}$$

$$\left\{G_L \hat{V}_2 + \left[bI_{R_1} + 3bI_{R_3} (2a^2 + b^2 - 1)\right]\right\} \sin\phi = - 2\omega a^2 Q_2 \tag{2.66}$$

The unknown phase shift ϕ may be determined from the ratio of the above equation as

$$\tan\phi = \frac{-2\omega a^2 Q_2}{a^2 I_{R_2}} = \frac{-2\omega Q_2}{I_{R_2}} \tag{2.67}$$

In practice for a reverse-biassed varactor diode the current due to the parasitic resistance will be very small and consequently the phase must be close to $-\pi/2$ as given for the lossfree case. Define

$$\phi = \delta - \pi/2, \qquad \delta \text{ small} \tag{2.68}$$

and therefore

$$\cos\phi = - \tan\delta = - I_{R_2}/2\omega Q_2$$

$$1/\delta = \frac{2\omega Q_2}{I_{R_2}} = \frac{- I_2}{I_{R_2}} \tag{2.69}$$

Equation (2.69) is the ratio of the second harmonic components of the test capacity current to the resistive current and is a measure of the quality of the device. It is independent of the input and output voltage depending only on the device parameters as measured by a large signal spectrum test. Furthermore equation (2.62) (the injected current into the output circuit) may be written as

$$i_{g_2} = j2\omega a^2 Q_2 (1 - j\delta) \tag{2.70}$$

which indicates the change in the current due to the presence of resistance.

The output voltage may be obtained from (2.65) and (2.66) by squaring and adding to give

$$G_L \hat{V}_2 + bI_{R_1}\left[1 + \frac{3I_{R_3}}{I_{R_1}}(2a^2 + b^2 - 1)\right] = \sqrt{(2\omega a^2 Q_2)^2 + a^2 I_{R_2}^{\;2}} \tag{2.71}$$

The left hand side of equation (2.71) can be simplified provided $I_{R_3}/I_{R_1} \ll 1$ and also the right hand member can be modified with the aid of (2.64) therefore

$$\hat{V}_2 \left(G_L + \frac{I_{R_1}}{V_T}\right) = 2\omega a^2 Q_2 \sqrt{1 + \delta^2}$$

or (2.72)

$$\hat{V}_2 = 2\omega a^2 Q_2 \sqrt{1 + \delta^2} \Big/ (G_L + g_1)$$

where

$$g_1 = I_{R_1}/V_T \tag{2.73}$$

which may be defined as the fundamental loss conductance. As the parasitic effects are reduced to zero, the lossfree situation is recovered.

The input circuit may be deduced by taking $\phi = -\pi/2$ so that $\cos\phi = 0$ and $\sin\phi = -1$. The input current is then approximated by

$$
\begin{aligned}
i_{in} = a\left[I_{R_1} + 3I_{R_3}\,(a^2 + 2b^2 - 1)\right] + 2\omega ab\, Q_2 \\
+ j\omega a\left[Q_1 + 3Q_3(a^2 + 2b^2 - 1)\right] - j2ab\, I_{R_1}
\end{aligned}
\tag{2.74}
$$

where as before $V_1 = \hat{V}_1 \cos\theta$

The input admittance is then given by

$$
\begin{aligned}
Y_{in} = \frac{i_{in}}{V_1} = \frac{2\omega\hat{V}_2\, Q_2}{V_T^{\,2}} + \frac{I_{R_1}}{V_T}\left[1 + \frac{3I_{R_3}}{I_{R_1}}\,(a^2 + 2b^2 - 1)\right] \\
+ j\omega\left[\frac{Q_1 + 3Q_3\,(a^2 + 2b^2 - 1)}{V_T} - \frac{2V_2\, I_{R_2}}{\omega V_T^{\,2}}\right]
\end{aligned}
\tag{2.75}
$$

Operation of the input circuit at the fundamental frequency is maintained by including a source inductance to cancel the capacitance term in equation (2.75).

The input conductance to the system is then given by

$$
\begin{aligned}
G_1 &= \frac{2\omega\,\hat{V}_2\, Q_2}{V_T^{\,2}} + \frac{I_{R_1}}{V_T}\left[1 + \frac{3I_{R_3}}{I_{R_1}}\,(a^2 + 2b^2 - 1)\right] \\
&\doteq \frac{2\omega\,\hat{V}_2\, Q_2}{V_T^{\,2}} + g_1
\end{aligned}
\tag{2.76}
$$

provided $I_{R_3}/I_{R_1} \ll 1$.

By (2.72) the input conductance may then be expressed as

$$
G_1 = \frac{a^2\, G_{21}^{\,2}}{G_L + g_1}\sqrt{1 + \delta^2} + g_1 \tag{2.77}
$$

where G_{21} is given by equation (2.54).

The complete equivalent circuit is shown in Figure 2.6.

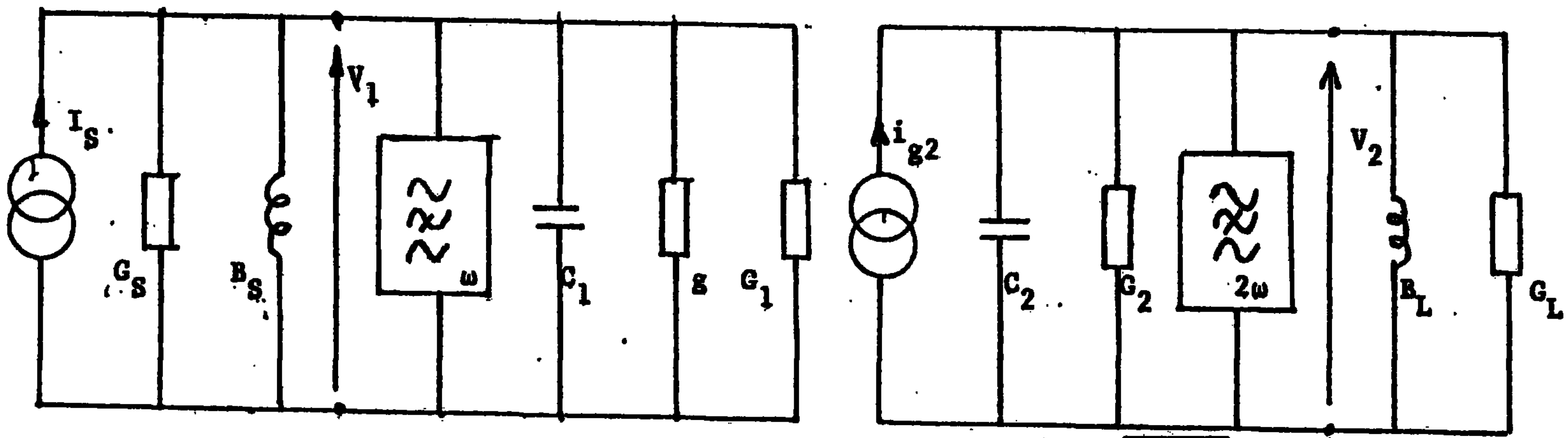

$V_1 = a\ V_T$

$B_S = j/\ C_1$

$C_1 = \left[Q_1 + 3Q_3\ (a^2 + 2b^2 - 1) - \frac{4Q_2\ V_{2\delta}}{V_T}\right] /V_T$

$g = g_1 = I_{R_1}/V_T$

$V_2 = \frac{2\omega a^2\ Q_2\sqrt{1 + \delta^2}}{G_L + g}\ (\cos\phi - j\sin\phi)$

$B_L = j/2\omega C_2$

$C_2 = \left[Q_1 + 3Q_3\ (2a^2 + b^2 - 1)\right] /V_T$

$G_2 = g_1 = I_{R_1}/V_T$

$$G_1{}' = \frac{a^2\ G_{21}{}^2}{G_L + g_1} \sqrt{1 + \delta^2}$$

$i_{g2} = j2\omega a^2\ Q_2\ (1 - j\delta)$ $\qquad \tan\delta = \delta = I_{R_2}/2\omega\ Q_2$ $\qquad \phi = \delta - \pi/2$

Figure 2.6

Equivalent Circuit of a Frequency

Doubler Including Losses

The input conductance consists of two parts:-

i) the reflected conductance of the output circuit (load plus device conductance),

ii) a conductance g_1 to absorb the power loss associated with the input circuit.

It remains now to determine the permissible values of the input signal in order that breakdown of the device can be prevented due to violation of equation (2.33).

$$a \cos \theta - b \sin 2\theta \leqslant 1 \qquad (2.78)$$

and therefore

$$a \leqslant \sec \theta - 2b \sin \theta \qquad (2.79)$$

This equation is plotted in Figure (2.7) and illustrates the permissible values of 'a' and 'b' which satisfy equation (2.33). But 'a' and 'b' are further constrained by equation (2.43), i,e.

$$\hat{V}_2 = 2\omega a^2 \, Q_2/G_L \qquad (2.80)$$

which may be rewritten as

$$a = \sqrt{b \, G_L/G_{12}} \qquad (2.81)$$

Equation (2.81) is also plotted with the ratio G_L/G_{12} as a running parameter. The point of operation of the multiplier must lie on one of these quadratic curves and lie within the permissible working range. For example if $G_L = G_{12}$ then maximum value for 'a' will be 0.68 and the maximum value of 'b' will be 0.47 as given by point P. If 'a' is reduced to say 0.6 then 'b' will reduce to 0.35 (point Q) on the curve $G_L/G_{12} = 1$.

The complete performance of the system can now be specified including for example the input power, output power and efficiency.

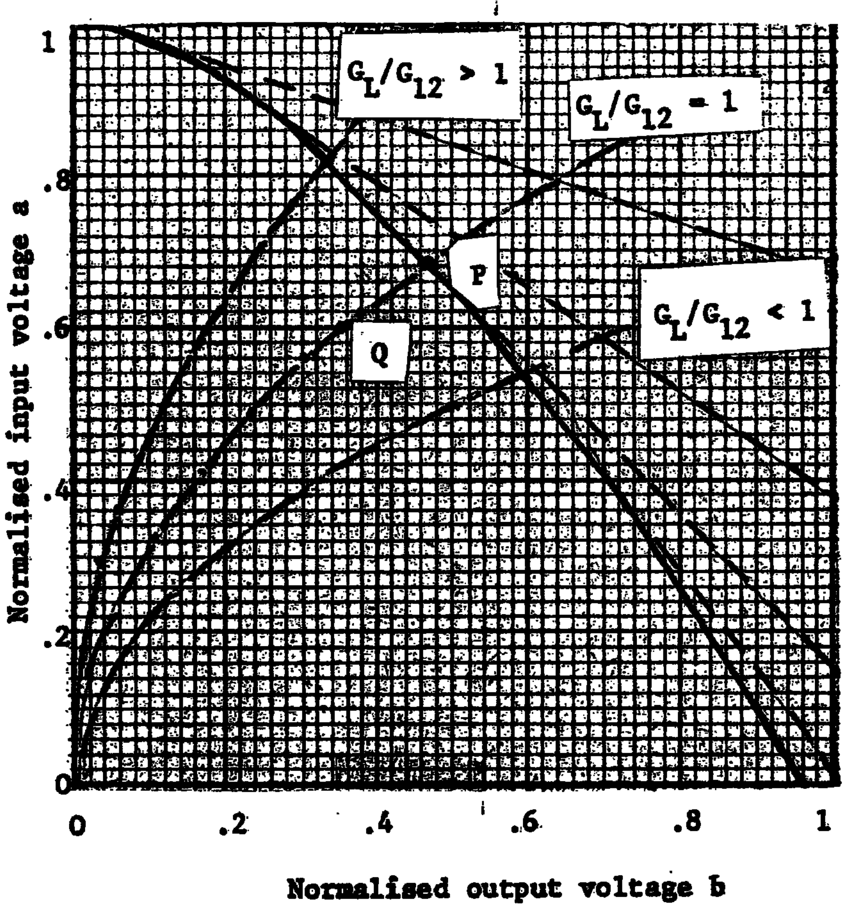

Figure 2.7

Operating Chart for Frequency Doubler

——————— limit of operation to prevent breakdown

—•—•— constant load conductance curves

2.8 Discussion

The aforegoing analysis shows that the performance of frequency multiplying circuits can be predicted in terms of the spectrum of the non-linear device to a sinusoidal drive. If the device characteristics are known the methods developed in this chapter are still applicable provided the Fourier Series coefficients can be evaluated.

Important ratios of spectral components which influence the performance of frequency multiplying systems have been identified. These are:-

(i) the transconductance $G_{12} = I_2/V_T$

(ii) a Quality Factor $1/\delta = I_2/I_{R_2}$

and (iii) the loss conductance $g_1 = I_{R_1}/V_T$

The above parameters are independent of input and output voltage and are properties of the non-linear device, obtainable from spectrum tests.

The conductance changing property of frequency multiplier systems has been demonstrated to depend on the transconductance (again a property of the device) and the possible use of a characteristic conductance to simplify design has been introduced.

A disadvantage of the proposed methods is the necessity to expand the Chebyshev representation of the device characteristic for a complex drive. Provided the spectrum of the device reduces rapidly for an increasing harmonic number the technique is acceptable.

The analyses presented here is being employed by D.F. Oxford* to design shunt and series frequency multiplying circuits using strip line and coaxial resonant circuits, and incorporating the effects of idler circuits into the analysis.

* Ph.D. research in frequency multiplying systems.

Suggestions for Further Investigations

1. Determination of transductance, quality factor and loss conductance from time domain portraits.

2. A numerical method of obtaining the modified spectrum when the device is stimulated with a complex drive.

CHAPTER 3

THE EXPONENTIAL DIODE WITH SERIES RESISTANCE

Static Characteristics

3.1 Introduction

In this chapter attention is focussed on the characteristics of a Schottky-Barrier diode whose current varies as the exponential of the junction voltage. All practical diodes possess parasitic spreading resistance in series with the diode junction. Any test circuit devised to verify analytic results will have a source resistance which increases the effective device resistance. When the source voltage is sufficiently large to drive the diode hard into conduction the bi-linear approximation is adequate. In other situations, such as the reverse-biased diode mixer circuit arranged to obtain minimum conversion loss, this approximation breaks down and the curvature in the neighbourhood of the diode turn-on voltage must be taken into consideration[7]. It is therefore necessary to solve the practical diode equation, i.e.

$$i = I_s \exp(\alpha V - \alpha i r) - I_s \tag{3.1}$$

All previous attempts[3,4] to solve this equation have used the power series expansion method which fails because of the slow rate of convergence.

This slow rate of convergence is due to the rapid change in the slope of the diode curve in the vicinity of the turn on voltage. The approach adopted in this work is to determine a functional expansion. It will be seen that the solution requires the sum of only two functional terms to obtain the necessary accuracy, the second term being a small correction to the first term. The rapid convergence of this two-term approximation may be attributed to the fact that each of the functions is written in a closed form and replaces the power series expansions of the aforementioned methods. As the two term expansion solution of equation (3.1) is original a complete derivation is given within this chapter.

3.2 The Normalised Equation

The solution to equation (3.1) is best approached by modifying it to a suitable mathematical form First, we rearrange the equation as

$$(i + I_s) = I_s \exp\left[(\alpha V + \alpha r I_s) - \alpha r (i + I_s)\right] \tag{3.2}$$

which leads to

$$I = A \exp(-\alpha r I) \tag{3.3}$$

where

$$A = I_s \exp(\alpha V + \alpha r I_s) \tag{3.4}$$

and

$$I = i + I_s \tag{3.5}$$

Further modification gives

$$I/A = \exp(-\alpha r A\, I/A) \tag{3.6}$$

which may finally be written as

$$x = \exp(-x/\varepsilon) \tag{3.7}$$

where

$$x = I/A = (i + I_s)/I_s \exp(\alpha V + \alpha r I_s) \tag{3.8}$$

and

$$\varepsilon = 1/\alpha r A = 1/\alpha r I_s \exp(\alpha V + \alpha r I_s) \tag{3.9}$$

Equation (3.7) is the simplest form of the equation (3.1) whilst equation (3.8) and (3.9) are the transformations which enable the solution, in terms of the original variables i, and V, to be recovered. It is of interest to note than this type of implicit exponential equation occurs in connection with black body radiation and with the stability of differential-difference equations (22). The method outlined above may be used to transform any equation of the form

$$Ai = B \exp(\alpha V + c - bi) + C, \qquad b > 0 \tag{3.10}$$

into equation (3.7) and therefore the results obtained for the diode equation may be of direct use in other areas of science.

3.3 The First Term Approximation

Now that the diode equation is reduced to its modified form, the variation of the roots of the equation can be displayed graphically for different values of the parameter ε. In Figure (3.1) the roots of equation (3.7) are shown as the intersections on the curves $y = x$ and $y = \exp(-x/\varepsilon)$. Also shown (broken lines) in Figure 3.1 are the approximate roots obtained if the exponential term is replaced by a linear approximation, i.e.

$$\exp(-x/\varepsilon) = 1 - x/\varepsilon \tag{3.11}$$

leading to

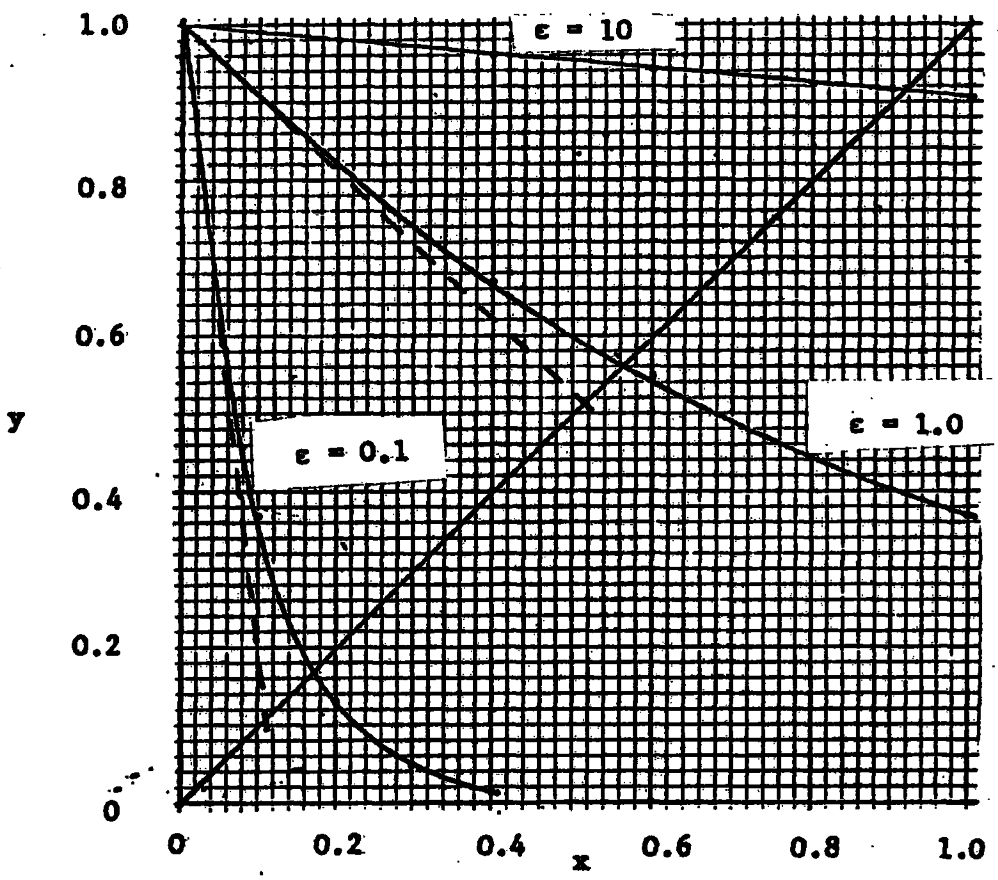

<u>Figure 3.1</u>

Exact and Approximate roots of the equation

$$x = \exp(-x/\varepsilon)$$

$$x \approx 1/(1 + 1/\varepsilon) \tag{3.12}$$

It will be seen that the ratio of the exact root to the approximate root varies from 1.01, through 1.096 to 1.7 as the parameter ε varies from 10, through 1.0 to 0.1. This argument suggests that it may be possible to find a better approximation by introducing a modifying factor to the solution of equation (3.7) in the form

$$x \approx f(\varepsilon)/(1 + 1/\varepsilon) \tag{3.13}$$

where $f(\varepsilon)$ is a slowly varying function with $f(\infty) = 1.0$. To determine the unknown function $f(\varepsilon)$, equation (3.13) is substituted into equation (3.7) to obtain

$$f(\varepsilon)/(1 + 1/\varepsilon) = \exp\left[-\frac{f(\varepsilon)}{\varepsilon\,(1 + 1/\varepsilon)}\right] \tag{3.14}$$

The logarithmic equivalent of (3.14) is

$$\ln f(\varepsilon) - \ln(1 + 1/\varepsilon) = -\,f(\varepsilon)/(1 + \varepsilon) \tag{3.15}$$

The function $f(\varepsilon)$ is greater or equal to unity and therefore $\ln f(\varepsilon)$ is always positive. Since $f(\varepsilon)$ changes slowly for large changes in ε then $\ln(f(\varepsilon))$ will change even more slowly. The second term in equation (3.15) i.e. $\ln(1 + 1/\varepsilon)$ behaves as $[-\ln(\varepsilon)]$ as ε approaches zero. The left hand side of equation (3.15) is therefore dominated by this latter term and it is therefore possible to neglect $\ln f(\varepsilon)$. This enables $f(\varepsilon)$ to be found as

$$f(\varepsilon) = (1 + \varepsilon)\ \ln\,(1 + 1/\varepsilon) \tag{3.16}$$

If (3.16) is now substituted into (3.13) the first term approximation to the root of (3.17) is obtained as

$$x \approx \varepsilon\ \ln\,(1 + 1/\varepsilon) \tag{3.17}$$

If ε is very large Figure 3.1 shows that x approaches unity and equation (3.17) then becomes

$$x \approx \varepsilon \ln (1 + 1/\varepsilon) \approx \varepsilon .\ 1/\varepsilon \to 1 \qquad (3.18)$$

On the other hand, if ε is small the root of equation (3.7) must approach zero and for this condition equation (3.17) becomes

$$x \approx \varepsilon \ln (1 + 1/\varepsilon) \approx \varepsilon \ln (1/\varepsilon) \to 0 \qquad (3.19)$$

Thus equation (3.17) has the correct asymptotic behaviour. For intermediate values of ε it will be seen from Figure 3.2 that (3.17) follows the general trend of the exact function but is not sufficiently accurate. In Figure 3.2 the exact function is computed by assigning values to x and calculating ε. The computed results from which Figure 3.2 is derived are given in Table 3.1.

3.4 The Two Term Approximation

The accuracy of the approximation may be further improved by obtaining a more accurate equation for $f(\varepsilon)$. This may be accomplished by assuming

$$f(\varepsilon) = f_o(\varepsilon) + f_1(\varepsilon) \qquad (3.20)$$

where $f_o(\varepsilon)$ is given by equation (3.16) and $f_1(\varepsilon)$ is assumed to be a small correction, i.e.

$$f(\varepsilon) = f_o(\varepsilon) \left[1 + f_1(\varepsilon)/f_o(\varepsilon)\right] = f_o(\varepsilon) \left[1 + z\right] \qquad (3.21)$$

where

$$z = f_1/f_o << 1 \qquad (3.22)$$

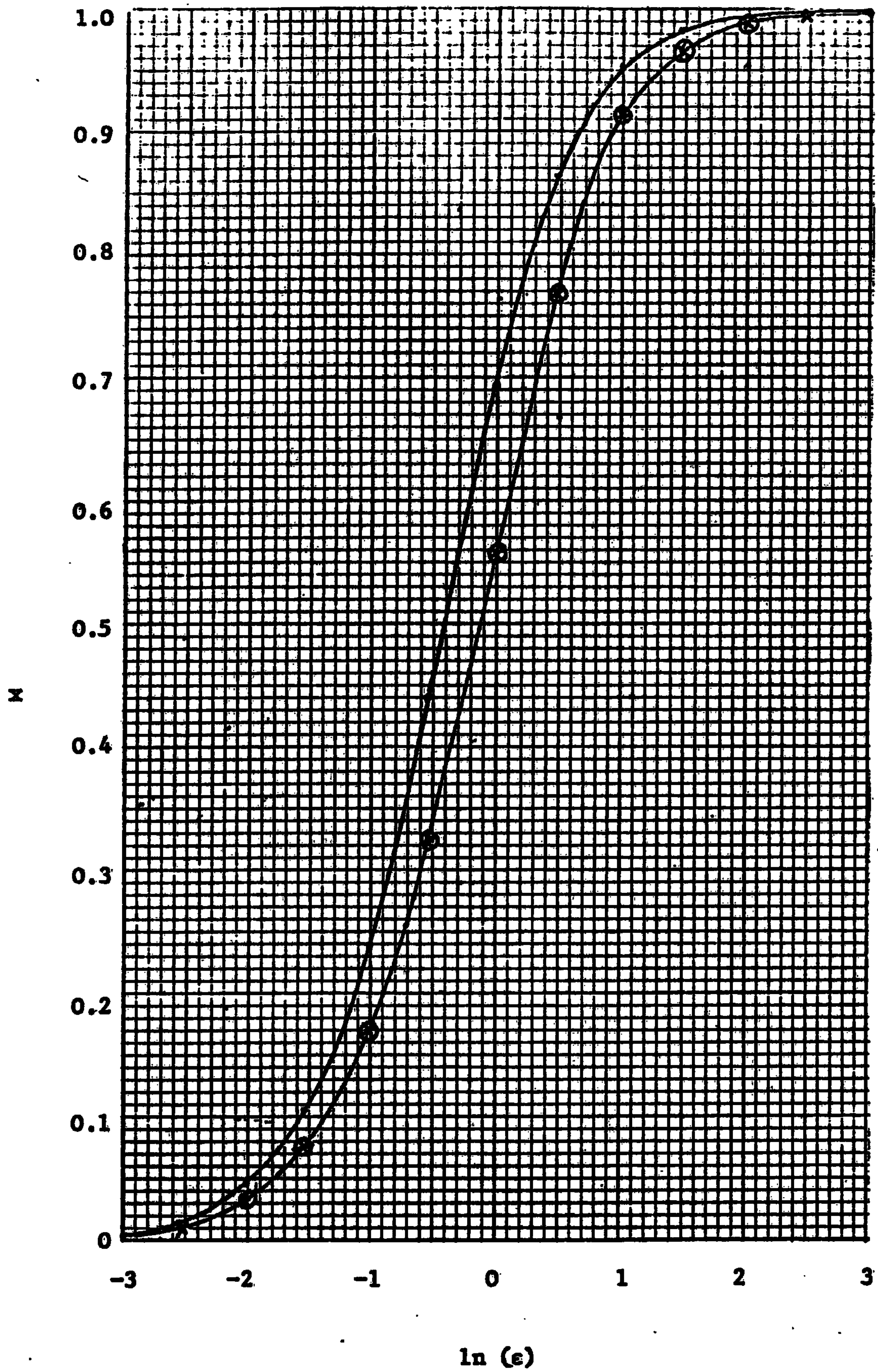

Figure 3.2

Solutions of $x = \exp(-x/\varepsilon)$

one term approximation

two term approximation

exact function

Table 3.1

ε	x	ε_r^*
.0001	.0009	.0000
.0003	.0024	.0002
.001	.0069	.0009
.003	.0174	.0029
.01	.0461	.0098
.03	.1060	.0294
.1	.2397	.0971
.3	.4399	.2888
1.0	.6931	.9631
3.0	.8630	2.9267
10.0	.9531	9.8959
30.0	.9836	29.8827
100.0	.9950	99.8774
300.0	.9983	299.8757
1000.0	.9995	999.8753
3000.0	.9998	2999.8790
9999.0	.9999	9998.9418

$^*\varepsilon_r$ calculated from inverse of equation (3.7) i.e.

$\varepsilon_r = -x/\ln(x)$

With this assumption (3.17) then takes the form

$$\ln\left[f_o(1 + z)\right] - \ln(1 + 1/\varepsilon) = - f_o(1 + z)/(1 + \varepsilon) \qquad (3.23)$$

which upon rearranging and cancelling common terms becomes

$$(1 + \varepsilon) \ln f_o + (1 + \varepsilon) \ln (1 + z) = - f_o z \qquad (3.24)$$

For small z the term ln (1 + z) may be replaced by z to give

$$(1 + \varepsilon) \ln f_o + (1 + \varepsilon) z = - (1 + \varepsilon)\left[\ln (1 + 1/\varepsilon)\right]z \qquad (3.25)$$

which is readily solved to give

$$z = \frac{- \ln f_o}{1 + \ln (1 + 1/\varepsilon)} \qquad (3.26)$$

The improved value for the function $f(\varepsilon)$ is now given by

$$f(\varepsilon) = (1 + z) f_o = f_o + zf_o$$

$$= (1+ \varepsilon) \ln (1 + 1/\varepsilon) - \frac{(1+ \varepsilon) \ln (1 + 1/\varepsilon)}{1 + \ln (1 + 1/\varepsilon)} \ln\left[(1+ \varepsilon) \ln (1 + 1/\varepsilon)\right] \qquad (3.27)$$

The two term approximation for x is finally obtained, i.e.

$$x = f(\varepsilon)/(1 + 1/\varepsilon)$$

$$= \varepsilon\ln (1 + 1/\varepsilon) - \frac{\varepsilon \ln (1 + 1/\varepsilon)}{1 + \ln (1 + 1/\varepsilon)} \ln\left[(1 + \varepsilon) \ln (1 + 1/\varepsilon)\right] \qquad (3.28)$$

The above is also plotted in Figure 3.2 where it is compared with the exact function from which it can be seen that the approximation to the exact solution is extremely good over a wide range of the variable ε. The computed results from which the graph of two term approximation shown in Figure 3.2 is derived are shown in Table 3.2

Table 3.2

ε	x	ε_r*
.0001	.0007	.0000
.0003	.00018	.0002
.001	.0052	.0009
.003	.0129	.0029
.01	.0034	.0098
.03	.0758	.0294
.1	.1713	.0971
.3	.3248	.2888
1.0	.5594	.9631
3.0	.7689	2.9267
10.0	.9119	9.8959
30.0	.9681	29.8827
100.0	.9901	99.8774
300.0	.9966	299.8757
1000.0	.9990	999.8753
3000.0	.9996	2999.8790
9999.0	.9999	9998.9418

*As for Table 3.1

$\varepsilon_r = -x/\ln(x)$

3.5 Solution in Terms of Initial Variables

Equation (3.28) has been shown to be a valid mathematical solution for the transcendental exponential equation, however to appreciate the physical implication of the solution it is necessary to transform equation (3.28) to the initial variables by means of (3.8) and (3.9). Before quoting the final result it is useful to examine the relation between ε and V, i.e.

$$1/\varepsilon = \alpha r I_s \exp(\alpha V + \alpha r I_s) \tag{3.29}$$

obtained by inverting (3.9). The multiplier of the exponential $\alpha r I_s$ may be incorporated into the argument of the exponential by introducing an auxiliary voltage V_o , i.e.

$$\alpha r I_s = \exp(-\alpha V_o) \tag{3.30}$$

Consequently equation (3.29) may now be written in the form

$$1/\varepsilon = \exp(\alpha V - \alpha V_o) = \exp(u) \tag{3.31}$$

where the term $\alpha r I_s$ in the argument of the exponential has been neglected since I_s is of the order of 10^{-9}, and

$$u = \alpha(V - V_o) \tag{3.32}$$

The two term approximation may finally be written as

$$i + I_s = \frac{1}{\alpha r}\ln(1 + e^u)\left[1 - \frac{\ln\left[(1 + e^{-u})\ln(1 + e^u)\right]}{1 + \ln(1 + e^u)}\right] \tag{3.33}$$

Graphical comparisons of the one-term and two term approximations with the exact diode equation are shown in Figures (3.3) and (3.4), respectively. The validity of the two term approximation is immediately apparent from Figure (3.4) and to appreciate its accuracy a numerical comparison is made in Table (3.3). The percentage error between the voltage recovered from the exact diode equation and the true voltage for a given current ranges from - 0.0028% at 1.9 volts, through - 0.1196% at 0.3 volts to - .0002% at 0.1 volts. The solution is an extremely good approximation to the exact diode equation. The accuracy is maintained for other values of x, r, and I_s and has been checked for values of r ranging from 10 to 1000 ohms.

3.6 <u>The Significance of the Logarithmic Form</u>

Although one term approximation is not sufficiently accurate it is useful to examine its behaviour as it highlights the physical nature of the device governed by an equation of the form

$$i + I_s = \frac{1}{\alpha r} \ln\left[1 + \exp \alpha \ (V - V_o)\right] \qquad (3.34)$$

If $V > V_o$, and since α is large (typically of the order of 40) then

$$\exp\left[\alpha(V - V_o)\right] >> 1 \qquad (3.35)$$

and equation (3.34) becomes

$$i + I_s \approx \frac{1}{\alpha r} \ \ln\left[\exp\left\{\alpha \ (V - V_o\right\}\right]$$

$$= \frac{V - V_o}{r} \qquad (3.36)$$

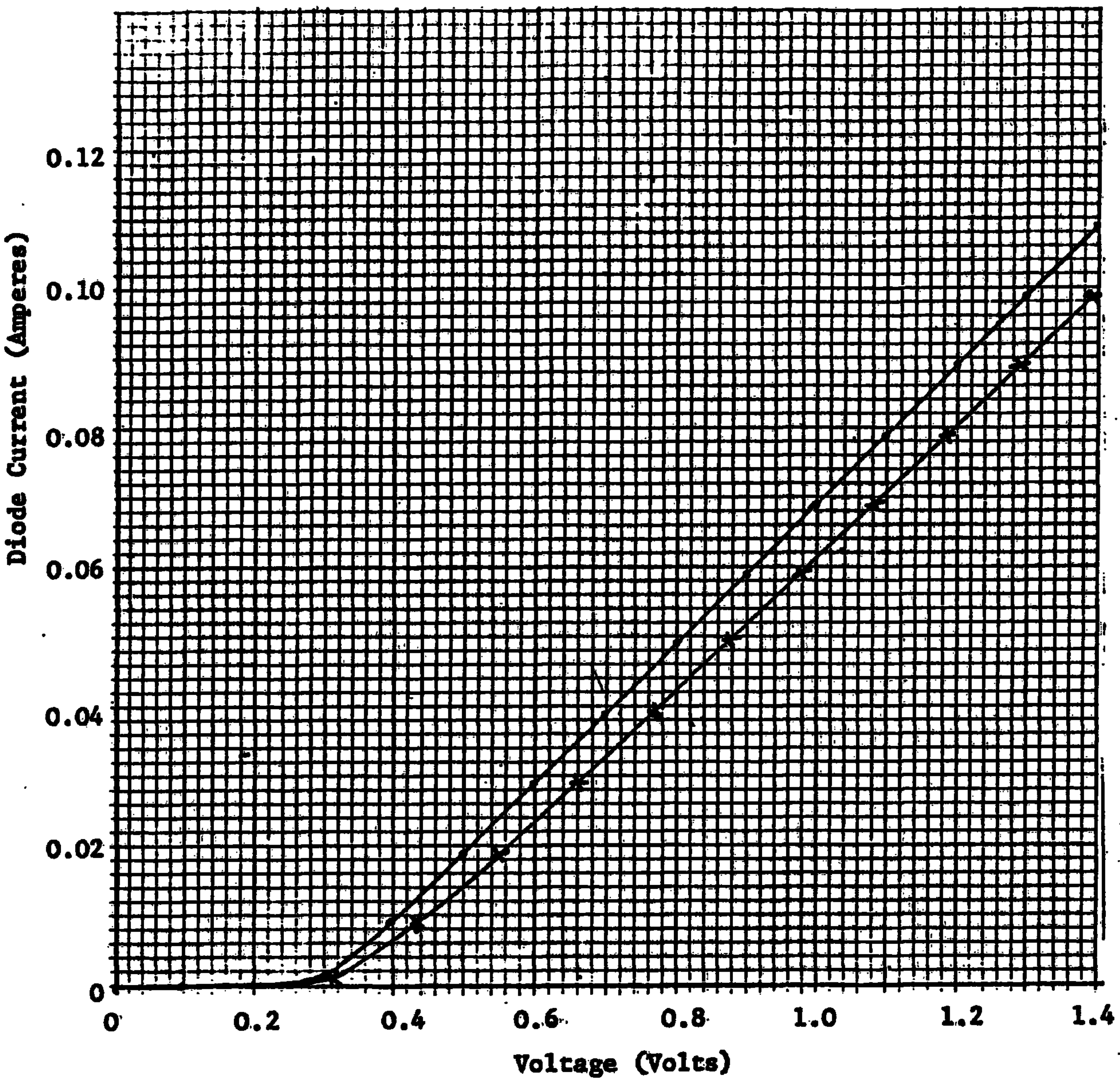

<u>Figure 3.3</u>

Comparison of one-term approximation with exact diode characteristic

——— one term approximation

—×—×—× diode characteristic $(i = I_s \exp(\alpha V - \alpha i r) - I_s)$

$\alpha = 40$, $r = 10$ ohms, $I_s = 10^{-8}$ amperes

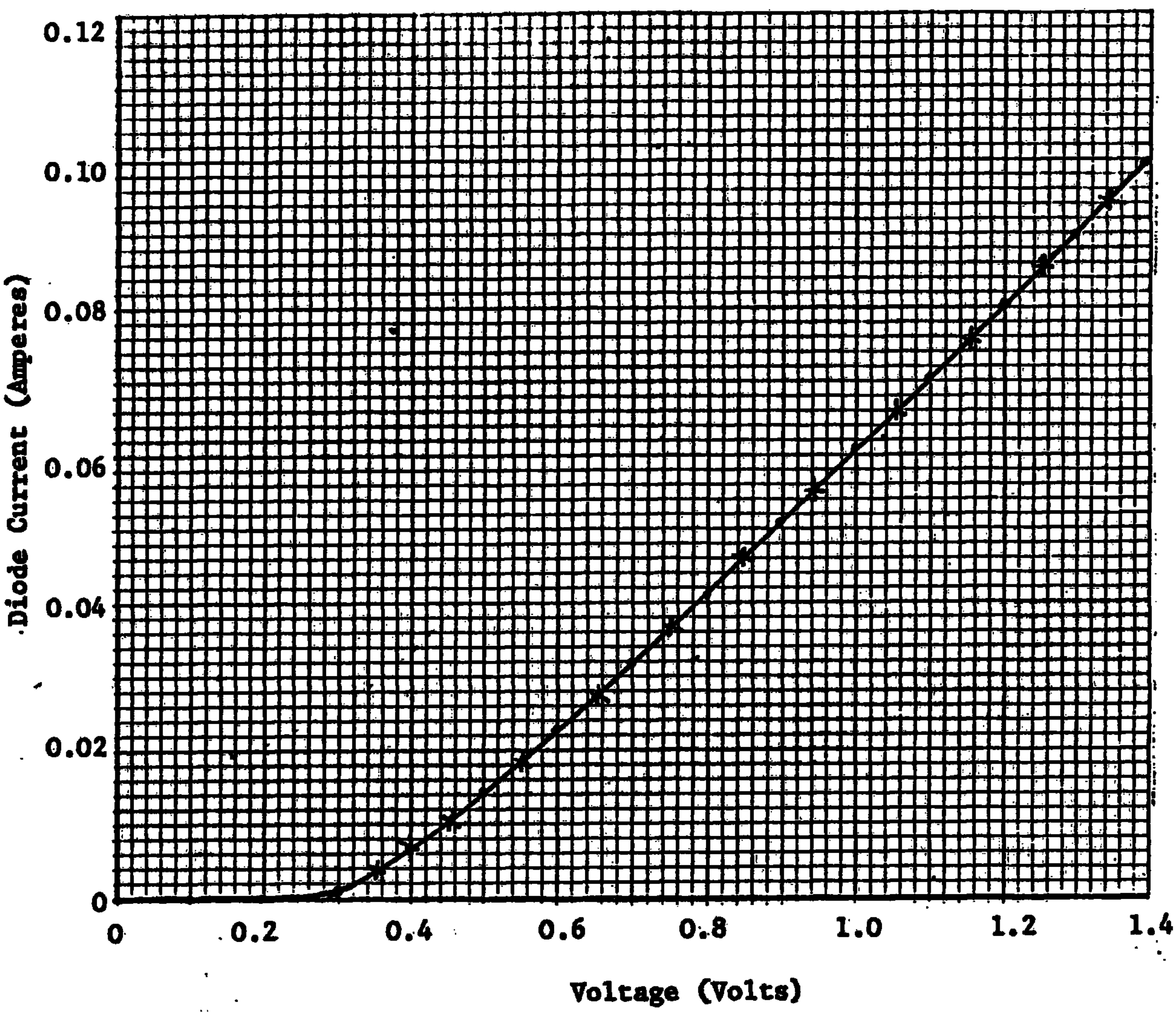

Figure 3.4

Comparison of two term approximation with exact diode characteristic

two term approximation

diode characteristic

$\alpha = 40$, $r = 10$ohms, $I_s = 10^{-8}$amperes

Table 3.3

Numerical comparison of one and two term approximations with exact diode equation

$\alpha = 40$, $r = 10$ ohms $I_s = 10^{-8}$ amperes $V_0 = 0.3107$

Voltage V	Current $(i + I_s)$ one term	Current $(i + I_s)$ two term	Voltage from two term
0	1×10^{-8}	1×10^{-8}	1×10^{-7}
.1	5.459×10^{-7}	5.458×10^{-7}	.0999
.2	2.963×10^{-5}	2.946×10^{-5}	.1999
.3	1.253×10^{-3}	1.053×10^{-3}	.2996
.4	8.996×10^{-3}	6.437×10^{-3}	.3987
.5	1.892×10^{-2}	1.445×10^{-2}	.4992
.6	2.892×10^{-2}	2.329×10^{-2}	.5995
.7	3.892×10^{-2}	3.248×10^{-2}	.6996
.8	4.892×10^{-2}	4.185×10^{-2}	.7997
.9	5.892×10^{-2}	5.135×10^{-2}	.8998
1.0	6.892×10^{-2}	6.093×10^{-2}	.9998
1.1	7.892×10^{-2}	7.056×10^{-2}	1.0998
1.2	8.892×10^{-2}	8.024×10^{-2}	1.1999
1.3	9.892×10^{-2}	8.996×10^{-2}	1.2999
1.4	1.089×10^{-1}	9.970×10^{-2}	1.3999
1.5	1.189×10^{-1}	1.095×10^{-1}	1.4999
1.6	1.289×10^{-1}	1.193×10^{-1}	1.5999
1.7	1.389×10^{-1}	1.291×10^{-1}	1.6999
1.8	1.489×10^{-1}	1.389×10^{-1}	1.7999
1.9	1.589×10^{-1}	1.487×10^{-1}	1.8999

Thus for $V > V_o$ the logarithmic form of equation (3.34) behaves linearly with slope $1/r$ which is precisely the manner in which the bi-linear approximation is used to represent diode behaviour when driven hard into conduction. Furthermore, if this straight line is extrapolated it cuts the V axis at $V = V_o$. This fact gives the physical interpretation to V_o as being the turn-on voltage of the diode and for $\alpha = 40$, $r = 10$, $I_s = 10^{-8}$ it is seen that

$$V_o = -\frac{1}{\alpha} \ln (\alpha r I_s) = 0.31 \text{ volts} \tag{3.38}$$

which is close to the empirically observed turn-on voltage. The fact that the turn on voltage of diodes appears to be independent of series resistance r may be explained by the fact that $\alpha r I_s$ is dominated by I_s and extremely large changes in r are required to produce a significant change in $\ln (\alpha r I_s)$.

When $V < V_o$ the exponential term in equation (3.34) becomes small compared to unity and then using (3.30) gives

$$i + I_s \approx \frac{\exp\left[\alpha \ (V - V_o)\right]}{\alpha r} = I_s \exp (\alpha V) \tag{3.39}$$

which tends to zero for negative voltage. This again is the manner in which the bi-linear approximation represents diode behaviour for reverse biased condition.

The aforegoing discussion suggests that it may be possible to obtain an approximation to the diode characteristic by assuming an equation of the form

$$i + I_s = \frac{1}{\alpha r_m} \ln \left[1 + \exp \alpha \ (V - V_1)\right] \tag{3.40}$$

where r_m is a modified resistance parameter to account for the slight reduction in slope of the exact curve as shown in Figure 3.3 and V_1 is chosen to represent the turn on voltage.

The appropriate parameters r_m, and V_1 may be obtained by expanding the two term approximation (equation 3.33) for $V > V_o$ to obtain

$$i + I_s \approx \frac{V - V_o}{r} \frac{1}{\alpha r} \ln\left[\alpha\ (V - V_o)\right] \qquad (3.41)$$

This equation is not linear in V, however, the curvature due to the logarithmic term is small and over practical working ranges may be linearised about $V = 2V_o$ to give

$$i + I_s \approx \frac{V\ (1 - 1/\alpha V_o)}{r} - (2 - \ln \alpha V_o - \alpha V_o)/\alpha \qquad (3.42)$$

This asymptote will intercept the V axis at

$$V_1 = \frac{\alpha V_o + \ln \alpha V_o - 2}{\alpha(1 - 1/\alpha V_o)} \qquad (3.43)$$

and the inverse of the slope will give the modified resistance parameter.

$$r_m = r/(1 - 1/\alpha V_o) \qquad (3.44)$$

The appropriate logarithmic approximation will then be given by equation (3.40) with the parameters r_m and V_1 given by equations (3.43) and (3.44), respectively. Graphical and numerical comparisons of the logarithmic approximation with the exact diode equation are shown in Figure (3.5) and Table (3.4) for diode parameters $\alpha = 40$, $r = 10$, $I_s = 10^{-8}$. The corresponding value of the turn-on voltage V_1 for these parameters as given by equation (3.43) is 0.35 volts which agrees with the intercept in Figure (3.5). The modified resistance r_m as given by equation (3.44) is 10.975 ohms, an increase of approximately 9% on the true series resistance. It should be noted that r_m is not directly proportional to r since V_o is dependent on r.

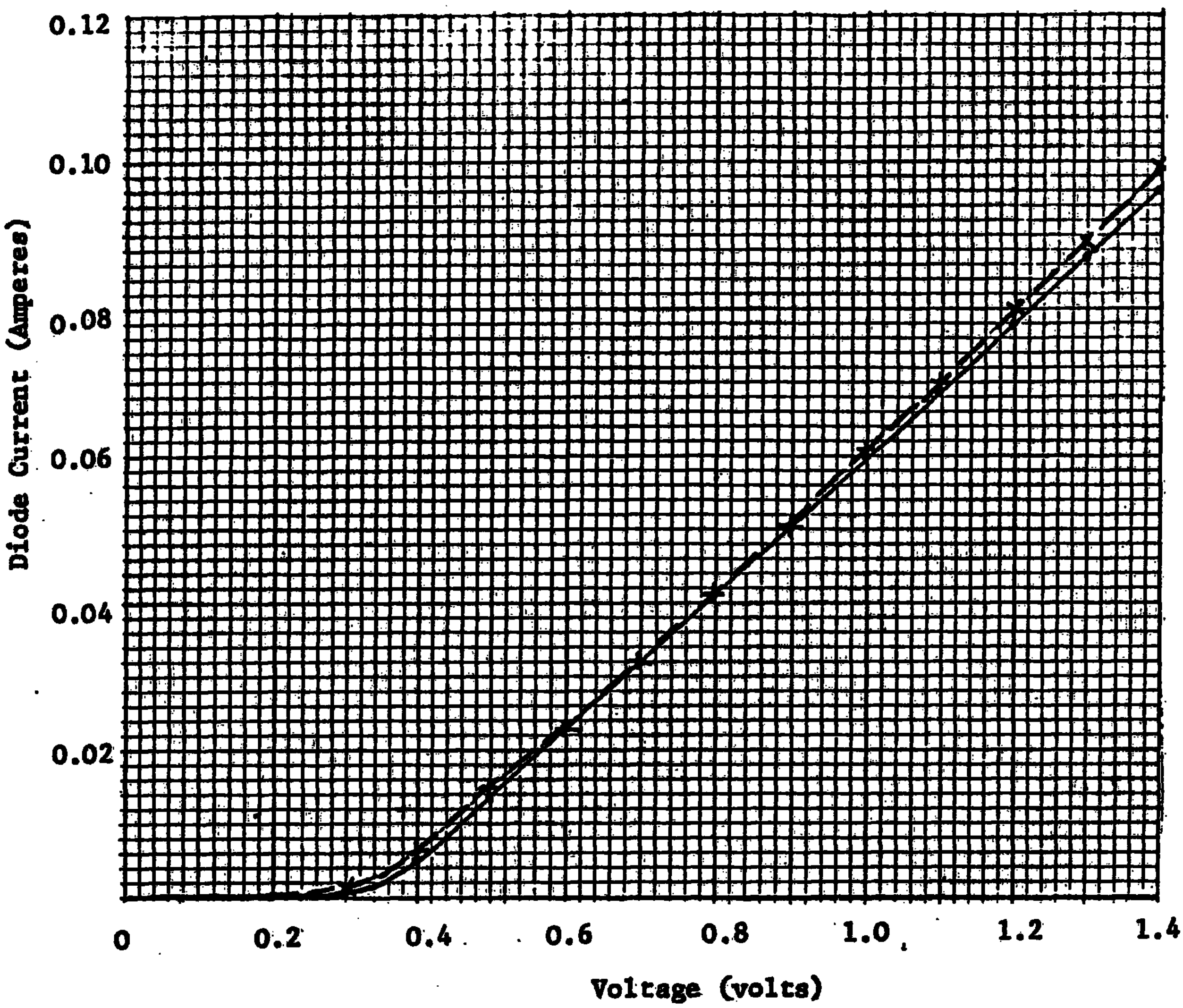

<u>Figure 3.5</u>

Comparison of translated one-term expansion with two-term approximation

—•—•— translated (logarithmic)

-*- -*- -*- two term approximation

Table 3.4

Comparison of logarithmic and two term approximations

$\alpha = 40, \quad r = 10$ ohms, $\quad I_s = 10^{-8}$ amperes

$V_0 = 0.3107$ volts

$V_1 = 0.352$ volts $\qquad r_m = 10.875$ ohms

voltage volts	two term amperes	logarithmic amperes
0	1×10^{-8}	1.8×10^{-9}
.1	5.458×10^{-7}	9.612×10^{-8}
.2	2.946×10^{-5}	5.242×10^{-6}
.3	1.053×10^{-3}	2.700×10^{-4}
.4	6.437×10^{-3}	4.724×10^{-3}
.5	1.445×10^{-2}	1.361×10^{-2}
.6	2.329×10^{-2}	2.280×10^{-2}
.7	3.248×10^{-2}	3.199×10^{-2}
.8	4.185×10^{-2}	4.119×10^{-2}
.9	5.135×10^{-2}	5.038×10^{-2}
1.0	6.093×10^{-2}	5.958×10^{-2}
1.1	7.056×10^{-2}	6.877×10^{-2}
1.2	8.024×10^{-2}	7.797×10^{-2}
1.3	8.996×10^{-2}	8.717×10^{-2}
1.4	9.970×10^{-2}	9.636×10^{-2}
1.5	1.095×10^{-1}	1.056×10^{-1}
1.6	1.193×10^{-1}	1.148×10^{-1}
1.7	1.291×10^{-1}	1.240×10^{-1}
1.8	1.389×10^{-1}	1.331×10^{-1}
1.9	1.487×10^{-1}	1.423×10^{-1}

It will be observed from Figure (3.5) that the two curves are an extremely good match in the vicinity of 0.7 volts, (approximately $2V_o$) but that they deviate slightly for other voltages. The choice of $2V_o$ as the point to fit the logarithmic curve is arbitrary. The main requirement is that the logarithmic curve should be fitted at a point beyond the curvature in the vicinity of the turn-on voltage. Other than this the point at which the two curves are made to fit will be largely dictated by the intended voltage swing imposed on the diode. For example if the maximum positive voltage is to be of the order 0.5 volts the fit can be made at say 0.45 volts which will clearly improve the accuracy of the approximation. If on the other hand a large voltage swing is anticipated a point about mid-way between the turn-on voltage and the maximum voltage will give a reasonably accurate representation. The determination of the parameters as r_m and V_1 when the two term approximation is linearised about a voltage differing from $2V_o$ is given in appendix C1.

With regard to the measure of the accuracy of the logarithmic approximation this will depend on the error norm used. In this respect Figure (3.6) illustrates the variation of the percentage error at different voltage levels from which it will be seen that the error is large for voltages below the turn-on voltage falls to the order of 2 percent at 0.7 volts and rises slowly to around 4 percent at 1.9 volts. The large percentage error at low values of voltage is due to the extremely small current level attained. The percentage error measures the deviation of the estimated point from its true value and takes no regard to the variation of the curve. The root mean square (r.m.s.) error the other hand gives a measure of the average deviation of the approximation curve from the true curve over the working range of the

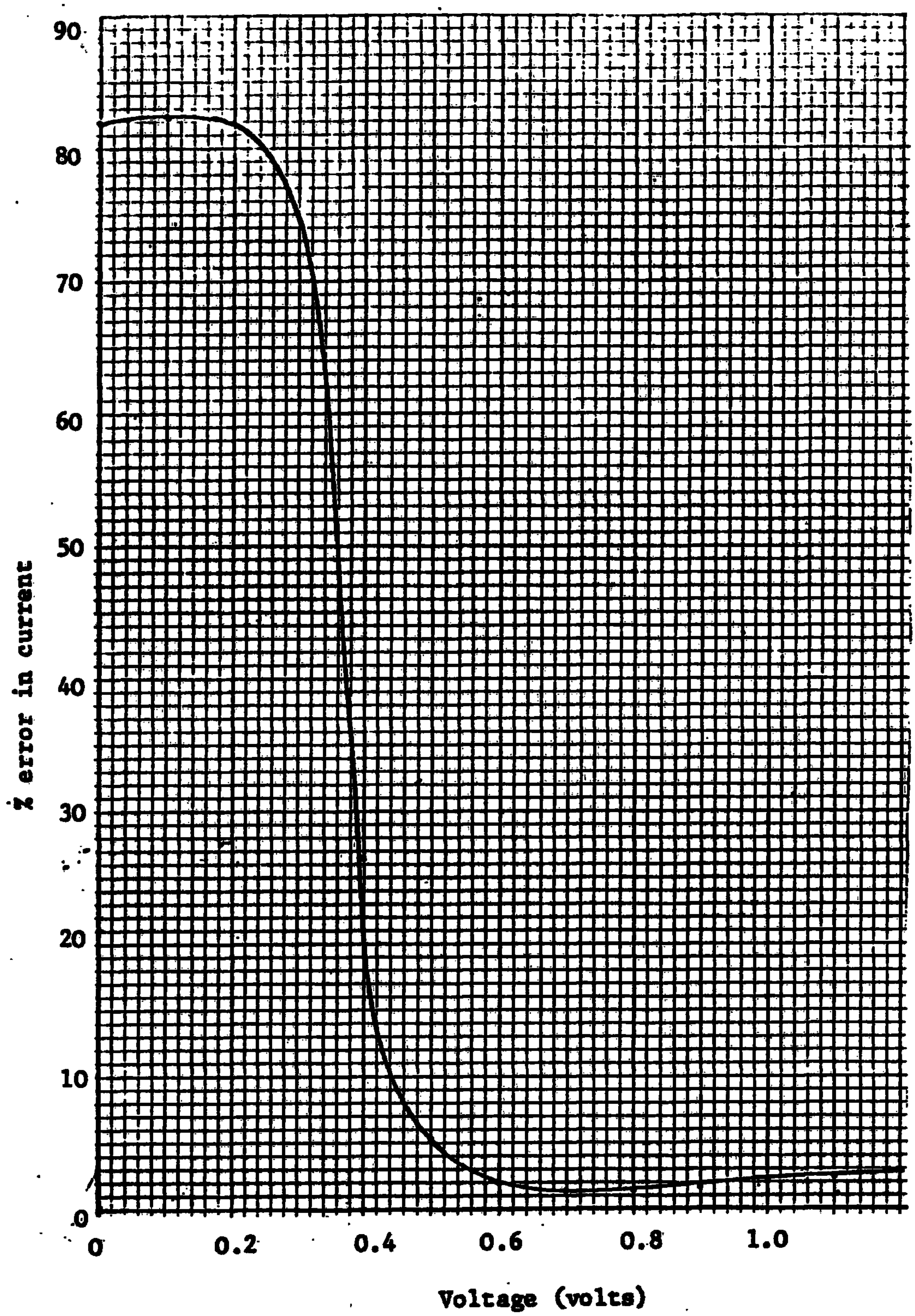

Figure 3.6

Variation of percentage error with applied voltage curve Figure (3.7) indicates the r.m.s. error over the working ranges covered. This curve shows a converse type behaviour to the percentage error curve giving a small error norm below the turn-on voltage and a considerably larger but roughly constant norm above the turn on level. This measure of error increases with increasing voltage range because it is proportional to the square of the area between the two curves.

3.7 Exponential Correction to the Bi-linear Model

In the previous section it has been shown how the logarithmic approximation can represent a diode having an asymptotic behaviour of a much used bi-linear model. Working from the logarithmic form it is also possible to produce a diode model which is bi-linear model withan exponential "cusp" correction as shown in Figure (3.8). The advantage of this model is that the two terms are additive whereas in the logarithmic model the bi-linear effect and the exponential curvature are included in a single function.

To obtain this useful approximate form, the logarithmic equation (3.40) is first expanded about the point $V = V_1$.

For $V \leq V_1$ equation (3.40) may be written as

$$i + I_s = \frac{1}{\alpha r_m} \sum_{k=1}^{\infty} (-1)^{k+1} \frac{\exp\left[k\alpha (V - V_1)\right]}{k} \qquad (3.45)$$

since the exponential term is less or equal to unity.

For $V \geq V_1$ equation (3.40) is rearranged as

$$(i + I_s) = \frac{1}{\alpha r_m} \ln\left\{\exp(\alpha (V - V_1))\left[1 + \exp(-\alpha (V - V_1))\right]\right\}$$

$$= \frac{V - V_1}{r_m} + \ln\left\{1 + \exp\left[-\alpha (V - V_1)\right]\right\}$$

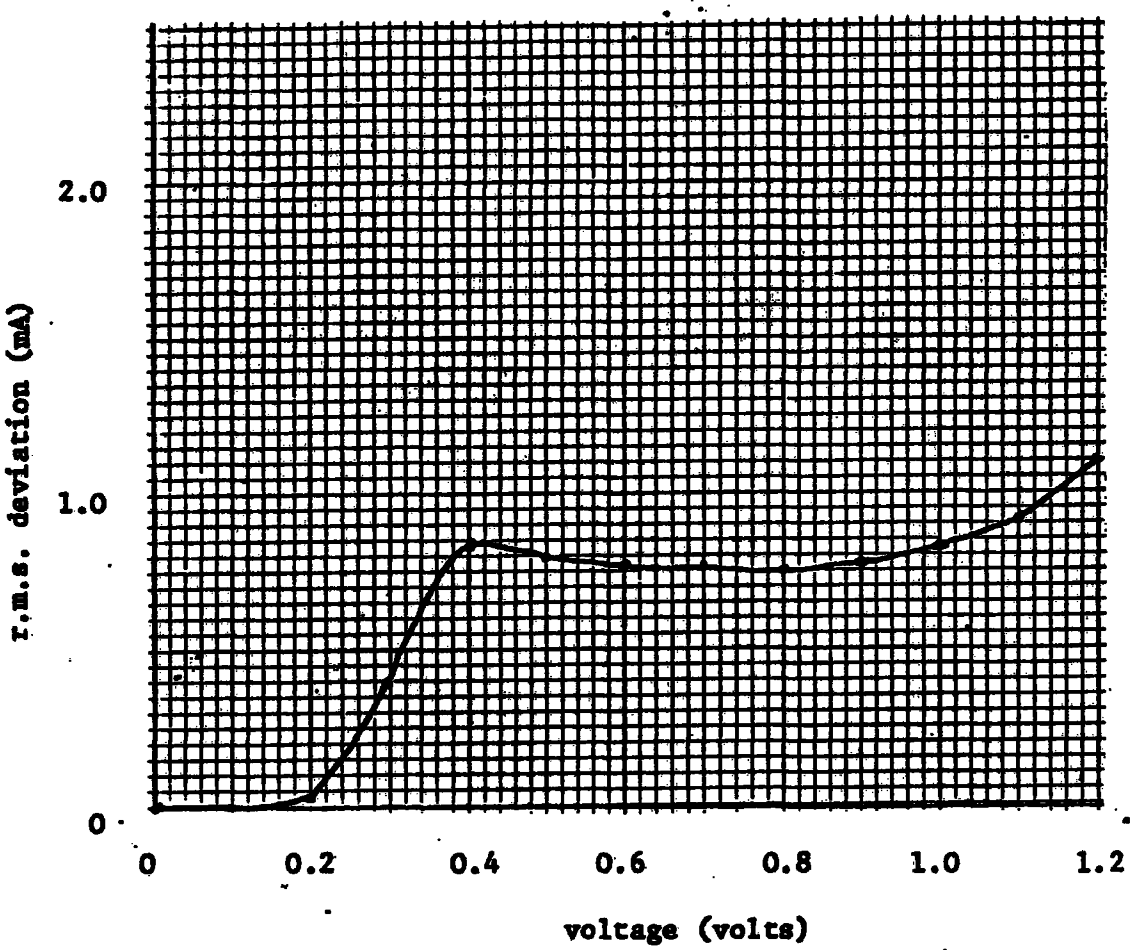

Figure 3.7

Variation of r.m.s. error with applied voltage

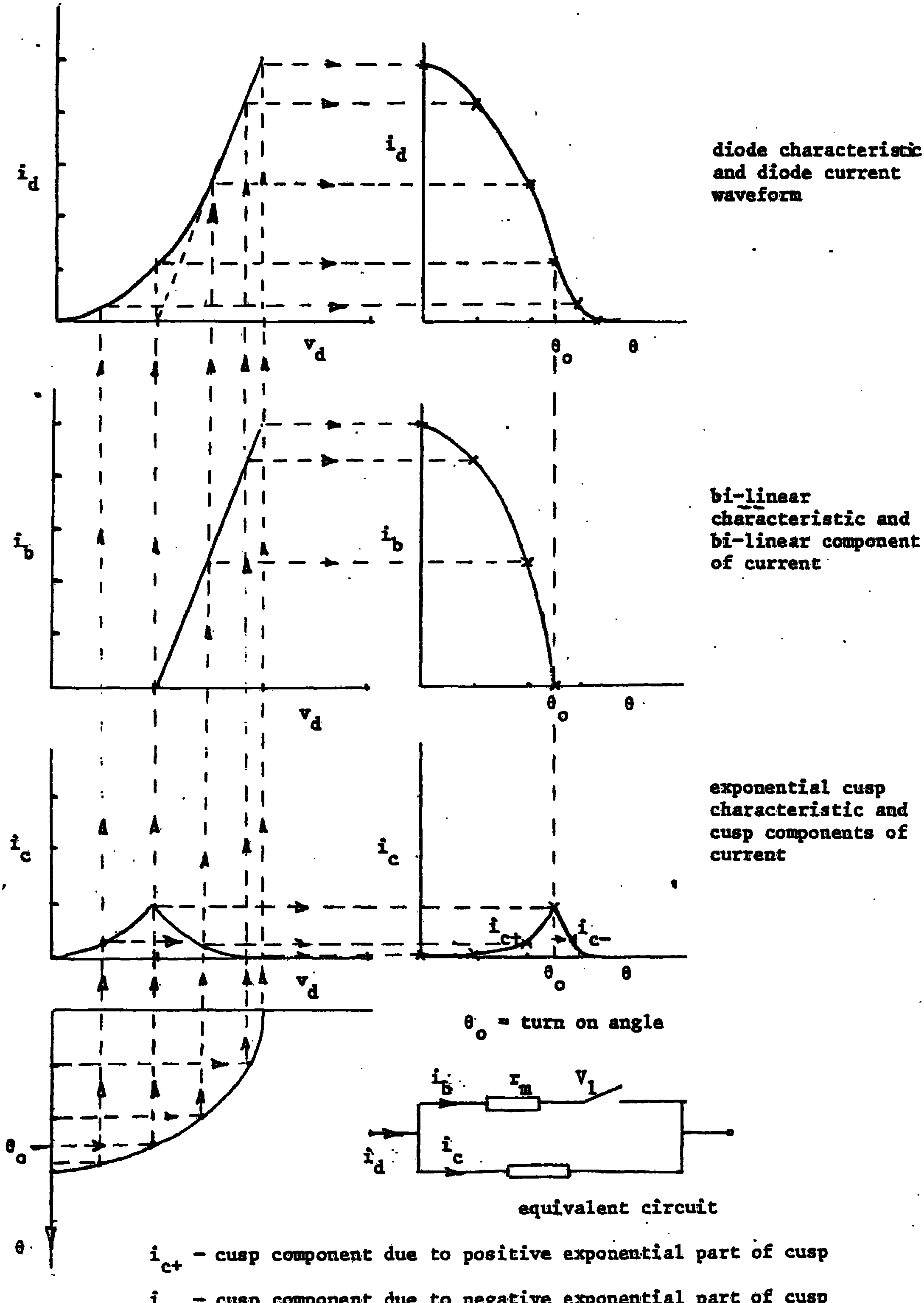

Figure 3.8

Cusp correction to bi-linear model

$$= \frac{V - V_1}{r_m} + \frac{1}{\alpha r_m} \sum_{k=1}^{\infty} (-1)^{k+1} \frac{\exp\left[-k\alpha\ (V - V_1)\right]}{k} \quad (3.46)$$

Evaluation of equations (3.45) and (3.46) will give identical numerical results as the logarithmic equation. Because of the large value of the parameter α the series of exponentials will rapidly approach zero for $V >> V_1$, i.e. the higher order terms of the series give negligible contribution when $V >> V_1$ and under such circumstances the first term of the series will suffice.

When $V = V_1$ the series in (3.45) and (3.46) will take on the value

$$(i + I_s) = \ln(2)/\alpha r_m \quad (3.47)$$

whilst the slope of the function at $V = V_1$ will be

$$\frac{d\ (i + I_s)}{dV} = \frac{1}{\alpha r_m}\left[\pm \alpha \frac{\exp\left[\pm \alpha\ (V - V_1)\right]}{1 + \exp\left[\pm \alpha\ (V - V_1)\right]}\right]$$

$$= \pm \frac{1}{2r_m} \quad (3.48)$$

Consider now the single exponential

$$\frac{1}{\alpha r_m} \ln(2) \exp\left[\pm \alpha\ (V - V_1)/\ln(4)\right] \quad (3.49)$$

When $V = V_1$ equation (3.49) takes on the value $\ln(2)/\alpha r_m$ and the initial slope is $1/2r_m$ which agrees with equation (3.47) and (3.48). Furthermore for $V \neq V_1$ the exponential decays rapidly to zero and thus has a similar asymptotic behaviour as equations (3.45) and (3.46). A comparison of equation (3.49) with the logarithmic approximation is shown in Figure (3.9). With this simple exponential approximation the solution may now be written,

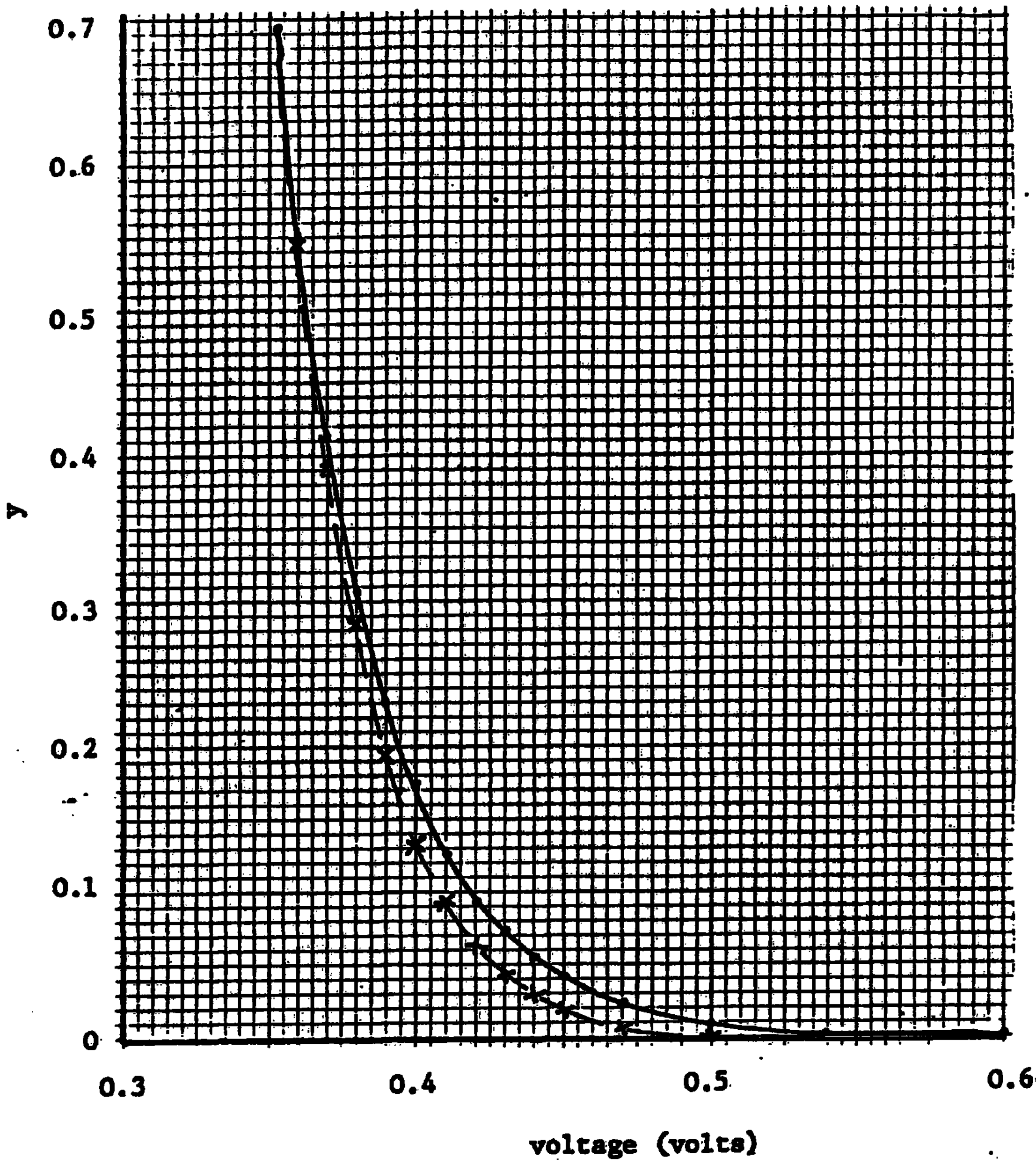

Figure 3.9

Comparison of curves

—x—x—x— $y = \ln(1 + \exp{-\alpha}(V - V_1))$ and

—•—•—•— $y = \ln(2)\exp\left[-\alpha(V - V_1)/\ln(4)\right]$

$V_1 = 0.352$ volts

for $V \leqslant V_1$

$$i + I_s = \frac{1}{\alpha r_m} \ln(2) \exp\left[\alpha (V - V_1)/\ln(4)\right] \tag{3.50}$$

and for $V \geqslant V_1$

$$i + I_s = \frac{V - V_1}{r_m} + \frac{\ln(2)}{\alpha r_m} \exp\left[-\alpha (V - V_1)/\ln(4)\right] \tag{3.51}$$

In this form the solution is seen to be the bi-linear approximation with exponential correcting terms to represent the diode curvature. Equations (3.50) and (3.51) have the additional advantage that when differentiated, to obtain the incremental time-varying parameters, they will give rectangular pulse waveform (obtainable from the bi-linear theory) with exponential correcting additive terms. Thus the problem of predicting the harmonic content of the current from equations (3.50) and (3.51) is identical to predicting the coefficients of the time varying conductance.

CHAPTER 4

THE EXPONENTIAL DIODE WITH SERIES RESISTANCE DYNAMIC CONSIDERATIONS

4.1 Introduction

In the previous chapter explicit equations were derived for the diode current in terms of the system voltage when the junction voltage is modified due to the presence of series resistance. This is a necessary prerequisite in the determination of the harmonic response to a sinusoidal driving voltage. The most useful approximation for this purpose is the bi-linear model with exponential correcting terms. In this way the effect of diode curvature may be compared with the predictions of the bi-linear model. In many practical applications the diode is driven with a sinusoidal voltage superimposed on a d.c. bias voltage, i.e.

$$V = -V_b + \hat{V}\cos\omega t \qquad (4.1)$$

The terms $(V - V_1)$ in equations (3.50) and (3.51) then take the form

$$-V_b - V_1 + \hat{V}\cos\omega t$$

$$\text{or } -V_2 + \hat{V}\cos\omega t \qquad (4.2)$$

where

$$V_2 = V_b + V_1 \qquad (4.3)$$

Thus V_2 may be regarded as a new turn-on voltage relative to the sinusoidal drive voltage which translates the diode characteristic along the V axis depending on the degree of bias V_b. Thus without loss of generality the terms $(V - V_1)$ may be replaced with $(V - V_2)$ where

$$V = \hat{V}\cos\theta, \quad \text{and} \quad \theta = \omega t \qquad (4.4)$$

With the time origin chosen so as to make the voltage drive cosinusoidal the current flowing in the diode is an even function of time and contains cosine terms only in its Fourier expansion i.e.

$$i(\theta) + I_s = \frac{a_o}{2} + \sum_{n=1}^{\infty} a_n \cos n\theta \tag{4.5}$$

where

$$a_n = \frac{2}{\pi} \int_o^{\pi} (i + I_s) \cos n\theta \, d\theta \tag{4.6}$$

4.2 <u>Low-level drive</u> $\hat{V} \leqslant V_2$

If the peak level of the local oscillator does not exceed the effective turn-on voltage V_2 then equation (3.50) suffices to predict the harmonic content. It is convenient to however rewrite it in the form

$$i + I_s = \frac{\ell n(2) \exp(-\alpha V_2/\ell n4) \exp(\alpha \hat{V} \cos\theta/\ell n4)}{\alpha r_m} \tag{4.7}$$

$$= K \exp(Z \cos\theta)$$

where

$$K = \ell n(2) \exp\left[(-\alpha V_2/\ell n4\right]/\alpha r_m$$

and (4.8)

$$Z = \alpha\hat{V}/\ell n(4)$$

The harmonic coefficients are then readily expressed in terms of the modified Bessel functions of the first kind, i.e.

$$a_n = 2K I_n(Z) \tag{4.9}$$

and the Fourier expansion for the diode current will then be

$$i(\theta) + I_s = K I_o(Z) + 2K \Sigma I_n(Z) \cos n\theta \tag{4.10}$$

In this form the effect of series resistance may be explained by observing that from equation (3.44) that as r increases, r_m increases and K decreases. Thus the percentage harmonic content is unchanged since K multiplies all harmonic components. Change of bias has a similar effect since only K is altered by a change in V_2.

It would clearly be inappropriate to use the bi-linear model for the low level drives under discussion. On the other hand if the series resistance was neglected and the exponential diode model assumed then the harmonic spectrum would have the form given by equation (4.10) but with

$$K' = I_s \exp(-\alpha V_b) \text{ and } Z' = \alpha\hat{V}$$

Since if r is zero then the diode current is (4.11)

$$i + I_s = I_s \exp \alpha(V - V_b) = I_s \exp(-\alpha V_b) \exp(\alpha\hat{V} \cos\theta)$$

It is of interest to compare the magnitudes of the currents given by equation (4.7) and the diode junction equation

$$i + I_s = I_s \exp\left[\alpha\hat{V} \cos\theta\right] \tag{4.12}$$

This comparison can be made by manipulating equation (4.7) into the form

$$i + I_s = I_s' \exp(-\alpha' V_b) \exp(\alpha' \hat{V} \cos\theta) \tag{4.13}$$

where

$$I_s' = \ln(2) \exp\left[-\alpha V_1/\ln(4)\right]\Big/\alpha r_m \tag{4.14}$$

$$\alpha' = \alpha/\ln 4 \tag{4.15}$$

For $\alpha = 40$, $I_s = 10^{-8}$, $r = 10$ ohms, and $V_b = 0$,
$I_s' = 10^{-10}\, I_s$ and $\alpha' = 29$.

Thus the effect of series resistance is to reduce the effective diode parameters considerably resulting in a much reduced current and consequent reduction in harmonic level. Therefore for these lowlevel drives it is not justifiable to ignore the series resistance.

4.3 Hard driven diodes

High level drives $V > V_2$

If the voltage drive is such that the effective turn on voltage V_2 is exceeded then the non-zero segment of the bi-linear part of the characteristic will contribute to the waveform and the harmonic components associated with it are found to be

$$\frac{a_o}{2} = \hat{V} \sin\left[\theta_o \; (1 - \theta_o)\right]/\pi r_m \quad , \tag{4.16}$$

$$a_n = \frac{\hat{V}}{n\pi r_m} \left(\frac{\sin\,(n-1)\,\theta_o}{n-1} - \frac{\sin\,(n+1)\,\theta_o}{n+1}\right) \tag{4.17}$$

where

$$\theta_o = \cos^{-1}(\hat{V}/V_2) \tag{4.18}$$

As can be seen from figure 4.1 the cusp current, i.e. the component of current flowing in the diode due to the cusp section of the characteristic is symmetrical for sufficiently large driving voltages. This condition will be achieved when the index of the negative exponential cusp exceeds a value of three for the exponential then is within 5% of zero. Thus, to obtain symmetrical cusp current the condition

$$\alpha\;(\hat{V} - V_2)/\ell n4 \geq 3$$

or

$$\hat{V} \geq V_2 + 3\ell n4/\alpha \tag{4.19}$$

must be satisfied. The term $3\ell n4/\alpha$ may be regarded as a measure of the excess of voltage beyond the effective turn-on voltage V_2 necessary to produce a symmetrical cusp current.

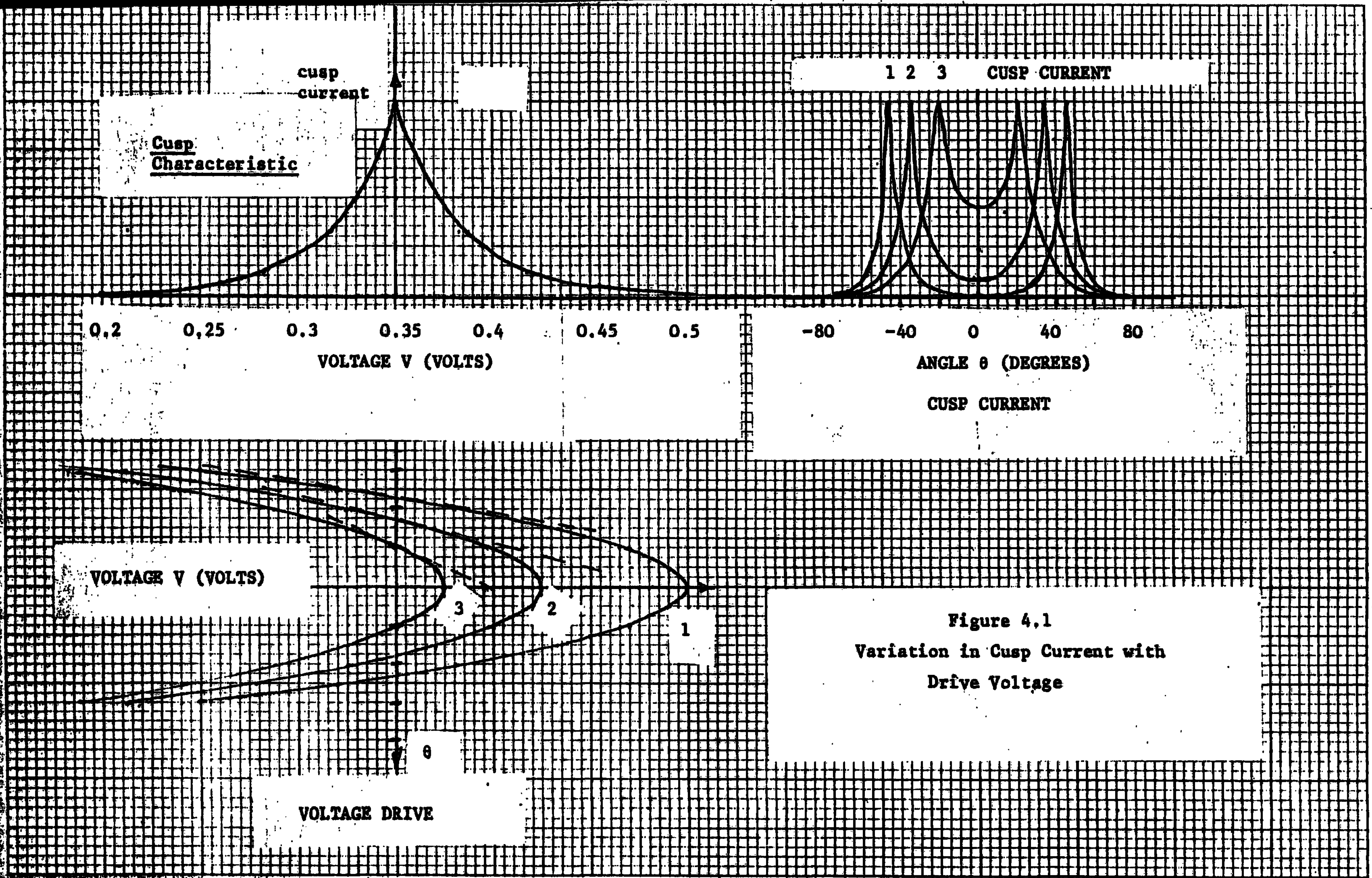

Figure 4.1
Variation in Cusp Current with
Drive Voltage

Curve 1 of Figure 4.1 illustrates the condition to produce a symmetrical cusp current. We see that the cosine voltage drive may be replaced by its tangent at the point $\theta = \theta_o$, for both exponential parts of the cusp, the curvature of the cosine wave only occurs when the exponentials have decayed essentially to zero and therefore give little contribution to the harmonic components. Changing the variable by

$$\theta = \theta_o - \phi_1 \tag{4.20}$$

where ϕ varies from θ_o to 0 as θ varies from 0 to θ_o, converts the negative cusp current i_{c-} equation

$$i_{c-} = \frac{\ell n2}{\alpha r_m} \exp\left[- \alpha\hat{V} (\cos\theta - \cos\theta_o)/\ell n4\right] \tag{4.21}$$

into

$$i_{c-} = \frac{\ell n2}{\alpha r_m} \exp\left[- \alpha\hat{V} (\cos\theta_o \cos\phi_1 + \sin\theta_o \sin\phi_1 - \cos\theta_o)/\ell n4\right] \tag{4.22}$$

Since α is a large parameter[23], it is possible to replace $\cos\phi_1$ and $\sin\phi_1$ by the leading terms of their respective power series expansions andobtain the required linearised form of

$$i_{c-} \simeq \frac{\ell n(2)}{\alpha r_m} \exp\left[(- \alpha\hat{V} \sin\theta_o\ \phi_1)/\ell n4\right] \tag{4.23}$$

In a similar manner, changing the variable to

$$\theta = \theta_o + \phi_2 \tag{4.24}$$

converts the positive exponential cusp current into the form

$$i_{c+} = \frac{\ell n(2)}{\alpha r_m} \exp\left[(- \alpha\hat{V} \sin\theta_o\ \phi_2)/\ell n(4)\right] \tag{4.25}$$

The harmonic components of the cusp current can now be determined from

$$a_n = \frac{2}{\pi} \int_{\theta_o}^{o} i_{c-} \cos n\,(\theta_o - \phi_1)\,(-\,d\phi_1)$$

$$+\frac{2}{\pi} \int_{o}^{\pi-\theta_o} i_{c+} \cos n\,(\theta_o + \phi_1)\,d\phi_2 \tag{4.26}$$

Since the range of both integrals completely traverses the range of the cusp the upper limits of the integrals in (4.26) may be replaced by infinity[23]. This allows both integrals to combine with cancellation of common($\sin n\theta_o \sin n\phi$)terms and therefore

$$a_n = \frac{4}{\pi}\,\frac{\ell n(2)}{\alpha r_m} \int_o^\infty \cos n\theta_o \cos n\phi \exp\left[(-\phi\alpha\hat{V} \sin \theta_o)/\ell n 4\right] d\phi \tag{4.27}$$

Equation 4.27 is readily integrated[24] to give

$$a_n = \frac{4}{\pi}\,\frac{\ell n(2)}{\alpha r_m} \cos(n\theta_o)\,\ell n 4\, \frac{\alpha\hat{V} \sin\theta_o}{\alpha^2\hat{V}^2 \sin^2\theta_o + (\ell n 4)^2\, n^2} \tag{4.28}$$

The effect of diode curvature may now be deduced from equation (4.28). The minimum value of $\sin\theta_o$ is 0.63 and this occurs when the equality is satisfied in equation (4.19) and V_2 is taken as $V_1 = 0.35$ i.e. zero bias conditions. The peak voltage will then be 0.45 volts. Thus $(\alpha\hat{V} \sin\theta_o)^2 = 128$ and will dominate the denominator of equation (4.28) if the harmonic number n is less than 8. Whilst this condition is satisfied (4.28) approximates to

$$a_n \simeq \frac{4}{\pi}\,\frac{\ell n(2)\;\ell n(4)}{\alpha r_m}\,\frac{\cos n\theta_o}{\alpha\hat{V} \sin\theta_o} \tag{4.29}$$

As the degree of overdrive beyond the turn-on voltage increases equation (4.29) will hold for even larger harmonic number. Thus the curvature of the diode contributes terms to the harmonic components which are proportional to $\cos n\theta_o$ and diminish as the drive level increases.

As the harmonic number increases the coefficients will eventually decrease to zero because of the presence of the n^2 term in the denominator of (4.28). The components due to the bi-linear portion of the characteristic on the other hand increase with drive voltage. Thus it may be concluded that diode curvature decreases in significance with increasing voltage drive.

The above results have been deduced on the basis of zero bias conditions. However, they are general and hold for other conditions which can be seen by observing that the term $\hat{V} \sin \theta_o$ may be expressed in the form

$$\hat{V} \sin \theta_o = V_2 \sqrt{\frac{\hat{V}^2 - V_2^2}{V_2^2}} = V_2 \sqrt{\chi} \tag{4.30}$$

where χ may be defined as the overdrive coefficient and equations (4.28) and (4.29) will hold for identical overdrive factors, regardless of $\hat{V}$ and V_2. Furthermore if the bias coefficient β is defined as

$$\beta = \alpha V_2 / \ell n 4 \tag{4.31}$$

then equation (4.28) may be written as

$$a_n \equiv \frac{4}{\pi} \frac{\ell n(2)}{\alpha r_m} \frac{\beta\sqrt{\chi} \cos n\theta_o}{\beta^2 \chi + n^2} \tag{4.32}$$

4.4 Intermediate drive levels

4.4.1 The positive cusp current

It remains now to consider the behaviour of the cusp current when peak level of the applied voltage is such that the negative exponential portion of the cusp is not completely traversed. This situation arises when

$$V_2 \leqslant \hat{V} \leqslant V_2 + 3\ell n 4/\alpha \tag{4.33}$$

With this restriction in voltage level, figure 4.1 illustrates that the positive exponential part of the cusp is fully traversed and that the tangent to the cosine drive voltage departs considerably from the true voltage within the range of the exponential decay and consequently the curvature of the cosine wave must be taken into account. This can be achieved by first changing the variable as defined in (4.24) and replacing cos ϕ by $1 - \phi^2/2$ and sin ϕ by ϕ to obtain

$$i_{c+} = \frac{\ell n(2)}{\alpha r_m} \exp\left[-\frac{\alpha\hat{V}}{\ell n(4)}\left(\frac{\phi^2}{2}\cos\theta_o + \phi\sin\theta_o\right)\right] \qquad (4.34)$$

As shown in Appendix (D1) equation (4.34) may be transformed into a gaussian curve by completing the square in the argument of the exponential. The positive cusp current is then given by

$$i_{c+} = A \exp - (q^2/2\sigma^2) \qquad (4.35)$$

where

$$\left.\begin{aligned} A &= \frac{\ell n(2)}{\alpha r_m} \exp\left[\frac{\alpha\hat{V}\sin\theta_o\tan\theta_o}{2\ell n4}\right] \\ q &= (\phi + \tan\theta_o) \\ \sigma &= \sqrt{\ell n(4)}/\alpha\hat{V}\cos\hat{\theta}_o \end{aligned}\right\} \qquad (4.36)$$

A graphical and numerical comparison of equations (4.35) with the positive cusp current is given in figure (4.2), and Appendix D2. Equation (4.35) defines a gaussian curve centred on $\phi = -\tan\theta_o$ with, (using probability nomenclature) a standard deviation of

$$\begin{aligned} \sigma &= \sqrt{\ell n(4)}/\alpha\hat{V}\cos\theta_o \\ &= \sqrt{\ell n4}/\alpha V_2 \qquad (4.37) \\ &= 1/\sqrt{\beta} \end{aligned}$$

Thus the standard deviation of the curve is independent of the over drive, depending only on the effective turn on voltage which may be controlled by the bias.

For small degrees of overdrive the curvature due to the peak of the cosine drive is reflected by the curvature of the gaussian curve near its origin. As the drive voltage increases the normal curve is offset and the point $\phi = 0$ will occur on the falling side of the normal curve, and eventually the positive cusp component will tend to an exponential decay as $(\phi^2 \cos \theta_o)/2$ becomes small compared to $\phi \sin \theta_o$.

The offset in the gaussian curve which controls the shape of the positive cusp current may be expressed in terms of the turn-on voltage and the drive voltage as

$$\mu = \tan \theta_o = \sqrt{(\hat{V}^2 - V_2^2)/V_2^2} = \sqrt{\chi} \qquad (4.38)$$

In terms of these two dimensionless parameters β and χ the constant A in equation (4.36) may be expressed as

$$A = \frac{\ln(2)}{\alpha\tau_m} \exp(\beta\chi/2) \qquad (4.39)$$

The harmonic contribution is then given by

$$a_{n+} = \frac{2}{\pi} \int_{\theta=\theta_o}^{\pi} \cos(n\theta)\, A \exp(-q^2/2\,\sigma^2)\, d\theta \qquad (4.40)$$

It is not possible to integrate (4.40) exactly but approximate expressions can be determined by using Laplaces method as shown in Appendix D3 providing cos $n\theta$ does not change too rapidly within the range of the normal curve. Examination of figure (4.2) shows that the most onerous condition is when the overdrive coefficient is zero and under such circumstances the method will become inaccurate for the harmonic numbers exceeding three. The accuracy and range of the method will improve as the overdrive coefficient increases as can be seen from figure (4.2). Furthermore the width of the gaussian curve will reduce as the bias coefficient increases resulting in improved accuracy of the method, which makes it attractive for the case of mixers arranged for low-loss conditions. With these comments in mind the harmonic contribution of the positive cusp current is shown to be

$$a_{n+} = \frac{\ln(2)}{\alpha r_m} \left\{ \frac{2}{\sqrt{2\pi\beta}} \exp\left(\frac{\beta\chi}{2}\right) \operatorname{erfc}\left[\sqrt{\frac{\beta\chi}{2}}\right] (\cos n\theta_o + n\sqrt{\chi} \sin n\theta_o) - \frac{2}{\pi\beta} n \sin n\theta_o \right\} \tag{4.41}$$

The worst case accuracy of equation (4.41) may be assessed by noting that as the overdrive coefficient is reduced to zero the wave-shape should match that dictated by the limit of equation (4.7) as the drive voltage equals the turn on voltage i.e. the "upper" limiting form of the low level drive equation equals the "lower" limiting form of the overdriven equation. Comparison of the exact spectrum of the low level case as given by equation (4.10) with the approximate spectrum of the overdriven case evaluated from (4.41) will therefore give an indication of the worst case accuracy of equation (4.41). This comparison is shown in table (4.1) for the bias coefficient β having values of 10.15 and 20, corresponding to peak drive levels of 0.352 and 0.692 volts and confirms the statements made with regard to the derivation of equation (4.41) The worst case accuracy may be improved by obtaining additional terms of the assymptotic expansion of equation (4.40) as shown in Appendix D3 . The effect of the second order terms is also indicated in table (4.1) where it will be

Table (4.1)

Comparison of Exact and Approximate spectrum of exponential cusp current

Overdrive factor $\chi = 0$

$$\frac{a_{n^*}}{\ln(2)/\alpha r_m} = \sqrt{\frac{2}{\pi\beta}} - \frac{n^2}{2\beta}\sqrt{\frac{2}{\pi\beta}}$$

$\alpha = 40$, $\hat{V} = V_2 = 0.352$ volts

Bias factor $\beta = \alpha\hat{V}/\ln(4) = 10.15$

Harmonic Number n	Exact Coefficient $2e^{-\beta} I_n(\beta)$	Approx Coefficient $\sqrt{2/\pi\beta}$	$n^2 \sqrt{2/\pi\beta}\ /2\beta$	$a_n^{\prime *}$
0	.253	.250	0	.250
1	.242	.250	.012	.238
2	.206	.250	.049	.201
3	.160	.250	.111	.139

$\alpha = 40$, $\hat{V} = V_2 = 0.692$ volts

Bias factor $\beta = 20$

0	.179	.178	0	.178
1	.175	.178	.005	.173
2	.162	.178	.018	.160
3	.143	.178	.040	.138
4	.119	.178	.071	.107

* All coefficients normalized by division by $\ln(2)/\alpha r_m$

observed that the worst case error is considerably reduced. The good correlation between these results for the worst case condition promotes confidence in the techniques used.

4.4.2 The negative cusp current

Finally it is necessary to determine the effect on harmonic response of the negative cusp current. The approach adopted in this range differs from that of the positive cusp current. It will be observed from figure (4.1) that the curvature of the cosine wave does not occur at the peak of the exponential. Thus the dominant effect is due to the almost linear sides of the wave and as the peak is approached the curvature reduces the rate of decay of the cusp current.

The change of variable

$$\theta = \theta_o - \phi \tag{4.42}$$

transforms the negative cusp current

$$i_{c-} = \frac{\ln(2)}{\alpha r_m} \exp\left[-\alpha\hat{V}(\cos\theta - \cos\theta_o)/\ln 4\right] \tag{4.43}$$

into an approximate expression

$$i_{c-} \approx \frac{\ln(2)}{\alpha r_m} \exp\left[-\alpha\hat{V}\left(\phi\sin\theta_o - \frac{\phi^2\cos\theta_o}{2}\right)/\ln 4\right] \tag{4.44}$$

where $\cos\phi$ and $\sin\phi$ have been replaced by the leading terms of their series. Since the dominant effect is one of exponential decay due to the $\phi\sin\theta_o$ term the exponential containing $(\phi^2/2)\cos\theta_o$ is approximated by the first two terms of its Taylor series expansion i.e.

$$i_{c-} \approx \frac{\ln(2)}{\alpha r_m}\left[\exp - (\alpha\hat{V}\sin\theta_o \cdot \phi/\ln 4)\right]\left[1 + \frac{\alpha\hat{V}\cos\theta_o}{2\ln 4}\phi^2\right] \tag{4.45}$$

A comparison of (4.45) with (4.43) is given in Figure (4.2) and Appendix D4. In terms of the overdrive and bias coefficients (4.45) becomes

$$i_{c-} \approx \frac{\ln(2)}{\alpha r_m} (1 + \beta\phi^2/2) \exp(-\beta\sqrt{\chi}\phi) \tag{4.46}$$

The harmonic contribution may now be obtained by direct integration and is shown in Appendix D5 to be

$$a_{n-} = \frac{2}{\pi}\frac{\ln(2)}{\alpha}\frac{\beta\sqrt{\chi}\cos n\theta_o + n\sin n\theta_o - \beta\sqrt{\chi}\exp(-\beta\sqrt{\chi}\theta_o)}{n^2 + \beta^2\chi}$$

$$-\frac{2}{\pi}\frac{\ln(2)}{\alpha r_m}\frac{\beta\sin n\theta}{n(n^2 + \beta^2\chi)} \tag{4.47}$$

$$+\frac{\beta}{2}\frac{\exp(-\beta\sqrt{\chi}\theta_o)}{(n^2 + \beta^2\chi)}\quad (\beta\sqrt{\chi}\theta_o)^2 + \frac{2(\beta^2\chi - n^2)\theta_o}{(n^2 + \beta^2\chi)} + \frac{2\beta\sqrt{\chi}(\beta^2\chi - 3n^2)}{(n^2 + \beta^2\chi)^2}$$

When the drive coefficient is zero, θ_o is zero and (4.47) correctly indicates that the negative cusp current contributes nothing to the harmonic content. As the drive coefficient increases the exponential term approaches zero and the harmonic content will tend to

$$a_n = \frac{2}{\pi}\frac{\ln(2)}{\alpha r_m}\frac{\cos n\theta_o}{\beta\sqrt{\chi}} \tag{4.48}$$

which is half the value given by equation (4.32) for the hard driven case - the remainder being produced by the positive cusp component.

4.5 The incremental conductance

The incremental conductance of the system (diode with series resistance) is readily determined as the derivative of the current with respect to the voltage.

For the low-level drive condition differentiation of equation (3.50) gives the normalised conductance as

$$\frac{g}{g_m} = \frac{1}{2}\exp \alpha(V - V_2)/\ln 4 \tag{4.49}$$

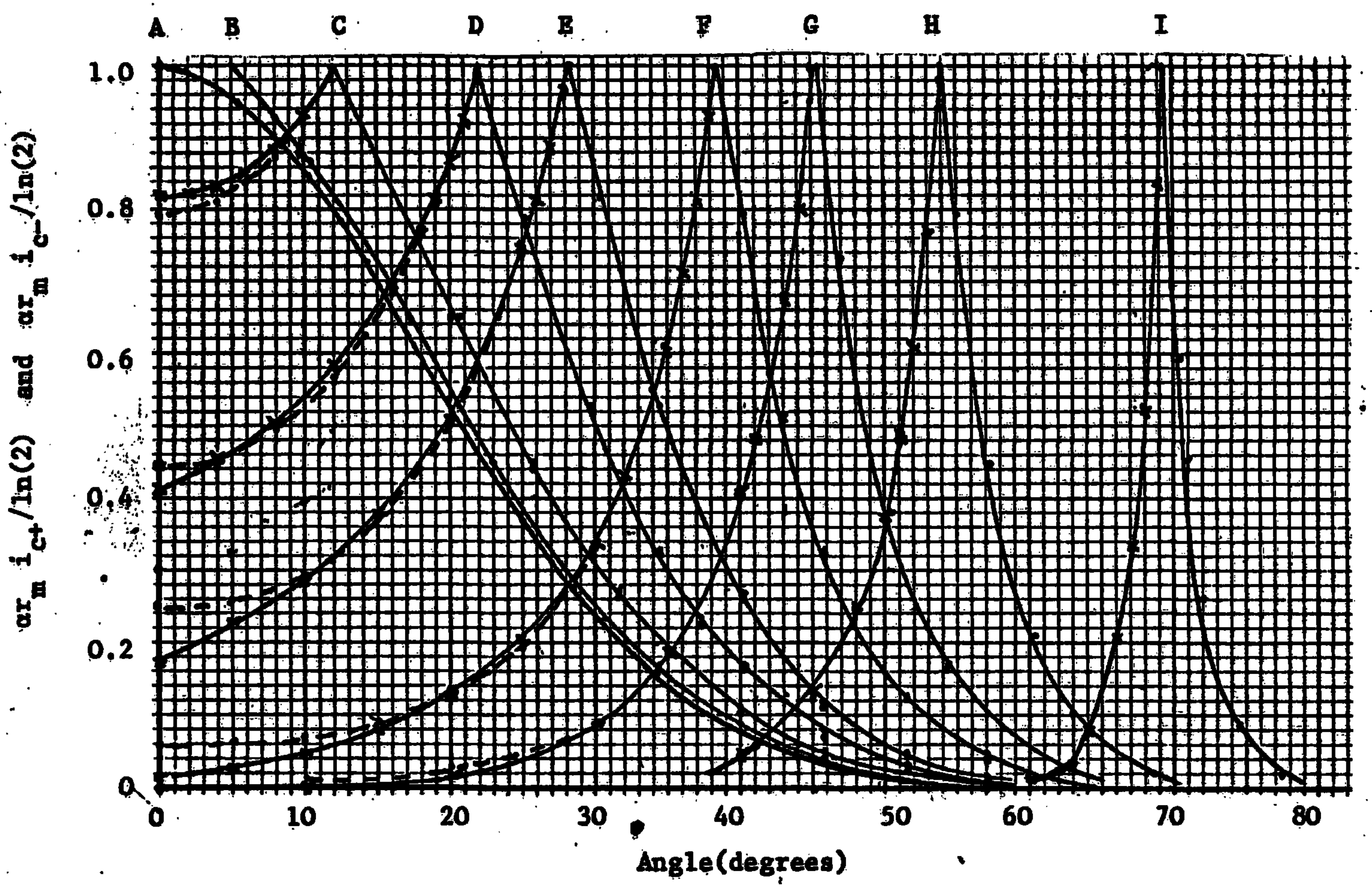

Curve	Peak Voltage Drive $\hat{V}$
A	0.352 volts
B	0.353
C	0.36
D	0.38
E	0.40
F	0.45
G	0.50
H	0.60
I	1.00

FIGURE 4.2

Comparison of exact and approximate cusp currents for $\alpha = 40$, $r = 10\Omega$, $I_s = 10^{-8}$ Amps.

Exact i_{c-} — Approximate i_{c-} — i_{c+} Exact and Approximate (see Appendix D2)

$$= \alpha r_m (i + I_s)/\ln 4$$

where

$$g_m = 1/r_m \tag{4.50}$$

Thus the harmonic components of the incremental conductance when the voltage varies cosinusoidally, i.e. the time varying parameters, may be obtained from the spectrum of the current given in equation (4.9).

When the voltage level is such that the diode is driven beyond the effective turn on voltage the incremental conductance has three components:-

(i) a rectangular pulse derived from the bi-linear segments.

(ii) an additive rising exponential cusp produced by the positive exponential portion of the cusp characteristic.

(iii) a subtractive exponential cusp due to the negative exponential part of the cusp characteristic.

Differentiation of the appropriate equations yields the following equations for the normalised incremental conductances.

$$\frac{g_1}{g_m} = H\ (V - V_2) \tag{4.51}$$

where H is the Heavyside shift operator,

$$\frac{g_+}{g_m} = \frac{1}{2} \exp\left[\alpha(V - V_2)/\ln 4\right]$$

$$= \frac{\alpha r_m}{\ln(4)} i_{c+} \tag{4.52}$$

$$\frac{g_-}{g_m} = -\frac{1}{2} \exp\left[-\alpha\ (V - V_2)/\ln 4\right]$$

$$= -\frac{\alpha r_m}{\ln 4} i_{c-} \tag{4.53}$$

The time varying parameters may then be easily determined as the combination of the spectrum of a rectangular pulse with the spectra of the cusp currents. For the hard driven diode it is immediately apparent that diode curvature has little effect since the spectra of the positive and negative cusp currents are equal. The critical range where diode curvature will be significant is when the applied voltage drive is within the range of the negative cusp portion of the characteristic since then the cusp current is not symmetrical. The waveforms of the time varying conductance as given by equations (4.51), (4.52), and (4.53) are shown in figure 4.3 for various levels of overdrive and clearly indicate the transition from a gaussian pulse to a rectangular pulse as the degree of overdrive increases.

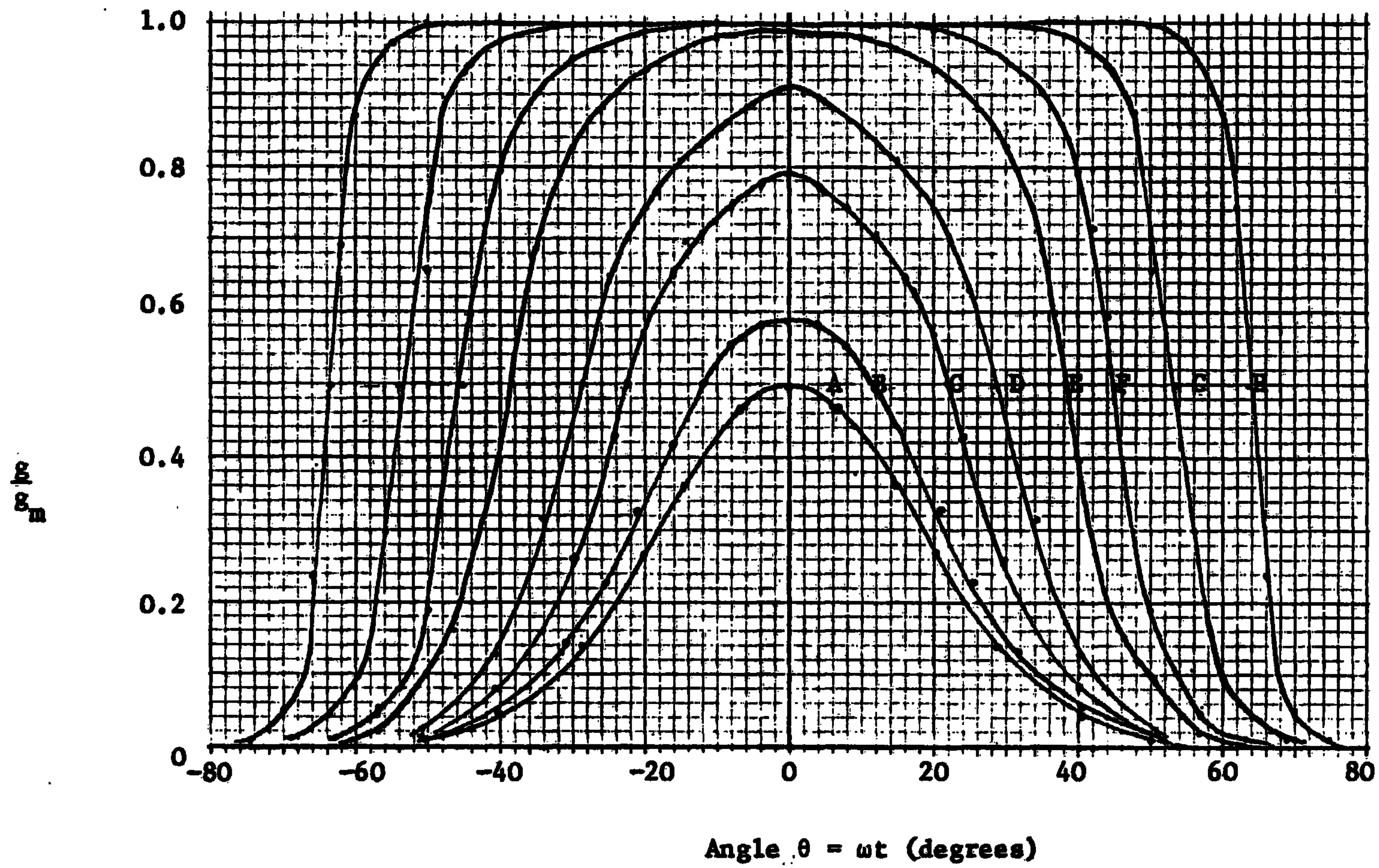

Curve	Peak Voltage Drive
A	.352 volts
B	.36
C	.38
D	.40
E	.45
F	.50
G	.60
H	1.00

Figure 4.3

Time Varying Conductance Waveforms
for different degrees of overdrive

CHAPTER 5

DELAYED DIODE CONDUCTION IN A LATTICE MIXER WITH CAPACITANCE

5.1 Introduction

In previous chapters studies have been made of the response to periodic drives of:-

(i) a predominately reactive device with parasitic resistance,

(ii) a non-linear resistive device with parasitic linear resistance.

In this chapter a study of a non-linear resistance system with capacitive parasitics is undertaken and the effect on the distribution of the local oscillator current between diode and capacitance is studied.

The system under discussion is shown in Figure 5.1 and is usually referred to as a lattice or double-balanced mixer. Numerical analyses (25, 26) have shown that current driven mixers are the most promising to obtain a low system noise figure and consequently the current driven case has been chosen for analysis.

The effect of parasitic capacitance on the small signal performance of lattice mixers has been investigated[10] but as in the case of single diode mixers the effect of capacitance on the local oscillator waveform is usually neglected because of the severe mathematical difficulties involved. The numerical procedures of Rustom and Howson[25], and Stracca[26], which used resistive models of a lattice mixer also neglected parasitic capacitance.

The analysis presented here clearly indicates that a significant modification in the distribution of the local oscillator current is produced due to the presence of capacitance. The capacitance of the system cannot change its voltage instantaneously and in order to reverse its polarity the system capacitance extracts current from the local oscillator source which prevents diode conduction for a period of time. Consequently a situation arises in which both the currents and voltages associated with each diode of the lattice are unknown and non-sinusoidal. The approach adopted in this chapter is to determine the waveshape of the diode current from which the spectral response of the system may be evaluated. Based on these findings Korolkiewicz[27] has investigated the effect of parasitic capacitance on the small signal performance of current driven lattice mixers.

5.2 Simple Theory of Lattice Mixer

A schematic diagram of a current driven lattice mixer is shown in Figure 5.1. The diodes are switched by the large local oscillator current I_p, at an angular frequency ω_p. The signal current i_s is at a frequency of ω_s. The switching of the diodes is made independent of the signal by making $|\hat{I}_p| >> |\hat{i}_s|$. The interaction of the pump and signal currents in the diodes produces currents at frequencies $\omega_s \pm n\omega_p$ in the output. By appropriate filtering at the output the components $\omega_o = \omega_s - n\omega_p$ can be selected. If $\omega_s > \omega_p$ then the output will be a low frequency version of the input signal.

During the positive excursion of the pump current diodes D_2 and D_4 do not conduct and the signal current is passed to the output transformer via the conducting diodes D_1 and D_3. During the negative excursion of the pump current diodes D_1 and D_3 are not conducting and the signal is passed to the output via the conducting diodes D_2 and D_4. However during the negative excursion of I_p the direction of the signal current in the output transformer is reversed. The current available at the output may therefore be represented as

$$i_o = \hat{i}_s S(t) \cos \omega_s t \tag{5.1}$$

where S(t) is a switching function, being +1 for positive I_p and -1 for negative I_p. Then

$$S(t) = \frac{4}{\pi} \sum_{n \text{ odd}}^{\infty} \frac{\cos n\omega_p t}{n} \tag{5.2}$$

and therefore

$$i_o = \frac{4\hat{i}_s}{\pi} \sum_{1}^{\infty} \frac{\cos \omega_s t \cos n\omega_p t}{n} \tag{5.3}$$

The above analysis is a simplified explanation of the frequency converting properties of the lattice mixer and more detailed treatments are readily available[5,28] The significant fact is that the switching function is always found to be symmetrical for all diodes of the lattice. It will now be shown that this symmetrical property is lost if the diode capacitance is included in the analysis.

5.3 The Effect of Diode Capacitance on the Switching of Bi-linear Diodes in Lattice Mixers

The switching of the diodes is independent of the high frequency input and low frequency output signals and therefore these small signals may be ignored when determining the response to the local oscillator, i.e. "pump" supply. As viewed from the local oscillator the equivalent circuit of the lattice configuration will be as shown in Figure 5.2(a) where the diode parasitics (diode junction capacitance C_j, diode package capacitance C_p, and diode series resistance r_s) have been included. At low frequencies reactance of the diode capacitances is sufficiently large for their effect to be neglected. As the frequency of operation is increased however they cannot be ignored. The diode junction capacitance is non-linear but because of the presence of the reverse connected diode each junction capacitance may be approximated[24,30] by a constant value given by

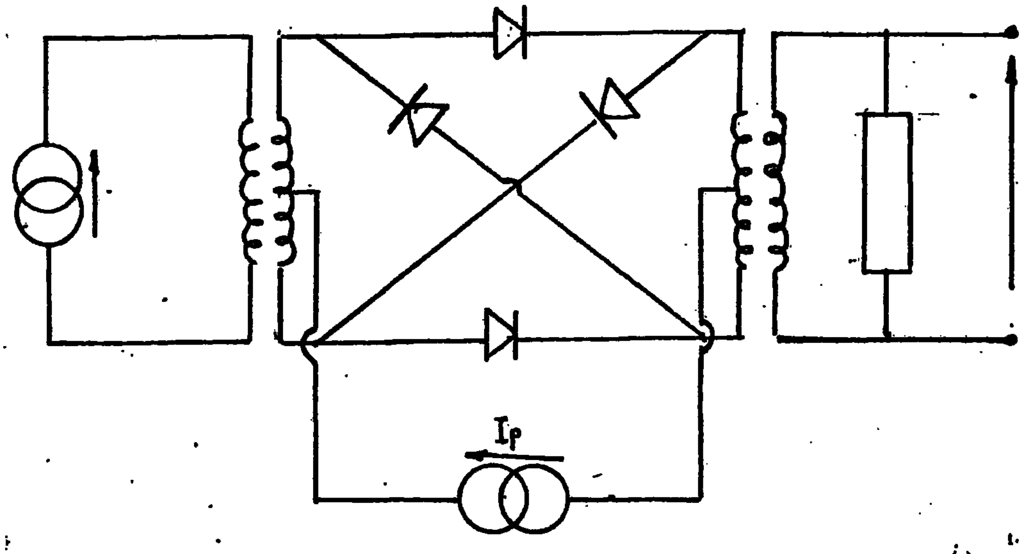

Figure 5.1

Current Driven Lattice Mixer

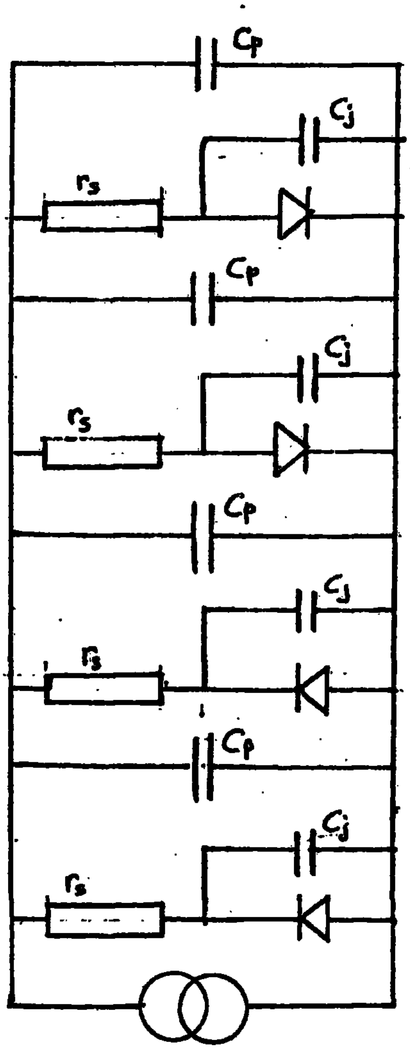

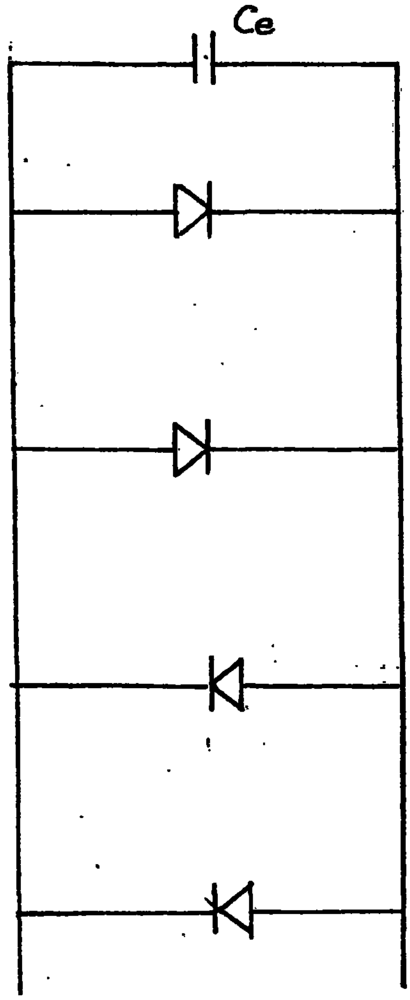

Figure 5.2(a) Figure 5.2(b)

(a) Large Signal Circuit of Lattice Mixer

(b) Simplified Large Signal Equivalent Circuit

$$C_j = (C_{j\,max} - C_{j\,min})/2 = C_o/2 \tag{5.4}$$

where $C_{j\,max}$ and $C_{j\,min}$ are the junction capacitances at the extremes of the operating conditions and C_o is the junction capacitance at zero diode voltage. The package capacitance C_p may be assumed constant, independent of frequency and level of local oscillator current drive. The diodes are assumed bi-linear with forward resistance r_f and for simplicity the reverse resistance is assumed infinite. The diodes are assumed to conduct when the voltage exceeds the turn-on voltage V_T. The simplified large signal equivalent circuit is therefore as shown in Figure 5.2(b), where

$$C_e = 4C_p + 2C_o \tag{5.5}$$

To understand the operation of the circuit assume that diodes D_2 and D_4 are conducting. As the pump current I_p approaches zero then the voltage V across the system will approach, $- V_T$. As the pump current becomes positive it cannot flow through diodes D_1 and D_3 since the voltage, $- V_T$, stored on the capacitance C_e holds these diodes in reverse bias. The total pump current must then be diverted through the capacitor to change the voltage to, $+ V_T$, according to

$$C_e \frac{dV}{dt} = I_p \sin \omega_p t \tag{5.6}$$

with $V = - V_T$, $t = 0$

By integrating (5.6) the voltage across the diodes is

$$V = \frac{2I_p}{\omega_p C_e} \sin^2 \left(\frac{\theta}{2}\right) - V_T \tag{5.7}$$

where

$$\theta = \omega_p t$$

The system voltage will therefore reach, $+ V_T$, when θ reaches the critical angle θ_c given by

$$\sin (\theta_c/2) = \sqrt{\omega_p C_e V_T / I_p} \tag{5.8}$$

At this angle diodes D_1 and D_3 are sufficiently forward biassed for conduction to be maintained and the pump current is diverted from the capacitor into the diodes. For angles exceeding θ_c the resistance of the diodes, $(r_f + r_s)/2$, is much smaller than the reactance of the capacitor and consequently the voltage across the system whilst the diodes are conducting approximates to

$$V = V_T + \frac{I_p \ (r_f + r_s)}{2} \sin \omega_p t \tag{5.9}$$

Typical current and voltage waveforms are shown in Figure 5.3.

The aforegoing argument shows that the diode - capacitor circuit of the lattice mixer produces a delayed conduction action in the diodes, and consequently the switching function which is necessary to analyse the small signal performance of the mixer is no longer an odd function and will therefore modify the behaviour of the mixer. Experimental evidence from tests conducted at 50 kHz on the circuit of Figure (5.2a) with parameter values chosen to simulate high frequency (1.5 GHz) behaviour verified that $\sin \theta_c/2$ was directly proportional to $\sqrt{C_e}$. However the coefficient of proportionality was found to differ significantly from $\sqrt{\omega_p V_T / I_p}$. This discrepancy can be accounted for by representing the diodes by the more realistic exponential functions as shown in the next section.

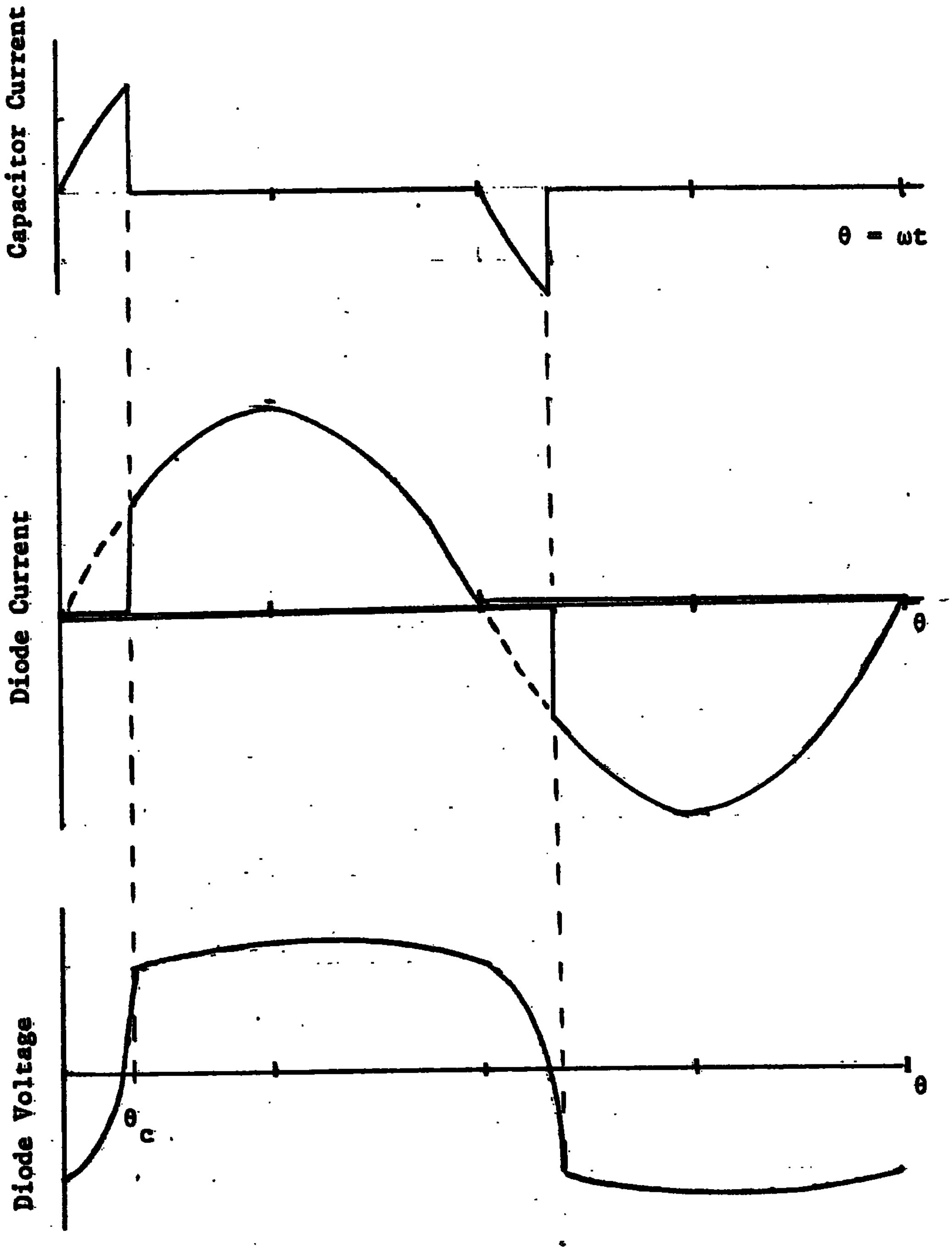

$$\sin\frac{\theta_c}{2} = \sqrt{\frac{V_T\,\omega C_e}{I_p}}$$

Figure 5.3

Large Signal Currents and Voltage

(Bi-Linear Diode Model)

5.4 The Effect of Diode Capacitance on the Switching of Exponential Diodes in Lattice Mixers

The equivalent circuit is again that of Figure 5.2a, but the currents in the diodes D_1 and D_3 are given by

$$i = I_s \exp(\alpha V) - I_s \tag{5.10}$$

and the currents flowing in D_2 and D_4 by

$$i = I_s - I_s \exp(-\alpha V) \tag{5.11}$$

The series resistance r_s is neglected since the switching action occurs near the turn on voltage where the diode resistance is still considerably larger than the series resistance. The current balance of the circuit is given by

$$C_e \frac{dv}{dt} + 2I_s \exp(\alpha V) - 2I_s \exp(-\alpha V) = \hat{I}_p \sin \omega_p t \tag{5.12}$$

which can be written as

$$\frac{\omega_p C_e}{\hat{I}_p} \frac{dV}{d\theta} + K \exp(\alpha V) - K \exp(-\alpha V) = \sin\theta$$

where

$$\theta = \omega_p t \tag{5.13}$$

and

$$K = 2I_s/\hat{I}_p$$

The exponential term can now be removed from the equation by means of the substitution

$$y = K \exp(\alpha V) \tag{5.14}$$

The diode currents are related to the variable y by

$$i_{D1} + i_{D3} = \hat{I}_p \; (y + 2I_s) \qquad (5.15)$$

where for matched diodes

$$i_{D1} = i_{D3} = \hat{I}_p \; (y + 2I_s)/2 \qquad (5.16)$$

The derivative in equation (5.13) transforms according to

$$\frac{dy}{d\theta} = \alpha \; K \; \exp \; (\alpha V) \; \frac{dV}{d\theta} = \alpha y \; \frac{dV}{d\theta} \qquad (5.17)$$

and therefore equation (5.13) becomes

$$\varepsilon \; \frac{dy}{d\theta} + y^2 - K^2 = y \; \sin \; \theta \qquad (5.18)$$

where $\varepsilon = \omega_p C_e / \alpha \hat{I}_p$ (5.19)

For practical diodes the parameters K and ε are typically of the order of 10^{-7} and 0.025 respectively at a frequency of 1.5 GHz and a pump current of 1 mA.

Figure 5.4 shows a graph of the zero slope isocline of equation (5.18). The effect of the small parameter K^2 may be noted by first observing that if $K^2 = 0$ the zero slope isoclines are given by

$$\begin{aligned} & y = 0 \\ \text{and} \quad & y = \sin \; \theta \end{aligned} \qquad (5.20)$$

The effect of the non-zero parameter K is therefore to divide the two isoclines as shown in Figure (5.4).

The effect of the small parameter ε multiplying the derivative is to make the isoclines of large gradient group close to the zero slope isocline as shown in Figure (5.5). Superimposed in Figure (5.5.) is an integral curve (solution curve) of equation (5.18) which closely

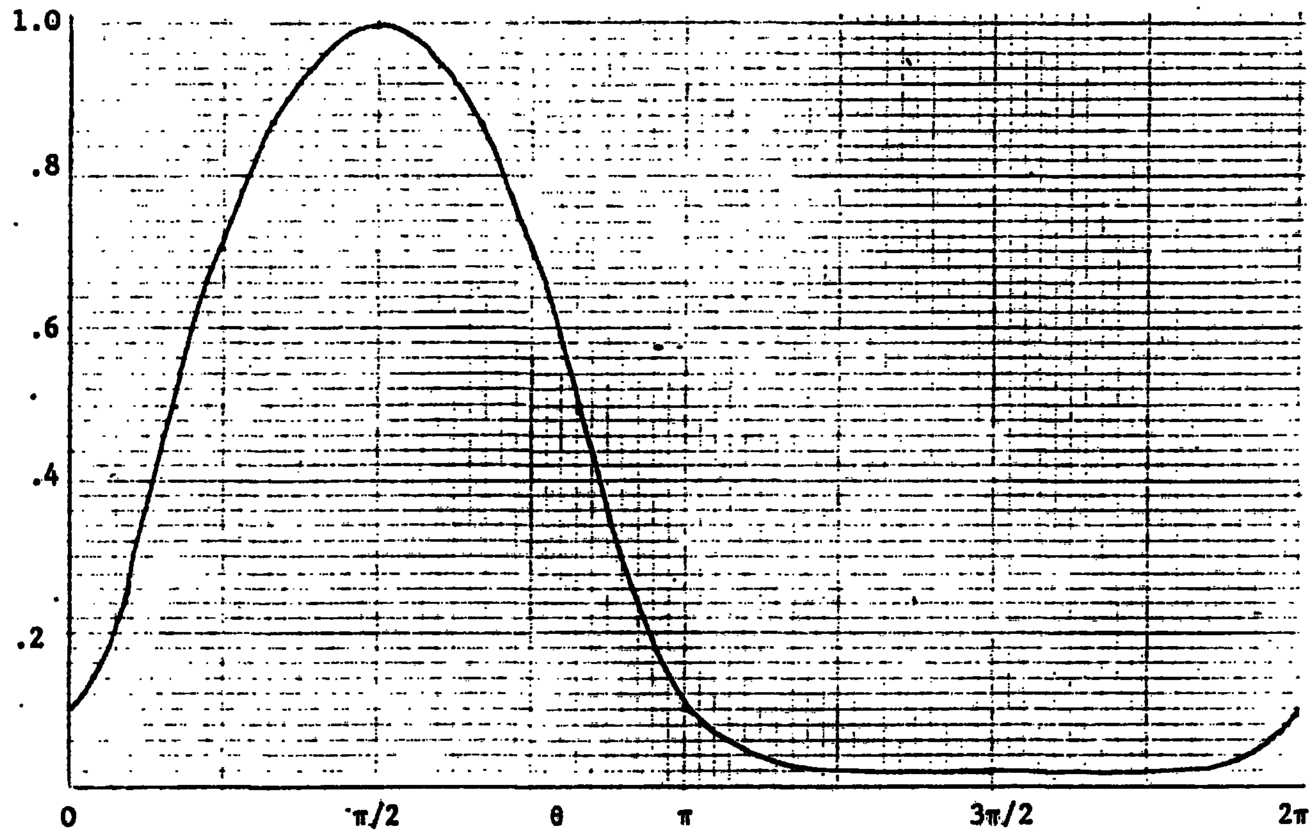

Figure 5.4

Zero slope isocline of equation

$$\varepsilon \frac{dy}{d\theta} + y^2 - K^2 = y \sin \theta$$

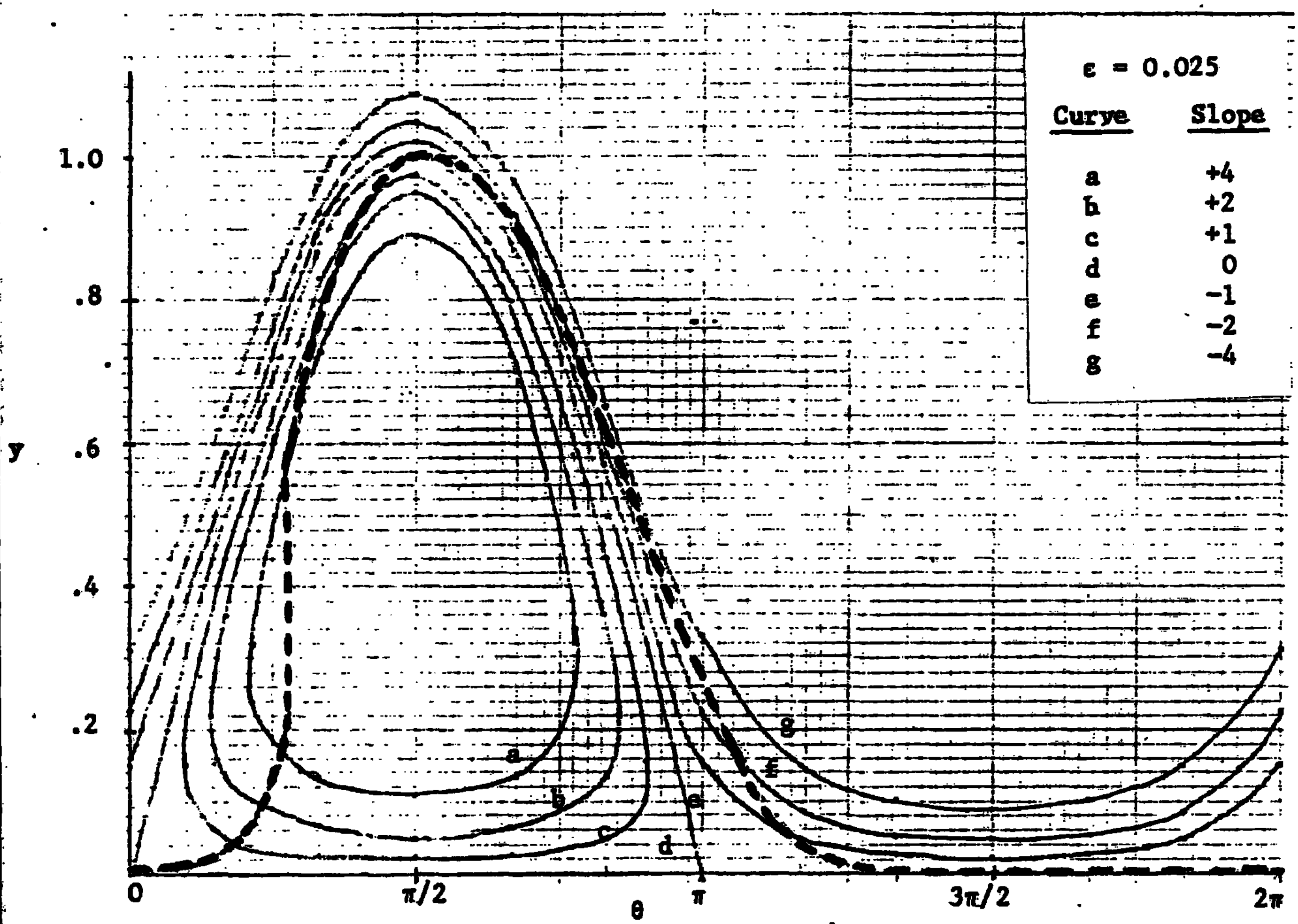

Figure 5.5

Isoclines of equation

$$\varepsilon \frac{dy}{d\theta} + y^2 - K^2 = y \sin\theta$$

——— isoclines

- - - - integral curve

Closed isocline contours have positive slope resembles the waveform predicted in section 5.3. To obtain a periodic solution equation (5.18) must be solved subject to the condition

$$y(0) = y(2\pi) \tag{5.21}$$

In engineering terms this is equivalent to choosing the initial switch on time such that the currents do not exhibit transients, and the system enters immediately into its steady state behaviour.

The solution to equation (5.18) is a function of the two parameters K^2 and ε but since K^2 is very much smaller than ε it is appropriate to develop a solution in the form of an asymptotic expansion in powers of K^2 i.e.

$$y(\theta, \varepsilon, K^2) = \sum_{n=0}^{\infty} K^{2n} \cdot y_n(\theta, \varepsilon) \tag{5.22}$$

where the functions $y_n(\theta, \varepsilon)$ are to be determined. From (5.18) and (5.22) the first term of the expansion (5.22) must satisfy

$$\varepsilon \frac{dy_o}{d\theta} + y_o{}^2 = y_o \sin\theta \tag{5.23}$$

and the periodicity condition (5.21).

It is shown in Appendix E1 that

$$y_o(\theta, \varepsilon) = \frac{\varepsilon \exp(-\cos\theta/\varepsilon)}{A + \int_0^\theta \exp(-\cos\phi/\varepsilon)\,d\phi} \tag{5.24}$$

To determine the constant of integration A in the above equation let the initial value $y_o(0) = \hat{y}_o$, then from (5.24)

$$\hat{y}_o = \varepsilon \exp(-1/\varepsilon)/A \tag{5.25}$$

and equation (5.24) becomes

$$y_o(\theta, \varepsilon) = \frac{\hat{y}_o \exp\ (1 - \cos\theta)/\varepsilon}{1 + \frac{\hat{y}_o}{\varepsilon} \exp(\ 1/\varepsilon) \int_0^\theta \exp(-\cos\phi/\varepsilon)\,d\phi} \tag{5.26}$$

Figure (5.5) shows that $\hat{y}_o$ is small and it is therefore convenient to let

$$\hat{y}_o = \exp\left[(\cos\theta_c - 1)/\varepsilon\right] \tag{5.27}$$

which shows that the constant θ_c lies in the range 0 to $\pi/2$.

In terms of the unknown constant θ_c equation (5.26) becomes

$$y_o\ (\theta,\ \varepsilon) = \frac{\exp\left[(\cos\theta_c - \cos\theta)/\varepsilon\right]}{1 + \frac{1}{\varepsilon}\exp\ (\cos\theta_c/\varepsilon)\ \int_0^\theta \exp\ (-\cos\phi/\varepsilon)\ d\phi} \tag{5.28}$$

This is clearly a very complex function, however it is immediately apparent that the periodicity condition cannot be satisfied since the integral in the denominator is always positive, the solution as given by (5.28) will tend to zero as θ increases. Furthermore, it is apparent that when $\theta < \theta_c$ the solution becomes large because of the form of the numerator. Thus the solution given by (5.28) does in fact represent the sudden increase in current. It is therefore necessary to investigate the nature of the solution as given by (5.28) in order to determine the region where this solution becomes inapplicable. This can be accomplished by making use of the fact that ε is small and employing Laplaces method as shown in Appendix E2 to evaluate the integral as θ varies over the range $(0-2\pi)$.

(i) <u>Range 1</u>, θ close to θ_c

$$y_o\ (\theta,\ \varepsilon) \simeq \frac{e^{\left[(\cos\theta_c - \cos\theta)/\varepsilon\right]}}{1 + \frac{1}{\sin\theta_c} + \frac{(\theta - \theta_c)}{\varepsilon}} \tag{5.29}$$

on using the result from Appendix E2

Let $\theta = \theta_c + \varepsilon\tau$ then

$$y_o\ (\theta,\ \varepsilon) \simeq \frac{e^{\left[\sin\theta_c \cdot \tau\right]}}{1 + \frac{1}{\sin\theta_c} + \tau}$$

When τ is negative the solution is exponentially small provided $\sin \theta_c$ is not zero. When τ is positive the solution is exponentially large. This indicates there is a rapid rise in the solution near $\tau = 0$ ($\theta = \theta_c$). This rapid rise takes place within an interval of order ε.

(ii) <u>Range 2,</u> $\theta_c < \theta < \pi$

From Appendix E2 in this range the integral is exponentially large and therefore

$$y_o\ (\theta,\ \varepsilon) \approx \frac{\exp\left[(\cos\theta_c - \cos\theta)/\varepsilon\right].\sin\theta}{\exp\left[(\cos\theta_c - \cos\theta)/\varepsilon\right]}$$

$$y_o\ (\theta,\ \varepsilon) \approx \sin\theta \qquad (5.31)$$

(iii) <u>Range 3,</u> $\pi < \theta \leq 2\pi$

In this range the integral is again exponentially large and with the aid of the result derived in Appendix E2 the solution can be written as

$$y_o\ (\theta,\ \varepsilon) \approx \frac{\exp\ (\cos\theta_c/\varepsilon)\ \exp\ (-\cos\theta/\varepsilon)}{\frac{1}{\varepsilon}\exp\ (\cos\theta_c/\varepsilon)\ \exp\ (-1/\varepsilon)\ \sqrt{2\pi\varepsilon}} \qquad (5.32)$$

$$= \sqrt{\frac{\varepsilon}{2\pi}}\exp\left[-(1+\cos\theta)/\varepsilon\right] \qquad (5.33)$$

In particular

$$y_o\ (\pi,\ \varepsilon) = \sqrt{\varepsilon/2\pi} \qquad (5.34)$$

and

$$y_o\ (2\pi,\ \varepsilon) = \sqrt{\frac{\varepsilon}{2\pi}}\exp\ (-2/\varepsilon) \qquad (5.35)$$

But the initial value of y at $\theta = 0$ is

$$y_o\ (0,\ \varepsilon) = \exp\left[(\cos\theta_c - 1)/\varepsilon\right] \qquad (5.35a)$$

and therefore $y(2\pi) \ll y(o)$. To have a periodic solution these two values must be equal. The reason for this discrepancy is that in the range

$\pi < \theta \leq 2\pi$ the approximation of neglecting K^2 is no longer valid.

In this range let

$$y = K^2 Y \tag{5.36}$$

so that equation (5.18) becomes

$$\frac{\varepsilon dY}{d\theta} + K^2 Y^2 = 1 - Y \sin\theta \tag{5.37}$$

Again by assuming an expansion of the form

$$Y(\theta, \varepsilon, K^2) = \sum_{n=0}^{\infty} Y_n(\theta, \varepsilon) K^{2n} \tag{5.38}$$

the equation governing Y_o can be seen to be

$$\frac{\varepsilon dY_o}{d\theta} + Y_o \sin\theta = 1 \tag{5.39}$$

By use of an integrating factor the solution is readily found to be

$$Y_o = \frac{1}{\varepsilon} \exp(-\cos\theta/\varepsilon) \int_{\theta}^{\theta} e^{\cos\theta/\varepsilon}\, d\phi \tag{5.40}$$

where θ_1 plays the role of an arbitrary constant and must be chosen so as to

(a) allow $K^2 Y_o(\theta, \varepsilon)$ to match with $y_o(\theta, \varepsilon)$ and

(b) to satisfy the periodicity condition.

(a) Matching

The behaviour of Y_o near θ_1 can be determined by putting

$$\phi = \theta_1 + \delta \tag{5.41}$$

and substituting in equation (5.40) to obtain

$$Y_o \simeq \frac{1}{\varepsilon} \exp(-\cos\theta/\varepsilon) \int_0^{\infty} \exp(\cos\theta_1/\varepsilon) \exp(-\sin\theta_1 \delta/\varepsilon)\, d\delta \tag{5.42}$$

In the range $\pi < \theta \quad \pi$, K^2Y_o must match with y_o as given by equation (5.33) i.e.

$$\frac{K^2 \exp(\cos\theta_1/\varepsilon)\exp(-\cos\theta/\varepsilon)}{\sin\theta_1} = \sqrt{\frac{\varepsilon}{2\pi}}\exp\left(-\frac{1}{\varepsilon}\right)\exp(-\cos\theta/\varepsilon) \tag{5.43}$$

and therefore both approximations vary with θ in the same manner provided

$$\frac{K^2 \exp(\cos\theta_1/\varepsilon)}{\sin\theta_1} = \sqrt{\frac{\varepsilon}{2\pi}}\exp\left(-\frac{1}{\varepsilon}\right) \tag{5.44}$$

(b) Periodicity

To produce periodicity $y_o(0) = K^2Y_o(2\pi)$. To determine the value of Y_o at 2π put $\phi = 2\pi - \delta$, $\cos\delta = 1 - \delta^2/2$, and $\theta = 2\pi$ toobtain

$$Y_o(2\pi) \simeq \frac{1}{\varepsilon}\exp(-\cos 2\pi/\varepsilon)\exp(1/\varepsilon)\int_0^\infty \exp(-q^2/2\varepsilon)\,dq \tag{5.45}$$

$$\simeq \sqrt{\pi/2\varepsilon}$$

and therefore

$$K^2\sqrt{\pi/2\varepsilon} = \exp\left[(\cos\theta_c - 1)/\varepsilon\right] \tag{5.46}$$

The solution will be complete when θ_c and θ_1 are determined from (5.44) and (5.46). This can be achieved by the elimination of K^2 from these two equations to give

$$\exp\left[(\cos\theta_1 + \cos\theta_c)/\varepsilon\right] = (\sin\theta_1)/2 \tag{5.47}$$

The approximate location of the roots of this equation are shown in Figure (5.6) where the fact that ε is small has been exploited to reveal that $\theta_1 \simeq \pi$ and $\theta_1 \simeq \pi - \theta_c$. The root near $\theta_1 = \pi$ leads to an unrealizable solution as seen from equation (5.42). To obtain a more accurate assessment of the root near to $\pi - \theta_c$ let

$$\theta_1 = \pi - \theta_c + \delta \tag{5.48}$$

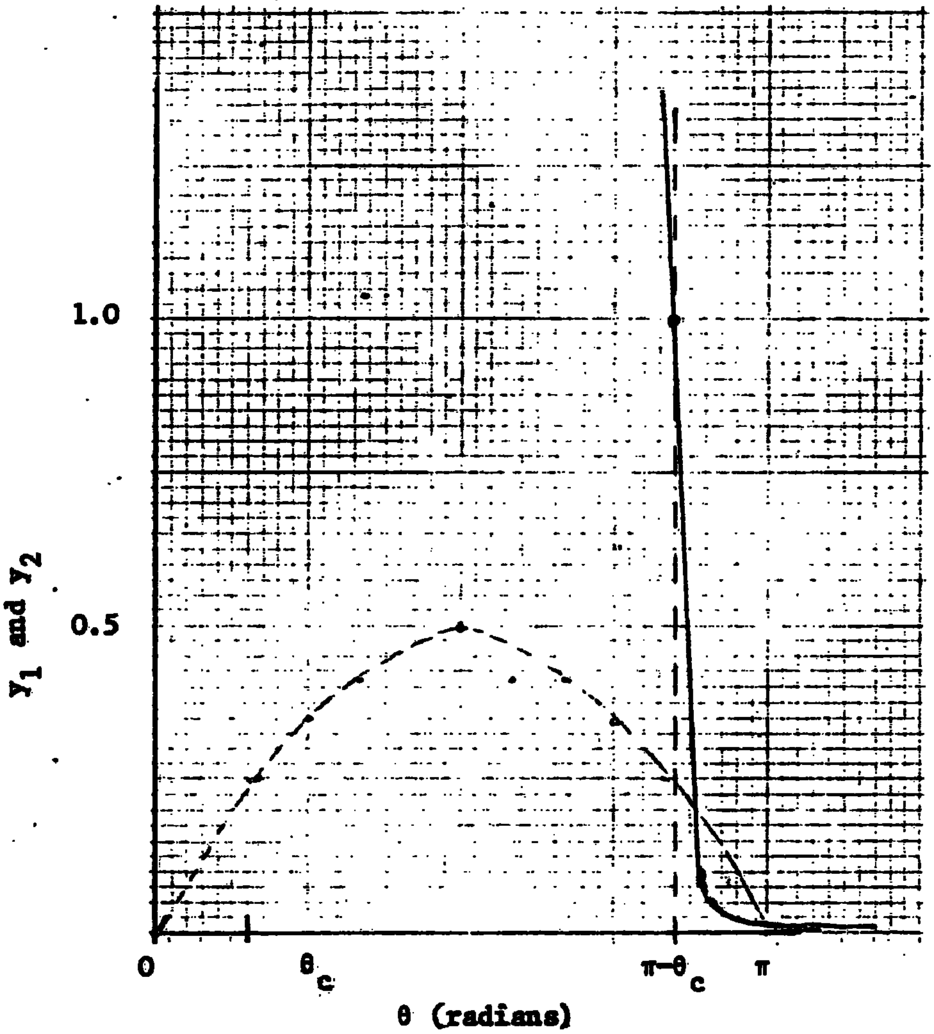

Figure 5.6

Approximate Location of roots

$\exp\left[(\cos\theta_1 + \cos\theta_c)/\varepsilon\right] = (\sin\theta_1)/2$

- - - - $Y_1 = (\sin\theta_1)/2$

——— $Y_2 = \exp\left[(\cos\theta_1 + \cos\theta_c)/\varepsilon\right]$

and so (5.47) becomes

$$\exp\,(-\,\delta \sin \theta_c/\varepsilon) = (\sin \theta_c)/2 \qquad (5.49)$$

which is easily solved to give

$$\delta = -\,\varepsilon \ln\left[\sin \theta_c/2\right] \Big/ \sin \theta_c \qquad (5.50)$$

To obtain θ_c, the conduction angle, put $\cos \theta_c - 1 = -\,2 \sin^2 (\theta_c/2)$ and substitute into (5.46) to obtain

$$\sin^2 (\theta_c/2) = \frac{\varepsilon}{2} \ln\left[(\frac{1}{K^2} \sqrt{\frac{2\varepsilon}{\pi}})\right] \qquad (5.51)$$

The logarithmic term in equation (5.51) is a slowly varying function of ε because it is dominated by the large parameter $(1/K^2)$ i.e.

$$\ln\left[(\frac{1}{K^2} \sqrt{\frac{2\varepsilon}{\pi}})\right] = 2 \ln (\frac{1}{K}) + \ln (2\varepsilon/\pi)/2$$

and therefore

$$\sin^2 (\theta_c/2) \simeq \varepsilon \ln(1/K) = \varepsilon \ln (\hat{I}_p/2I_s) \qquad (5.52)$$

over a large range of ε.

Experimental investigation detailed in Chapter 7 verifies that equation (5.52)is a reasonable estimate of the conduction angle θ_c, for restricted values of ε and K. Further experimental work is required to test the validity of equation (5.52) for general values of ε and K.

Comparison of equation (5.8) and (5.52) shows that the two equations would give identical results if V_T in equation (5.8) is taken as $\ln(\hat{I}_p/2I_s)/\alpha$.

5.5 Conclusions

It has been shown that the diode parasitic capacitance significantly changes the waveform of the diode currents in the sense that conduction is delayed up to a critical angle θ_c depending on the circuit parameters and the drive level. The delay in conduction will significantly effect the harmonics generated by the diodes and will consequently effect the small signal frequency converting properties of the lattice mixer. This delay in diode conduction has not been discussed previously in the literature dealing with lattice mixers and obviously opens up a new area of investigation[27]. In this work the significant fact is the use of matched asymptotic expansions to obtain accurate quantitative information relating to the conduction angle; the simpler bi-linear approximation however offers valuable insight into the mechanism of the delay. It is the author's strong belief that perturbation methods are a valuable tool to the engineer and the analytic information so obtained may often be more useful than information obtained by numerical experimentation with mathematical models representing electronic systems.

Suggestions for further investigation

In high frequency circuits it is standard practice to obtain sinusoidally varying current drives from voltage sources via series tuned circuits. If a lattice mixer is driven from such a source then it must satisfy the following equations

$$\omega_p C_e \frac{dV_d}{d\theta} + I_s \exp(\alpha V_d) - I_s \exp(-\alpha V_d) = i \qquad (A)$$

$$\frac{d^2 i}{d\theta^2} + \frac{1}{Q}\frac{di}{d\theta} + i = \frac{\hat{V}_p \cos\theta}{\omega_p L} - \frac{i}{L}\frac{dV_d}{d\theta} \qquad (B)$$

The pump current in equation (A) is controlled by the filter equation (B), where Q is unloaded magnification factor of the tuned circuit, L is the inductance and V_p is the voltage drive level. Does this system balance similar to the system of equation (A) (i will be sinusoidal for infinite Q), or is there a significant difference?

Further experimental work is required to test the validity of equation (5.52) over a wider range of the variables.

CHAPTER 6

COMPUTER AIDED MEASUREMENT OF HARMONIC AMPLITUDES AND PHASES

6.1 Introduction

From the analyses and discussions presented in previous chapters it will be appreciated that the spectral content of the response of non-linear systems to periodic drives is of paramount importance in the understanding, predicting and design of frequency converting networks. It has also been demonstrated in Chapter 2 that there is a unique relationship between the characteristic of a non-linear device or system and its spectral components generated by a sinusoidal drive. In order to verify predicted spectrum from mathematical analysis, and to determine device characteristics from spectral components, the magnitude and phase of the components relative to a fundamental drive function must be measured.

The circuit and systems discussed in previous chapters may be used at any frequency but find great applicability at high frequencies. The spectral response at these frequencies is therefore a wide-band system with a very high fundamental frequency which imposes stringent conditions (linearity in gain and phase) on the electronic circuitry associated with the measurement of the spectrum. There are commercially available harmonic measuring system (usually called harmonic or spectrum analysers) but these only measure harmonic amplitudes and do not give harmonic phase information. To resolve some of these problems it was decided to design and construct a spectrum analyser system which would fulfill the following functions:

(i) to obviate the high frequency problems by down converting the original signals to a lower frequency by a sampling technique known as aliasing. This process is performed by a commercially available instrument known as a Vector Voltmeter which converts a signal whose spectrum lies within the range 1 MHz to 1000 MHz to a 20 kHz signal having identical wave shape, and therefore the same relative spectrum.

(ii) to design a computer based system which would compute the harmonic components in both magnitude and phase of the 20 kHz wave shape. The 20 kHz replicas of the input drive and output response are sampled and then "trapped" or stored by transient recorders. The stored information is then transferred to a mini-computer for processing and the harmonic content is made available as a numerical print out. The transfer of the data from the transient recorders is under the control of the computer and a single cycle of the waveform to be analysed is transferred for processing. The time origin of this wave is chosen by appropriate settings of the transient recorder so that it corresponds to the peak of the sinusoidal drive; in this way the harmonics are computed relative to a cosinusoidal drive.

6.2 Signal Sampling

The theory of sampling is well established and documented [31], however to understand the performance and associated errors of the proposed analyser system the pertinent theorems and proofs are given in Appendix F1.

The principle of aliasing is embodied in result number 7, of Appendix F1 and displayed graphically in Figure (6.1). The signal to be down converted is periodic and therefore has a discrete spectrum the lowest frequency of which is ω_L all other components being multiples of this frequency. The signal is non-return to zero (N.R.Z) sampled at a sampling frequency ω_s. The two frequencies (ω_L and ω_s) are incommensurate so that there exists a remainder ω_1 such that

$$\omega_L = k\,\omega_s + \omega_1 \qquad (6.1)$$

where k is an integer.

For simplicity take the case of $k = 1$ and consider first the translations in frequency as expressed by

$$\sum_{n=-\infty}^{+\infty} F(\omega - n\omega_s) \tag{6.2}$$

From Figure (6.1) it will be seen that the component at ω_L translates direct to ω_1. The component at $2\omega_L$ requires two translations, the first transfers $2\omega_L$ to $\omega_L + \omega_1$ and the second translates this to $2\omega_1$, i.e. $n = 2$ in equation (6.2) when $\omega = 2\omega_L$. Similarly, the third harmonic at $3\omega_L$ requires three translations etc. The n which controls the translation is associated with the harmonics of the impulse sequence formed at the leading edges of the sampling intervals. Each harmonic of the signal spectrum requires a different harmonic of the impulse sequence to produce the alias conversion. Equation 6.1 also indicates that the set of frequencies $n\omega_1$ form a residue class modulo ω_s, which is an interesting algebraic interpretation of aliasing. In this manner the component at ω_L and associated harmonics are translated to ω_1 and multiples of ω_1. Other groupings of the harmonics also occur around ω_L and its harmonics as shown in Figure 6.1. If the integer k is taken as 2 there will be two groupings of the harmonics as shown in Figure 6.1 and therefore in general there will be k groupings of harmonics between ω_1 and ω_L for any choice of k.

Secondly, consider the effect of the distortion on amplitude of the translated spectra as dictated by the Sampling Function multiplier

$$Sa\ (\omega\, T_s/2) \tag{6.3}$$

This function passes through zero when ω is a multiple of ω_s. As can be seen from Figure 6.1 amplitude distortion is present in all harmonic groupings but is least significant in the lowest frequency group. Furthermore, by correct choice of ω_1 and ω_s for a given ω_L the distortion of this lowest order group can be reduced by compressing the spectra into the frequency range where the sampling function is approximately unity. Finally, phase distortion also occurs due to the presence of the term

$\omega_L = \omega_s + \omega_1,\ k = 1$

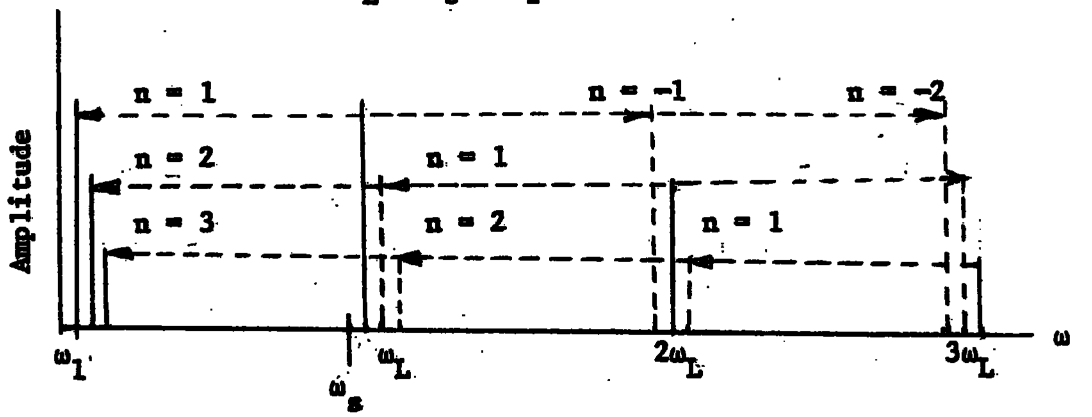

Signal Aliasing (k = 1)

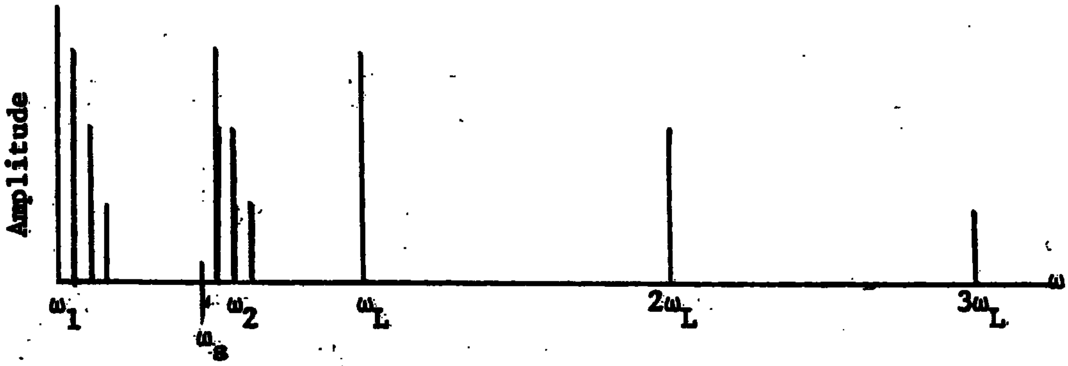

$\omega_L = 2\omega_s + \omega_1$

Signal Aliasing (k = 2)

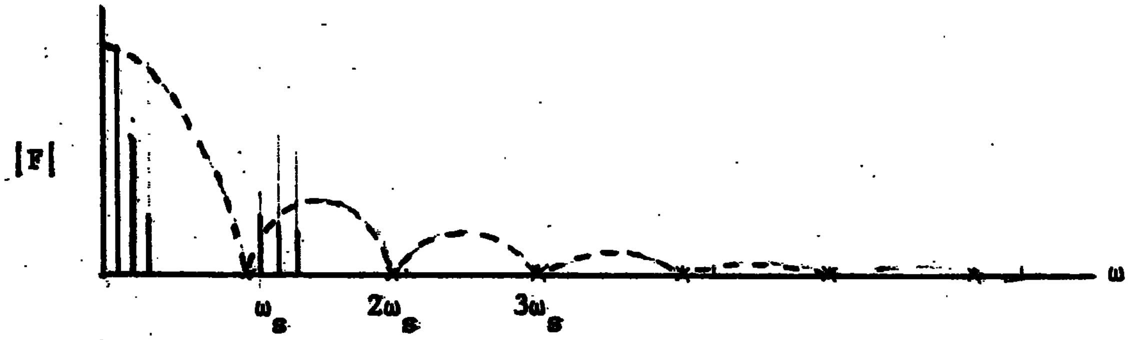

Amplitude Distortion

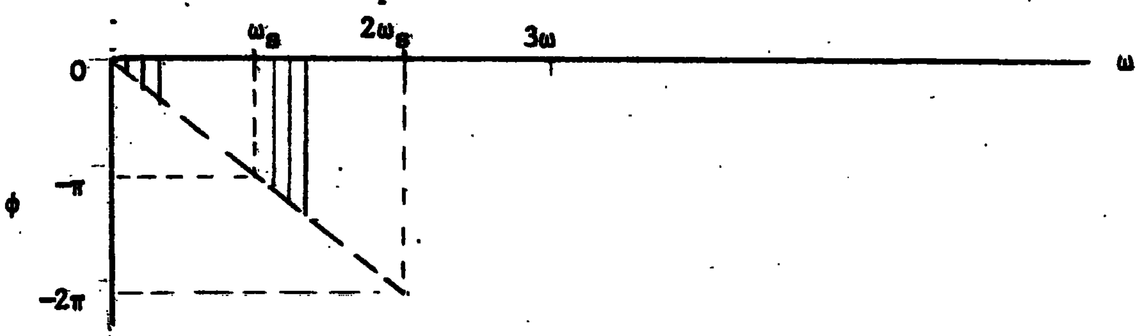

Phase Distortion

Figure 6.1

Frequency down converting by Aliasing

$$\exp\left(-j\omega\, T_s/2\right) \tag{6.4}$$

This phase error increases from zero to π radians as ω varies from 0 to ω_s hence this error can be kept small provided the highest harmonic of ω_1 is much less than ω_s.

If k is greater than unity the higher harmonic groups may easily be removed by means of a low pass filter. The output signal after aliasing is therefore a low frequency replica of the original high frequency signal.

The 20 kHz signals (replicas of the cosine drive signal and the periodic response signal) are then stored in the transient recorders. To perform this function each transient recorder samples its signal again using N.R.Z. type samples with the sampling frequency ω_s being much higher than the basic 20 kHz. The principle is embodied within result 7 of Appendix F1 and illustrated graphically in Figure (F1) of that Appendix. It will be seen that if the original signal is strictly band limited then the sampling frequency ω_s must be greater than twice the highest frequency present in the original spectrum. The spectrum to be analysed however is a Fourier series and although the harmonic amplitudes tend to zero the signal is not strictly band limited. Thus the tail of the first harmonic group will intermingle with the lower order harmonics of the second grouping producing an aliasing error. To reduce this error the sampling frequency must be significantly higher than the anticipated highest measurable harmonic. In the proposed system, the maximum sampling rate of the transient recorders is 5 MHz, which corresponds to a sampling interval of 0.2 μ sec. The recorders are capable of storing 1024 samples and the number of samples in one cycle of the 20 kHz signals is 250. If it is required to measure up to ten harmonics of the signal (i.e. up to 200 kHz) then the amplitude distortion introduced by sampling will be

$$\frac{\sin\left[\omega T_s/2\right]}{\omega T_s/2} = \frac{\sin\,(\pi\omega/\omega_s)}{\pi\,\omega/\omega_s}$$

and the phase distortion will be

$$\exp\,(-\,j\omega\,T_s/2) = \exp\,(-\,j\,\pi\omega/\omega_s)$$

The amplitude and phase distortion at 200 kHz will therefore be

$$1 - \frac{\sin\left[\pi\,(.2/5)\right]}{\pi\,(.2/5)} = 0.0026$$

$$= .26\%$$

and $\pi\,(.2/5)$ $= .1257$ rads

$= 7.2$ degrees

The sampling of the signal will not therefore introduce significant errors in the results.

During each sampling interval the 'held' level is converted into an eight bit binary number, the signals having first been scaled to lie between 0 and 1 volt by the transient recorder input amplifiers. Thus the range 0 - 1 volt is resolved into $2^8 = 256$ possible levels giving a possible error of $\pm$ 1/512 on each sample.

Once triggered the transients recorders can store four complete cycles of the 20 kHz waves. The two recorders are arranged in a master-slave configuration. The slave recorder is first "armed" and is triggered electronically from the master at the same instant as the master is triggered manually by the operator. The two signals stored in separate instruments are therefore locked in time with each other. In this way a point in the cosine drive signal which occurs at the same time as a point on the response signal are placed in identical store addresses in the two transient recorders. The two stored signals are displayed on monitor oscilloscopes by repetitively reading through the recorder stores. Each recorder is equipped with store address indicators which can be set by the operator to any address in the range 0 to 1024. Once set, the portion of the waveform stored in locations having a lower address than the indicator setting can be intensified on the monitor oscilloscope using intensity modulation. In this manner the address at which the peak of the cosine drive occurs may be determined, which is also the address in the slave recorder of the start of the response signal. In a similar way the address of the sample at the end of the cycle can be determined. A typical intensified record of a waveform is illustrated in Figure 6.2.

6.3 Transfer of data to computer

The sampled and held waveform of the system response stored in the slave transient recorder is transferred to the computer under programme control. The timing diagram of the transient recorder is shown in Figure (6.3). The digital output 'enable' is grounded permanently thus the transient recorder is always enabled. The digital output 'request' is connected to the CB 2 terminal of the digital port of the computer. Whilst CB 2 is held at logic level 1 under computer control digital output is unavailable. When the programme sets CB 2 low the transient recorder output flag is set high to indicate digital output is available and the first sample stored as an eight bit digital word is placed on the 8 bit parallel bus system. At the same time as word 1 is placed on the bus the transient recorder sets the data ready signal high. This level is passed to the computer by the CA 1 terminal of the computer interface. The programme tests terminal CA 1 to determine whether word 1 is available and then jumps to a programme area which transfers word 1 to computer memory. The CB 2 output is then set high by programme which is interpreted by the transient recorder as word off request. When word 1 is removed from the bus and the data ready flag sets to zero, the programme then tests CA 1 and if low sets CB 2 low to request the next word. The "handshaking" process continues in this manner until all 1024 digital words are transferred.

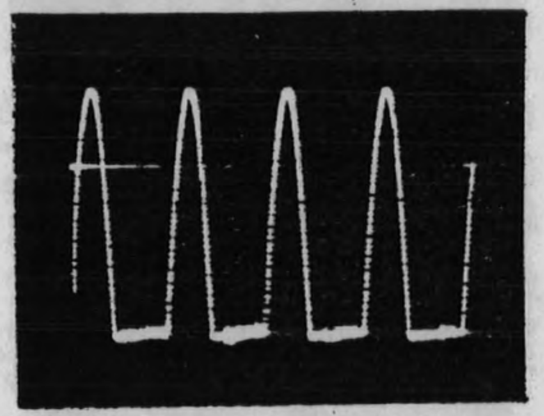

(a) 1024 samples of response waveform

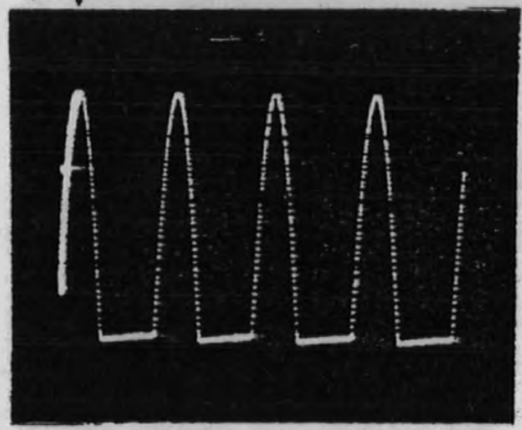

(b) enhanced brightness of samples before start of cycle (address No. 47)

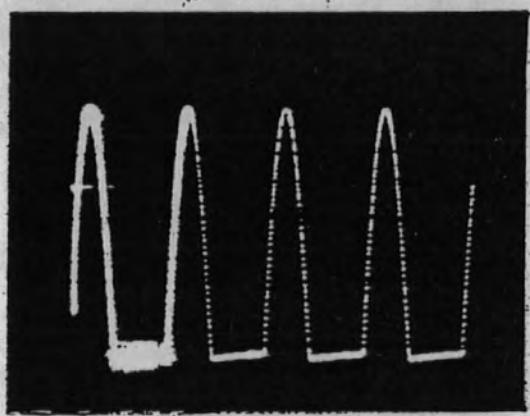

(c) enhanced brightness to end of first cycle (address No. 295) Samples per cycle = 248

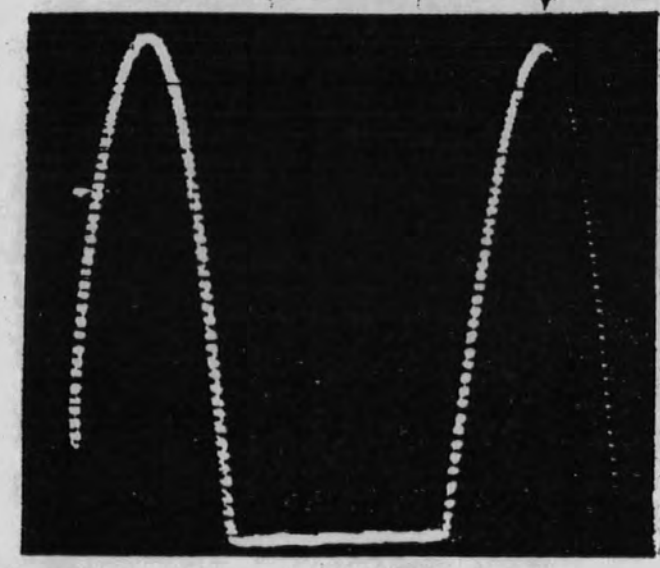

(d) enlargement trace of (c)

Figure 6.2

Location of start and finish address numbers

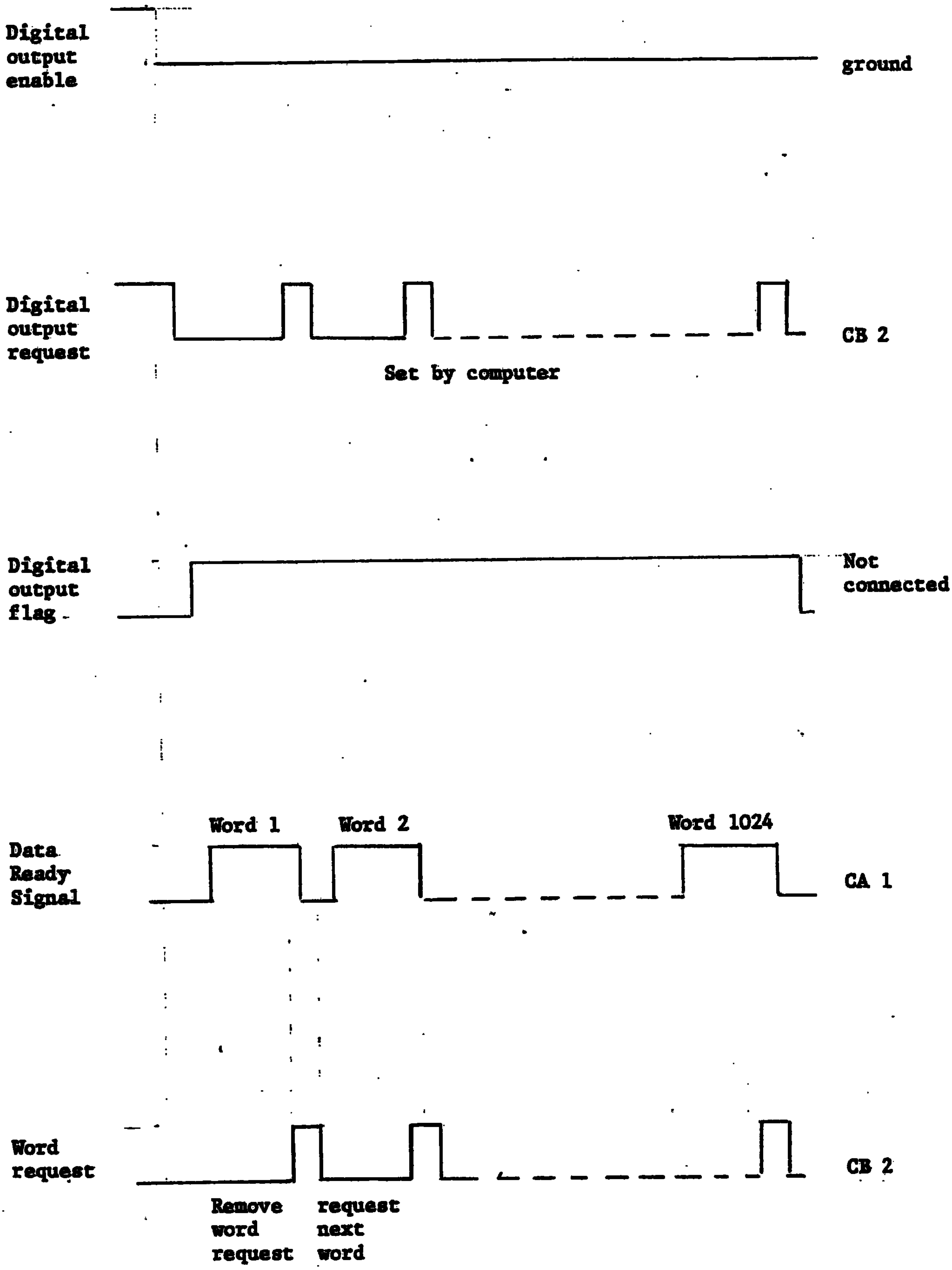

Figure 6.3

"Handshaking" signals between Computer and Transient Recorder

The addresses of the start and finish of one complete cycle of the response signal (previously set on the transient recorders) are entered into the computer from the keyboard together with scale information relating to the amplifier settings on the transient recorder. The data associated with one cycle of the waveform is then processed by a Fourier Analysis Programme stored in the computer and the harmonic components are displayed on a line printer. A copy of the programme which transfers the data and evaluates the harmonic components is shown in Appendix F2 and a schematic diagram of the complete measuring system is shown in Figure (6.4).

6.4 Errors introduced prior to transfer of data to computer

(A) False Period Error

The length of the data record i.e. one cycle, to be transferred from the transient recorder to the computer is determined manually by the operator. The timing of the system is such that approximately 250 samples are taken per cycle. Thus each sample corresponds to approximately 1.5 degrees. Practically it is very difficult to determine the peaks of the cosine drive exactly using brightness intensity and consequently the data record transferred to the computer may be longer or shorter than an exact cycle by ±3 degrees. The periodic wave analysed by the computer is therefore not exactly the wave stored in the recorder. As shown in Appendix F3 an error is introduced in the coefficients of the harmonics due to the false assessment of periodic time. This error affects both the amplitude and phase of the measured response and furthermore would produce higher harmonic distortion even in a strictly bandlimited signal.

The most significant term in the expansion for the modified coefficient $\overline{C_k}$ is given by

$$\overline{C_k} = C_k \exp (jk\epsilon\pi) \, Sa(k\epsilon\pi) \approx C_k \exp (jk\epsilon\pi) \tag{6.5}$$

where Sa is the sampling function.

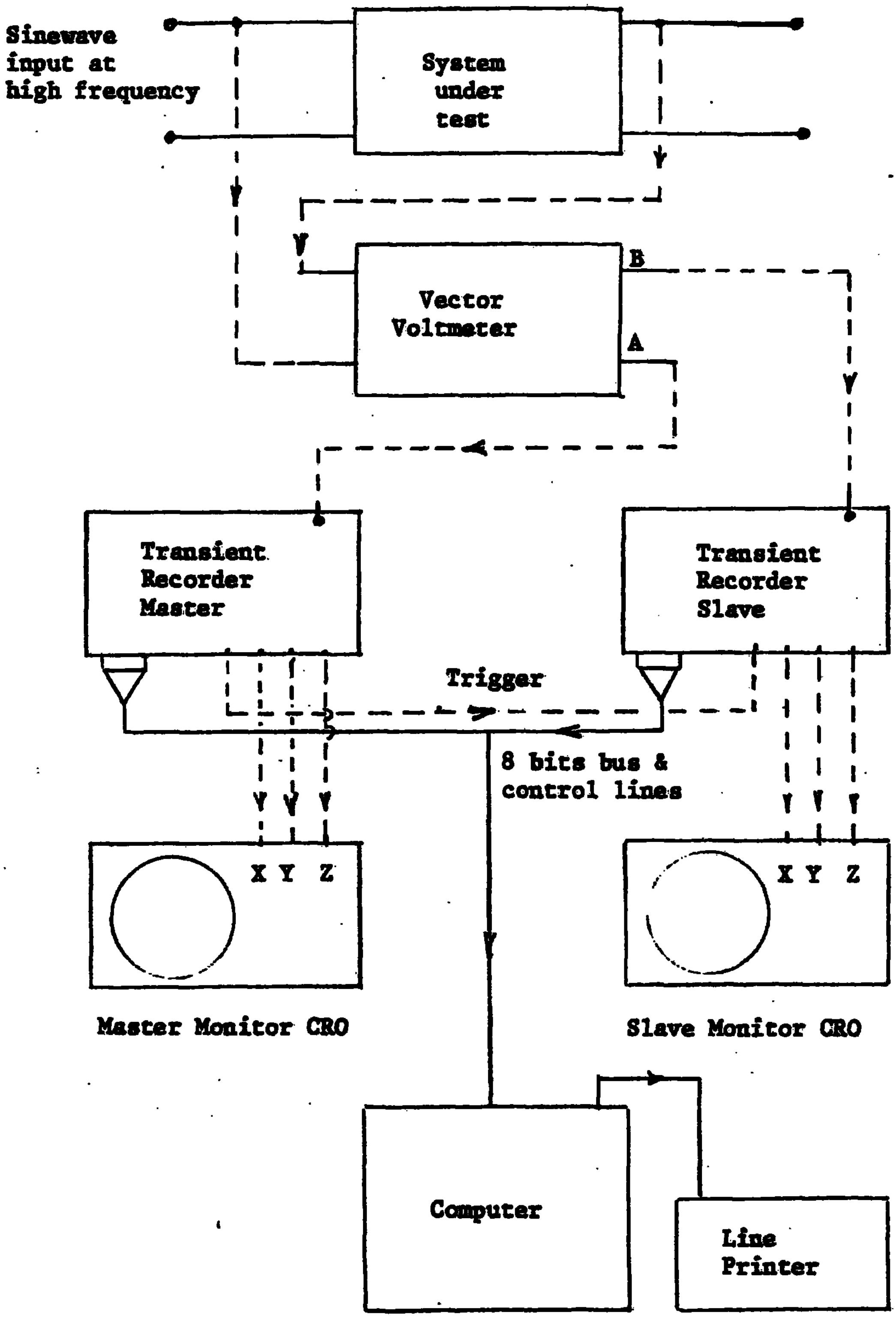

Figure 6.4

Schematic Diagram of New Spectrum Analyser System provided $k\varepsilon \ll 1$ which shows that the most significant effect of the false periodic time is to produce phase distortion, and the degree of phase distortion is directly proportional to the harmonic number. For an error $\varepsilon = 3/360$, the phase distortion produced in say the tenth harmonic will be approximately 15 degrees.

(B) Quantising Error

The samples stored in the transient recorder are subject to quantising error. It is shown in Appendix F4 that the worst case error introduced into the calculation of the cosine and sine coefficients is given by

$$2K\,(1 + p\pi/N)/\pi M \tag{6.6}$$

where p is the harmonic number

N is the number of samples per cycle

M is the number of quantising levels

K is the scale factor of the measuring system

For $N = M = 256$ the absolute errors for $p = 1$ and $p = 10$ are

2.52×10^{-3} x Volts Full Scale

and

2.79×10^{-3} x Volts Full Scale

The percentage error in the coefficient depends on the coefficient magnitude and if the ~~wave under investigation is of the order of half the~~ full scale voltage this would be equivalent to approximately 0.5% error.

6.5 Proving tests

The system was tested with a sine wave supplied from a low distortion test oscillator, (overall percentage harmonic distortion < 0.1%) at a frequency of 20 kHz. The level of the wave was set using a previously calibrated digital voltmeter having an accuracy of 0.1%. Typical results

```
N1=                327

N2=                577
RESISTOR VALUE=              1
VOLTS FULL SCALE=             1
DC VALUE=              .508832204
COS TERM             SIN TERM
 .506837055              -.018973962



MAGNITUDE              PHASE
 .507192085               2.14392476
```

Test Voltage 0.351V r.m.s. cosine wave (.497 Volts peak)

Signal Source 0.1% low distortion test oscillator

Level set by 0.1% digital voltmeter

Error = .507 - .497 = 0.01

% Error = 2%

Phase Error = 2 degrees

<u>Table 6.1</u>

Typical results for a sine wave test

MEASURED HARMONIC COMPONENTS

MAGNITUDE (volts)	PHASE (degrees)
.633510169	-39.6120908
.0365117742	-.522469663
.209514155	-88.8190931
.036402948	-1.04429366
.123732409	-87.973642
.0362221412	-1.56486357
.0862831829	-87.0368509
.0359700885	-2.08353177
.0649641794	-85.9634814
.0356478628	-2.59962862
.0509991472	-84.6982494
.0352568175	-3.11241832
.0410187089	-83.1708032
.0347985975	-3.62110308
.0334570152	-81.2885897

Harmonic	Theoretical	Error	% Error	Phase (deg)
1	.637	2.6×10^{-3}	0.4	0.4
3	.212	2.2×10^{-3}	1.05	1.2
5	.127	3.3×10^{-3}	2.7	2.0
7	.091	4.9×10^{-3}	5.75	3.0
9	.071	5.7×10^{-3}	8.8	4.04
11	.058	6.8×10^{-3}	13.0	5.3
13	.049	7.9×10^{-3}	19.4	6.8
15	.042	9.4×10^{-3}	28.6	8.7

Test Voltage 1 Volt peak-peak Square Wave at 20 kHz

Table 6.2

Measured and Theoretical Harmonics of a Square Wave

from such a test are shown in Table (6.1). The system was then tested with a square wave and the measured spectrum was compared with the theoretical spectrum in Table (6.2).

6.6 Discussion

The sine wave tests on the spectrum analyser system reveal that the basic accuracy of the system is approximately 2% with a phase error of two degrees. The error in amplitude is due to the combined effects of sampling, quantising, numerical computing errors, and the basic accuracy of the input amplifiers of the transient recorders. Because the test was referenced to a cosine wave the majority of the phase error may be due to false measurement of period since the phase distortion due to sampling is approximately 0.7 degrees for the sampling rates used.

The results of the square wave test showed that up to the fifteenth harmonic could be measured with an absolute error varying from 2.6×10^{-3} to 9.4×10^{-3} where full scale is unity (0.5 volts peak). The percentage errors range from 0.4% at fundamental to 28.6% at the fifteenth harmonic. The large percentage errors at the higher harmonics are perhaps misleading in the sense that they appear large because of division by the small amplitude.

The phase error ranges from 0.4 degrees at fundamental to 8.7 degrees at the fifteenth harmonic. This error appears to be dominated by the sampling process which accounts for phase shifts between 0.72 and 10.8 degrees. The error due to false period measurement in this test would be small since the wave was referenced to the edges of the square wave which can be accurately set up by visual means using the brightness intensity. This choice of reference point explains why the odd harmonic have phase angles of the order of 90 degrees, since the system measures phase relative to a cosine wave.

It is interesting to observe that the system indicates the presence of even harmonics of almost constant amplitude. As shown in Appendix F3 false period measurement introduces such effects. Additionally the digital nature of the computed results may also produce these additional frequencies. The constant level of these even harmonics, not present in the test wave form, suggests that this is the "noise" level of the system, where the term noise is meant to encompass all unwanted effects generated internally within the system.

The system can be improved in a number of ways. The data transfer "handshaking" is set up using BASIC programming language and consequently is slow because of the interpretation time of each BASIC statement. Considerable improvement in speed of transfer can be achieved by setting up the "handshaking" using machine code.

Sampling errors (especially phase error) and false periodic measurement errors can be reduced by taking more samples per cycle. This would require a greater computational effort but this can be overcome by using F.F.T. (Fast Fourier Transform) algorithms. The software of the system could easily be extended to produce graphs of waveforms and the spectrum.

CHAPTER 7

EXPERIMENTAL RESULTS

7.1 Introduction

In this chapter experimental evidence is presented to support the theoretical results derived in previous chapters. The experimental procedures are described and comparisons between theoretical and practical results are presented for the major areas of investigation, which were

(i) device identification from spectral response (discussed in Chapter 2),

(ii) static characteristic of exponential diodes with series resistance (discussed in Chapter 3),

(iii) spectral response of exponential diodes with series resistance to sinusoidal drive, (discussed in Chapter 4),

(iv) effect of parasitic capacitance on the large signal waveforms of lattice mixers, (discussed in Chapter 5).

7.2 Device identification from spectral response

A varactor diode, type BA111, was tested at a 100 kHz by two methods.

Method 1

The first method of test was to bias the diode at various negative voltages and to determine the incremental capacitance by application of a small alternating voltage superimposed on the d.c. level. A Q meter was then used to produce resonance at this frequency. From a knowledge of the inductance and capacitance set on the Q meter the extra capacitance provided by the varactor diode is then readily evaluated. The test circuit was as shown in Figure 7.1a. The capacitor C_b is a blocking capacitor to isolate the Q meter circuit from the dc bias. The value of the blocking capacitor is of the order of 10^6 times larger than the capacitance of the varactor diode and consequently had negligible effect on the measurement. The shunt combination of R_s and C_s represents the input impedance of an oscilloscope used to detect resonance. The resistance in series with the d.c. bias supply is included to reduce the alternating current through the bias supply to an acceptably small level and at the same time maintain a reasonably high Q factor for the circuit. When resonance is achieved the incremental capacitance of the varactor diode is given by

$$C_i = (1/\omega^2 L) - (C_q + C_s) \tag{7.1}$$

<u>Method 2</u>

The second method of test was to measure the spectrum produced by the varactor diode when driven with a large signal sinusoidal voltage superimposed on the d.c. bias and to compute the device characteristic as outlined in Chapter 2. The test circuit is as shown in Figure 7.1b. The sinusoidal supply had a fifty ohm internal resistance and the current was detected by monitoring the voltage across a fifty ohm series resistance. The capacitor C_b is a bypass capacitor so that the current at a fundamental frequency of 100 kHz, does not pass through the d.c. bias supply. Direct current is prevented from flowing because of the reverse bias on the diode. From manufacturers specifications, and the results of the previous incremental tests, an average value of incremental capacitance is approximately 40 pF. At a test frequency of 100 kHz the reactance of the reverse biassed diode is of the order of 40 kΩ as compared with the total series resistance of the test circuit of 100Ω. Even at the tenth harmonic the varactor diode would offer a reactance of 4 kΩ and therefore the series resistance has a negligible effect on the harmonic generating properties of the diode.

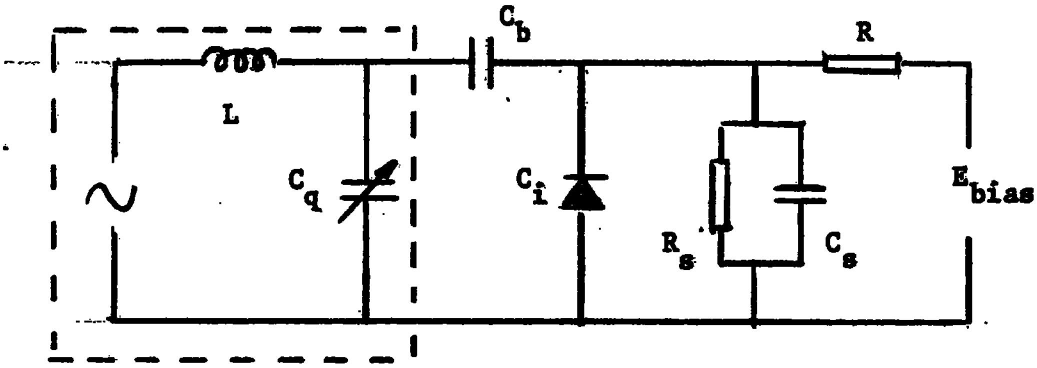

Figure 7.1a

Test Circuit to Determine Incremental Capacitance
Using Q Meter f = 100 kHz

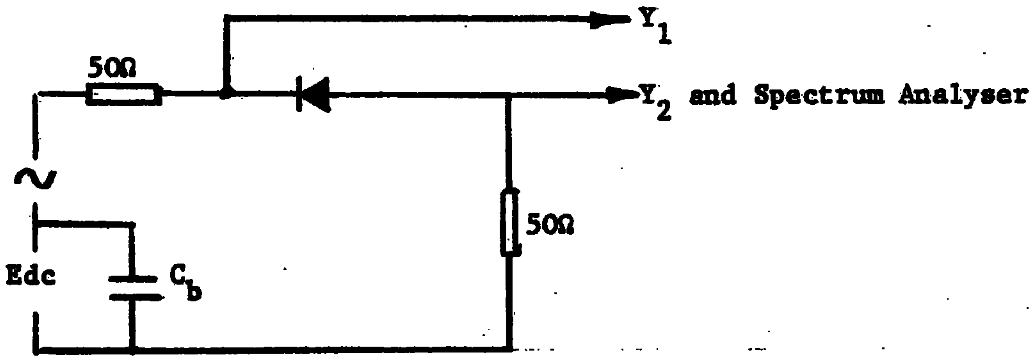

Figure 7.1b

Test Circuit to Determine Spectral Response of
Varactor Diode

To determine the device characteristic from the current spectrum use is made of the basic law

$$i = \frac{dq}{dt} = \frac{dq}{dV_d}\,\frac{dV_d}{dt} = C_i(V_d)\,\frac{dV_d}{dt} \tag{7.2}$$

where C_i is the incremental capacitance, V_d is the voltage across the diode which equals the drive voltage of the test circuit since resistance loss is negligible. The drive to the circuit is

$$V = V_d = \hat{V}\cos\theta - E, \quad \theta = \omega t, \quad E > 0 \tag{7.3}$$

where to prevent the diode entering into the conduction region the condition $\hat{V} \leq E$ must be imposed, and E is the d.c. bias voltage. Equation (7.2) now becomes

$$i = C_i\,\frac{d}{dt}\,(\hat{V}\cos\theta - E)$$

$$= -\hat{V}\omega C_i \sin\theta \tag{7.4}$$

The diode current is of the form

$$i = \sum_1^{\infty} I_n \sin n\theta \tag{7.5}$$

and to obtain equality in equation (7.4) the incremental capacitance must contain no sine terms, and therefore

$$C_i = C_o/2 + \sum_1^{\infty} C_n \cos n\theta \tag{7.6}$$

Consequently (7.4) may be rewritten as

$$\sum_1^{\infty} I_n \sin n\theta = -\omega\hat{V}\sin\theta\left[C_o/2 + \sum_1^{\infty} C_n \cos n\theta\right] \tag{7.7}$$

To balance the harmonics on either side of equation (7.7) then

$$C_{2p} = \frac{\mp 2}{\omega\hat{V}} \sum_{2p+1}^{\infty} I_n, \qquad p = 0, 1, 2 \ldots\ldots \tag{7.8}$$

and

$$C_{2p+1} = \frac{-2}{\omega \hat{V}} \sum_{2p+2}^{\infty} I_n, \qquad p = 0, 1, 2 \ldots\ldots \tag{7.9}$$

which represents the incremental time varying coefficients in terms of the harmonic currents, and therefore the incremental capacitance may be obtained as

$$C_i = C_o/2 + \sum_{1}^{\infty} C_n T_n (V/\hat{V}) \tag{7.10}$$

The large signal test was performed with a bias voltage of − 6 volts and a peak sinusoidal drive of 5.95 volts (4.2 V rms) at a frequency of 100 kHz. The measured spectrum developed across the 50Ω monitor resistor is given in Table 7.1. Converting to current and using equations (7.8) and (7.9) gives the time varying components which are shown in Table 7.2. The device characteristic may then be identified by use of equation (7.10). Table 7.3 summarizes the values of C_i for various values of deviation from the bias voltage. The values deduced from the spectral response of the device are plotted in Figure 7.2 where they are compared with the results obtained from the Q meter test.

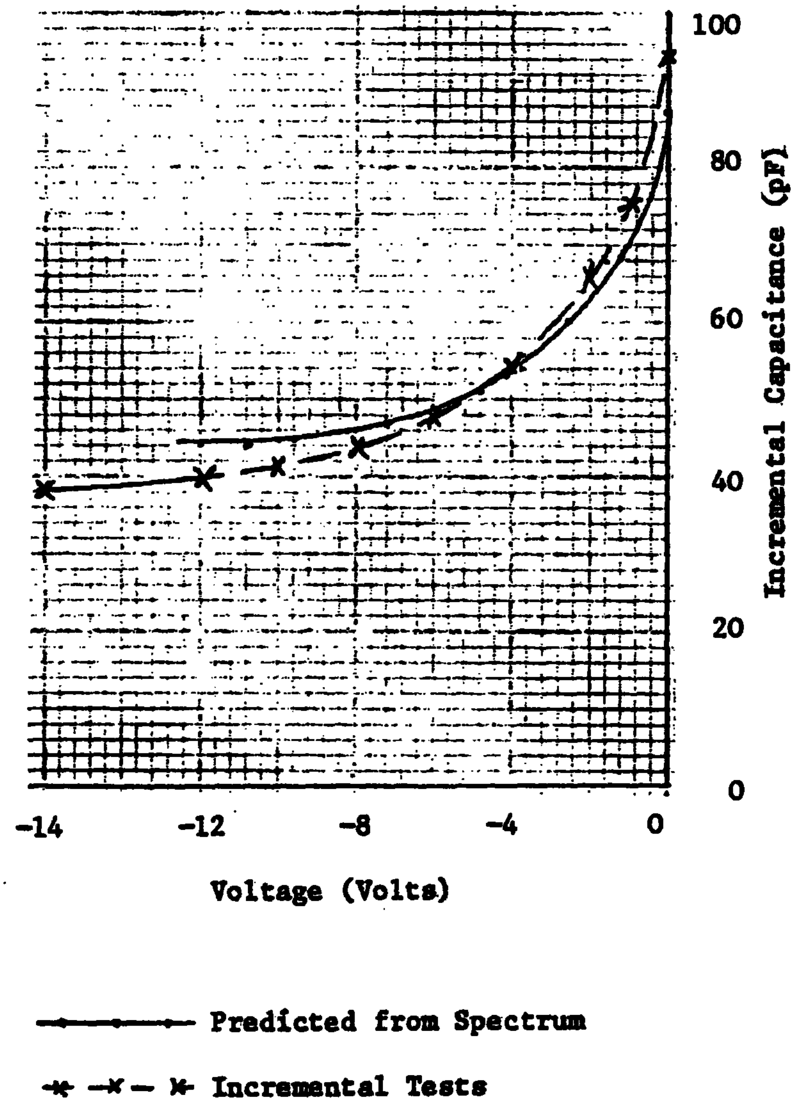

<u>Figure 7.2</u>

Comparison of Varactor Characteristic as Predicted from Spectrum and Measured on Q Meter

TABLE 7.1

Measured Spectral Coefficients

Frequency (kHz)	Voltage (mv)
100	6.8
200	0.9
300	0.44
400	0.16
500	0.08
600	0.04
700	0.024
800	0.01

TABLE 7.2

Coefficients of Incremental Capacitance

C_0	111.335 pF
C_1	16.83
C_2	8.247
C_3	3.18
C_4	1.58
C_5	0.758
C_6	0.364
C_7	0.1516

Table 7.3

Evaluation of Device Characteristic

$\Delta V = V - E$	0	1.19	2.38	3.56	4.75	5.94
$x = \Delta V/a$	0	.2	.4	.6	.8	1.0
$\frac{C_o}{2} T_o(x)$	55.7	55.7	55.7	55.7	55.7	55.7
$C_1T_1(x)$	0*	± 3.36	± 6.72	± 10.08	± 13.44	± 16.8
$C_2T_2(x)$	- 8.3	- 7.57	- 5.6	- 2.3	+ 2.3	+ 8.23
$C_3T_3(x)$	0	+ 1.78	+ 2.94	+ 2.94	+ 1.09	± 3.13
$C_4T_4(x)$	+ 1.58	+ 1.09	- 0.13	- 1.33	- 1.33	+ 1.58
$C_5T_5(x)$	0	± 0.64	± 0.67	+ 0.06	+ 0.75	± 0.76
$C_6T_6(x)$	- .364	- .13	+ .28	+ .27	- .27	+ .364
$C_7T_7(x)$	0	+ .15	± .04	± .15	+ .03	± .15
$x \geq 0$	48.68	51.16	54.74	60.21	67.97	86.71
$x \leq 0$	48.68	47.01	45.76	45.11	44.83	45.03

* Use upper sign for $x \geq 0$

Use lower sign for $x \leq 0$

7.3 Static Characteristics of the Exponential Diode with Series Resistance

To compare the theoretical predictions of the two-term approximation with measured results obtainable from tests on practical diodes it was first necessary to ascertain the primary parameters of the diodes, i.e. α, I_s, and r_s.

For the condition when the series resistance drop ir_s is much smaller than the diode voltage V, the defining exponential law

$$i = I_s \exp(\alpha V - \alpha i r_s) - I_s \qquad (7.11)$$

may be approximated and rearranged as

$$\ln(i) = \alpha V - \ln(I_s) \qquad (7.12)$$

Thus by plotting ln(i) against V the parameters α and I_s may be determined from the slope and intercept of the graph of the measured results.

When the diode current is such that the series resistance drop cannot be ignored then equation (7.11) may be rearranged as

$$\ln(i\exp(\ V)) = \alpha r_s i + \ln(I_s) \qquad (7.13)$$

A graph of the experimental results in the form of equation (7.13) will therefore give αr_s as the slope and a second independent determination of $\ln(I_s)$ from the intercept.

The test circuits usedto determine the parameters are shown in Figures (7.3a) and (7.3b). The voltmeters used for these tests were four digit, high input resistance (1 MΩ) voltmeters previously checked against a six digit, 0.01% standard and their accuracies confirmed as 0.1%. In both test circuits the resistance of the voltmeter across the series monitor resistor is sufficiently high so that the current through the monitor resistor is greater than 99% of the diode current.

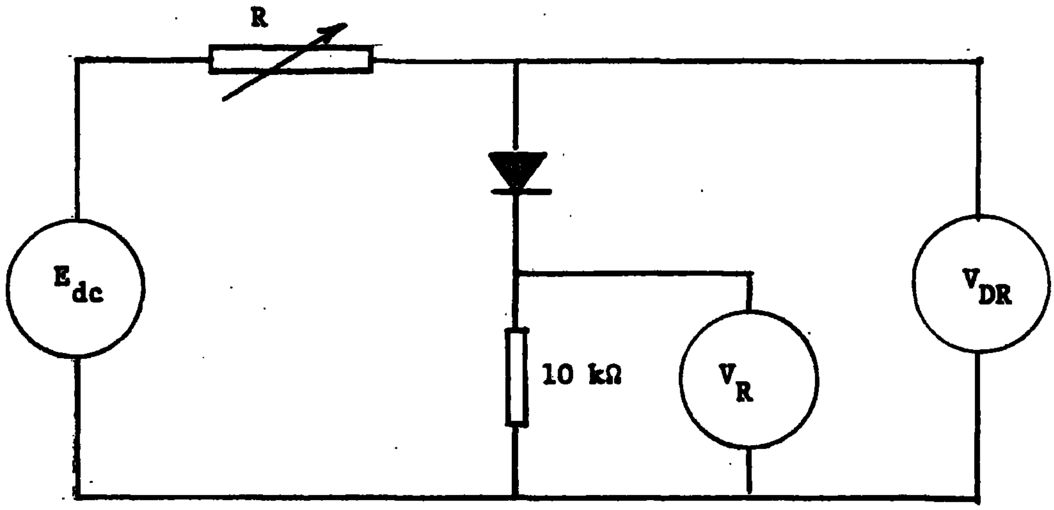

Figure 7.3(a)

Test circuit to determine α and I_s

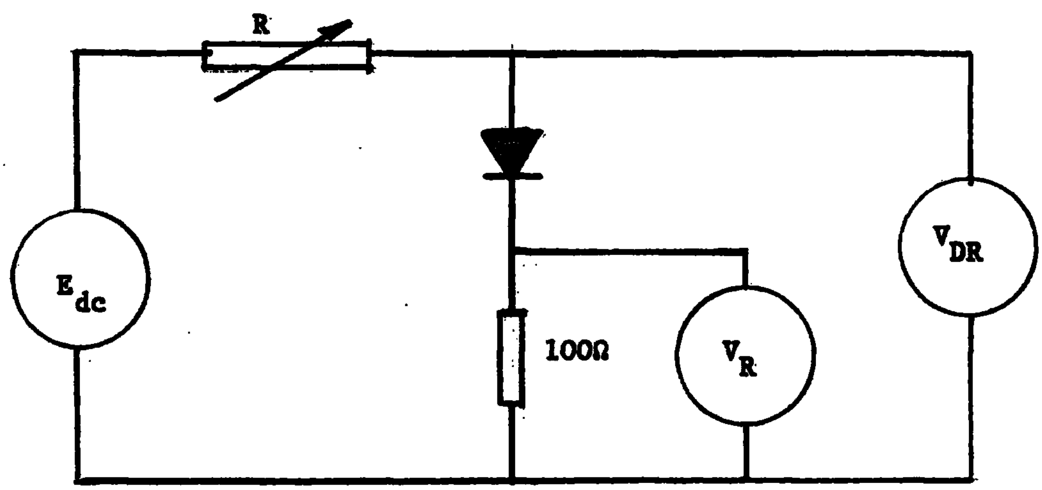

Figure 7.3(b)

Test circuit to determine r and I_s

Typical test results are shown in Tables (7.4) and (7.5) together with appropriate calculations. The test results for four diodes are displayed in graphical form in Figures (7.4) to (7.11) and a summary of the parameters determined from these tests are shown in Table (7.6).

The parameters obtained from the aforementioned tests were used in the two term approximation to predict the static characteristic of the experimental diode with series resistance. A typical set of results for these calculations is shown in Table (7.7). The first set of calculations (Table 7.7a) predicts the current flowing in a diode with an additional 100 ohms series resistance. The second set of results (Table 7.7b) predicts the current flowing in a diode when only the parasitic series resistance is present. Also shown in Table 7.7 are calculated diode currents assuming the logarithmic model of the diode. Table (7.7c) and (7.7d) show results when the logarithmic curve is fitted at two different voltages, the first for use in a hard driven situation and the second for use in a low-level drive situation.

The static characteristics predicted for the four diodes are shown in Figure (7.12) to (7.15) where a comparison is made with practical results obtained from measurements on the test circuit of Figure (7.3b). Also superimposed on these graphs are the predicted characteristics of the diodes including only their parasitic series resistance. The practical results shown for comparison purposes, were obtained by subtracting the voltage drops produced in the source and monitor resistors from the voltage applied to test circuit shown in Figure (7.3b).

Table 7.4

Typical Set of Results for the Determination of α and I_s

Diode Type HP 5082-2817

V_{RD}(mV)	V_R(mV)	$V_D = V_{RD} - V_R$(mV)	i (amps)
150	.51	149.5	5.1×10^{-8}
160	.78	159.3	7.8
170	1.2	168.8	1.2×10^{-7}
180	1.75	178.3	1.75
190	2.54	186.5	2.54
200	3.65	196.4	3.65
210	4.98	205.2	4.98
250	15.7	334.3	1.6×10^{-6}
300	41.1	258.6	4.14
400	115.1	284.9	1.151×10^{-5}
500	199	299	1.99
600	289	311	2.89
700	382	318	3.82

From the graph of above results in Figure (7.8)

$V_d = .342$ volts $\quad i = 10^{-4}$ amps

$V_d = .164$ volts $\quad i = 10^{-7}$ amps

$$\ln(i) = \ln(I_s) + \alpha V_d$$

$$\therefore \alpha = \text{slope} = \frac{\ln(10^{-4}) - \ln(10^{-7})}{.342 - .164}$$

$$= (\ln 1000)/.178 = 38.8$$

To find I_s add the following

$$\ln(10^{-4}) = \ln(I_s) + .342\alpha$$

$$\ln(10^{-7}) = \ln(I_s) + .164\alpha$$

$$\ln(I_s) = \frac{\ln(10^{-11}) - 19.6328}{2}$$

$$= -22.480618$$

$$\therefore I_s = 1.725 \times 10^{-10}$$

Table 7.5

Typical Set of Results for the Determination of I_s and r_s

Diode Type 5082-2817

i(mA)	V_R(mA)	V_{RD}(mV)	V_D(mV)	i exp(V) (mA)
5.0	500	992	492	2.56×10^{-8}
4.5	450	936	486	2.91
4.0	400	877	477	3.67
3.5	350	820	470	4.20
3.0	300	760	460	5.32
2.5	250	701	451	6.29
2.0	200	640	440	7.70
1.5	150	577	427	9.57
1.0	100	510	410	1.23×10^{-7}
0.5	50	438	388	1.44

From graph of above results in Figure (7.9)

$$\text{Intercept} = 1.73 \times 10^{-7} \text{ mA}$$
$$= 1.73 \times 10^{-10} \text{ amps}$$

$$\text{Slope} = \alpha r = \frac{\ln(1.73 \times 10^{-7}) - \ln(3.5 \times 10^{-8})}{4(\text{mA})}$$

$$= \frac{\ln(17.5/3.5)}{4} = 0.40236$$

$$r = 0.40236/\alpha = 0.40236/38.8$$

$$= 0.01037 \text{ Volts/mA}$$

$$= 10.37 \text{ ohms}$$

Table 7.6

Measured Diode Paramaters

Diode Type	Sample No.	α	r_s (ohms)	I_s (amps)
HP 5082-2800	1	37.54	22.65	3.4×10^{-9}
	2	37.54	22.02	3.0×10^{-9}
HP 5082-2811	1	37.14	9.04	8×10^{-10}
HP 5082-2817	1	38.81	10.37	1.73×10^{-10}
HP 5082-2835	1	38.16	8.05	8.9×10^{-9}

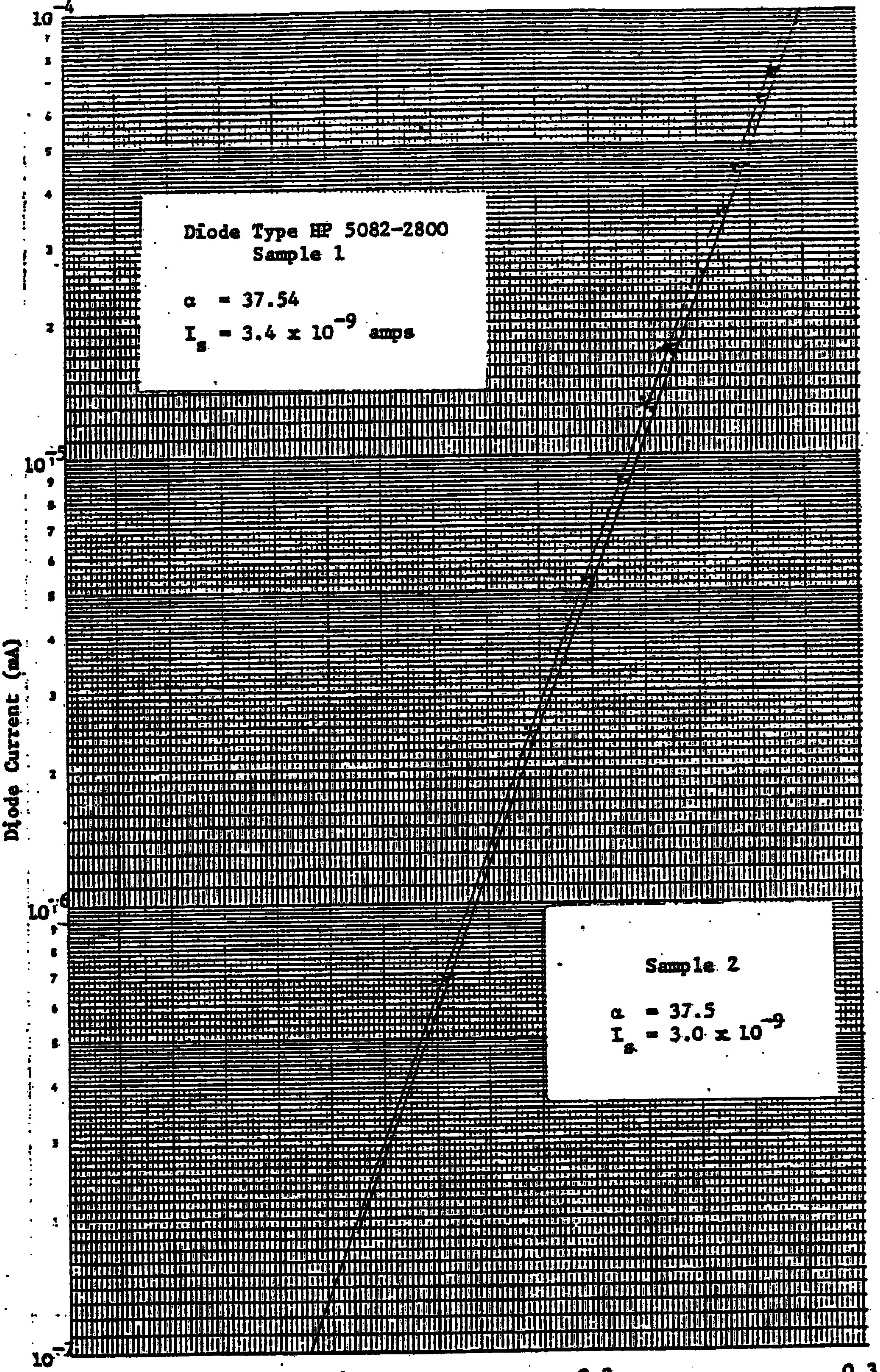

Figure 7.4

Determination of α and I_s

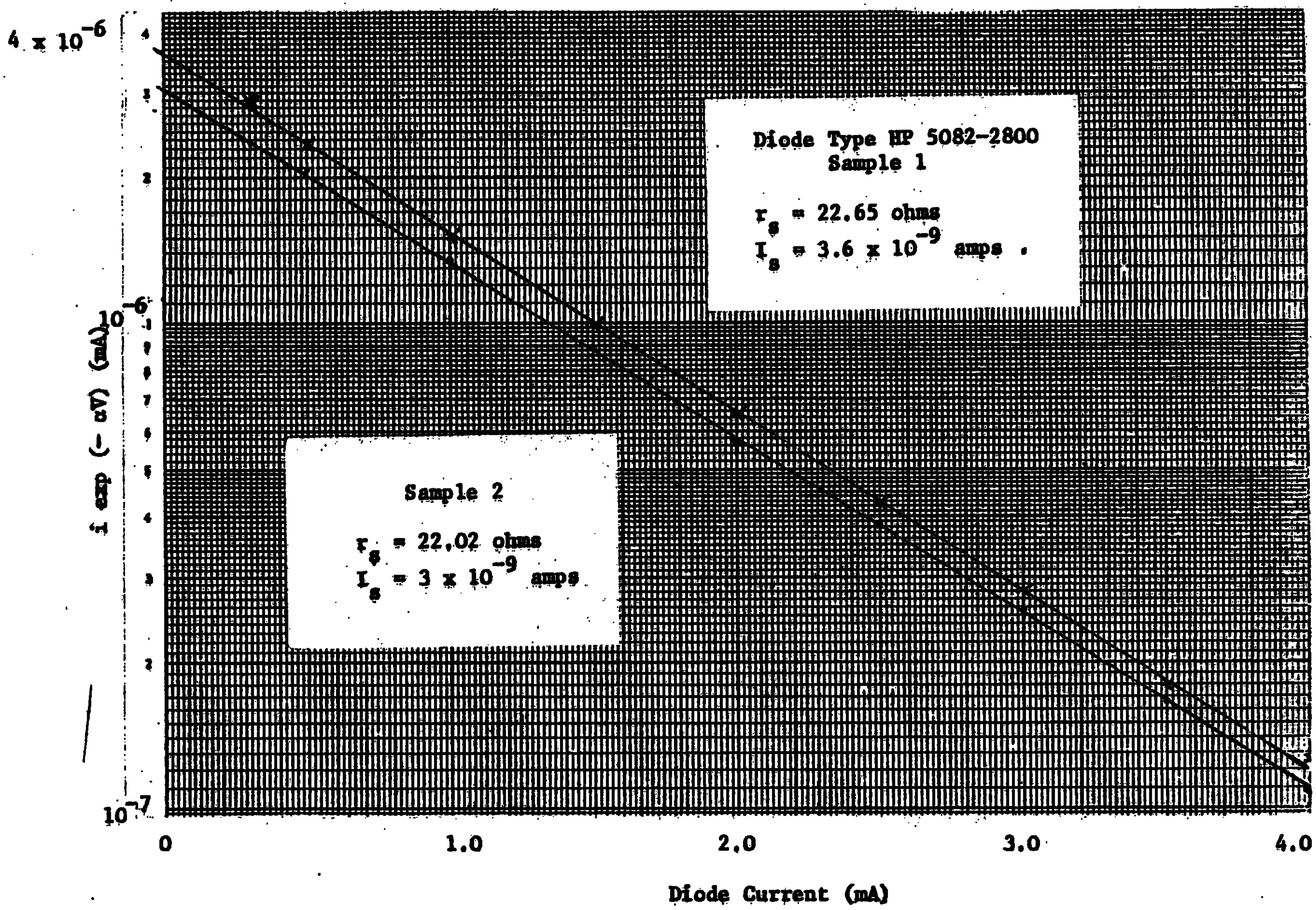

Figure 7.5

Determination of r_s and I_s

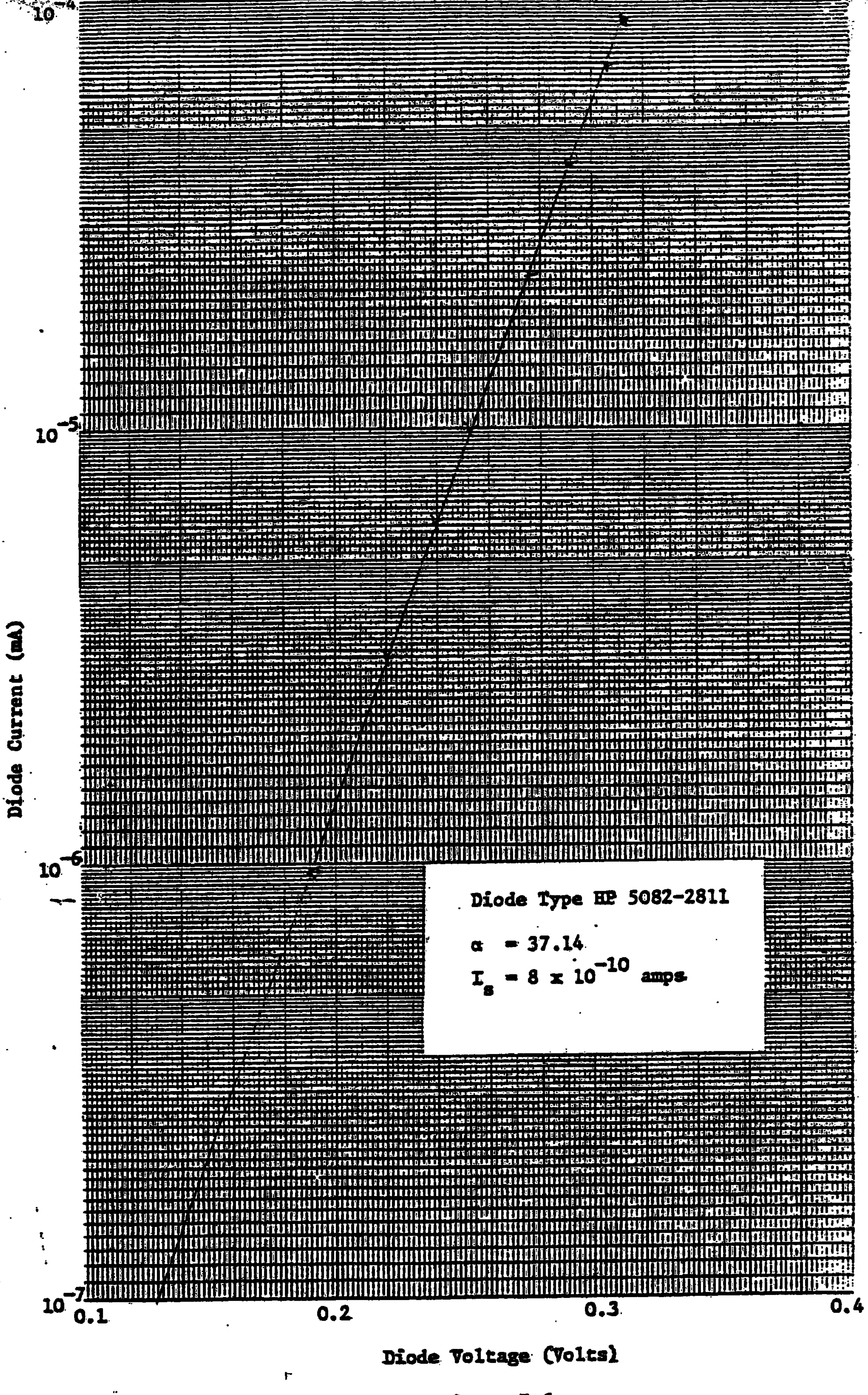

Figure 7.6

Determination of α and I_s

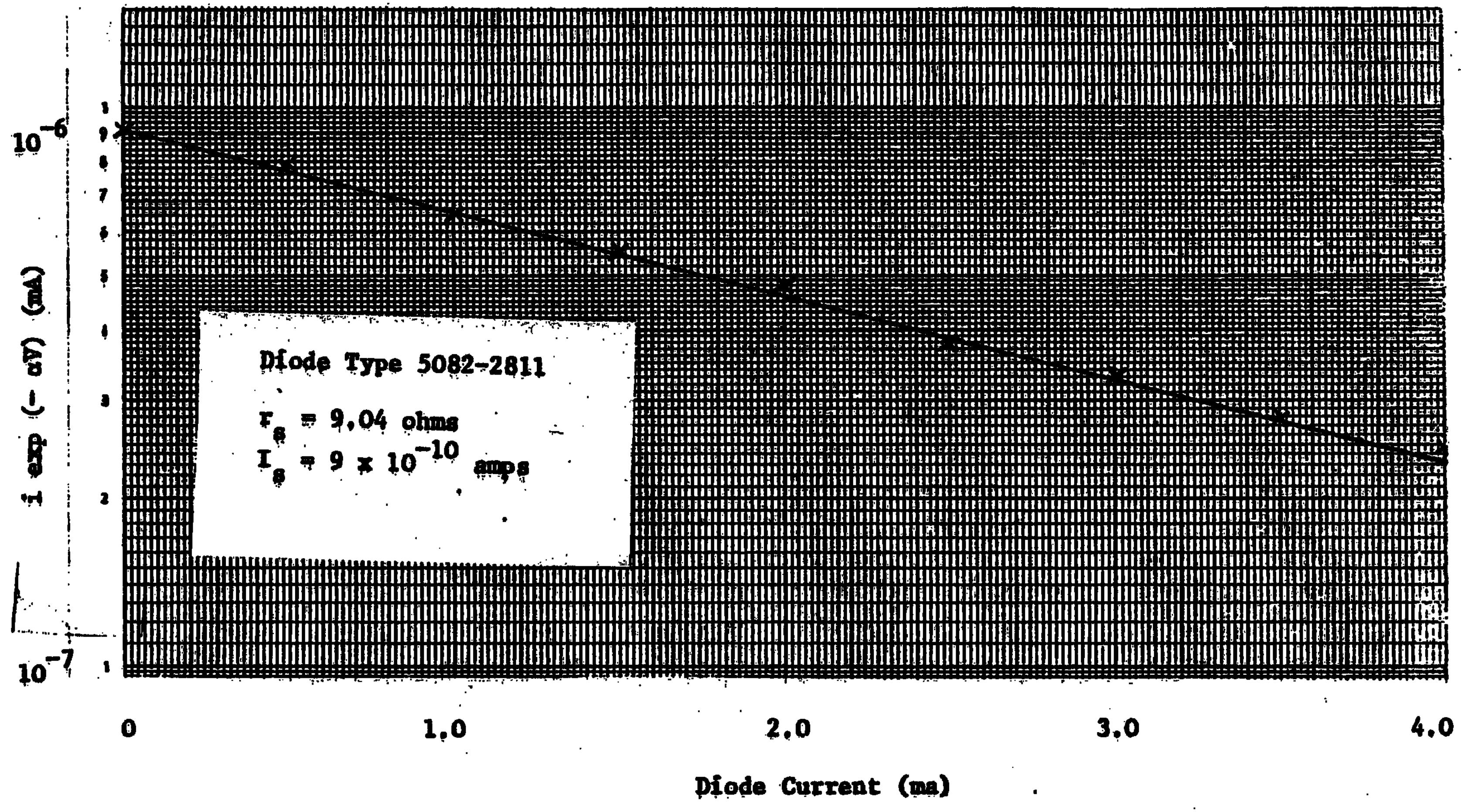

Figure 7.7

Determination of r_s and I_s

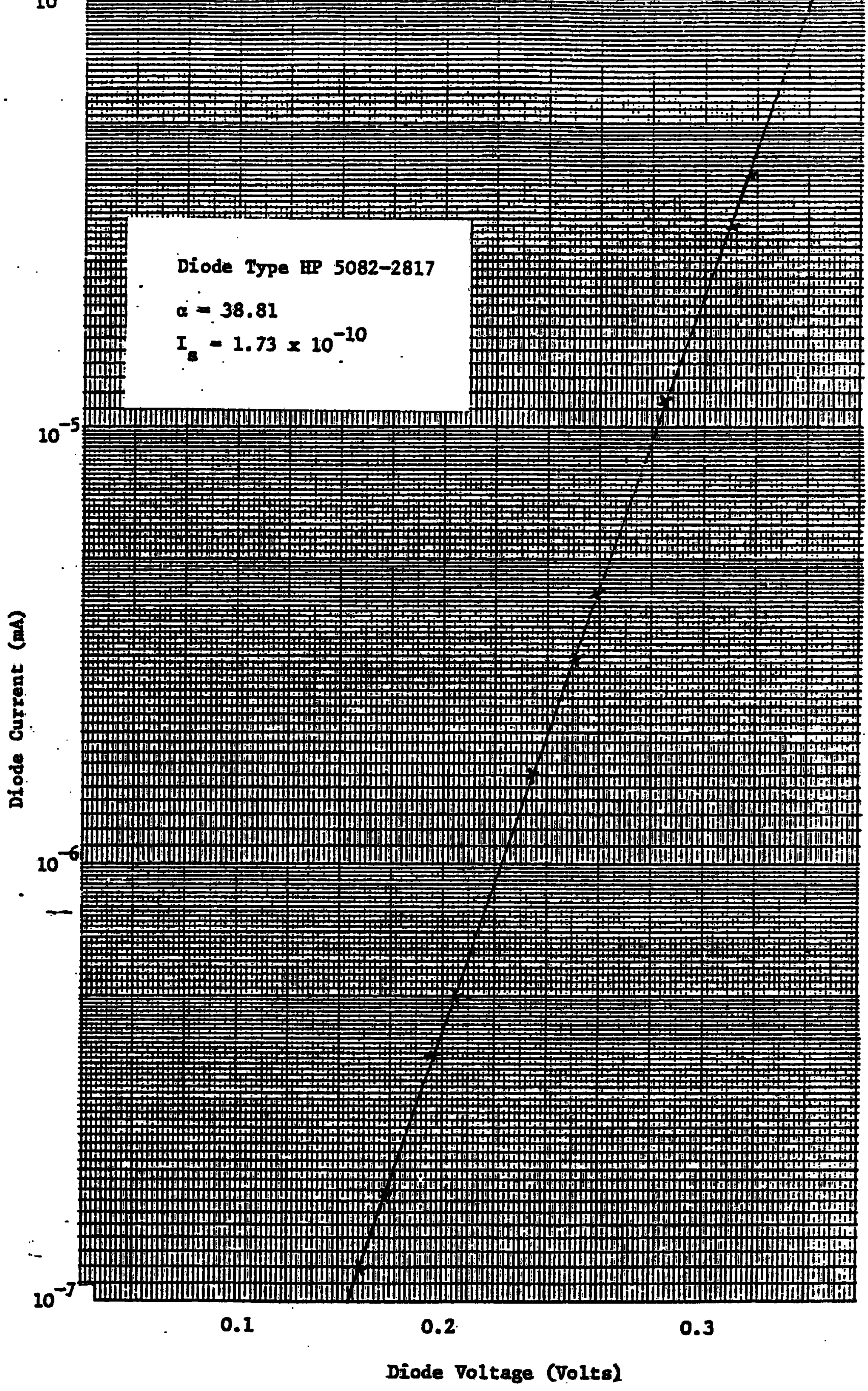

Figure 7.8

Determination of α and I_s

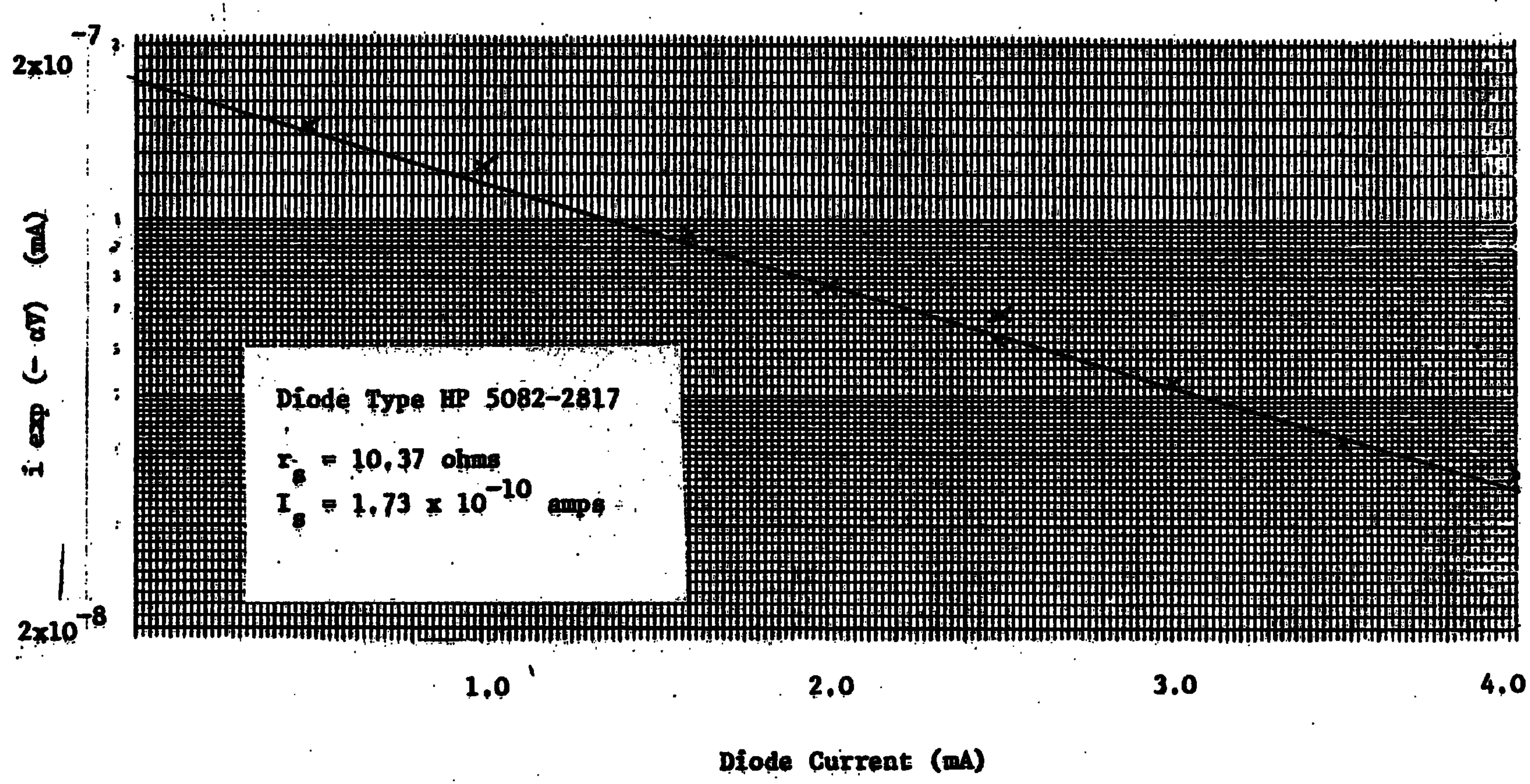

Figure 7.9

Determination of r_s and I_s

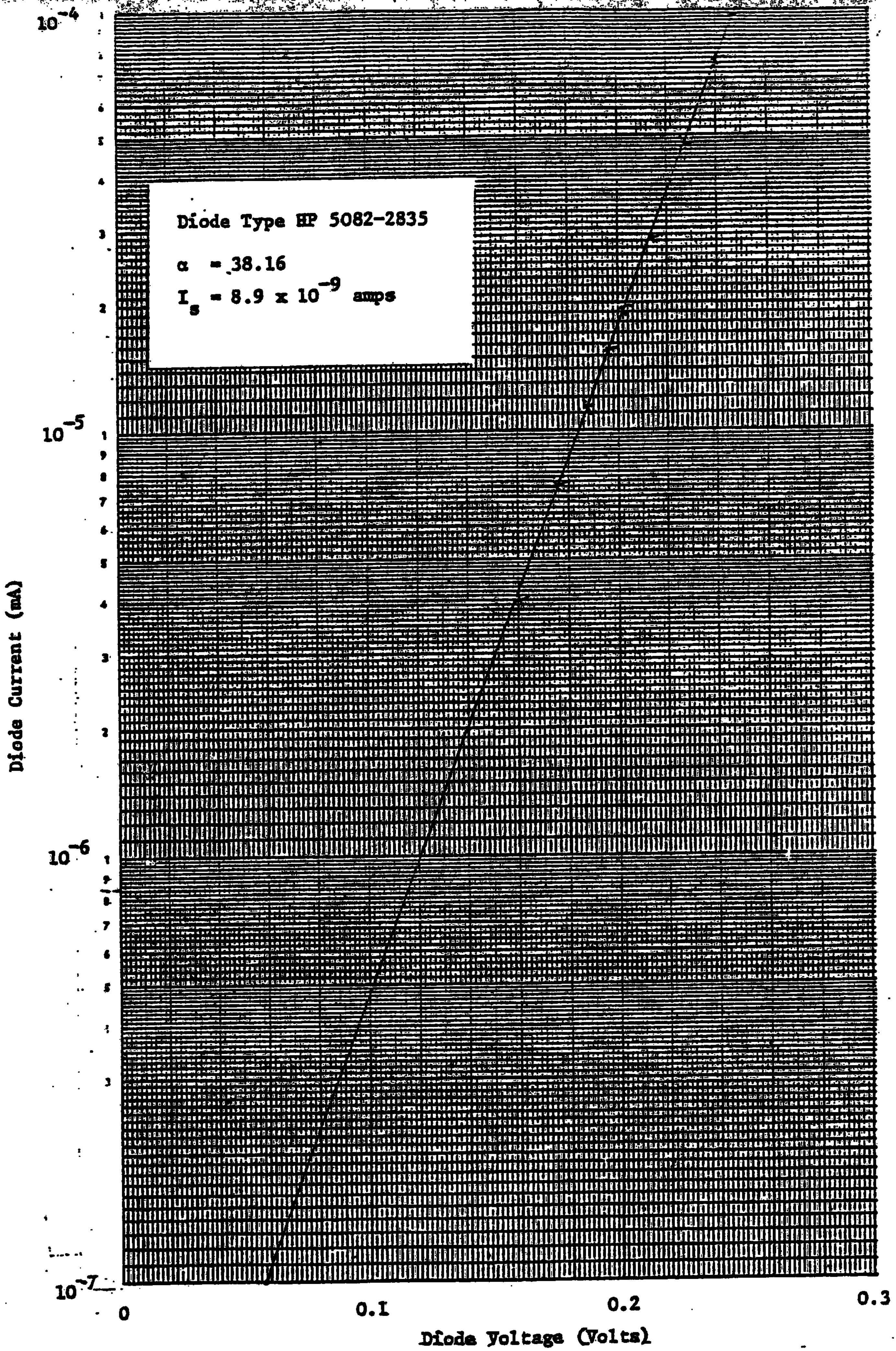

Figure 7.10

Determination of α and I_s

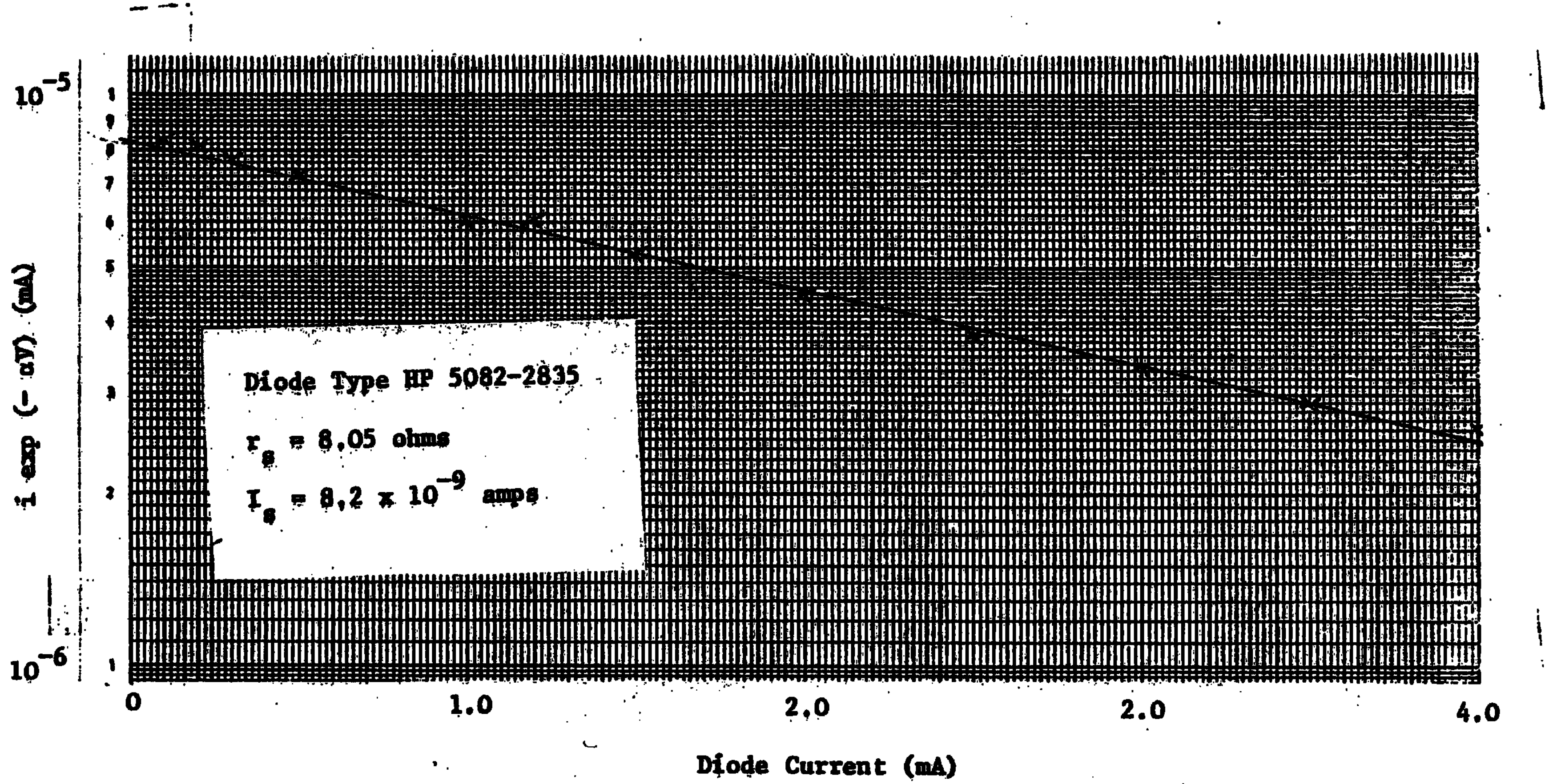

Figure 7.11

Determination of r_s and I_s

TABLE 7.7

TABLE 7.7a: Diode Type HP5082-2835

α = 38.16 R + r_s = 108.05 I_s = 8.9E-09

V_o = .267631882

Voltage (Volts)	Diode Current (Amps)
.36	4.7581399E-03
.3	4.23096831E-03
.74	3.70727001E-03
.69	3.27417972E-03
.63	2.75961676E-03
.57	2.25256403E-03
.5	1.67491326E-03
.45	1.27639828E-03
.38	7.53482229E-04
.33	4.2743669E-04
.3	2.66502658E-04
.27	1.43541887E-04
.23	4.72841467E-05
.95	5.55398314E-03
.99	5.90928757E-03
1	5.99824689E-03

TABLE 7.7b: Diode Type HP5082-2835

α = 38.16 r_s = 3.05 I_s = 3.9E-09

V_o = .335685394

Diode Voltage (Volts)	Diode Current (amps)
.39	5.11466656E-03
.38	4.38333364E-03
.37	3.7031169E-03
.36	3.07906832E-03
.35	2.51561801E-03
.34	2.01622068E-03
.245	9.91780413E-05
.345	2.25774337E-03
.355	2.78952589E-03
.335	1.79127875E-03
.32	1.21660343E-03
.31	9.15273622E-04
.3	6.74894314E-04
.285	4.13652752E-04
.27	2.45983558E-04
.255	1.43286606E-04

TABLE 7.7 continued

TABLE 7.7c Logarithmic Approximation

Diode Type HP 5082-2835

α = 38.16 $R + r_s$ = 108.05 I_s = 8.9E-09

V3=	.55		
V0=	.267631882		
V1=	.303723187	RM=	118.077686
.88	4.88048869E-03		
.81	4.28765865E-03		
.76	3.86420862E-03		
.67	3.10199875E-03		
.62	2.6785498E-03		
.59	2.42448251E-03		
.52	1.83170626E-03		
.46	1.32407825E-03		
.4	8.20930074E-04		
.36	5.01119488E-04		
.34	3.56839055E-04		
.3	1.38626596E-04		
.25	2.68736953E-05		

TABLE 7.7d Logarithmic Approximation

Diode Type HP 5082-2835

α = 38.16 $R + r_s$ = 108.05 I_s = 8.9E-09

V3=	.35		
V0=	.267631882		
V1=	.271437726	RM=	142.426152
.5	1.60480741E-03		
.45	1.25392028E-03		
.44	1.18380223E-03		
.4	9.04016175E-04		
.36	6.27974908E-04		
.32	3.67755812E-04		
.29	2.04005093E-04		
.275	1.40464757E-04		
.21	1.68491246E-05		
.26	9.17282307E-05		
.25	6.72560275E-05		

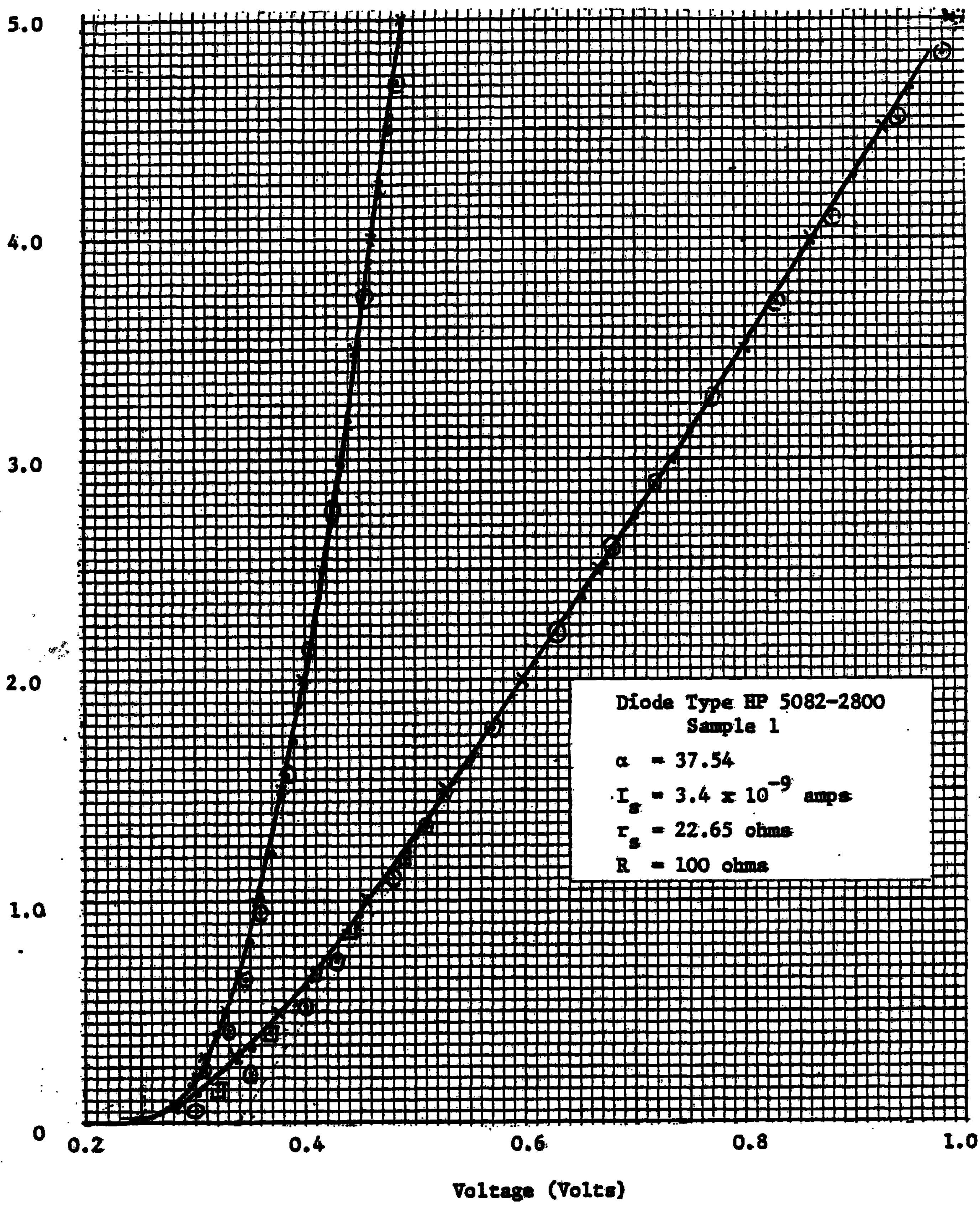

Figure 7.12

Diode Static Characteristics

Predicted current (two term approximation)

Predicted current (logarithmic approximation) Bilinear fitted at 0.7 volts

Logarithmic approximation fitted at 0.45 V

Measured diode current

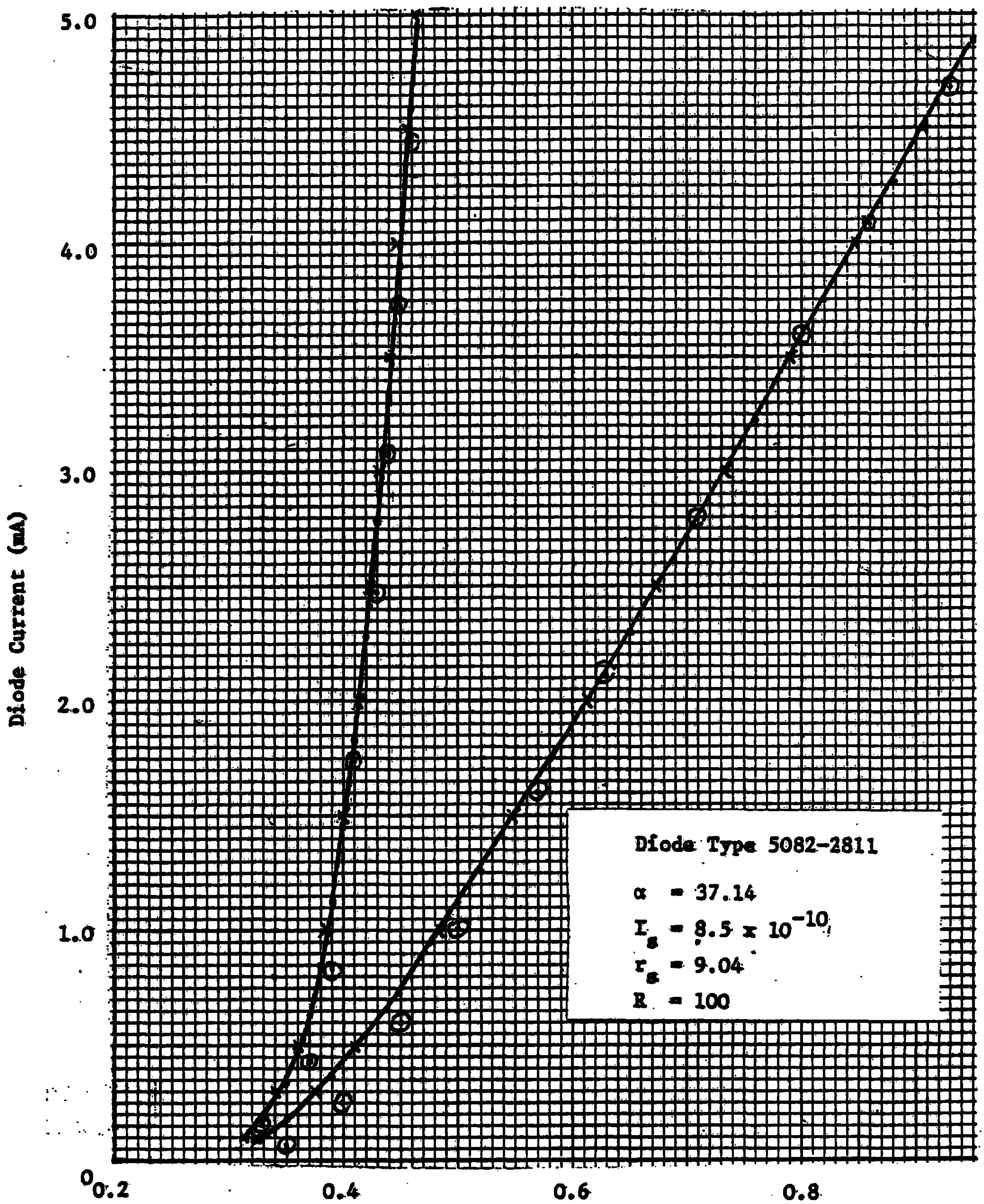

Figure 7.13

Diode Static Characteristics

Predicted current (two term approximation)

Predicted current (logarithmic approximation)

Bilinear section fitted at 0.7 Volts

× × × Measured diode current

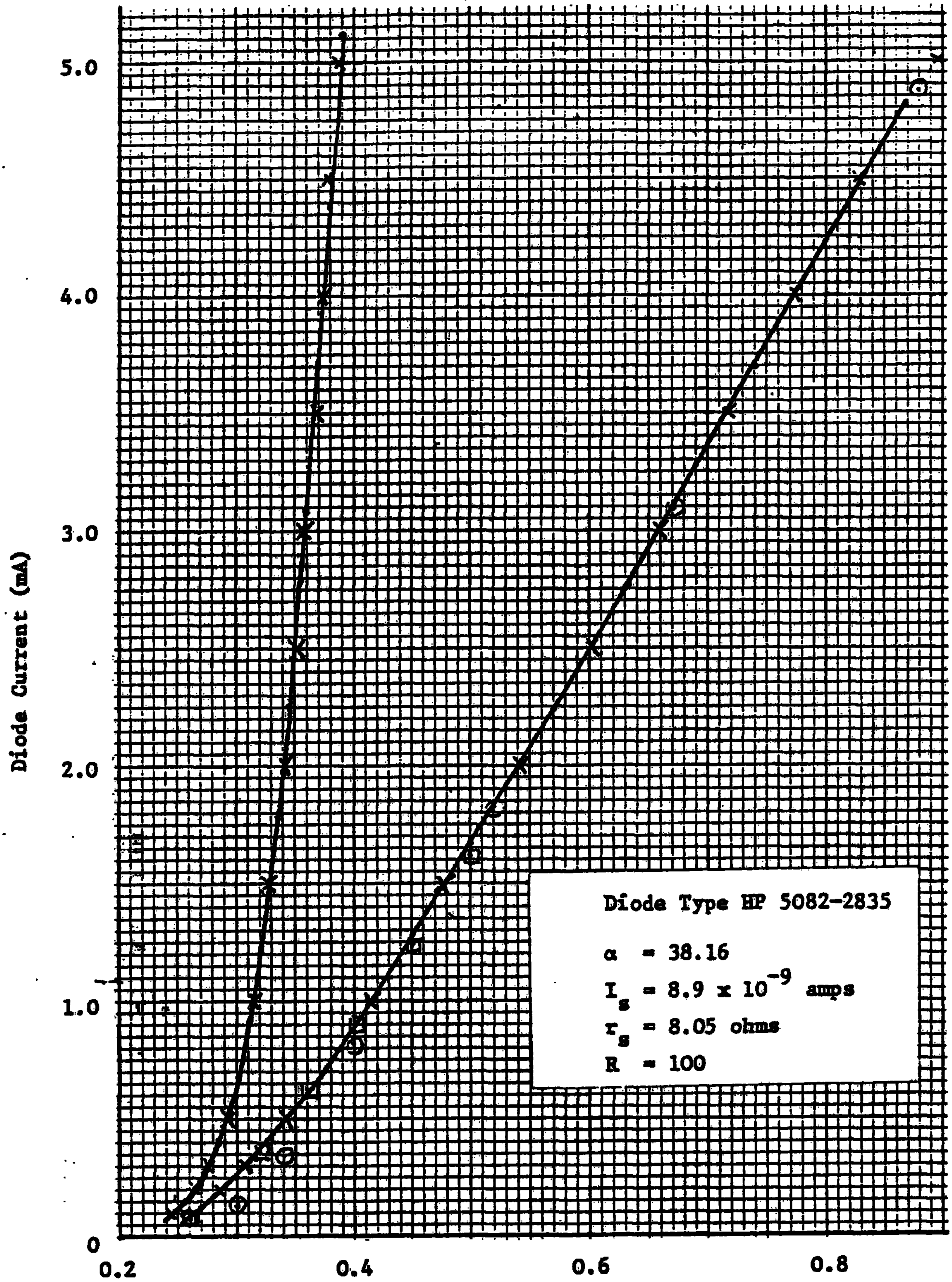

Figure 7.14

Diode Static Characteristics

Predicted diode current (two term approximation)

Predicted current (logarithmic approximation)

Bilinear fitted at 0.55V

logarithmic fitted at 0.35V

Measured diode current

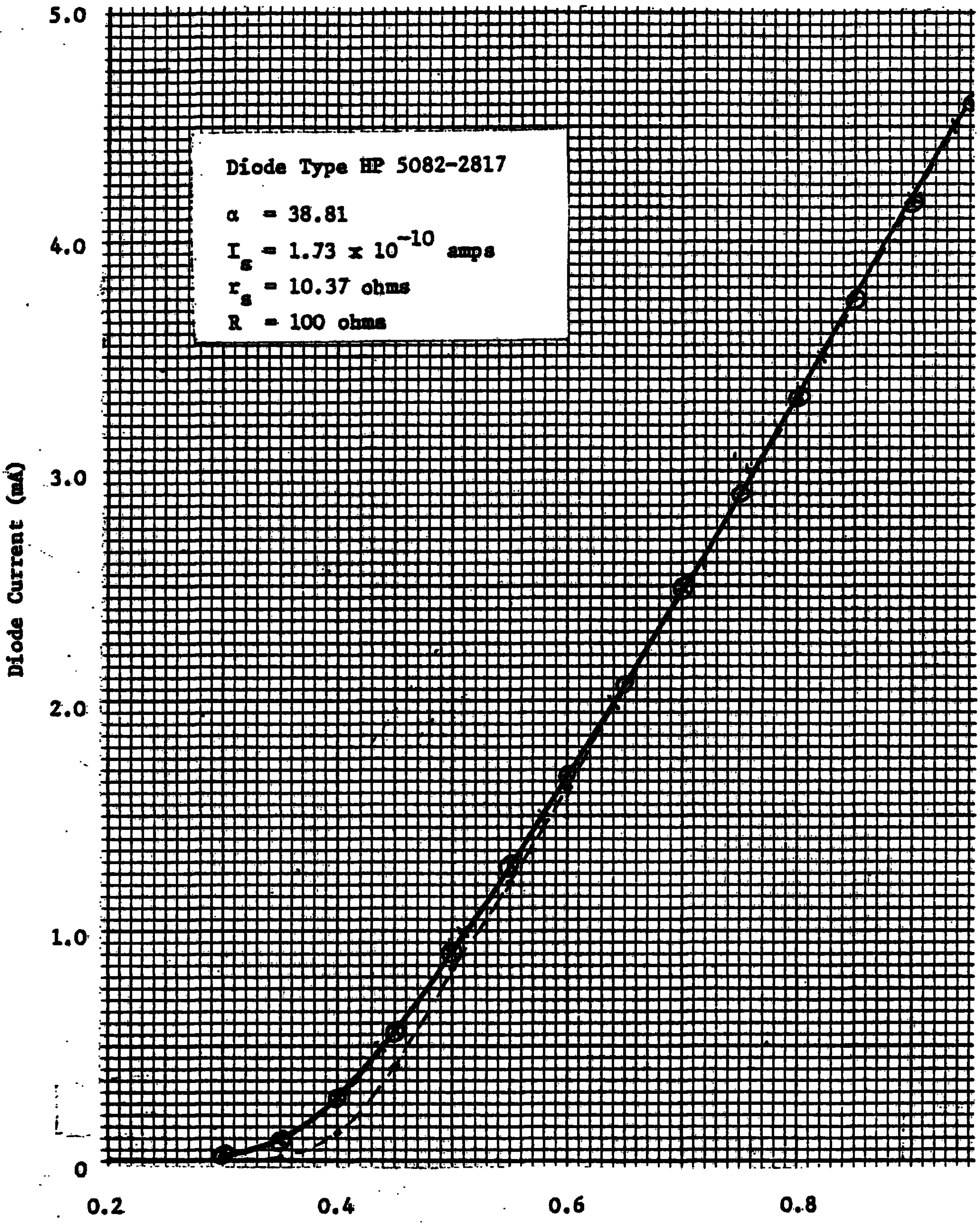

Figure 7.15

Diode Static Characteristics

Predicted diode current (two term approximation)

Predicted current (logarithmic approximation) Bi-linear fitted at 0.7 Volts

Measured diode current

7.4 Comparison of predicted and measured waveforms

For these tests the diode was driven from a low distortion sinusoidal test oscillator. The level of the test voltage was set by measuring the open circuit voltage of the oscillator with a digital voltmeter having an accuracy of 0.1%. With the diode and the monitor resistor R_m connected as shown in Figure 7.16, the transient recorders (T.R.) were adjusted to store the waveforms of the voltage V_D and V_R. As explained in Chapter 6 a single cycle of the diode current waveform was transferred to the computer. By a suitable modification of the Fourier Analysis programme the magnitudes of the samples of the current waveform were made available as a numerical print out on the line printer. A typical set of measured sample levels for various voltage drives are shown in Appendix G1. These measured sample levels were then compared with results predicted from the bi-linear model with exponential correcting cusps. The numerical values as given by this model are shown in Appendix G2 and a graphical comparison between the measured and theoretical results is shown in Figure 7.17. The programmes required to print out the samples of the current waveform and to evaluate the theoretical formulea [equation (3.50) and (3.51)] are shown in Appendix G3.

7.5 Comparison of predicted and measured spectrum

(a) Low frequency tests at 20 kHz

The diodes were tested using the system shown in Figure 7.16. The sampled waveforms stored in the Transient Recorders were transferred to the computer and one cycle of the measured diode current was harmonically analysed using the Fourier analysis programme. A typical set of results are shown in Appendix G4 for various levels of voltage drive. The harmonic content as given by the equations derived in Chapter 4 was also computed and are shown in Appendix G5. Comparisons of the predicted and measured spectral decomposition for various voltage drives are shown in graphical form in Figure 7.18.

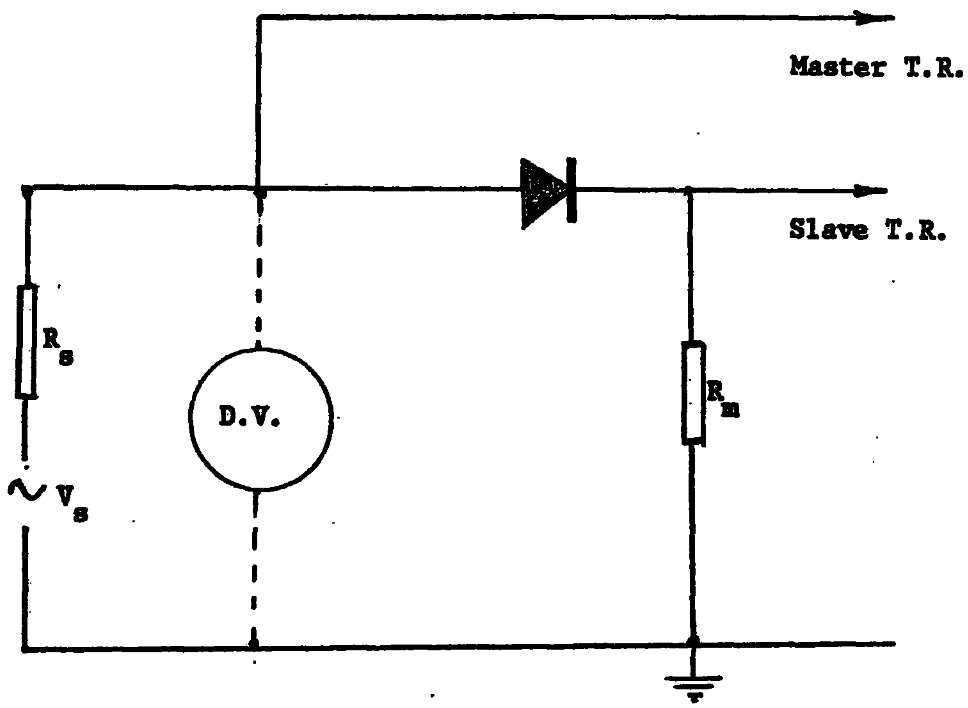

Figure 7.16

Test circuit for measurement of diode current

T.R. Transient Recorder

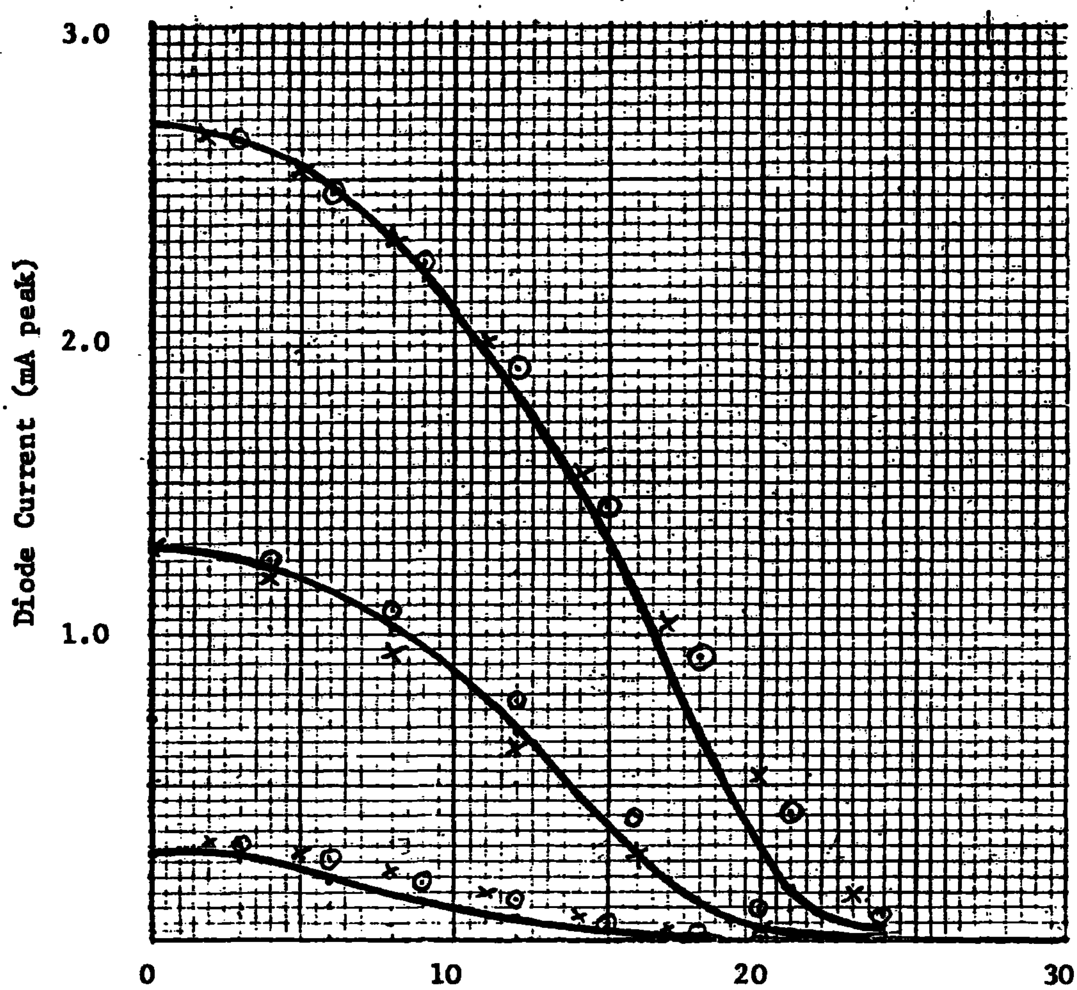

Sample Number

Figure 7.17

Predicted and measured diode current waveforms

Diode Type HP 5082-2800

——— Predicted (Bi-linear + exponential cusps)

× Decreasing measured current

⊙ Increasing measured current

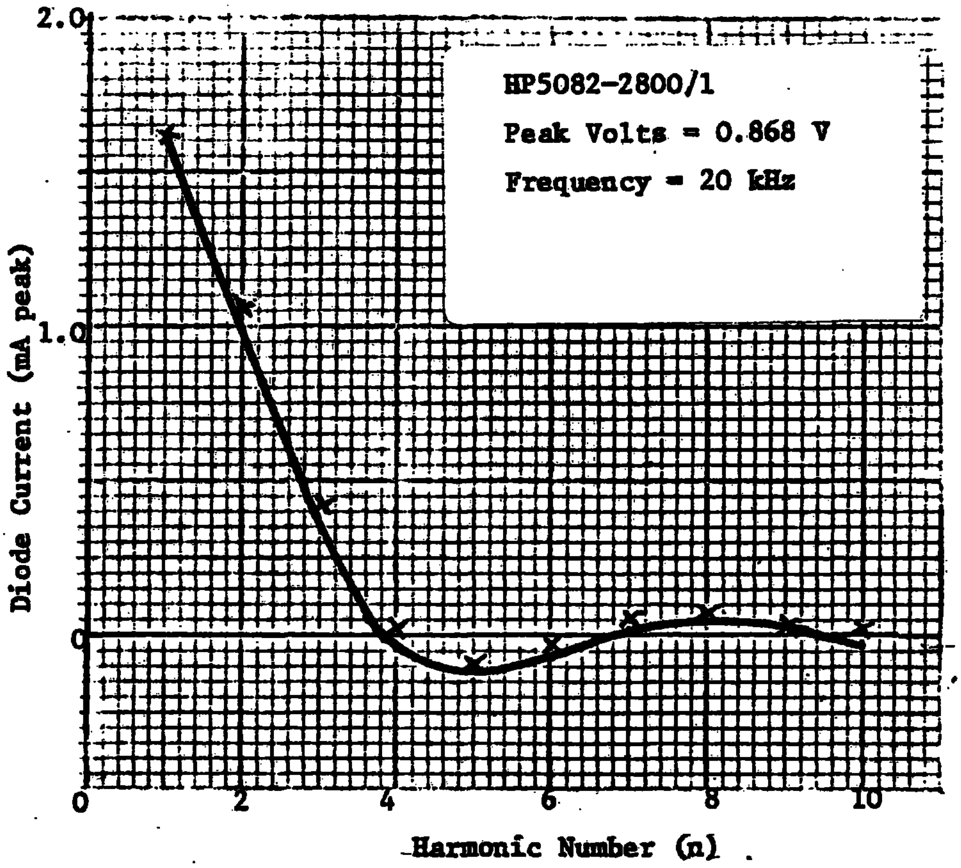

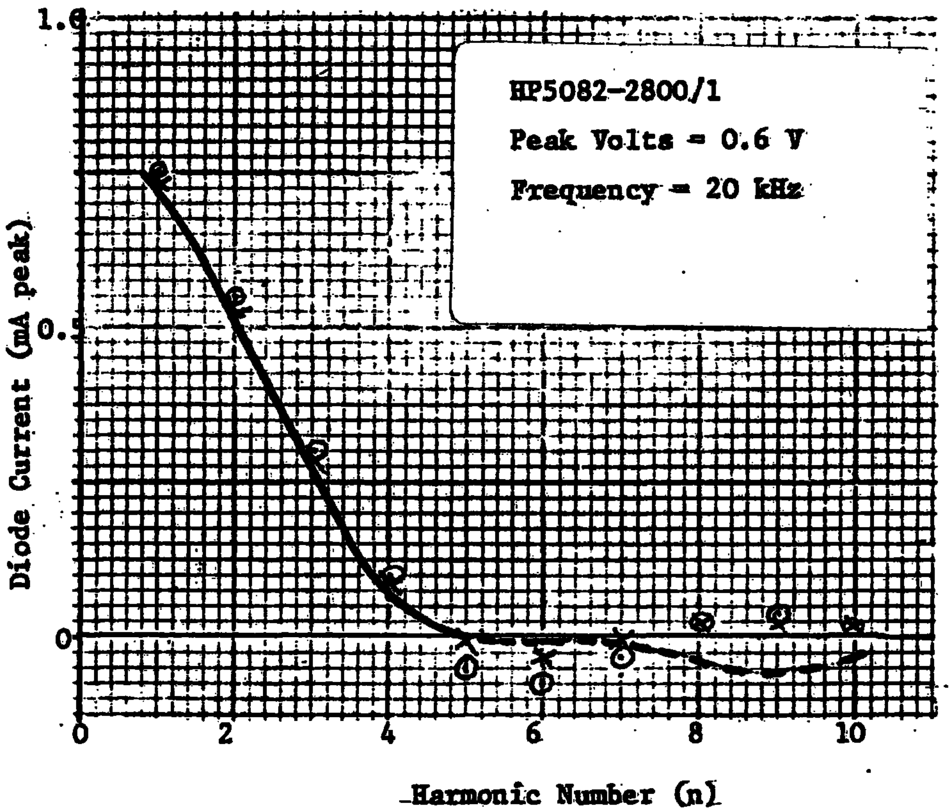

Figure 7.18 (a and b)

Comparison of predicted and measured spectrum

——— Predicted (Bi-linear+exponential cusps)

⊙ Predicted (Bi-linear)

× Measured

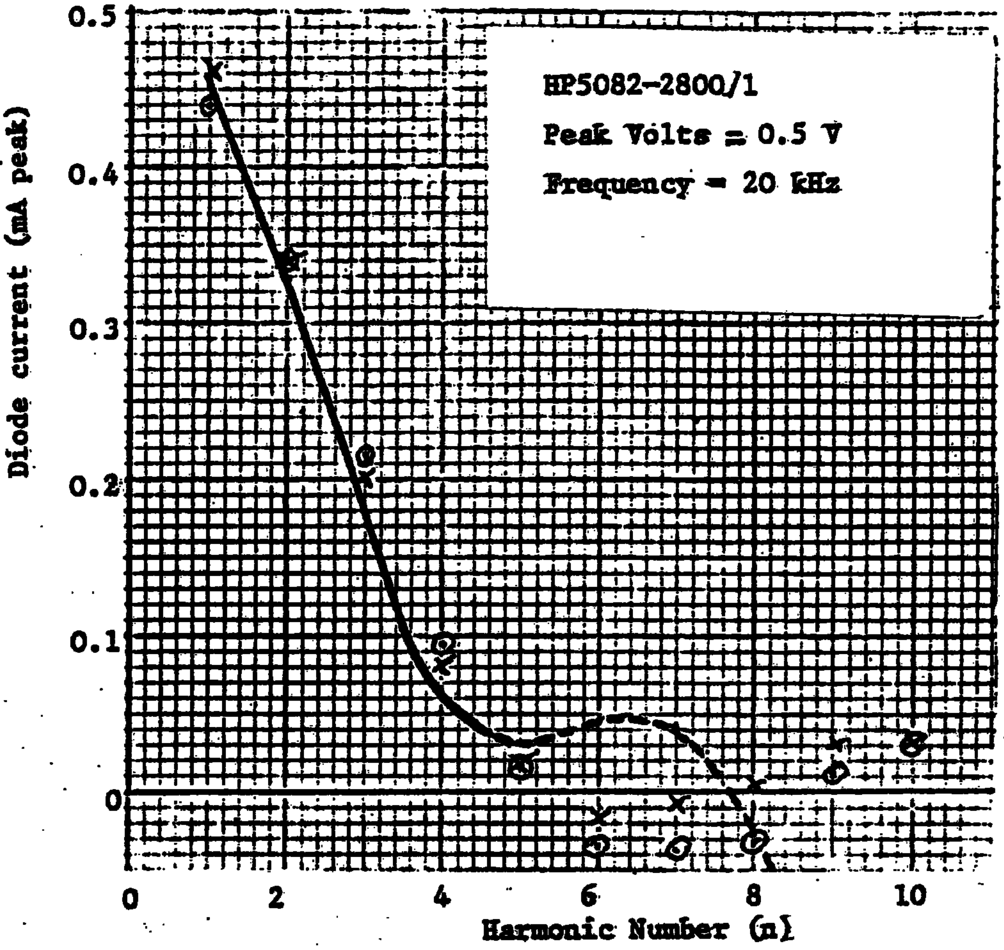

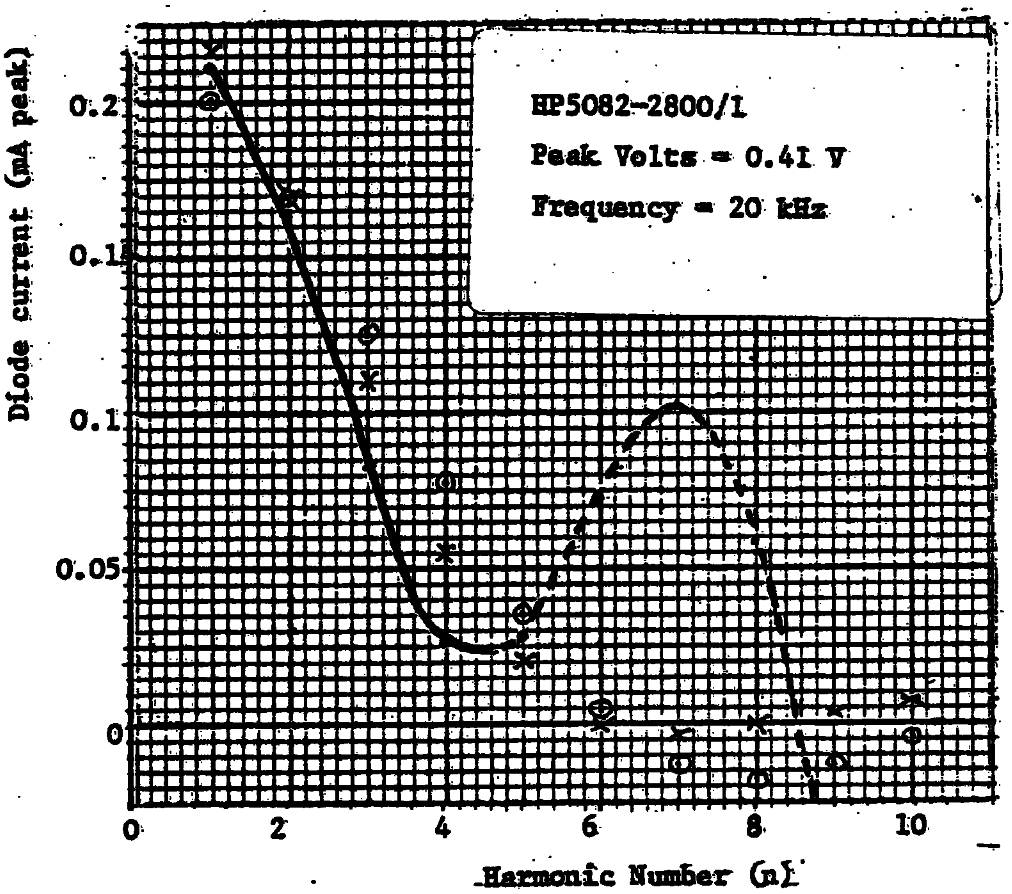

Figure 7.18 (c and d)

Comparison of predicted and measured spectrum

——— Predicted (bi-linear with exponential cusp)

⊙ Predicted (Bi-linear)

(b) High frequency tests at 10 MHz

Tests were carried out at 10 MHz using a low distortion sine wave oscillator. The open circuit output voltage of the oscillator was set to the desired drive level by means of the vector voltmeter. With the diode and 50 ohm monitor resistor connected to the 10 MHz source the supply voltage and diode current were monitored by the vector voltmeter. The 20 kHz replicas of the 10 MHz waveforms were then stored in the transient recorders and passed to the computer for Fourier analysis.

The 20 kHz replicas of the diode voltage and current wave-forms are shown in Figure 7.19 together with a time-domain portrait of the diode characteristic. Figure 7.20 shows graphical comparisons between predicted and measured harmonic content of the diode current waveshape. The measured test results obtained as a numerical print out from the computer and the theoretical results are shown in Appendix G6.

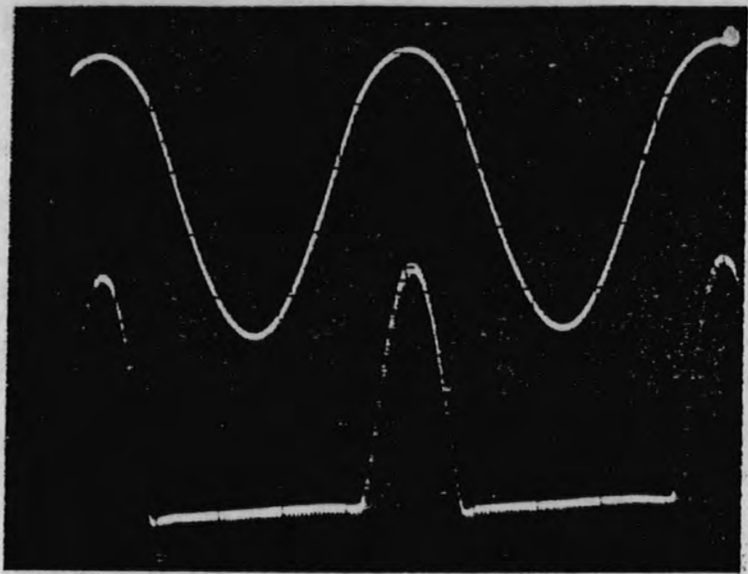

(a) Upper Trace
Voltage across diode and monitor resistance

(open circuit voltage = 0.5 V peak)

(b) Lower Trace
Voltage across monitor resistance

peak current = 1.7 mA

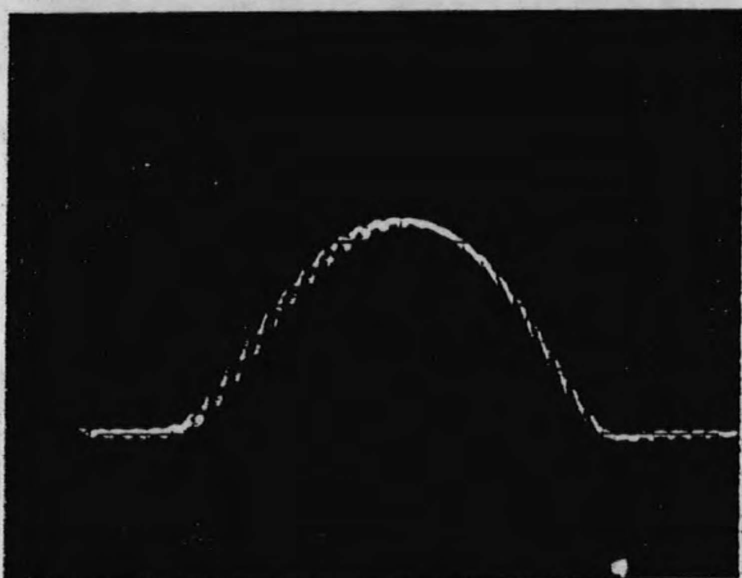

Voltage across monitor resistance

Expanded time scale

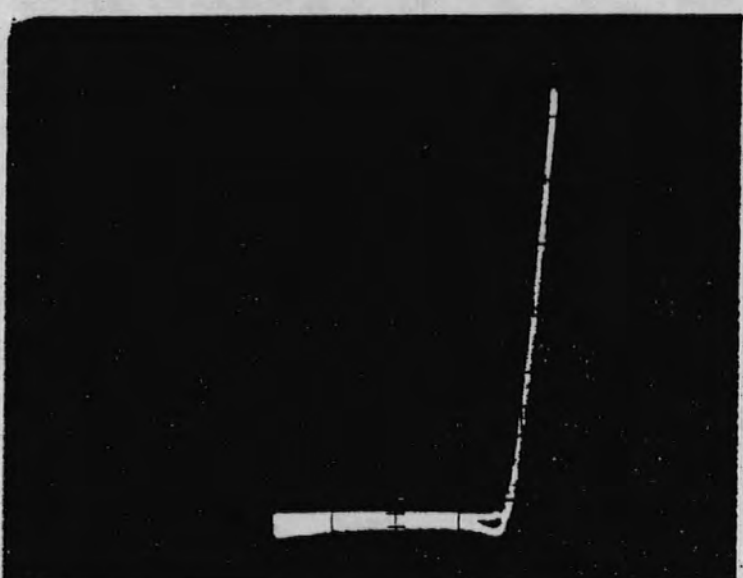

Time domain portrait
(Loop formed near turn-on voltage represents the effects of diffusion capacitance)

Peak voltage = 0.5 V
Peak current = 1.7 mA

Figure 7.19

20 kHz Replicas of 10 MHz waveforms

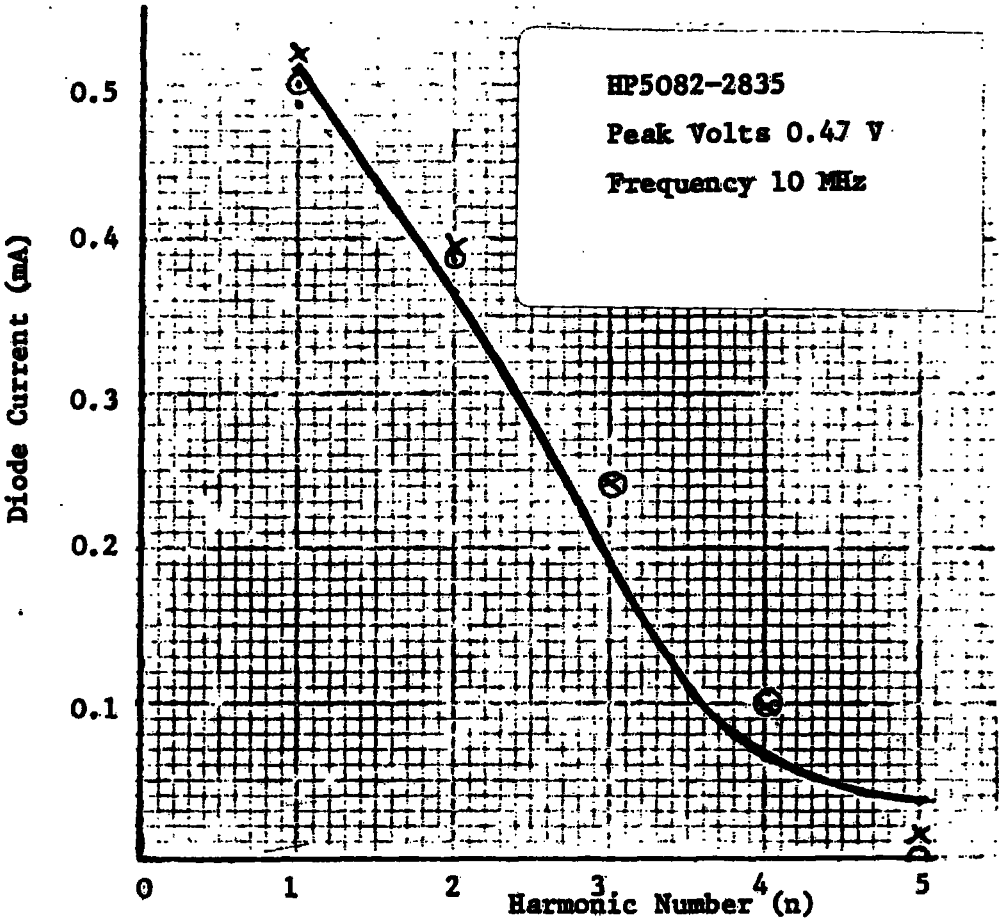

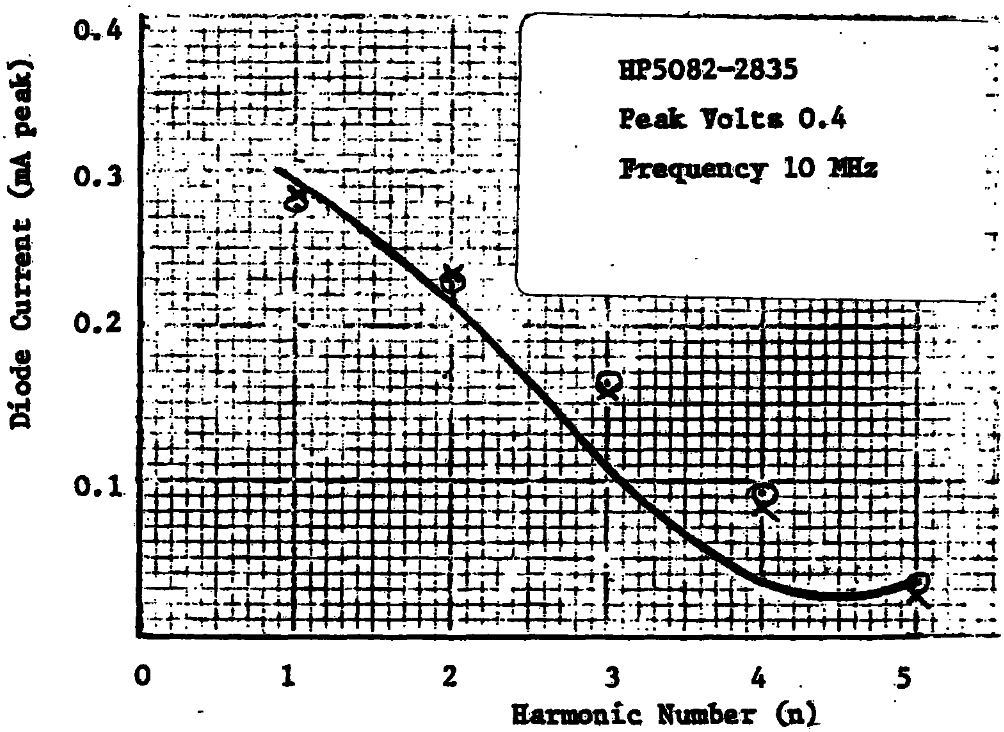

Figure 7.20

Comparison of Predicted and Measured Spectrum

——— Predicted (Bi-linear + Exponential Cusps)

⊙ Predicted (Bi-linear)

× Measured

7.6 Effect of parasitic capacitance on Lattice array of diodes

An analogue model of a lattice array of diodes was constructed and tested at 50 kHz. The diodes used were type HP 5082-2833 and from preliminary tests the diode parameters where found to be $\alpha = 36.5$, $r_s =$ 11.3 ohms and $I_s = 8 \times 10^{-10}$ amperes.

The diode current and voltage were monitored and typical waveforms are shown in Figure 7.21 for different values of parasitic capacitance which clearly indicates the nature of the predicted delay in diode conduction. Figure 7.22 gives a graphical comparison of the predicted and measured delay angle for various values of parasitic capacitance.

The harmonic content of the diode current may be predicted by assuming that the diode current is zero for angles less than the delay angle θ_c and sinusoidal for θ_c to π. The theoretical and measured harmonic components of the diode current are shown in Figure 7.23.

The harmonic spectrum of the voltage across the diodes may be obtained by integrating the expression for the capacitor current. A comparison between theoretical and measured values of harmonic components are shown in Figure 7.24.

7.7 Discussion of Results

(a) Device Identification

The results presented in section 7.2 relating to device identification by spectral response clearly indicate the feasibility of the proposed method. The incremental capacitance variation with applied voltage is obtained from a simple spectral test in a straight forward manner as compared with a tedious point by point incremental test using a Q-meter. The time varying incremental capacitance coefficients are also obtained as part of the process of determining the device characteristic which is an added advantage of the method. The difference between the two curves shown in Figure 7.2 may be due to

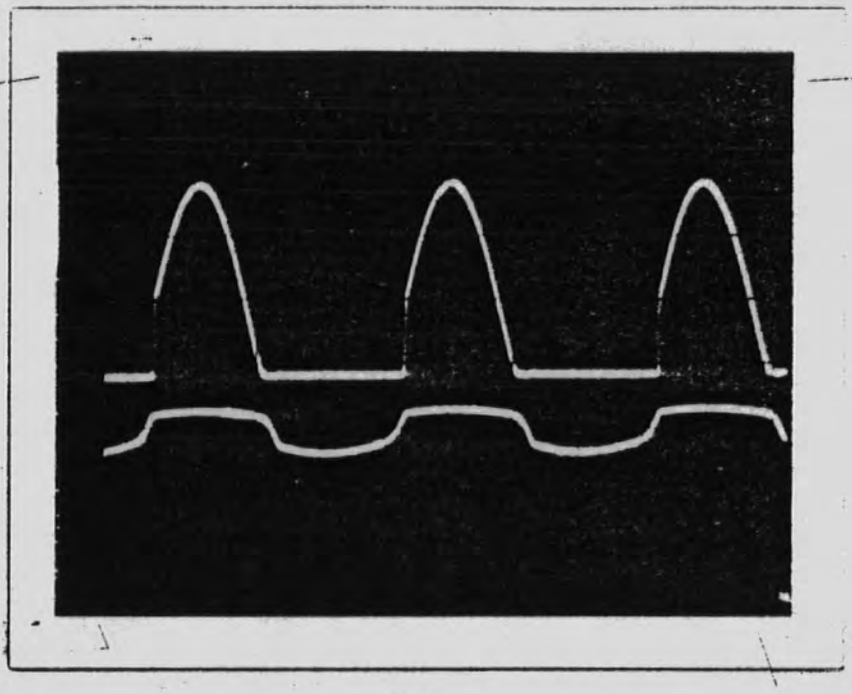

(a)

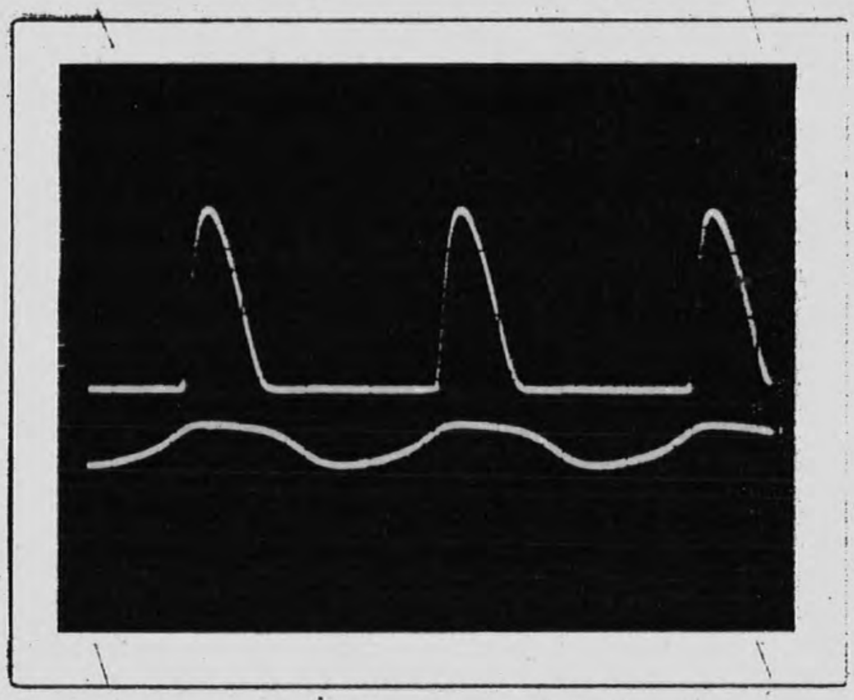

(b)

Figure 7.21

Current and Voltage waveform in Lattice array of diodes

Upper Traces are diode current

Lower Traces are diode voltage

(a) Small parasitic capacitance

(b) Larger parasitic capacitance

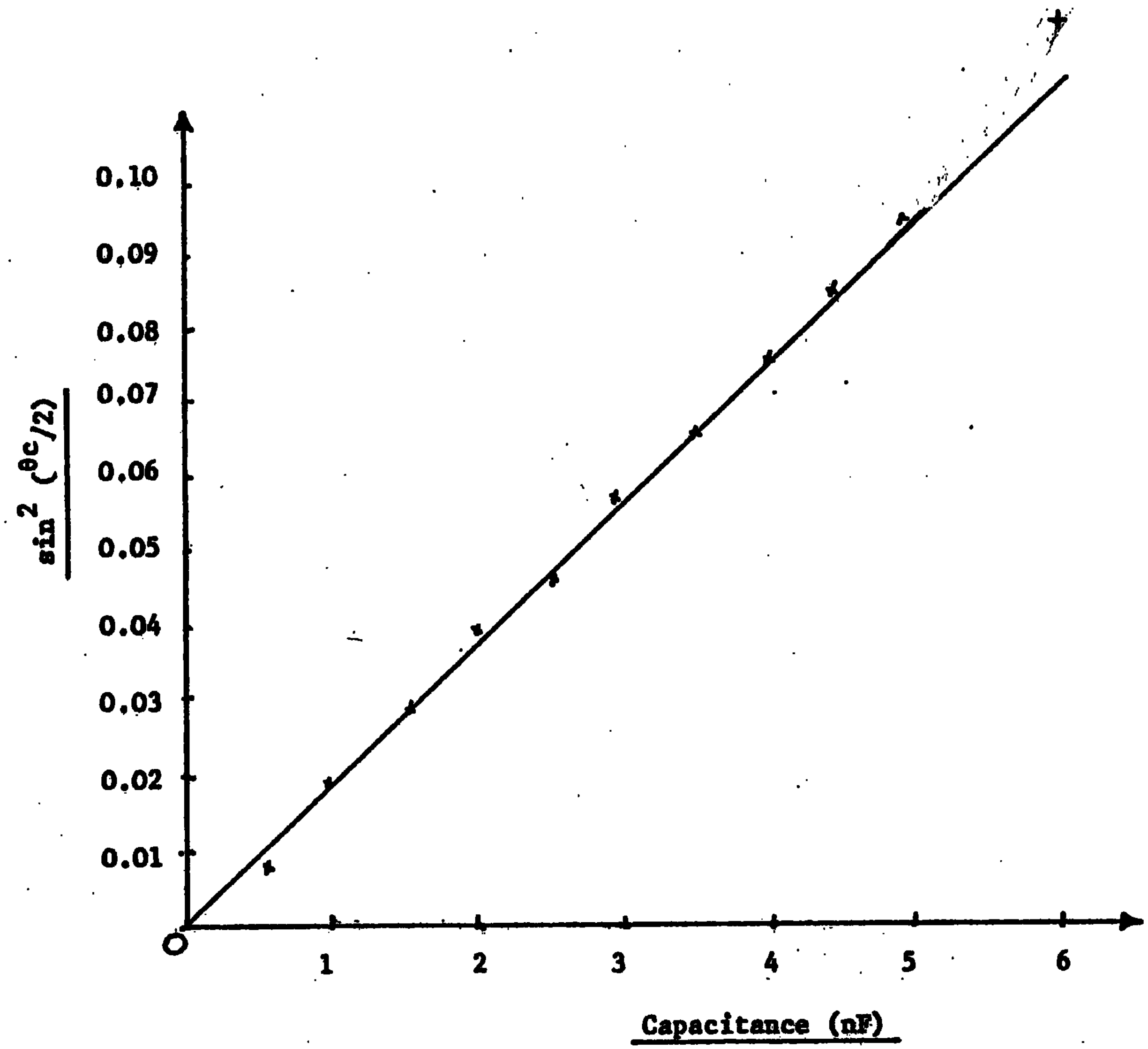

Figure 7.22 Theoretical and measured values of delay angle against diode capacitance C_e

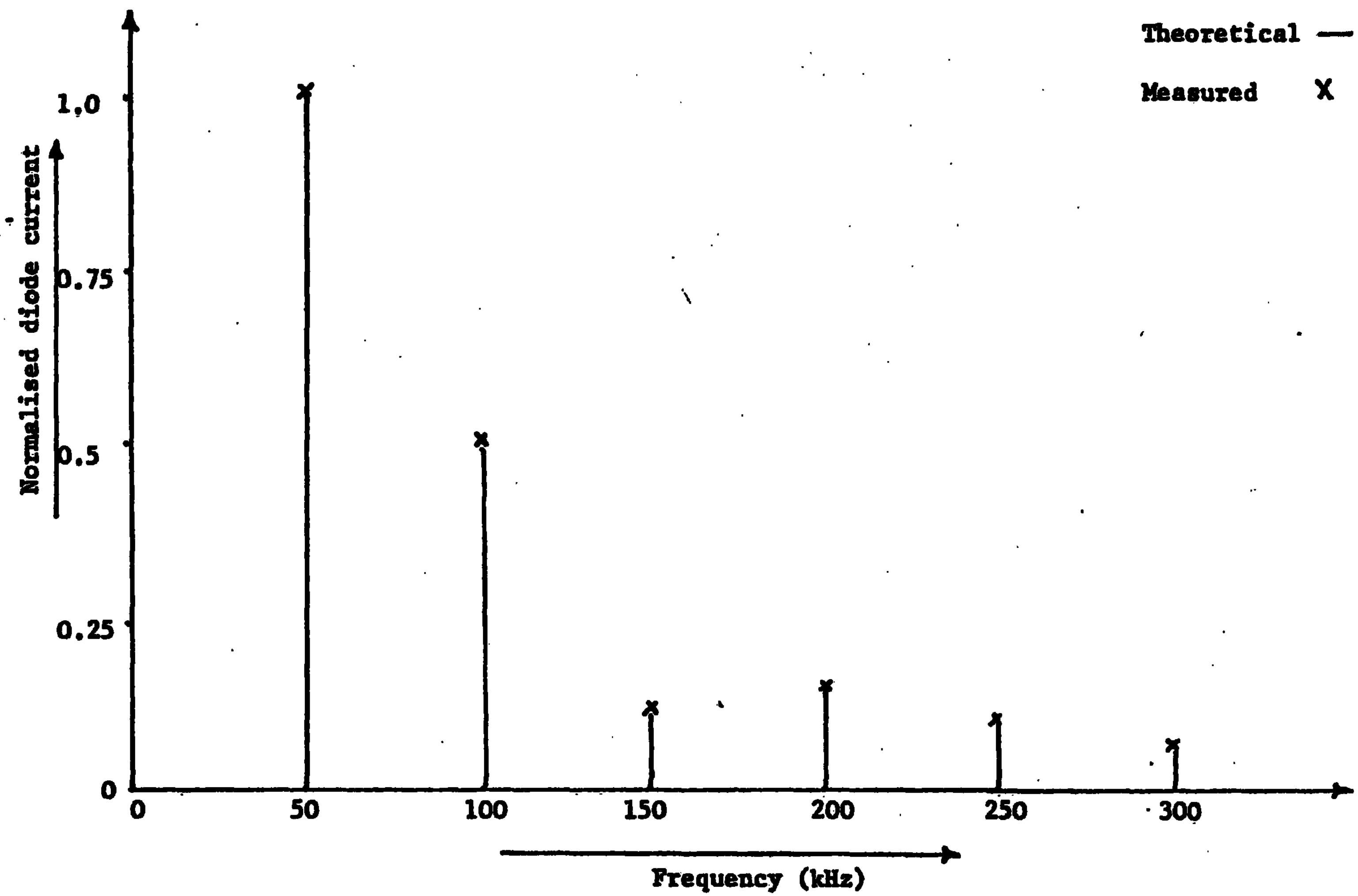

Figure 7.23 Frequency spectrum of the diode current

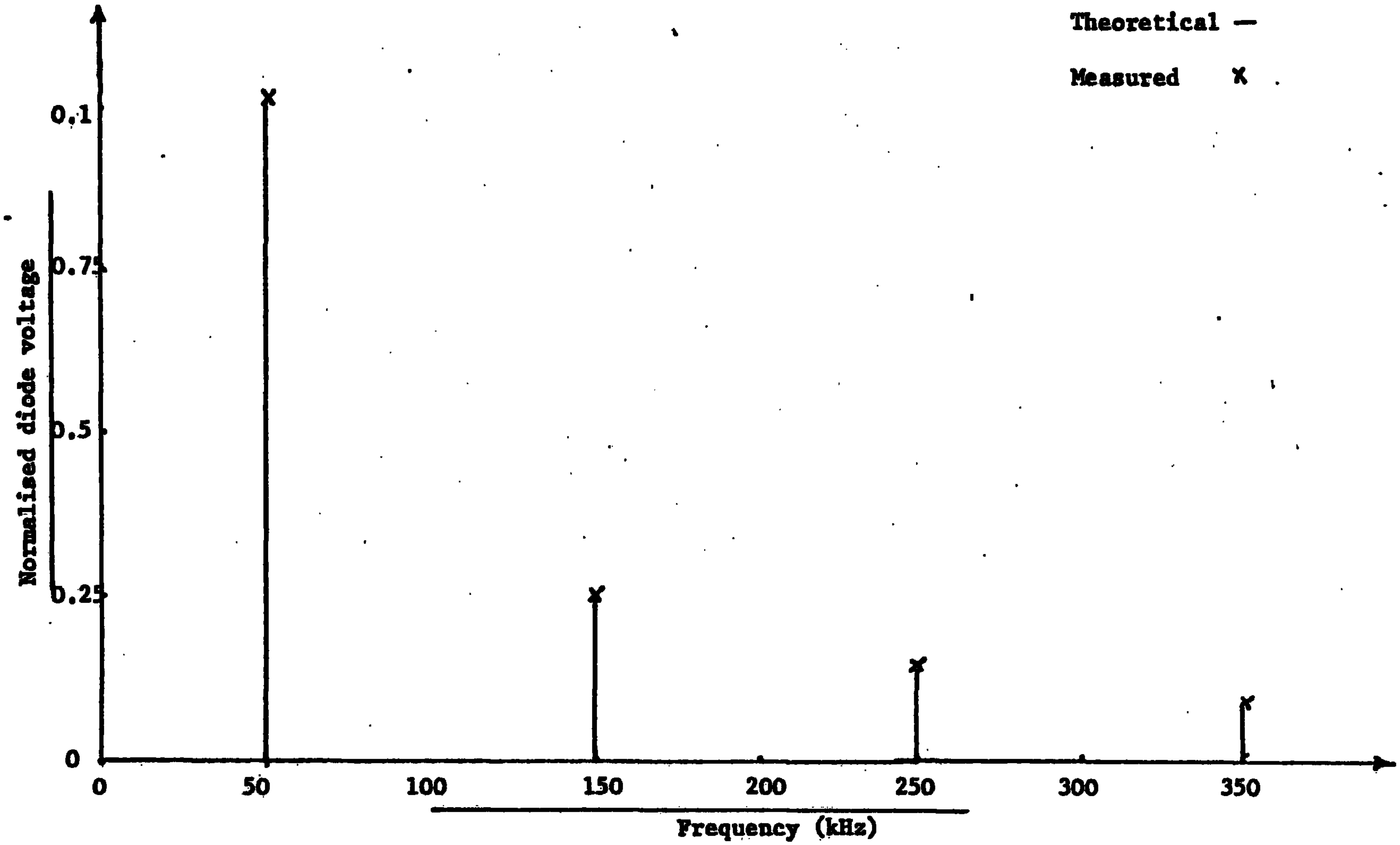

Figure 7.24 Frequency spectrum of the voltage waveform

(i) the small number of harmonics used to identify the device and,

(ii) error involved in the measurement of the harmonic components.

This measurement error compounds the basic error involved when representing a device characteristic by a polynomial of finite degree.

Thus if the device characteristic is based on the measurement of n harmonics the mathematical difference between the device characteristic and the n^{th} degree Chebyshev polynomial is approximately I_{n+1} [20] provided the harmonic components are measured with no error. If each harmonic component is subject to an addition measurement error ε_n, then the practical difference between the two curves will be $|I_{n+1}| + \sum_{1}^{N} |\varepsilon_n|$.

As explained in Chapter 2 the coefficients of the spectral response to a sinusoidal drive have importance in their own right since ratios of these test coefficients identify many of the significant parameters of frequency converting networks.

(b) Static Characteristics of Exponential Diodes

The comparisons of the measured static characteristics of the exponential diode with series resistance and the two term approximation are excellent. The solution presented in Chapter 3 will predict accurately the diode current for a wide ranges of diode parameters, series resistance and applied voltage.

The logarithmic model, introduced as a simplification of the two term approximation, introduces errors in the vicinity of the diode turn-on voltage when the translation has been established for high working voltages. This is not considered a serious deficiency in the model since it has been shown (Chapter 4, Section 4.3) that diode curvature is of decreasing importance in the spectral response with high drive voltages. For low level drive voltages the technique of fitting the logarithmic approximation at lower voltages show that the model can be chosen to match the diode curvature near the turn-on voltage (Figure 7.12 to 7.15).

The comparisons between measured and predicted waveforms (Figure 7.17) show good agreement and the transition of the diode current from a gaussian pulse to an offset sinewave is clearly evident. The major errors introduced in these results are due to :-

(i) determining the effective zero current level since the samples stored in the transient analyser are all offset and lie above zero,

(ii) identifying the sample which corresponded to the peak current level,

(c) Spectral Response of Exponential Diodes.

Consider first the situation with high drive levels (Figure 7.18a). For this condition the predicted and measured spectral response are in close agreement up to the tenth harmonic. The contributions from the exponential cusp are of the order of 0.1% of the contribution from the bi-linear segments as can be seen from the numerical print out in Appendix G5. The theoretical discussion in section 4.3 also indicates that diode curvature is of small significance for such drive levels. It may therefore be concluded, based on experimental and theoretical investigations, that diode curvature may be ignored for large drive levels.

As the drive level is reduced (Figure 7.18b) it will be seen that the bi-linear approximation is adequate up to the tenth harmonic, although slightly over-estimating the measured response. The effect of the correction due to the contribution from the exponential cusps is to reduce the predicted level to slightly below the measured results. For harmonic numbers exceeding five the cusp corrections become excessive and do not improve on the accuracy of the bi-linear model.

For lower voltage levels still (Figure 7.18c and d) the pattern of behaviour is similar but with the bi-linear contribution having increasing error. The exponential cusp corrections are in the correct direction but are too large and clearly are divergent for harmonic numbers in excess of five.

Similar remarks hold for the tests carried out at 10 MHz only in these cases it appears that the bi-linear approximation is adequate even at these low drive levels.

In concluding that the bi-linear approximation is adequate to predict the harmonic response up to the fifth harmonic it should be appreciated that an adaptive bi-linear approximation is being used. Thus the bi-linear model used for the hard drive case would be very inaccurate if used in the low drive level situation.

For low-level drives the bi-linear contributions to the spectral content are inaccurate at higher harmonic numbers and a simple corrective term is still required since the exponential cusp correction term is diverging in this region. Examination of the numerical print-outs in Appendices G5 and G6 reveal that the term responsible for the divergence of the cusp correction is the positive exponential part of the correction.

A re-examination of the equation for the positive and negative exponential cusp contributions shows that the integrands for both systems were approximated in similar ways, [Equations (4.34) and (4.46)] but whereas the negative component admitted direct integration the positive cusp component could only by approximately integrated using Laplaces method. The exact integration of the negative cusp components results in terms of the form

$$(n^2 + \beta^2\chi)^{-1}$$

appearing in the equation which prevent divergence of the expressions for large n or small χ. However, the approximate integration of the positive cusp components, gives rise to terms in n and n^2 in the expansion which will eventually dominate the magnitude of the expression as n increases. Thus the asymptotic expansion of the integral for the positive exponential cusp components becomes non-uniform for increasing harmonic number. The possibilities of obtaining a uniform expansion will be considered later.

(d) Effect of parasitic capacitance on switching of diodes in Lattice Array

The predicted and measured delay angle of conduction are in good agreement for a wide range of parasitic capacitance met in practice. The predicted harmonic components produced by the delayed conduction phenomena also agreed closely with the measured values. As explained in Chapter 5 the curvature of the diodes plays a significant role in the determination of the conduction angle. Delayed conduction in diodes with stray capacitance is an unusual effect, yet basic conceptual appreciation is readily gained by application of the bi-linear diode model, although the more refined analysis incorporating the exponential nature of the diode is necessary to obtain quantitative information.

7.8 Suggestions for Further Investigation

The concept of time varying portraits, introduced in this work as a generalisation of static characteristic, is worthy of further investigation. It is easily displayed on an oscilloscope, and as has been previously mentioned, the presence of resistive and reactive components is immediately apparent from the shape of the portrait. The possible use to select high grade components from batch production may well be a useful addition to a production line. The technique may possible extend to other areas e.g. linearity of amplifiers, identification in control systems etc.

For a linear resistive element it is trivial to show that the area under the i-v characteristic equals the average power per cycle when the device is sinusoidally excited.

For non-linear resistive elements MacFarlane[32] introduced the idea of content and co-content i.e.

$$vi = \int i dv + \int v di$$

where $\int i dv$ is the content C and $\int v di$ is the co-content Cc. Thus instantaneous power

$$p = C + Cc$$

In linear resistive systems C = Cc. In non linear resistive systems C $\neq$ Cc, whilst both C and Cc are positive quantities.

For a linear reactive element the time varying portrait will be an ellipse. Again it is trivial to show that the rectangle bounded by the ellipse which has maximum area represents four-times the peak stored energy. Extending the concept of content and co-content to reactive elements it is readily shown that the content is positive whilst the co-content is negative.

For a linear resistive-reactive system the time-varying portrait is an inclined ellipse. As pointed out in Chapter 2 these are readily separated so that a measure of device or system quality Q may be obtained from geometrical constructions on the time domain portrait.

In view of the above results is it possible to find geometrical constructions for non-linear time varying portraits which would measure average power and energy storage? The feasibility of identifying a device from its spectral response to a sinusoidal stimulus has been established. However, more experimental investigations are still necessary especially at higher frequencies where the measurement of the effects ofresistive loss on the spectrum requires evaluation. Harmonic current is detected as a voltage across a monitor resistance, and the system source will in general contain resistance. A method of "stripping" the effects of source and monitor resistance from the measured spectrum will need to be developed.

The asymptotic evaluation of the integral to obtain the spectral components due to the positive exponential cusp requires further analysis. One disadvantage of the method proposed in Chapter 4 is the assumption that $\cos n\theta$ remains dominated by the exponential decay of the other member of the integrand. Clearly for sufficiently large harmonic number n the $\cos n\theta$ term will eventually oscillate faster than the rate of decay of the exponential. This effect is possibly enhancing the degree of nonuniformity of the proposed expansion. To overcome such effects the replacement of cos $n\theta$ by exp $(-jn\theta)$, generalisation into the complex plane, and using the method of steepest descent[23] as shown in Appendix G7 results in the following.

Degree of overdrive $\sqrt{\chi} = 0$

$$a_{n+} \simeq \frac{\ln(2)}{\alpha r_m} \sqrt{\frac{2}{\pi\beta}} \exp\,(-\,n^2/2\beta)$$

Degree of overdrive $\sqrt{\chi} > 0$

$$a_{n+} \simeq \frac{2\ln(2)}{\pi\alpha r_n} \frac{\cos\,(n\theta_o + \psi)}{\sqrt{n^2 + \beta^2\chi}}$$

where $\tan\psi = n/\beta\sqrt{\chi}$

The above equations do not diverge with increasing harmonic number n. For sufficiently large β the harmonic contribution may be approximated by

$$a_{n+} = \frac{\ln(2)}{\alpha r_m}\sqrt{\frac{2}{\pi\beta}}\,(1 - \frac{n^2}{2\beta})\ , \quad \sqrt{\chi} = 0$$

which is also the limiting form of equation (4.41) used to compile Table 4.1.

CHAPTER 8

CONCLUSIONS

The theory developed in Chapter 2 and the supporting experimental results in Chapter 7 clearly indicate the feasibility of identifying a device (or system) from its spectral response to a sinusoidal drive. This new approach to non-linear spectral analysis avoids the need to develop the response waveform into its harmonic components. The method suggested is well suited to situations where the mathematical model of the device (or system) is difficult, or perhaps impossible, to ascertain. The process is easily computerised, and providing the problem of wide-band high frequency testing can be resolved, the amount of information made available is proportional to the sophistication of the supporting "software". The concept of time-varying portraits provides another view of non-linear elements. These novel concepts have not been investigated previously and some useful areas for future investigations have been indicated. The latter sections of Chapter 2 indicate that it is possible to design frequency converting systems directly from a knowledge of spectra which obviates the need for the device characteristic, i.e. parameters of the device are represented by the magnitude of specific harmonic components in the test spectrum. This approach would therefore give indications of the best device to use for specific purposes, which is of considerable value to designers and could be a criterion for device manufacturers. Just as important is the fact that system parameters (for example, input and output admittances (or impedances), transfer parameters, characteristic admittance (or impedance), loss coefficients may be identified in terms of the test spectrum.

In Chapter 3 the static characteristics of an exponential diode with series resistance were studied. The presence of resistance considerably modifies the harmonic generating properties of the diode. In this case the natural mathematical model takes the form of an implicit equation in terms of the unknown current and is an example of a situation where it was previously impossible to obtain an explicit representation of the device characteristic. However, by an application of a variation of parameter technique an explicit representation of the device is found as a functional expansion. The theoretical and practical investigations revealed that only two terms of this expansion are necessary to obtain highly accurate results over the entire practical working range of the diode. Interpretation of the form of this expansion revealed that it was possible to devise two additional diode models (the logarithmic model and the bi-linear model with exponential cusp correction). The validity of these models is adequately supported by the experimental evidence in Chapter 7. The model incorporating the exponential cusp correction is significant in the sense that the reproductive nature of the exponential function with respect to differentiation implies that the small signal incremental parameters may be obtained in the same manner as the diode spectrum.

The prediction of the spectral response of the exponential diode with series resistance has been solved and experimentally verified. A uniform expansion for the harmonic contribution of the positive exponential cusp current which is valid for large harmonic numbers has been obtained and extends the range of validity of the methods proposed in this report.

The effect of delayed conduction in lattice diode mixers is highly significant. It has been shown[25] that in the absence of capacitive effects the conversion loss and noise figure of these mixers is considerably improved when driven by an oscillator having a high output impedance. As a consequence of the prediction of delayed conduction as obtained in Chapter 5 it has been shown[27] that a compromise must be made between the need to have a high source impedance for low noise figure and a reduced source impedance to minimise the delay in diode conduction.

The new technique used to measure spectral content described in Chapter 6 has proved to be a versatile and accurate system being capable of assessing harmonic content up to frequencies of the order of 50 MHz. Again the "software" system may be readily extended to give graphical outputs of waveform and spectrum if so desired. Performance at higher frequencies may also be possible with the aid of a purpose-designed sampling unit to accomplish the alias conversion.

The results presented here are of importance in their own right as they have led to a conceptual and quantitative appreciation of factors governing the harmonic generating properties of non-linear devices. They are also a means to an end with the response to the local oscillator determined, the small signal performance must also be obtained. Therefore the manner in which the results may be applied has been indicated (i,e. equivalent circuits of multipliers, incremental conductances, and switching functions).

The philosophy adopted in the theoretical investigations has been to use techniques with strong convergence properties since the classical power series expansions converge too slowly. The application of these techniques to frequency converting circuits has clarified certain aspects of performance and opened up a number of new avenues of investigation.

REFERENCES

1. Torrey, H.C., & Whitmer, C.A., 'Crystal Rectifiers', (M.I.T. Radiation Laboratory Series), Vol. 15., New York; McGraw-Hill, 1948.
2. Kahng, D., 'Conduction Properties of the Au-n Type Si Schottky Barrier', Solid State Electron, 6, p. 281, 1963.
3. Mill, H.D., 'On the Equation $i = I_s$ (exp (V - Ri) - 1)', I.B.M. Journ, 11, pp. 553-554, 1967.
4. Katib, M.K., 'Evaluation of Harmonic Generating Properties of Schottky Barrier Diodes', Ph.D. Thesis, Durham, 1976.
5. Howson, D.P., 'Rectifier Modulators with Frequency Selective Terminations', Proc. I.E.E., Vol. 107, Part B, pp. 261-272, Jan 1960.
6. Rafuse, R.P., 'Low Noise and Dynamic Range in Synmametric Mixer Circuits', Proc. of the 1st, Biennial Cornell Conf., Pub. Cornell Univ., pp. 147-154, 1967.
7. Glover, K.J., Gardiner, J.G., & Howson, D.P., 'Double-Tuned Modulator Calculations using an Improved Diode Model', The Radio and Electronic Engineer, Vol. 42, No. 1, pp. 37-44, Jan. 1972.
8. Liechti, C.A., 'Down-Converters using Schottky Barrier Diodes', IEEE Trans., Vol. ED-17 No. 11, pp. 975-983, Nov. 1970.
9. Fleri, A.F., & Cohen, L.D., 'Non-Linear Analysis of the Schottky Barrier Mixer Diode', IEEE Trans., Vol. MTT-21, No. 1, pp. 39-43, Jan 1973.
10. Mania, L., & Stracca, G.B., 'Effect of the Diode Junction Capacitance on the Conversion Loss of Microwave Mixers', IEEE Trans., Vol. Comm-22, No. 9, pp. 1428-1435, Sep. 1974.
11. Leeson, D.B., & Weinreb, S., 'Frequency Multiplication with Non-Linear Capacitors - a Circuit Analysis', Proc. Inst. Radio Engrs., 46, p. 2076, 1959.

12. Scanlan, J.O., & Laybourn, P.J.R., 'Large Signal Analysis of Varactor Harmonic Generators without Idlers'.

13. Scanlan, J.P., & Laybourn, P.J.R., 'Analysis of Varactor Harmonic Generators with Arbitrary Drive Levels', Proc. IEEE., Vol. 14, No. 11, pp. 1598-1604, Nov. 1967.

14. Petrov, B.Y., 'Stability of Steady States of Varactor Frequency Multipliers', Radio Engineers and Electronic Physics, Vol. 21, Part 6, pp. 81-89, 1976.

15. Gardiner, J.G., & Wagiealla, M.Z., 'The Step Recovery Diode in Series Mode Harmonic Generation', Report No. 144, Postgraduate School of Electrical and Electronic Engineering, University of Bradford, March 1973.

16. Nayfeh, A., 'Perturbation Methods', John Wiley & Sons, 1973.

17. Lewis, L.T., 'Harmonic Analysis for Non-Linear Characteristics', Trans. A.I.E.E., 73, Part 1, pp. 693-699, 1954.

18. Douce, J.L., 'A Note on the Evaluation of the Response of a Non-Linear Element to Sinusoidal and Random Signals', I.E.E. Monograph No. 257M, pp. 88-91, Oct 1957.

19. Karybakus, C.A., 'A Review of the Describing Function Calculations of Double Valued Characteristics, The Inverse Problem', Int. J. Control, Vol. 17, No. 5, pp. 955-963, 1973.

20. Snyder, M.A., 'Chebyshev Methods in Numerical Approximations', Pentice Hall, 1966.

21. Holt, A.G.J., Attikouzel, J., and Chapman, R., 'Chebyshev Approximations for Distributed RC Networks', Proc. I.E.E., pp. 815-817, May 1975.

22. Kahan, W.M., 'Numerical equation Solver for any Equation f(x) = 0', Hewlett Packard Journal. pp. 20-26, December 1979.

23. Carrier, G.F., Krook, M., and Pearson, C.E., 'Functions of a Complex Variable', McGraw-Hill Inc, pp. 249-254, 1966.

24. Gradshteyn, I.S., and Ryzhik, I.M., 'Tables of Integrals Series and Products', Academic Press, 1965.

25. Rustom, S., and Howson, D.P., 'Mixer Noise Figure using an Improved Resistive Model', Int. J. Electronics, Vol. 41, 1976.

26. Stracca, G.B., 'Noise in Frequency Mixers using Non-linear Resistors', Atta Feq., Vol. 6, 1971.

27. Korolkiewivz, E., and Kulesza, B.L.J., 'Influence of Capacitance on Performance of Balanced Microwave Mixers', Electronic Letters, Vol. 17, No. 3, pp. 144-146, 1980.

28. Kulesza, B.L.J., 'General Theory of a Lattice Mixer', Proc. I.E.E. Vol. 8, No. 9, 1971.

29. Fei, F.S., and Mattauch, R.J., 'High Frequency Resistive Mixer Diode Analysis Capacitance Analysis', Proc. I.E.E.E., Vol. 64, pp. 141-143, 1976.

30. Rafuse, R.P., 'Low Noise and Dynamic Range in Symmetrical Mixer Circuits', Proc. of the 1st Bienial Conference, pp. 147-154, 1967.

31. Papoulis, A., 'Circuits and Systems', Holt, Rinehart and Winston Inc., 1980.

32. MacFarlane, A.G.J., 'Engineering System Analysis', Harrop and Co Ltd., pp. 38-44, 1964.

APPENDICES

APPENDIX A

A1. List of Publications

A2. Publications

Appendix A

Publications

Armstrong, R., 'Magnetic induction in materials of varying permeability', MSc Thesis, September 1974.

Armstrong, R., 'Magnetic effects of large currents involved in U shaped array in lengthwise graphitisation', Private report to Anglo Great Lakes Corporation, Report No. RD 144, June 1975.

Armstrong, R., 'Four terminal network theory applied to tap staggering', Int. J. Elect. Enging Educ., Vol. 14, pp. 359-363, 1977.

Armstrong, R., 'Predicting the electrical performance of arc furnaces', IEE J. Elect. Power Appl., Vol. 1, No. 3, pp. 86-90, August 1978.

Armstrong, R., Korolkiewicz, E., and Kulesza, B.L.J., 'Large signal waveforms in microwave balanced mixer with capacitance', Proc. IEE, Vol. 125, No. 8, pp. 728-729, August 1978.

Armstrong, R., and Ince, A., 'Un diagramme operatorie pour les fours a arc', Journal du four electrique and des industries electrochemîques No. 6, pp. 21-29, June-July 1979.

Armstrong, R., 'The electric arc furnace - useful teaching system', Int. J. Elect. Enging. Educ., Vol. 17, pp. 51-57, 1980.

Armstrong, R., and Kulesza, B.L.J., 'An approximate solution to the equation $x = \exp(-x/\varepsilon)$', The Bulletin of the Institute of Mathematics and Its Application. Vol. 17, No. 2/3, Feb/March 1981.

Armstrong, R., and Korolkiewicz, E., 'Application of Resonant Circuit Theory to Matching Networks', Int. J. Elect. Eng., Ed., Vol. 18, Sept 1981.

An Approximate Solution to the Equation $x = \exp(-x/\epsilon)$

R. ARMSTRONG, AFIMA
and B. L. J. KULESZA
Department of Physics and Electronics, University of Durham
Department of Electrical Engineering and Physical Electronics, Newcastle-upon-Tyne Polytechnic

A PROBLEM of importance in the analysis of resistive mixers is to determine the current flowing in an exponential diode with series resistance in terms of the applied voltage and the circuit parameters. The system is characterised by the equation

$$I = \bar{I}_s \exp(\alpha V - \alpha Ir) - I_s. \tag{1}$$

By means of the substitutions

$$x = (I + I_s)/I_s \exp(\alpha V + \alpha r I_s) \tag{2}$$

$$\varepsilon = 1/\alpha r I_s \exp(\alpha V + \alpha r I_s) \tag{3}$$

equation (1) may be transformed into its essential mathematical form of

$$x = \exp(-x/\varepsilon) \tag{4}$$

which has the equivalent inverse form of

$$x = -\varepsilon \ln(x). \tag{5}$$

Asymptotic expansions of (4) or (5) are readily obtained for large or small values of the parameter ε.

(*i*) ε large

$$x \sim 1 - \varepsilon^{-1} + \tfrac{3}{2}\varepsilon^{-2} + \ldots \quad \text{as } \varepsilon \to \infty; \tag{6}$$

(*ii*) ε small

$$x \sim \varepsilon \ln(1/\varepsilon) - \varepsilon \ln(\ln 1/\varepsilon) + \ldots \quad \text{as } \varepsilon \to 0. \tag{7}$$

We now seek a solution to equation (4) valid for all ε which is asymptotically correct for both large and small ε. To do this we first replace the exponential term by its linear approximation of $1 - x/\varepsilon$ to give

$$x \approx 1/(1 + 1/\varepsilon). \tag{8}$$

To refine the solution we assume that

$$x = f(\varepsilon)/(1 + 1/\varepsilon) \tag{9}$$

where $f(\varepsilon)$ is a slowly varying modulating function, with $f(\infty) = 1$. Substituting (9) into (5) expanding, and neglecting $\ln(f)$ we obtain

$$x = \varepsilon \ln(1 + 1/\varepsilon). \tag{10}$$

To determine a two term expansion we write

$$f = f_0(1 + z), \quad f_0 = (1 + \varepsilon)\ln(1 + 1/\varepsilon) \tag{11}$$

substitute into (9) and expand for small z to obtain

$$x = \varepsilon \ln(1 + 1/\varepsilon) - \frac{\varepsilon \ln(1 + 1/\varepsilon)}{1 + \ln(1 + 1/\varepsilon)} \ln[(1 + \varepsilon)\ln(1 + 1/\varepsilon)]. \tag{12}$$

Examination of equation (12) reveals that it has the same asymptotic forms as (6) and (7) for large and small ε. Equation (12) is shown in graphical form in Fig. 1 and compared with the exact solutions, these being obtained by assigning values to x and calculating ε. The two term expansion is thus seen to be an extremely good approximation to the exact solution.

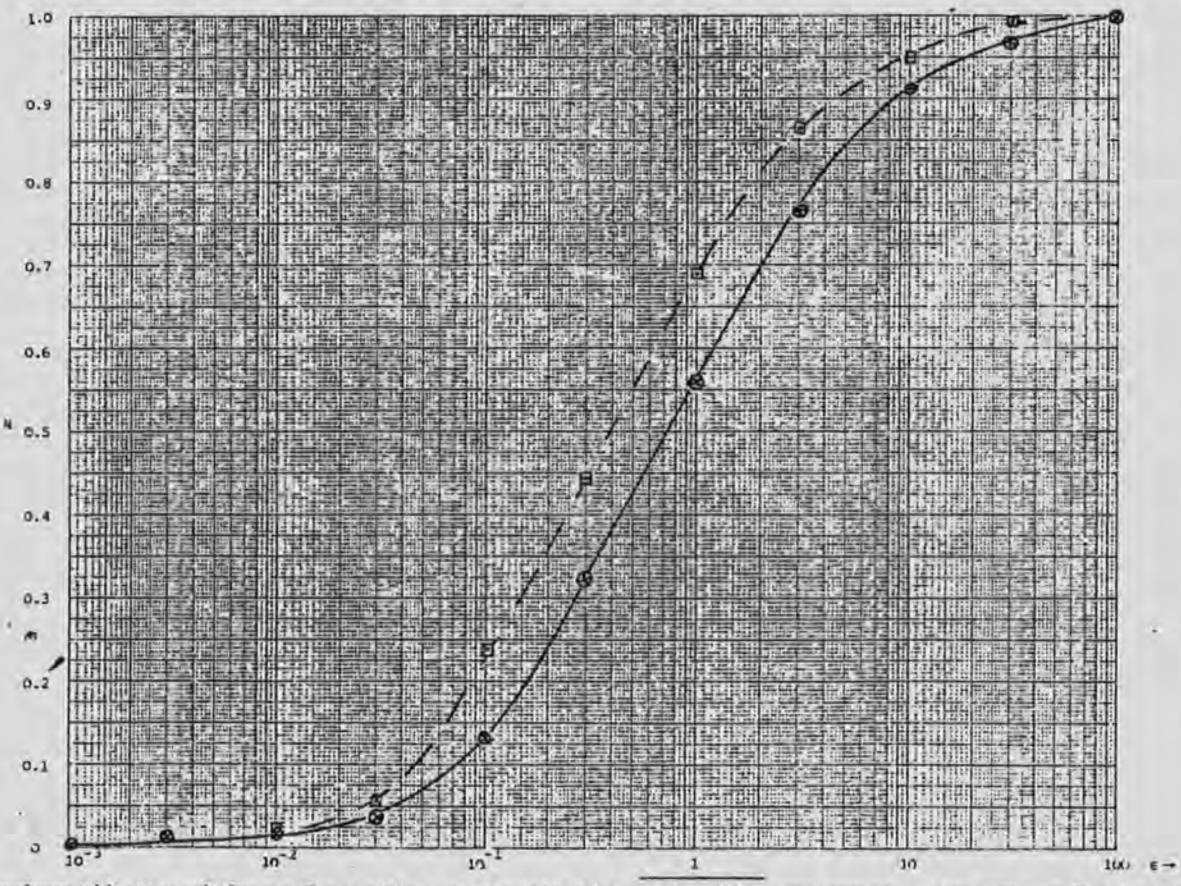

Fig. 1. Comparisons with exact solution. —⊟— — —⊟—, one term expansion; —×———×—, two term expansion; —⊖———⊖—, exact solution

LARGE SIGNAL WAVEFORMS IN A MICROWAVE BALANCED MIXER WITH CAPACITANCE

Indexing terms: Mixers (circuits), Solid-state microwave circuits

Abstract

The correspondence describes the effect of the diode capacitance on the current and voltage waveforms developed in a current-driven balanced mixer operating at microwave frequencies. It is shown that the current through the 'on' diode is a truncated halfwave sinewave, the angle of truncation being a function of the diode capacitance, drive level and the diode incremental resistance at the origin. The closed-form solution for the angle of truncation provides valuable insight into the deterioration in performance of balanced mixers at microwave frequencies owing to diode parasitic capacitance.

Introduction

A large variety of balanced mixers are available in integrated circuit form with operating frequency ranges of the order of 100 MHz. At microwave frequencies, however, the 2-diode balanced and the 4-diode double-balanced mixers are still inevitably used. These two mixer circuits have been comprehensively analysed in many publications assuming that the current through each diode is sinusoidal during conduction. At low frequencies this assumption is valid, but at microwave frequencies the diode parasitic capacitance considerably alters the large signal waveform, in that the current waveform through the 'on' diode is a truncated halfwave rectified sinewave, as shown in Fig. 1. This effect of the diode capacitance has not been observed and analysed in any literature relating to mixer performance. Experimental results using a low-frequency model are found to be in good agreement with the theoretical predictions. A Fourier analysis on the diode current waveform shown in Fig. 1 and the resulting voltage waveform developed across each diode also shows good correlation with the practical results.

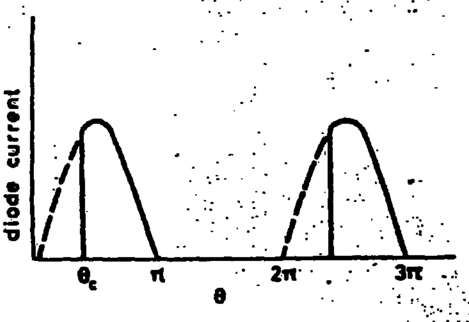

Fig. 1
Truncated half-wave rectified sinewave

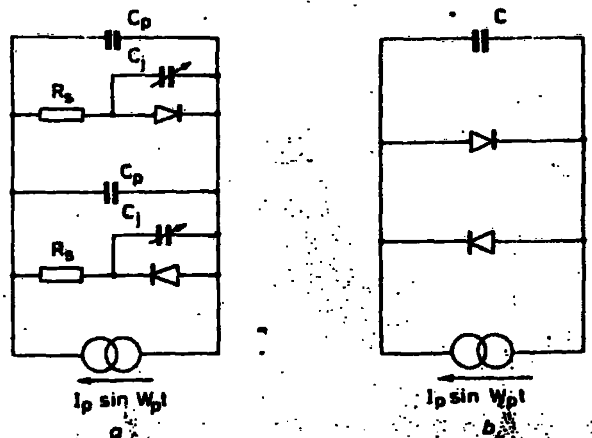

Fig. 2
Equivalent circuits of the mixer as seen by the local-oscillator current drive

Analysis

The circuit including the diode parasitics seen by the local-oscillator current drive for a balanced 2-diode mixer is shown in Fig. 2*a*. This circuit is also valid for a 4-diode double-balanced mixer if each diode shown in Fig. 2*a* represents the appropriate two diodes in parallel. Experimental investigations indicated that a 100% change in the value of the diode series resistance R_s did not significantly affect the current waveform and hence its effect has been neglected in the analysis. It has been shown[1,2] that the diode junction capacitance C_j can be approximated by a constant value given by

$$C_j \approx C(0) \approx [C_{j_{max}} - C_{j_{min}}]/2 \tag{1}$$

where $C(0)$ is the value of C_j at zero voltage. The effective total capacitance across the diodes is therefore

$$C = 4C_p + 2C_j \quad \text{(double-balanced mixer)}$$

or

$$C = 2C_p + C_j \quad \text{(balanced mixer)}, \tag{2}$$

where C_p is the diode package capacitance.

The equivalent circuit to be analysed therefore reduces to that shown in Fig. 2*b* and is governed by the following differential equation:

$$\frac{CdV}{dt} + nI_s\left[\exp(\alpha V) - \exp(-\alpha V)\right] = I_p \sin \omega_p t, \tag{3}$$

where $\alpha = q/KT$, I_s is the diode saturation current and $n = 2$ for a double-balanced mixer or $n = 1$ for a balanced mixer. It is convenient at this stage to introduce the following normalised parameters:

$$\theta = \omega_p t, \tag{4a}$$

$$K = nI_s/I_p \tag{4b}$$

$$\epsilon = \omega_p C/\alpha I_p = \omega_p C r_b K/n \tag{4c}$$

where

$$r_b = \left.\frac{dV}{dI}\right|_{I=0} = \frac{1}{\alpha I_s}$$

Substituting the normalised parameters of eqn. 4 and a new variable defined by

$$y = K\exp(\alpha V) \tag{5}$$

eqn. 3 becomes

$$\epsilon\frac{dy}{d\theta} + y^2 - K^2 = y \sin\theta \tag{6}$$

The analytical solution to this nonlinear differential equation is difficult, but an approximate expression for the angle of truncation θ_e can be obtained by solving eqn. 6 in two regions:

$$K^2 \ll y^2$$

and

$$y^2 \ll K^2$$

and matching these two solutions to satisfy the condition of periodicity for y. The condition $K^2 \ll y^2$ corresponds to the part of the cycle when the diode is fully conducting and therefore the diode current is much greater than I_s. On the other hand, when the diode is in the reverse biased region the condition $y^2 \ll K^2$ is applicable. The angle of truncation θ_e is then given by

$$\sin^2(\theta_e/2) = \frac{\epsilon}{2}\log\{\exp[(2\epsilon/\pi)^{1/2}/K^2]\} \tag{7}$$

Eqn. 7 may be further simplified for a practical diode to

$$\sin^2(\theta_e/2) \simeq A\epsilon/2 \tag{8}$$

where A represents the logarithmic term in eqn. 7 and can be regarded as a constant since it varies slowly for large changes in ϵ.

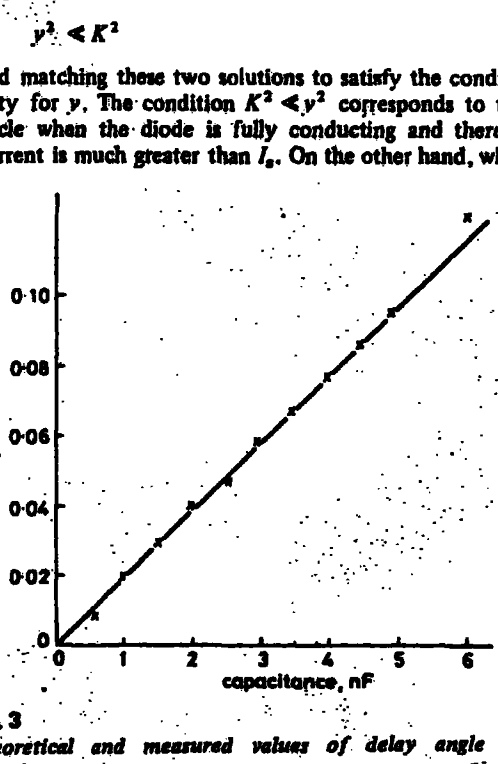

Fig. 3
Theoretical and measured values of delay angle against diode capacitance

x measured results
— theoretical results

Experimental results

A low-frequency equivalent circuit, shown in Fig. 2*b*, was constructed using Schottky barrier diodes. A test frequency of 50 kHz was chosen so that the inherent capacitive effect of the diodes was negligible. The high-frequency performance of the diodes was simulated by an external capacitor. The magnitude of this capacitor was determined by scaling a typical parasitic capacitive value in the ratio of working frequency (1 GHz) to the test frequency. Preliminary tests carried out on the diodes (type HP 2833) indicated that $I_s = 8 \times 10^{-7}$ A and $r_b = 3{\cdot}4 \times 10^7\,\Omega$. The current drive was adjusted so that the normalised current-drive factor K was 7×10^{-7}.

Fig. 3 shows a comparison of the theoretical values of θ_e with measured values for varying values of capacitance. The divergence between the theoretical and practical results for large values of capacitance may be explained by the fact that the assumption of a sharp turn on of the diode current is no longer valid in that region. The effect of the truncated angle θ_e on the frequency spectrum of the diode current and voltage was also found to be in close agreement with the measured results.

Conclusion

Saleh[3] has shown that the optimum performance of a balanced mixer in the absence of the diode parasitics is obtained when the time varying resistance $r(t)$ of the pumped diodes is a square wave. The diode capacitance in the case of practical microwave balanced mixer causes the current waveform to be truncated and hence the suggested optimum performance can never be practically obtained.

Acknowledgments

The authors wish to gratefully acknowledge the valuable assistance given by Prof. P.H. Roberts, Department of Mathematics, University of Newcastle upon Tyne.

1st March 1978

R. ARMSTRONG
E. KOROLKIEWICZ

Department of Electrical & Electronic Engineering
Newcastle upon Tyne Polytechnic
Ellison Building
Ellison Place
Newcastle upon Tyne NE7 8ST
England

B.L.J. KULESZA

Department of Physics & Electronics
University of Durham
South Road
Durham DH1 3LE
England

References

1 FEI, F.S., and MATTAUCH, R.J.: 'High frequency resistive mixer diode capacitance analysis', *Proc. IEEE*, 1976, 64, pp. 141–143
2 RAFUSE, R.P.: 'Low noise and dynamic range in symmetric mixer circuits'. Proceedings of the 1st Biennial Cornell conference, 1967, pp. 147–154
3 SALEH, A.A.M.: 'Theory of resistance mixers' (MIT Press, 1971), pp. 54–55

SPTC124E

Predicting the electrical performance of arc furnaces

R. Armstrong

Indexing term: Arc furnaces

Abstract: The paper develops a method of predicting the electrical performance of arc furnaces. The technique is based on a power chart derived from an equivalent phasor diagram. Comparisons with other methods of prediction and with practical observations are made. An approximate form of the operating chart is also presented which is applicable to systems having a low resistance/reactance ratio.

List of principal symbols

E_a = level of arc voltage
V_s, V_a = r.m.s. values of supply voltage and fundamental component of arc voltage
e_1, e_2, e_3 = instantaneous values of arc voltages
v_1, v_2, v_3 = instantaneous values of supply voltages
i_1, i_2, i_3 = instantaneous values of supply currents
R = system resistance
X = system reactance
ϕ = intrinsic phase difference between V_s and V_a
δ = system angle $\tan^{-1}(R/X)$
ρ = radius of normalised operating circle
S = apparent power
P = power
Q = reactive power
subscript b refers to base values

1 Introduction

The electric arc furnace is at present the most efficient way of producing special-alloy steels in quantities required to meet the needs of industry. In these times when great emphasis is placed on the conservation of energy, it is imperative that the energy consumed by arc furnaces is fully utilised. This requires a method of accurately predicting the electrical performance which can easily be applied by personnel responsible for arc-furnace operations.

A number of manufacturers have installed arc furnaces to augment their supply of these special-alloy steels. In such instances the production engineer in charge of the furnace usually has a metallurgical background, yet is required to make decisions regarding the electrical performance of the furnace. Again there is a need for a method to assist him in his decisions.

This paper outlines a method of predicting the electrical performance of arc furnaces. The method is based on an equivalent phasor diagram, the derivation of which highlights some of the salient features of the system. The power chart, derived from the phasor diagram, can be used without resorting to the underlying theory and has the added advantage that variations in all the quantities involved can be visualised.

Paper T223 P, received 30th May 1978

Mr. Armstrong is with the Department of Electrical & Electronic Engineering, Newcastle upon Tyne Polytechnic, Ellison Building, Ellison Place, Newcastle upon Tyne NE1 8ST, England

2 The arc furnace power diagram

In order the analyse the behaviour of an electric arc furnace system we make the following assumptions:

(*a*) The 3-phase supply to the furnace is balanced and sinusoidal.

(*b*) The phases of the arc furnace system are electrically balanced.

(*c*) The voltage developed across each arc is constant during conduction at level E_a and reverses each half cycle.

(*d*) The arcs fire symmetrically with 120° phase displacement.

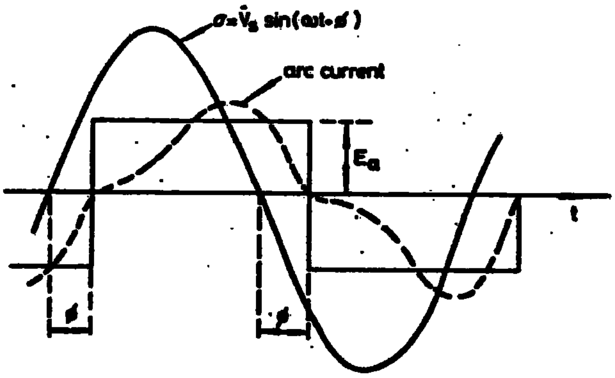

Fig. 1 *Typical voltage and current waveforms*

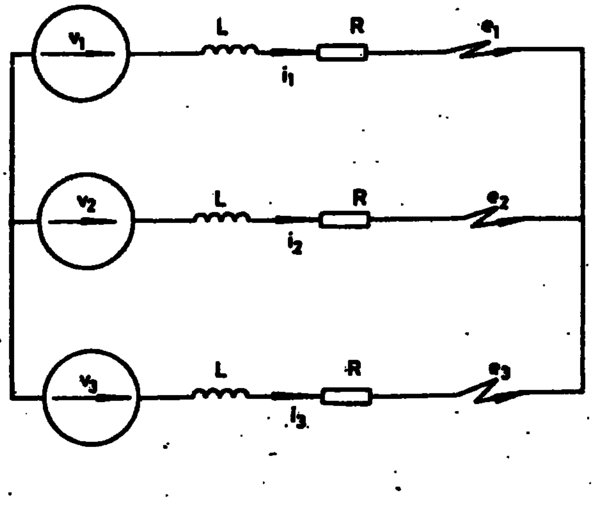

Fig. 2 *Equivalent circuit of a 3-phase arc furnace*

0140–1327/78/223P–0086 $1·50/0

The arcs can only be maintained when the applied voltage is in excess of the level E_a consequently there is an inherent phase delay ϕ between the supply and arc voltages as shown in Fig. 1. The equivalent circuit of a 3-phase arc furnace is shown in Fig. 2 and the solution of the differential equation of the system is shown in Appendix 8.1, from which it will be seen that for stable arcs (arcs which conduct for a full half cycle) the following condition must be satisfied:

$$\cos(\phi + \delta) = V_a/2\rho(R/X)V_s \qquad (1)$$

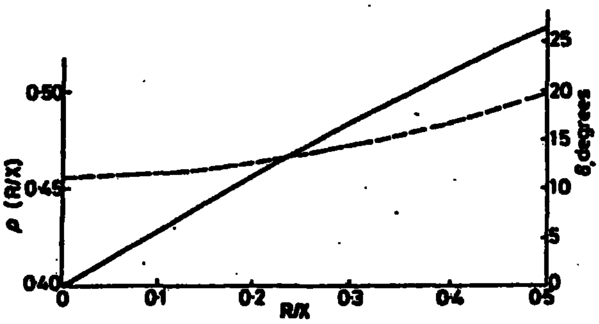

Fig. 3 *Variation of ρ and δ with system parameters*

——— ρ
——— δ

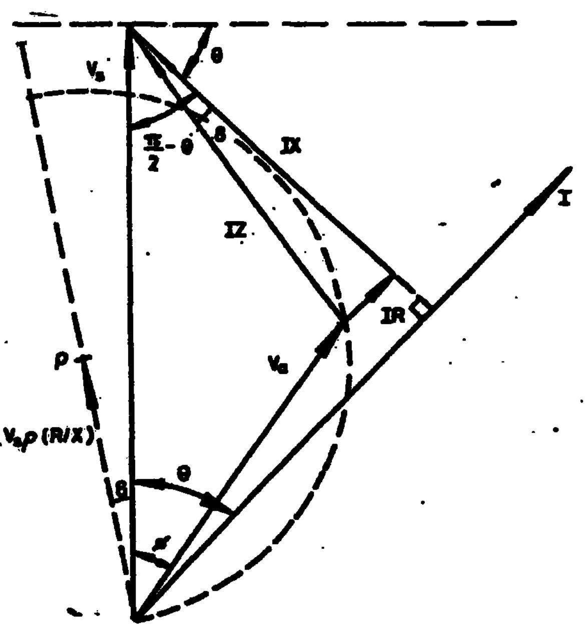

Fig. 4 *Equivalent phasor diagram for a 3-phase arc furnace*

The variation in system angle δ and the function ρ for different values of R/X are shown in Fig. 3, and, for given values of R/X and V_s, eqn. 1 represents a semicircle of radius $\rho(R/X)V_s$ inclined to the vertical axis by the angle δ as shown in Fig. 4, the centre of the semicircle being at point P. Also shown in Fig. 4 are the resistance and reactance voltage drops. The complete Figure is, in fact, the phasor diagram representing the relationships between the fundamental components of the various voltages and currents existing in the system.

The power diagram indicated in Fig. 5 is obtained by multiplying all sides of the V_s, V_a, IZ triangle by V_s/Z, and rotating through an angle δ. The diagram can be made universal by dividing all sides of the triangle by a base MVA, defined by

$$S_b = V_b I_b \qquad (2)$$

where the base voltage V_b is taken as the phase value of the furnace supply voltage and the base current given by

$$I_b = V_b/Z \qquad (3)$$

In the normalised diagram the radius of the operating circle is $\rho(R/X)$. The stable region of the diagram is to the right of the line indicating the theoretical limit of instability which is shown in Appendix 8.2 to be

$$\phi_c = \tan^{-1}\left\{\frac{(\rho\pi\cos\delta)/3}{1 + (\rho\pi\sin\delta)/3}\right\} \qquad (4)$$

If required, other limits of operation may be superimposed on the diagram, e.g. the transformer rating and the maximum allowable arc voltage.

For systems whose R/X ratio is less than 0·2, which is typical for systems fed direct from the 275 kV system, an interesting approximation is possible. We first observe from Fig. 3 that the radius of the operating circle is 0·46 and the centre of the circle is almost on the Q axis. Considering now the case where R is zero, the radius of the circle is 0·456 and the centre lies on the Q axis. These two circles are approximately coincident; the second circle may be regarded as the first circle rotated through an angle. This allows an approximate power chart to be drawn, assuming R to be zero, as shown in Fig. 6 where the arc power loci have been superimposed.

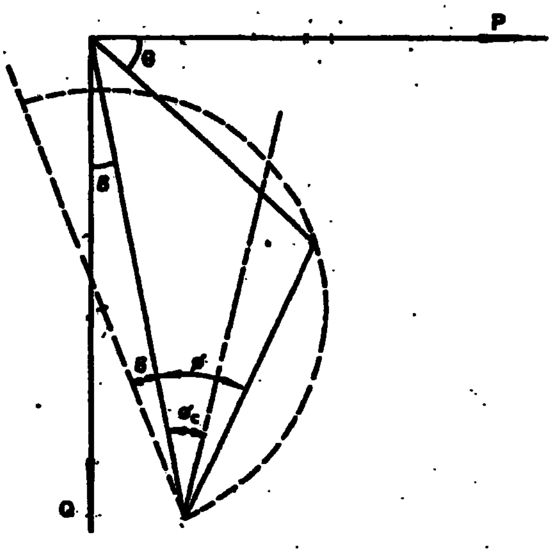

Fig. 5 *Power chart for a 3-phase arc furnace*

3 Comparisons with other methods of prediction

To illustrate the use of the power chart a specimen calculation is shown below, the appropriate power chart being shown in Fig. 7. The example is relevant to a system published by Freeman and Medley[1] and a comparison with their results is illustrated in Fig. 8.

3.1 Specimen calculation

System $Z = (456 + j2772) \times 10^{-6}\,\Omega$

$Z = 2809 \times 10^{-6}\,\Omega$

Base voltage $V_b = 525/\sqrt{3} = 303$ V

Base current $I_b = V_b/Z = 303 \times 10^6/2809 = 108$ kA

Base MVA/phase $S_b = V_b I_b = 303 \times 108 = 33$ MVA/ph

$R/X = 456/2772 = 0{\cdot}1645$

From Fig. 3 $\delta = 9{\cdot}34$ degrees

$p(R/Z) = 0{\cdot}46$

The normalised arc power P_a is determined by subtracting the normalised I^2R loss from the total input power.

Comparisons were also made with results published by Paschkis and Persson[2] for a system with a R/X ratio of 0·24. This is desirable since Freeman and Medley based their calculations on the concept of an operational reactance, whereas the results of Paschkis and Persson are based on a square-wave arc voltage and include the effects of harmonics in the current waveform. This comparison is indicated in Fig. 9.

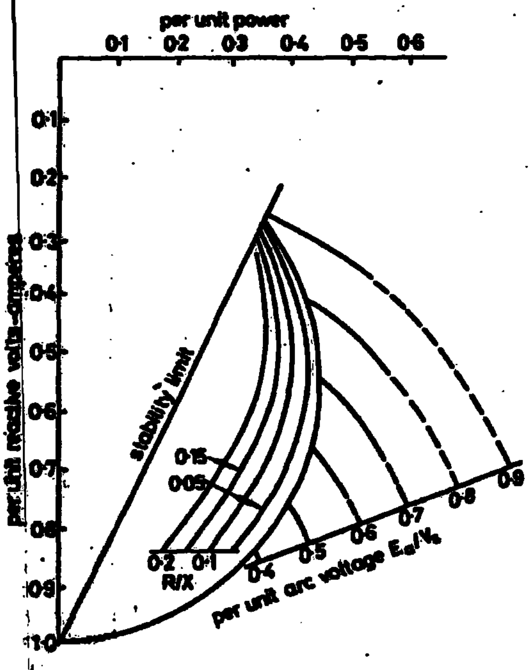

Fig. 6 *Approximate power chart*

4 Comparison with practical results

The chart was also used to predict the performance of a 150 ton, 50 MVA arc furnace, and the results so obtained compared with measured operating conditions. A summary of the comparison is given in Table 1 where the power and MVA are 3-phase values.

Table 1: Comparison with practical results

Tap voltage	predicted			measured		
	P	MVA	p.f.	P	MVA	p.f.
550	44·2	60·4	0·743	46·8	60·3	0·711
525	43	64	0·682	45·3	62·4	0·658
475	36·8	55·8	0·656	37	56	0·59
425	29·3	40·4	0·719	32·5	41·3	0·744
375	28·6	39·7	0·725	26·6	33·3	0·762
325	18·25	25·9	0·707	19·3	25·8	0·725
275	12·86	17·9	0·725	13·8	18·0	0·746
200	7·34	10·63	0·68	7·5	11·2	0·68

5 Conclusions

The results of Freeman and Medley fall off more rapidly than those produced from the chart for high levels of arc current. Their calculations are based on the concept of an operating reactance which is 15% greater than the short circuit reactance. The difference in the two sets of results at high current levels is probably because the operating reactance is dependent on current level and not strictly constant.

Comparison with the results of Paschkis and Persson show that the values obtained from the chart are lower for high current levels. This is because the operating chart does not include the effects of harmonic components of currents which will become more significant at high levels of current.

The operating chart therefore gives results which are comparable with other published results over the lower range of arc currents and are intermediate for higher current levels.

The results shown in Table 1 indicate that the operating chart gives excellent predictions of actual operation. When using the chart in practice it would be more convenient to scale the diagram in actual power levels. Having selected a particular tap voltage the arc-voltage level is marked on the operating circle. Since the arc voltage varies with slag basicity[3] better results will be achieved by using measured values of arc voltage rather than values computed from arc length. For a given furnace installation with a known R/X ratio the arc-power curve can also be drawn on the diagram giving immediate indication of arc power.

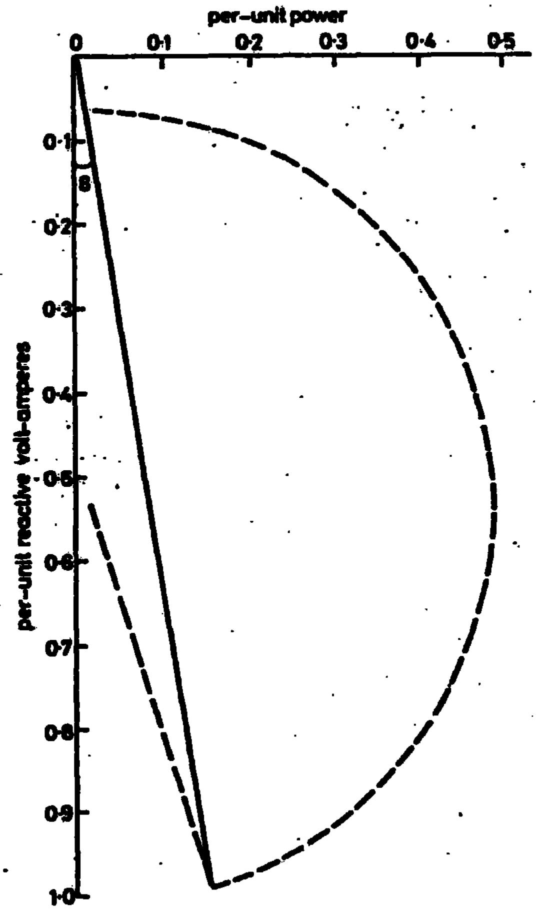

Fig. 7 *Power chart for system discussed in Section 3*

6 Acknowledgment

I wish to acknowledge advice and help given by A. Ince of Anglo Great Lakes Corporation and also the help of Round Oak Steelworks, Brierly Hill.

7 References

1 FREEMAN, E.R., and MEDLEY, J.E.: 'Efficient use of power in electric arc furnaces', *IEE J. Electr. Power Appl.*, 1978, 1, pp. 17–24

2 PASCHKIS, V., and PERSSON, J.: 'Industrial electric furnaces and appliances' (Interscience, 1960) p. 220

3 PIROZHNIKON, V.E.: 'Effects of slag on thermal process in electric furnaces', *Stal*, March 1967, pp. 222–224

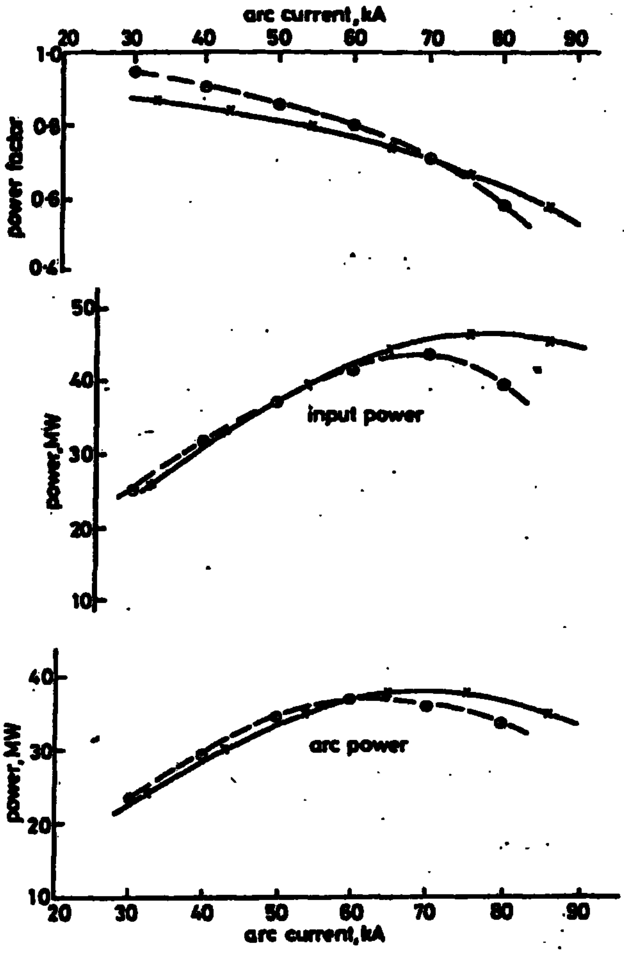

Fig. 8 *Comparison of results*

–x–x– operating chart
–o–o– Freeman and Medley

8 Appendixes

8.1 Determination of the phase angle ϕ

Let D be the differential operator defined by

$$D(\cdot) = \left(L\frac{d}{dt}+R\right)(\cdot) \tag{5}$$

then the system shown in Fig. 2 is governed by

$$v_1 - e_1 + e_2 - v_2 = Di_1 - Di_2 \tag{6}$$

$$v_2 - e_2 + e_3 - v_3 = Di_2 - Di_3 \tag{7}$$

$$i_1 = -(i_2 + i_3) \tag{8}$$

where e_1, e_2, and e_3 represent the square-wave arc voltages each displaced by 120° in accordance with assumption (*a*).

Eliminating v_2, v_3, i_2 and i_3 we see that i_1 is governed by

$$Di_1 = v_1 - \frac{2}{3}\left(e_1 - \frac{e_2+e_3}{2}\right) \tag{9}$$

Since the arc current can only be maintained providing the applied voltage exceeds the level E_a then a phase shift ϕ must exist between v_1 and e_1 and to include this effect in the analysis we write

$$v_1 = \hat{V}_s \sin(\omega t + \phi) \tag{10}$$

The equivalent arc voltage on the left-hand side of eqn. 9 is discontinuous and the current i_1 is given below for the time intervals indicated:

$$i_1 = A_1 \exp(-\omega t R/X) + \frac{\hat{V}_s}{Z}\sin(\omega t + \phi - \alpha) - \frac{2}{3}\frac{E_a}{R}$$

$$0 < \omega t < \pi/3$$

$$= A_2 \exp(-\omega t R/X) + \frac{\hat{V}_s}{Z}\sin(\omega t + \phi - \alpha) - \frac{4}{3}\frac{E_a}{R}$$

$$\pi/3 < \omega t < 2\pi/3$$

$$= A_3 \exp(-\omega t R/X) + \frac{\hat{V}_s}{Z}\sin(\omega t + \phi + \alpha) - \frac{2}{3}\frac{E_a}{R}$$

$$2\pi/3 < \omega t < \pi \tag{11}$$

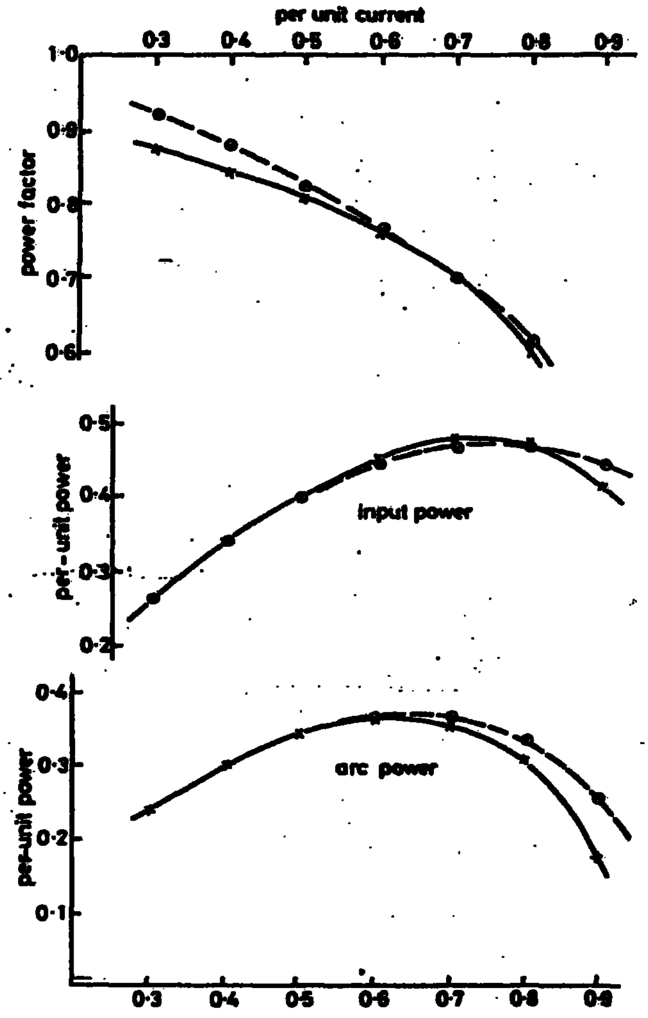

Fig. 9 *Comparison of results*

–x–x– operating chart
–o–o– Paschkis and Persson

In the above equation there are four unknowns, namely A_1, A_2, A_3 and ϕ. Eliminating A_2 and A_3 and using the condition that i_1 is zero at $\omega t = 0$ and $\omega t = \pi$ we find that ϕ must satisfy the condition

$$\frac{\hat{V}_s}{Z}\sin(\phi-\alpha) = 2\frac{E_a}{3R}\left(\frac{1-x^2}{1-x+x^2}\right) \qquad (12)$$

where

$$\alpha = \tan^{-1}(X/R)$$

and

$$x = \exp(\pi R/3X).$$

By putting $\alpha = (\pi/2-\delta)$ and rearranging we find that

$$\cos(\phi+\delta) = \frac{2E_a}{3\hat{V}_s}\frac{\sqrt{1+R^2/X^2}}{R/X}\;\frac{x^2-1}{x^2-x+1} \qquad (13)$$

The above equation can be expressed in terms of the r.m.s. level of the supply voltage and the r.m.s. level of the fundamental component of the square-wave arc voltage to obtain

$$\cos(\phi+\delta) = V_a/2\rho(R/X)V_s \qquad (14)$$

where the function $\rho(R/X)$ is given by

$$\rho(R/X) = \frac{3}{\pi}\frac{R/X}{\sqrt{1+R^2/X^2}}\left(\frac{x^2-x+1}{x^2-1}\right)$$

$$x = \exp(\pi R/3X) \qquad (15)$$

Eqn. 14 defines a semicircle of radius $\rho(R/X)$ where V_a/V_s is the normalised arc voltage. As a special case we observe that as R tends to zero then

$$\rho = 9/2\pi^2 \approx 0{\cdot}45 \qquad (16)$$

and

$$\cos\phi = \pi^2 V_a/(9V_s) \approx V_a/(0{\cdot}9V_s) \qquad (17)$$

With the phase shift between V_s and E_a established, the r.m.s. level of the fundamental component of the arc voltage can be used to determine the fundamental component of current.

8.2 Arc stability

At $t = 0$, the rate of change of the arc current must be greater than zero for the arc to establish. If di/dt is negative at $t = 0_+$ then the arc current is attempting to flow in a negative direction whilst the arc voltage is positive which is not possible.

In the region $0 < \omega t < \pi/3$ the current is characterised by

$$\frac{di_1}{dt}+\frac{Ri}{L}1 = \frac{\hat{V}_s}{L}\sin(\omega t+\phi)-\frac{2}{3}\frac{E_a}{L}. \qquad (18)$$

At $t = 0$, $i_1 = 0$ and the onset of arc instability is given by $di/dt = 0$ and the above equation indicates that the critical angle ϕ_c is given by

$$\sin\phi_c = \frac{2}{3}\frac{E_a}{\hat{V}_s} = \frac{\pi}{6}\frac{V_a}{V_s} \qquad (19)$$

But also

$$\cos(\phi_c+\delta) = V_a/2\rho V_s \qquad (20)$$

and therefore

$$\sin\phi_c = \frac{\pi}{3}\rho(R/X)\cos(\phi_c+\delta) \qquad (21)$$

which has solution

$$\phi_c = \tan^{-1}\frac{\rho\pi\cos\delta/3}{1+\pi\rho\sin\delta/3} \qquad (22)$$

whilst the limiting value of ϕ_c as R tends to zero is

$$\phi_c = \tan^{-1}(3/2\pi) \qquad (23)$$

Examination of the expression for the critical angle reveals that the presence of resistance improves arc stability.

Int. J. Elect. Enging Educ., Vol. 17, pp. 51–57. Manchester U.P., 1980. Printed in Great Britain

THE ELECTRIC ARC FURNACE — A USEFUL TEACHING SYSTEM

R. ARMSTRONG
Department of Electrical Engineering and Physical Electronics, Newcastle upon Tyne Polytechnic, England

1 INTRODUCTION

Of necessity the various techniques used in solving electrical engineering problems are taught separately, with the inevitable result that the student is presented with a set of apparently disjoint facts. It is therefore of immense educational value to study a system which draws on a variety of principles. Such a system is the electric arc furnace which has the following salient features.

(i) The system is non-linear by virtue of the electric arc.
(ii) A linearising technique is required to make the systems amenable to analysis.
(iii) The differential equation of the system must be examined in the time domain to determine a fundamental constraint on the solution.
(iv) Fourier Series may be used to obtain steady state behaviour of the system.
(v) The fundamental constraint mentioned in (iii) enables the steady state solution to be represented by a locus diagram which can be converted into a universal power chart, which gives accurate assessments of current, power, volt-amperes and power factor. This obviates the necessity to evaluate complex formulae and gives a visual insight into the variations of the various quantities under consideration.
(vi) The problem exhibits a form of instability, which may be predicted from the differential equation.

Practical details can often stimulate students' interest and the following will be helpful in this respect. A typical three-phase arc furnace may have an electrical rating of 50 MVA and be capable of melting 150 tons of steel in three hours. The currents taken by such furnaces can be as high as 70–80 KA at voltage levels variable between 200 to 550 volts (line) in steps of 25 volts. The energy liberated[1] per hour has been estimated to be 96 MJ (27 KWh) per cubic cm of arc volume at temperatures of the order of 10,000 to 18,000 °C. When the arc is conducting, the voltage across the arc is approximately constant.

2 ELECTRO-MAGNETIC EFFECTS

The arcs are struck between the charge (scrap to be melted) and three vertical graphite electrodes, the electrodes being positioned at the corners of an equilateral triangle. Some interesting practical effects can be explained by examination of the magnetic forces set up between the electrodes. Assuming balanced currents, application of the simple magnetic force rule

$$F = B \times I \text{ Newton/metre} \tag{1}$$

shows that the force on an electrode has the form

$$F = \frac{\mu_o \sqrt{3} I^2}{8\pi a} \{1\, i + \cos 2\omega t\, i + \sin 2\omega t\, j\} \tag{2}$$

where 'a' is the electrode separation and i and j lie in the plane perpendicular to the electrode axis, i being perpendicular to a plane parallel to the 'yellow' and 'blue' electrodes.

The above expression indicates that the force possesses a constant 'repulsive' part and a rotating part ($\cos 2\omega t\, i + \sin 2\omega t\, j$). These forces are not sufficiently large to deflect or break the electrodes, but a force of the same basic nature also acts on the arcs which are flexible. If the arc length is too long[2] the constant repulsive force deflects the arc towards the side of the furnace bath which may damage the expensive refractory lining of the furnace. The rotating force on the other hand has an advantageous effect in that it causes the arc to rotate around the base of the electrode producing even wear. Proximity effects cause the current to flow in the outer parts of the electrode. Since the complete electrode is formed by joining short lengths at screw joints this turning moment can unscrew the electrode joints should the phase sequence be wrong.

3 ELECTRICAL ASPECTS

For analytic convenience we will examine the electrical performance of a single-phase arc furnace. The three-phase arc furnace may be[3] analysed by the same technique.

3.1 *The intrinsic phase shift*

The electrical system of a single phase arc furnace is as shown in Fig. 1. As mentioned in section 2, the arc voltage can be regarded constant at a level E during conduction and reverses each half cycle and consequently the non-linear V-i arc characteristic need not be considered if the arc voltage is expressed as a square wave. However it cannot be assumed that the arc begins to conduct at the same instant as the supply voltage passes through zero, and so we incorporate an intrinsic phase shift ϕ into the analysis by specifying the supply voltage as

$$v = \hat{V} \sin(\omega t + \phi) \tag{3}$$

The intrinsic phase shift ϕ is unknown and must be determined as part of the solution.

The differential equation of the system is

$$\frac{L di}{dt} = \hat{V} \sin(\omega t + \phi) - e(t) \tag{4}$$

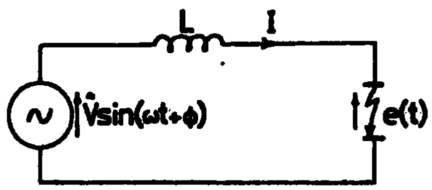

FIG. 1 Electrical system of a single-phase arc furnace.

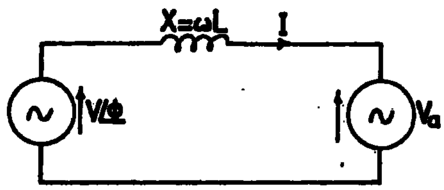

FIG. 2 Equivalent circuit for the fundamental component of current.

where $e(t)$ represents the square-wave arc voltage mentioned previously. The solution to equation (4) is

$$i = A - \frac{\hat{V}}{X}\cos(\omega t + \phi) - \frac{E\omega t}{X} \tag{5}$$

At time $t = 0$, the arc begins to conduct and the current i commences to rise from zero and therefore

$$A = \frac{\hat{V}}{X}\cos\phi \tag{6}$$

At $\omega t = \pi$, the current must fall to zero prior to re-establishing itself in the negative direction and hence

$$0 = A - \frac{\hat{V}}{X}\cos(\pi + \phi) - \frac{E\pi}{X} \tag{7}$$

Eliminating A between equations (6) and (7) we find that the intrinsic phase delay must satisfy the condition

$$\cos\phi = \pi E/2\hat{V} \tag{8}$$

and hence

$$A = \pi E/2X \tag{9}$$

3.2 *Frequency domain solution*

At this stage we could use the time domain solution (equations (5) (8) (9)). However, it is more illuminating to consider the frequency domain solution. To do this we represent the square wave arc voltage by its Fourier Series and use the principle of superposition. The equivalent circuit for the fundamental component of current is then as shown in Fig. 2. This equivalent system contains only sinusoidally varying quantities of the same frequency and we are at liberty to represent its behaviour by a phasor diagram. In doing this we must retain the fact that ϕ is not arbitrary but is constrained by equation (8) and in keeping with all steady state sine-wave behaviour we represent all voltages and currents by their r.m.s. values.

Rewriting equation (8) in terms of r.m.s. values we see that the constraint on

ϕ is given by

$$\cos\phi = \frac{\pi^2 V_a}{8V} = \frac{V_a}{2\rho V} \tag{9}$$

where

$$\rho = \frac{4}{\pi^2} \simeq 0.4. \tag{10}$$

As shown in Fig. (3), equation (9) can be regarded as representing a semicircle of radius ρV. Fig. 4 shows this semicircle with the reactance drop superimposed, which allows the power factor angle to be displayed. This phasor diagram can be converted to the power chart of Fig. 5 by multiplying all sides of the V, V_a, IX triangle by V/X. Furthermore the diagram can be made universal by dividing all sides by a base MVA,

$$S_b = I_b V_b \tag{11}$$

where the base voltage is taken as the supply voltage and the base current is given by

$$I_b = V_b/X \tag{12}$$

We see immediately from the power chart that for a given input voltage there is a maximum fundamental input power and that all other power levels can be transmitted at two possible power factors, and two associated current levels.

3.3 *Effects of higher harmonics*

Only voltages and currents at the same frequency can interact to produce power. Since the supply voltage is derived from an infinite source (the grid system) it is constrained to be sinusoidal and hence knowledge of the funda-

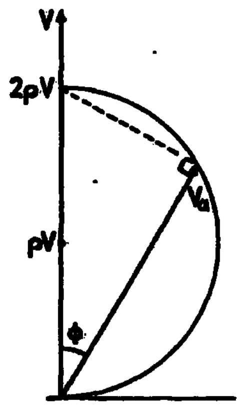

FIG. 3 Phasor representation of the constraint $\cos(\phi) = V_a/2\rho V$.

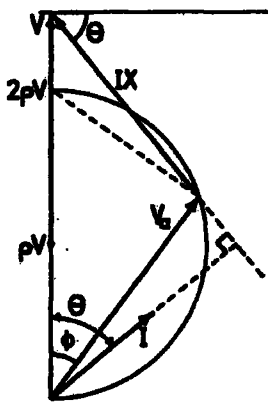

FIG. 4 Phasor diagram of the fundamental components of voltage and current.

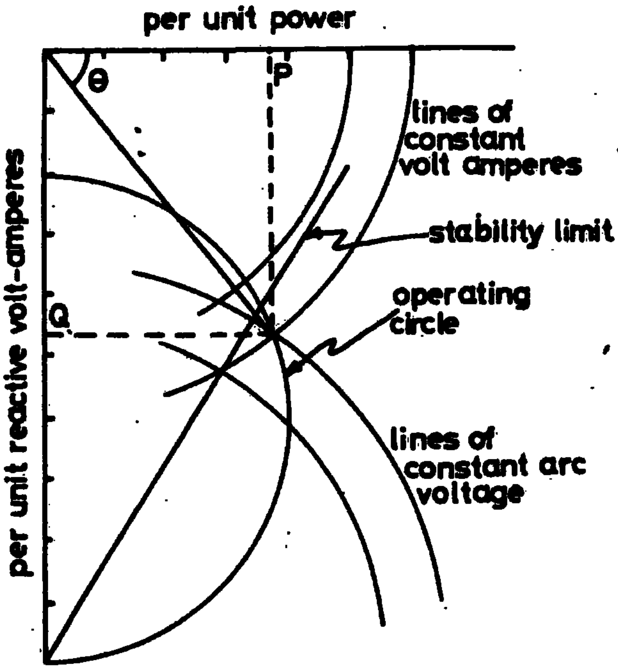

FIG. 5 Power chart for a single-phase arc furnace.

mental component of current is sufficient to predict input power. The higher harmonics, however, do contribute to the r.m.s. value of the current and hence to the power factor. The harmonics in the current waveform reduce approximately as $1/n^2$ because the harmonic voltage falls as $1/n$ whilst the reactance increases as n. In practice the error introduced by these components can be ignored.

3.4 *Arc stability*

A practical problem associated with arc furnaces is setting the levels of the system such that the arc is stable i.e. conducts for a full half-cycle. It is interesting to observe that this is the converse of the switchgear problem of extinguishing the arc as quickly as possible.

A $t = 0$ the rate of change of the arc current must be greater than zero for the arc to establish. If di/dt is negative then the arc is attempting to flow in a negative direction whilst the arc voltage is positive, which is not possible. Examination of equation (4) indicates that di/dt is zero at $t = 0$ when the intrinsic phase angle ϕ has the critical value ϕ_c given by

$$\sin \phi_c = E/\hat{V} = \pi V_a/4V \tag{13}$$

But also

$$\cos \phi_c = V_a/2\rho V \tag{14}$$

and therefore

$$\tan\phi_c = \rho\pi/2 = 2/\pi \qquad (15)$$

$$\phi_c = 32.5°$$

4 CONCLUSIONS

It is interesting to observe that rotating magnetic fields have significance in areas other than electrical machines. The magnitude of the magnetic forces is not important but the analysis is relevant since it reveals the fundamental mechanism causing arc deflection and rotation.

From a mathematical point of view the circuit problem of the arc furnace is solved once the time domain solution has been found. The r.m.s. current, power, and power factor may be obtained by well-known methods. However, a deeper insight into the performance of the system is obtained from the alternative viewpoint of the frequency domain solution. Replacing the square wave arc voltage by its fundamental component (i.e. its describing function) is valid because of the filtering action of the series inductance on the higher harmonics of current. This approximation then allows conventional circuit theory to be used to produce a locus diagram. The conclusion to be drawn here is that even though a solution to a problem is known, an alternative viewpoint may add considerable engineering information and emphasize important aspects of performance.

It is considered that the system studied in this article is sufficiently simple to allow the student to see the significance of the various techniques used to obtain a meaningful engineering solution.

5 REFERENCES

[1] Freeman, E. R., and Medley, J. E., 'Efficient use of power in electric arc furnaces', *IEE J. Elect. Power Appl.*, 1, pp. 17–24, (1978).

[2] Schwabe, W. E., 'Ultra high power furnaces', *Iron and Steel Eng.*, pp. 132–137, (Sept. 1969).

[3] Armstrong, R., 'Predicting the electrical performance of arc furnaces', *IEE J. Elect. Power Appl.*, 1, No. 3, pp. 86–90, (1978).

ABSTRACTS–ENGLISH, FRENCH, GERMAN, SPANISH

The electric arc furnace — a useful teaching system

A simplified study of problems relating to an electric arc furnace system is presented as a means of illustrating a variety of principles required to produce a meaningful solution. Features discussed in the article are: Rotating magnetic fields; Linearisation technique; Time domain solution; Frequency domain solution; Locus diagram; Stability limit.

Le four à arc électrique: un système utile d'enseignement

Une étude simplifiée des problèmes relatifs à un four à arc électrique est présentée comme illustration de la variété des principes nécessaires à l'obtention d'une solution réaliste. Les éléments discutés dans cet article sont: champs magnétique rotatifs; technique de linéarisation; solution dans le domaine temps; solution dans le domaine fréquence; diagramme des lieux; limites de stabilité.

R. ARMSTRONG
Senior Lecturer Dept of Electrical Engineering & Physical Electronics

UN DIAGRAMME OPÉRATOIRE POUR LES FOURS A ARC

A. INCE
Development Manager
Anglo Great Lakes Corporation
Newcastle upon Tyne

Le rendement des fours à arc est d'une importance capitale en aciérie électrique. Concevoir le programme opératoire d'un four à arc pour l'adapter à diverses conditions relève généralement de l'empirisme. Même si un programme satisfaisant a été établi, il n'en demeure pas moins qu'on peut se demander si l'utilisation de la puissance est effectivement la meilleure possible. Comme les ressources mondiales en énergie diminuent et que son coût augmente, les opérateurs de fours à arc subissent une pression constante en vue d'en assurer une utilisation optimale.

Il est donc évident qu'il est désirable de disposer d'une méthode de prévision des performances des fours à arc, capable d'être directement utilisée par les métallurgistes. Cet article se propose de répondre à cette demande en décrivant la construction et l'emploi d'un diagramme opératoire pour les fours à arc. Basé sur des principes bien connus, il peut être utilisé sans recours à la théorie et possède cet avantage que les effets des variations des divers paramètres électriques : puissance, tension, intensité, facteur de puissance, pour diverses longueurs d'arc peuvent être visualisées et mesurées simultanément.

On exposera ici seulement la construction et l'utilisation du diagramme. Les lecteurs intéressés par les implications théoriques ou par des comparaisons avec des résultats pratiques de mesures pourront se reporter à l'article d'Armstrong (1).

Liste des symboles utilisés

- V : tension entre phases (prise du transformateur)
- I : intensité
- R : résistance
- X : réactance
- P : puissance active (MW)
- Q : puissance réactive (MVAr)
- S : puissance (MVA)
- V_a : tension d'arc.

Les indices b concerneront les grandeurs rapportées à l'unité (explications ci-dessous).

DESCRIPTION DU DIAGRAMME OPERATOIRE

Le diagramme relatif à un four à arc triphasé, valable pour un rapport « résistance/réactance » inférieur à 0,2, est représenté figure 1. Le diagramme est universel car il s'applique à tous les fours quelles que soient puissances et tensions ; ceci implique qu'il ne doit pas être retracé pour chaque valeur de la tension appliquée ou de la tension d'arc. Cette adaptabilité est obtenue en considérant toutes les variables comme des fractions d'une certaine valeur de base (égale à l'unité) définie ci-dessous.

Tension de base V_b

Elle est définie comme la tension par phase correspondante à la prise du transformateur. Par exemple, pour une tension entre phases de 525 V, la tension de base (égale à l'unité) sera $525/\sqrt{3} = 303$ V et une lecture « normalisée » (c'est-à-dire rapportée à l'unité) de 0,7 doit correspondre à une tension réelle de $0{,}7 \times V_b = 212$ V.

Intensité de base I_b

Elle est définie par le rapport de la tension de base V à la réactance de court-circuit du système soit

$$I_b = V_b/X \quad \text{(intensité de court-circuit)}$$

Puissance apparente de base S_b

Elle est définie comme le produit de la tension de base par le courant de base.

$$S_b = V_b\, I_b \text{ (MVA)}$$

Toutes les puissances mesurées sur le diagramme représentent une fraction de la puissance de base en MVA.

Ainsi une lecture de 0,3 correspond à une puissance réelle de

$$0{,}3 \times S_b \text{ (MW par phase)}$$

alors qu'une puissance réactive de 0,4 indique une valeur réelle de

$$0{,}4 \times S_b \text{ (MVAR par phase)}$$

Comme on peut le voir sur la figure 1, l'axe unitaire ou normalisé relatif aux puissances (axe P) est horizontal et l'axe unitaire relatif aux puissances réactives (axe Q) est vertical. Le cercle opératoire (lieu géométrique de tous les points possibles de fonctionnement) est un demi-cercle de rayon

$$9/2\pi^3 \approx 0{,}45 \text{ unité centré sur l'axe Q à}$$
$$Q = 1 - 9/2\,\pi^3 \approx 0{,}55 \text{ unité}.$$

La limite de stabilité de l'arc est indiquée par la droite xy, la région stable se situant à droite.

Le point de fonctionnement « a » se trouve à l'intersection du cercle opératoire et de l'arc de cercle correspondant à une tension d'arc constante. Noter que la tension d'arc est aussi représentée par une fraction de la tension de base.

La longueur du segment joignant l'origine au point de fonctionnement (oa) donne à la fois la puissance totale (VA) et l'intensité. La projection de ce segment sur l'axe P donne la puissance active alors que sa projection sur l'axe Q donne la puissance réactive. Enfin l'angle entre cette droite et l'axe P est l'angle de phase Ø (facteur de puissance cos Ø).

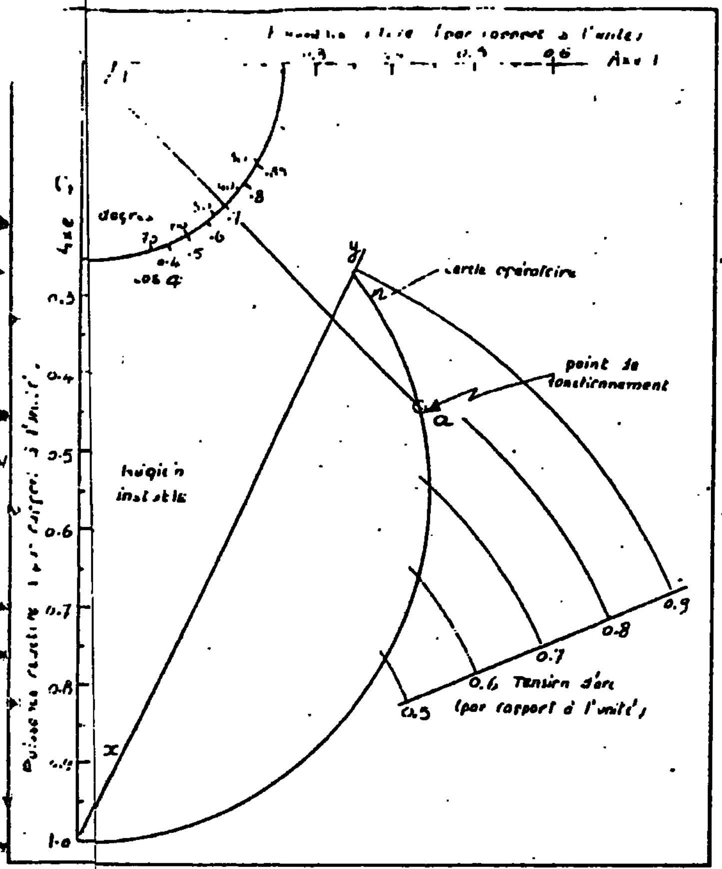

Fig. 1. — Le diagramme opératoire.

Exemple 1

Les principales particularités du diagramme étant exposées, nous allons maintenant l'illustrer par un exemple. Le système étudié sur la figure 3 et correspondant au diagramme de la figure 2 est celui publié par Freeman et Medley (2).

Le four fonctionne sur la prise de tension maximale à 525 V avec un arc de 15,25 cm (6 inches). La tension d'arc (*) est donnée par

$$V_a = 30 + 12 \times \text{longueur d'arc (cm)}$$
$$= 30 + 12 \times 15{,}25 = 213 \text{ volts}$$

Nous pouvons maintenant établir les valeurs des grandeurs-unités (valeurs de base).

Tension de base : $V_b = 525/\sqrt{3} = 303$ V.

Réactance totale : $X = (2\,342 + 430).10^{-6} = 2\,772.10^{-6}\ \Omega$.

Courant de base : $I_b = V/X = 303/2\,772.10^{-6} = 109$ KA.

Puissance de base MVA :

$$S_b = V_b . I_b = 303 \times 109 = 33 \text{ MVA}$$

Tension d'arc (rapportée à l'unité) : $V_a/V_b = 213/303 = 0{,}7$.

Du diagramme de la figure 2 nous pouvons extraire les valeurs suivantes et les convertir en valeurs réelles.

TABLEAU I

Grandeurs	Rapportée à l'unité	Réelle	Segment sur le diagramme
Puissance	0,45	14,85 MW/phase	
P. réactive VA	0,55	18,15 MVAr/ph.	
VA totaux	0,71	23,43 MVA/ph.	a d
Intensité	0,71	77,39 KA	a e
Angle de phase	50°	50°	o a
Cos ⊘	0,642	0,642	o a

(*) *La tension d'arc dépend aussi de la basicité du laitier (3).*

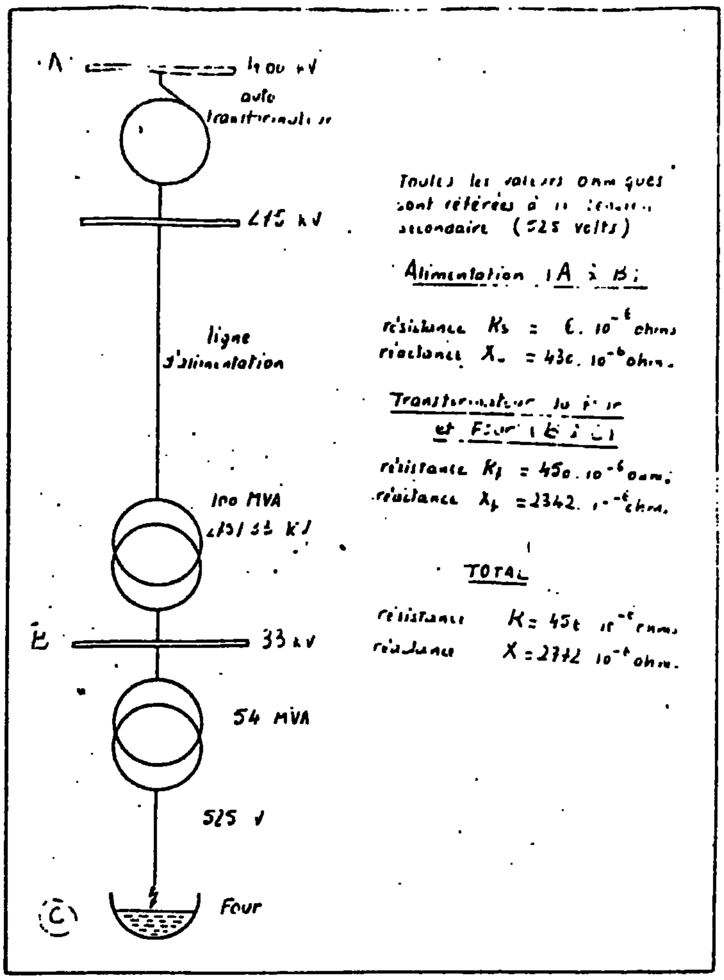

Fig. 3. — Schéma de l'installation relative à l'exemple 1.

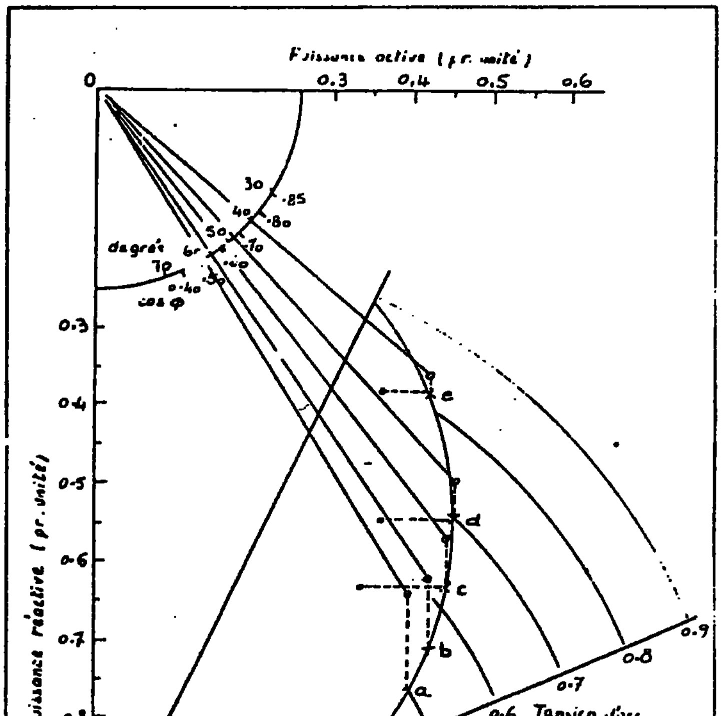

Fig. 2. — Exemple n° 1. Détermination des puissances actives et réactive fournies au transformateur ainsi que la puissance dans l'arc.

...e four est équilibré; chaque phase fournit la même ...issance de telle sorte que la puissance totale est :

$$P = 3 \times 14{,}85 = 44{,}55 \text{ MW}$$

et de même, les VA totaux sont

$$S = 3 \times 23{,}43 = 70{,}29 \text{ MVA}$$

Les valeurs obtenues ci-dessus (sauf l'intensité) sont celles qui pourraient être lues sur les instruments appropriés placés au point A (fig. 3) du montage. Si l'instrumentation de contrôle se situe en B les valeurs fournies par le diagramme ne correspondent plus. Pour trouver les valeurs réelles en B nous devons soustraire la puissance et les pertes réactives relatives à la portion d'équipement comprise entre A et B. Ceci est réalisé comme suit :

Pertes ohmiques entre A et B : $I^2.R_s$ (R_s = résistance dite « de source »).

Pertes rapportées à l'unité :

$$I^2R_s/S_b = \frac{I^2.R_s}{I_b^2.X} = \frac{I^2{,}pu.(R_s)}{X}$$ (pu = par rapport à l'unité).

Dans cet exemple l'intensité rapportée à l'unité est 0,71 donc la puissance correspondante perdue dans la section AB est

$$(0{,}71)^2 \frac{6.10^{-6}}{2\,772.10^{-6}} = 0{,}001$$

Ainsi, la puissance rapportée à l'unité et parvenant au transformateur du four est

$$0{,}45 - 0{,}001 = 0{,}449$$

La soustraction peut aussi être opérée sur le diagramme et correspond à un déplacement vers la gauche de 0,01 pu.

En comparant avec la puissance totale, cette perte est insignifiante et peut être négligée.

Une telle situation est classique pour un four alimenté par un réseau THT :

Les pertes réactives entre A et B sont $I^2.X$, soit en rapportant à l'unité

Le tableau II résume les résultats.

TABLEAU II			
Grandeurs	Rapportées à l'unité (d'après le diagramme	Reelles Par phase	3 phases
Puissance totale	0,45	14,85	44,55 MW
VArs totaux	0,55	18,15	54,45 MVAr
MVA totaux	0,71	23,43	70,29 MVA
Intensité	0,71	77,39 KA	— KA
Angle de phase	50°	50°	50°
Facteur de puissance	0,642	0,642	0,642
Pertes à l'alimentation			
en puissance	0,001	0,33	0,099 MW
réactives	0,08	2,64	7,92 MVAr
Entrée au transformateur du four			
Puissance	0,449	14,8	44,45 MW
VArs	0,47	15,51	46,53 MVAr
MVA	0,66	21,78	65,34 MVA
Angle de phase	47°	47°	47°
Cos Ø	0,682	0,682	0,682
Pertes totales	0,08	2,64	7,92 MW
Puissance dans l'arc	0,37	12,21	36,63 MW
Rendement	82 %	82 %	82 %

$$\frac{I^2.X_s}{S_b} = \left(\frac{I^2}{I_b^2}\right)\left(\frac{X_s}{X}\right) = I^2_{pu}\left(\frac{X_s}{X}\right) = (0{,}71)^2 \frac{430.10^{-6}}{2\,772.10^{-6}} = 0{,}078 \sim 0{,}08$$

Ainsi la puissance réactive parvenant au transformateur de four est

$$0{,}55 - 0{,}08 = 0{,}47$$

La puissance totale est représentée par le segment o b soit 0,66 unité ce qui correspond à une puissance d'entrée de 0,66 × S = 0,66 × 33 = 21,78 MVA par phase soit au total 3 × 21,78 = 65,34 MVA.

L'angle de phase qui serait mesuré en B est celui compris entre le segment ob et l'axe P. Il est de 47 degrés ce qui donne un facteur de puissance cos Ø = 0,682.

Nous constatons que la puissance reçue par le transformateur du four est supérieure à sa puissance nominale et, en conséquence, l'opération avec les conditions précédentes ne peut être envisagée que pendant un temps limité.

Nous pouvons maintenant calculer la puissance effective dans l'arc en soustrayant les pertes totales de la puissance d'entrée.

Variation de la tension d'entrée

Quand on calcule le rendement d'un four pour diverses tensions d'alimentation, il n'est pas exact d'admettre que la résistance et la réactance dites « de sources » (entre A et B dans l'exemple précédent) sont constantes. Ceci est dû au fait que la valeur de la haute tension d'entrée du transformateur a été référée à 525 V. Pour une autre prise (tension VT) les nouvelles valeurs correspondantes (primées ci-après) sont données par :

$$R'_s = \left(\frac{VT}{525}\right)^2 \times R_s$$

$$X'_s = \left(\frac{VT}{525}\right)^2 \times X_s$$

$$\text{Total des pertes (rapportées à l'unité)} = \frac{I^2.R}{I_b^2.X} = I^2_{pu}\,\frac{R}{X} = (0{,}71)^2 \cdot \frac{456.10^{-6}}{2\,772.10^{-6}} = 0{,}083 \sim 0{,}08$$

La puissance dans l'arc rapportée à l'unité est alors 0,45 — 0,08 = 0,37 ce qui est équivalent à la distance a d du diagramme. En valeur réelle ceci donne 12,21 MW par phase (36,63 MW au total).

Finalement on accède au rendement.

$$\text{Rendement} = \frac{\text{Puissance dans l'arc} \times 100}{\text{Puissance totale d'entrée}} = \frac{c\ d \times 100}{a\ d} = \frac{0{,}37 \times 100}{0{,}45} = 82\ \%$$

Ainsi pour fonctionnement sous 425 V les valeurs appropriées sont :

$$R'_5 = 0{,}6553 \times 6 \times 10^{-6} \quad 4.10^{-6}$$
$$X'_5 = 0{,}6553 \times 430 \times 10^{-6} = 281.10^{-6}$$

La nouvelle tension de base est $425/\sqrt{3} = 245$ V.

La réactance totale du système est $(281 + 2\,342).10^{-6} = 2\,623.10^{-6}$ ce qui donne un courant de base de $245/2\,623.10^{-6} = 93{,}3$ KA et une nouvelle puissance totale de $93{,}3 \times 245 = 22{,}8$ MVA.

La suite du calcul est inchangée.

Exemple 2

Supposons maintenant que le four fonctionne sous 425 V et que l'on demande de calculer la tension d'arc correspondant au maximum de puissance utile. Pour cela, nous devons calculer les puissances dans l'arc pour diverses valeurs de la tension d'arc.

Ainsi, si la tension d'arc est 0,7 pu on a :

Tension de base $V_b = 424/\sqrt{3} = 245$ V.

Réactance totale $X = 282 + 2\,346.10^{-6} = 2\,624.10^{-6}$.

Courant de base $I_b = V_b/X = 93$ KA.

Pour une tension d'arc de 0,7 pu nous tirons du diagramme.

Puissance d'entrée pu = 0,45.

Courant (pu) = 0,72.

Rapport total R/X = 0,173.

Pertes = $(0{,}72)^2$ (0,173) = 0,09.

Puissance dans l'arc Pa = 0,45 — 0,09 = 0,36.

Ce calcul est répété pour diverses tensions d'arc, les résultats étant résumés dans le tableau 3.

TABLEAU III

Tension d'arc	Intensité	Pertes	Puissance d'entrée	Puissance dans l'arc
0,70	0,72	0,09	0,45	0,36
0,75	0,67	0,078	0,445	0,367
0,80	0,60	0,062	0,425	0,363
0,85	0,525	0,048	0,390	0,342

Ces résultats sont maintenant transcrits sur le diagramme comme le montre la figure 4. La puissance maximale dans l'arc correspond au point a. Le segment a b représente les pertes et donne le point opératoire b. Le fonctionnement au point c demanderait un courant de 0,72 unité avec un cos Ø de 0,63 pour établir une puissance d'arc de 0,36 unité. D'un autre côté, l'opération au point b fournit une puissance d'arc de 0,37 unité pour un courant réduit à 0,65 unité et un cos Ø supérieur (0,69). Nous constatons également que la courbe de puissance dans l'arc est insensible à de petites variations proches du maximum et si d est pris comme point de fonctionnement nous obtenons une puissance d'arc de 0,365 (variation de 1,35 % par rapport à l'optimum) pour un courant de 0,6 unité (réduction de 0,7 %) avec un nouvel accroissement du facteur de puissance à 0,72.

Le point de fonctionnement b pour obtenir la puissance d'arc maximale étant déterminé, les autres paramètres requis (intensité, cos Ø ...) sont calculés comme dans l'exemple 1. Le lecteur pourra vérifier que les valeurs indiquées au tableau 4 correspondent à un fonctionnement au maximum de puissance d'arc.

Exemple 3

Le premier exemple correspondait à une tension d'alimentation fixe et une longueur d'arc fixe alors que pour le second la tension était fixe et la longueur d'arc variable.

Maintenant, considérons une longueur d'arc fixe avec des tensions variables.

TABLEAU IV

Grandeurs	Rapportées à l'unité	Réelles par phase
Puissance	0,44	10,0 MW
VArs	0,46	10,5 MVAr
MVA	0,65	14,8 MVA
Courant	0,65	60,5 kA
Cos Ø	0,69	0,69
Pertes		
Pertes totales en puissance	0,075	1,7 MW
Pertes VAr « source »	0,045	1,0 MVAr
Entrée au four		
Puissance	0,44	10,0
VArs	0,415	9,5
MVA	0,62	14,0
Cos Ø	0,73	0,73
Tension d'arc	0,76	186 V
Puissance d'arc	0,37	8,4 MW

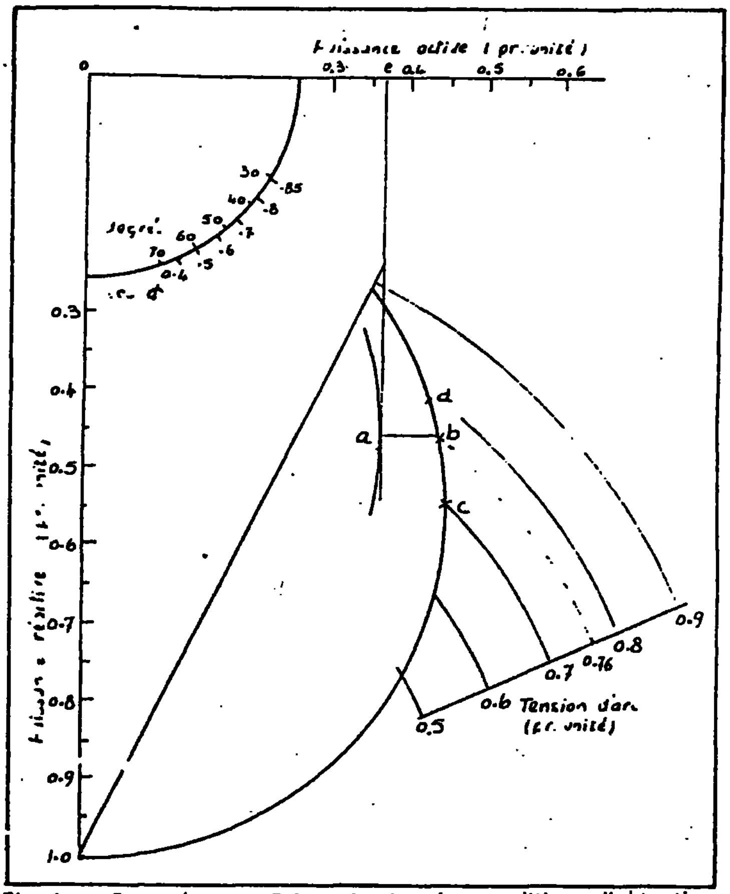

Fig. 4. — Exemple n° 2. Détermination des conditions d'obtention de la puissance maximale dans l'arc.

Une telle situation correspond peut-être à un four chargé en continu. Comme il travaille généralement en « bain plat », nous pouvons supposer que la longueur d'arc est fixée, par exemple à 10,16 cm (4 inches), pour éviter l'usure excessive des réfractaires. Pour utiliser pleinement la puissance investie, on peut se demander s'il est possible de travailler en continu avec le transformateur à sa puissance maximale soit 54 MVA (18 MVA par phase).

Pour résoudre ce problème nous testerons diverses tensions d'alimentation et calculerons pour chacune les conditions de travail. Cette analyse s'effectue de la même manière que pour l'exemple 1 et les résultats en sont résumés dans le tableau 5, les points de fonctionnement apparaissant sur la figure 5.

TABLEAU V

Tension VT	$\left(\frac{VT}{525}\right)^2$	$R' .10^{-6}$	$X' .10^{-6}$	$R.10^{-6}$	$X.10^{-6}$	V_b	V_a/V_b	I_b	S_b	$18/S_b$	X'_b/X	R/X	Point de fonctionnement
525	1,00	6	430	456	2 772	303	0,5	109	33	0,55	0,155	0,165	a
475	0,8185	4,9	352	455	2 694	274	0,55	102	28	0,64	0,131	0,169	b
425	0,6533	3,9	282	454	2 624	245	0,62	93	23	0,78	0,107	0,173	c
375	0,5102	3,06	219	453	2 561	216	0,7	84	18	1,00	0,086	0,177	d
325	0,3832	2,3	165	452	2 507	188	0,81	75	14	1,28	0,066	0,180	e
Prise tension	MVA totaux	Pertes réactives	MVA au four		Pertes	Puissance totale	Puissance arc	Cos Ø	Valeurs réelles MVA	Intensité	Puissance arc	Cos φ	Rendement
										KA	MW		
525	0,87	0,12	0,765	> 0,55	dépasse la puissance nominale du transformateur								
475	0,84	0,092	0,765	> 0,64									
425	0,785	0,066	0,735	< 0,78	0,11	0,445	0,335	0,62	16,9	73	7,7	0,62	75 %
375	0,72	0,046	0,685	< 1,00	0,09	0,45	0,36	0,68	12,33	60,5	6,48	0,68	80 %
325	0,58	0,022	0,565	< 1,28	0,06	0,425	0,365	0,76	7,9	43,5	5,11	0,76	86 %

Ces résultats montrent qu'il est nécessaire d'opérer à 425 V ou au-dessous. Avec 375 V au lieu de 425 V nous constatons que la puissance d'arc est réduite de 15,5 % pendant que le courant diminue de 27 % pour une augmentation du cos Ø de 0,62 à 0,68.

Cette diminution de puissance peut augmenter le temps d'opération mais, en contre partie, l'accroissement du facteur de puissance et la réduction corrélative des coûts peut rendre l'opération à 375 V économiquement souhaitable.

CONCLUSIONS

Pour utiliser le diagramme, on doit se souvenir des points suivants :

— Le rapport R/X ne doit pas dépasser 0,2. Un diagramme plus sophistiqué valable pour des rapports R/X supérieurs est fourni par Armstrong (1).

— Dans cet article, la tension d'arc est liée à sa longueur par la formule

$$V = 30 + 12\ X\ (cm)$$

mais comme l'a noté Pirozhnikov (3) la tension d'arc varie considérablement avec la basicité du laitier et il est préférable d'utiliser une valeur expérimentale de V.

— La résistance et la réactance « de source » (réseau fournisseur) doivent aussi être connues. En vue d'obtenir les performance maximales les informations nécessaires doivent être demandées aux responsables du réseau.

— Le diagramme fournit des indications raisonnables pour un travail sur « bain plat », mais pour les conditions de fusion avec formation des « puits », tout ce qu'on peut en espérer est qu'il permette d'obtenir les valeurs moyennes de performances électriques.

— Avec un four non équilibré sur ses 3 phases on note des différences entre les valeur effectives et les valeurs précalculées.

Les exemples présentés dans cet article montrent que le diagramme opératoire permet d'effectuer une « simulation » capable de conduire à un programme d'utilisation approprié.

Bien que quelques connaissances complémentaires (par exemple l'effet de la basicité du laitier) soient souhaitables, il doit déjà amener les métallurgistes à déterminer par eux-mêmes des conditions de marche satisfaisante, et dans de nombreux cas, améliorées.

Il est sans doute exact de dire que l'opération au four à arc, étant plus un art qu'une science, fait partie des domaines de la technologie.

Le diagramme proposé permet cependant d'éclairer certains mystères techniques mais il est certain que pour

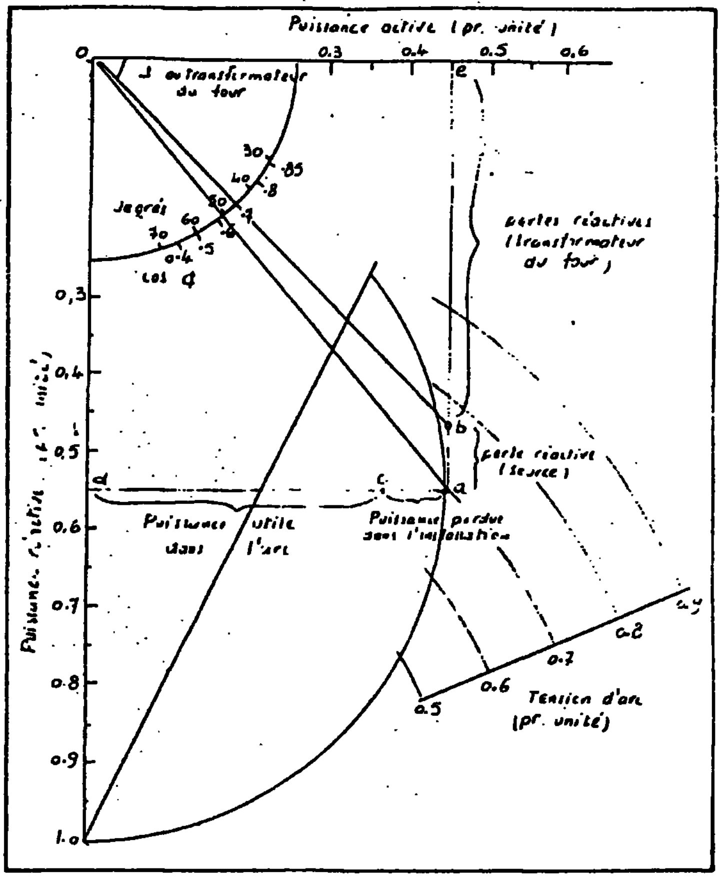

Fig. 5. — Exemple n° 3. Recherche de la tension optimale.

l'évaluation des résultats, la compétence et l'expérience sont encore nécessaires. Le succès d'un diagramme de ce genre dépend de son application à des conditions variées et ceci doit être effectué avec la coopération des aciéristes. Il est souhaitable que l'utilisation du diagramme, pendant des périodes de travail bien contrôlées, donne lieu à une collecte de résultats qui permettront les comparaisons entre les valeurs réelles et les valeurs prédites.

REFERENCES

1. Armstrong (R.). « Predicting the performance of electric arc furnace ». I.E.E. Journal on Electric Power Applications.
2. Freeman (E.R.) et Medley (J.E.). Efficient use of power in electric arc furnaces. I.E.E. Journal on Electric Power Applications. February 1978, vol. 1, n° 1, p. 17-24.
3. Pirozhnikov (V.E.). Effects of slag on thermal process in electric furnaces. Stal, March 1976 p. 222-224.

Int. J. Elect. Enging Educ., Vol. 18, pp. 351–358. Manchester U.P., 1981. Printed in Great Britain

APPLICATION OF RESONANT CIRCUIT THEORY TO MATCHING NETWORKS

R. ARMSTRONG and E. KOROLKIEWICZ
School of Electronic Engineering, Newcastle upon Tyne Polytechnic, England

1 INTRODUCTION

In high frequency communication systems, matching the source impedance to the load impedance is important, to prevent reflections and consequent distortion. Transmitters should transfer the maximum amount of power to the aerial, whilst in receiving systems low power levels also dictate maximum power transfer conditions. High frequency systems must accommodate modulated signals, and the bandwidth of a matching network must be adequate to allow the side bands to propagate. The basic building block of such matching networks is the parallel or series tuned circuit. This article shows how the theory of resonant circuits may be used to design apparently complex matching networks[1–3]. An example is given to illustrate the design process using both analytical and graphical methods. From an educational point of view the student sees the tuned circuit from a different aspect whilst the graphical method of solution is an excellent example on the use of a Smith Chart.

2 THE BASIC BUILDING BLOCK

Consider the problem of matching two resistors, R_s to R_m at a single frequency by means of the network shown in Fig. 1(a). As viewed from the terminals AB the matching network and the load appear as a parallel circuit as shown in Fig. 1(b). This network is equivalent to the three-element shunt network of figure 1(c).

The dynamic resistance is

$$R_D=(R_m^2+X_{L1}^2)/R_m \tag{1}$$

and the equivalent parallel inductive reactance is

$$X_{LD}=(R_m^2+X_{L1}^2)/X_{L1} \tag{2}$$

For matching at a single frequency it is required to choose values of X_{L1} and X_{C1} such that $R_D=R_S$ and from equation (1) it will be seen that X_{L1} must be given by,

$$X_{L1}=\sqrt{R_m(R_S-R_m)} \tag{3}$$

Equation (3) shows that R_S must be greater than R_m to make X_{L1} inductive. From Fig. 1(c) the magnitude of X_{C1} must equal the effective inductive re-

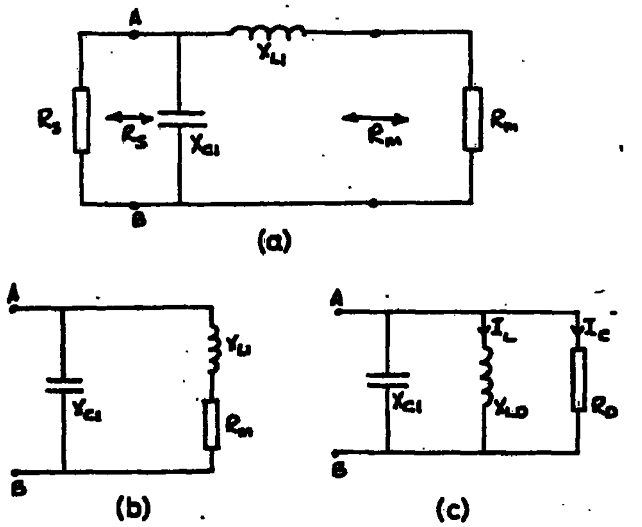

FIG. 1 LC matching section when $R_s > R_m$ and its equivalent parallel network.

actance at the working frequency and therefore,

$$X_{C1} = (R_m^2 + X_{L1}^2)/X_{L1} \tag{4}$$

The Q factor of the resonant circuit in Fig. 1(c) is defined as the ratio of the current I_L in the inductance to the current I_R in the resistance at resonance i.e.,

$$Q_1 = I_L/I_R = R_D/X_{LD} \tag{5}$$

Substituting equations (1) and (2) into equation (5), the Q factor of the resonant circuit in Fig. 1(c) is,

$$Q_1 = X_{L1}/R_m \tag{6a}$$

When R_s is connected across AB the loaded Q is given by,

$$Q_{1L} = Q_1/2 \tag{6b}$$

which determines the bandwidth of the network shown in Fig. 1(c).

If the terminating resistance values are specified, then the Q, and hence the bandwidth are automatically fixed. Alternatively, from equation (1) with $R_D = R_s$ it is easily shown that,

$$R_m = R_s/(1 + Q_1^2) \tag{7}$$

from which R_m may be determined if R_s and Q_1 are specified.

To match from a low resistance R_m to a high resistance R_L the matching network is reversed as shown in Fig. 2 and identical analysis yields,

$$X_{L2} = (R_m[R_L - R_m])^{\frac{1}{2}} \tag{8}$$

$$X_{C2} = (R_m^2 + X_{L2}^2)/X_{L2} \tag{9}$$

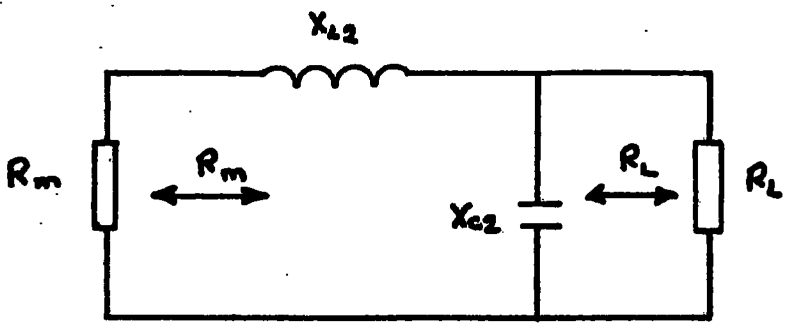

FIG. 2 LC matching section when $R_m < R_L$.

$$Q_2 = X_{L2}/R_m \tag{10}$$

$$R_m = R_L/(1+Q_2^2) \tag{11}$$

In a majority of high frequency applications it is often necessary to match between a complex impedance and 50Ω. This can be done readily using the above theory. For example, if the source impedance is complex then the R_s of figure 1(a) is the effective parallel resistance of the source and the effective parallel susceptance is included as part of X_{C1}. Alternatively, in Fig. 2 the complex impedance may be regarded as a resistor R_m in series with a reactance which is included as part of X_{L1}. In both cases the above theory is sufficiently general to design the matching networks.

The range of complex impedances that can be matched to a 50Ω load by each of the two LC matching networks can be readily obtained[4] and are shown in Fig. 3.

3 π MATCHING NETWORKS

For the simple L-C networks analysed in section (2) the bandwidth is automatically fixed by the specified source and load resistances. If it is required to specify the bandwidth in addition, then the π network shown in Fig. 4(a) may be used. Such a network also has the advantage of being able to match any complex impedances. By splitting the π network into two simple *LC* sections as shown in Fig. 4(b) the value of R_m may be chosen to achieve the desired bandwidth. For matching, the required R_m is given by equations (7) and (11).

$$R_m = R_s/(1+Q_1{}^2) = R_L/(1+Q_2{}^2) \tag{12}$$

This equation shows that the node with the highest terminating resistance has the largest Q and hence dictates the bandwidth of the system.

It is shown in the appendix that constant Q curves on the Smith Chart are described by the following equation of a circle

$$U^2 + (V + 1/Q)^2 = 1 + 1/Q^2 \tag{13}$$

where U and jV are the real and imaginary axes on the Smith Chart of the

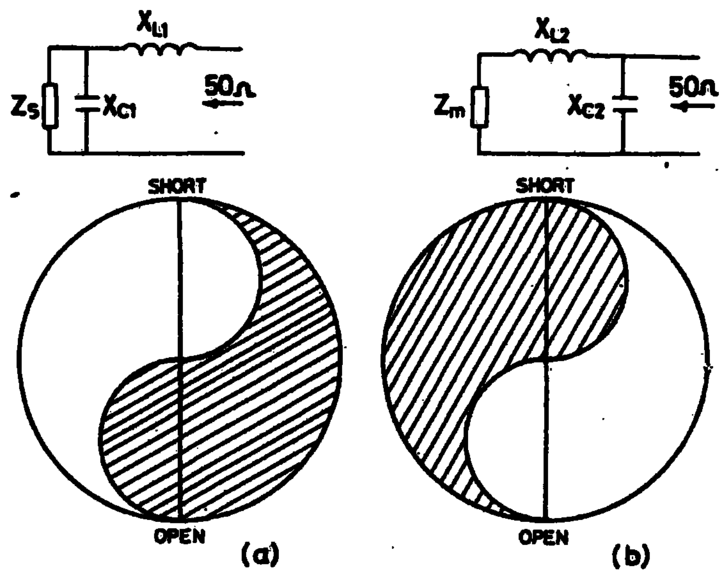

FIG. 3 (a) Shaded region shows range of complex impedance Z_s that can be matched to 50Ω using circuit shown in Fig. 1. (b) Shaded region shows range of complex impedance Z_m that can be matched to 50Ω using circuit shown in Fig. 2.

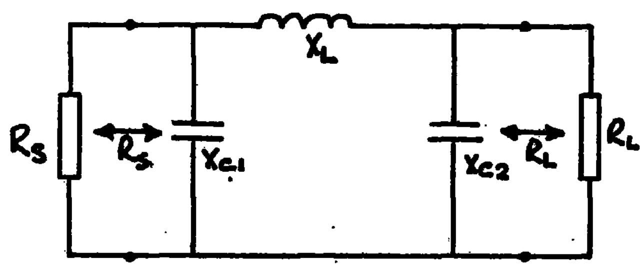

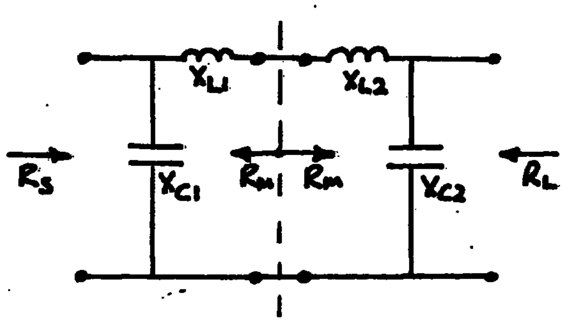

FIG 4 π matching section.

voltage reflection coefficient. It is possible therefore to use the Smith Chart to evaluate the elements of the π matching network as shown in the following example.

4 EXAMPLE

Suppose it is necessary to match an output admittance $(0.01+j0.02)S$ of an amplifier to a 50Ω load and the required value of Q being 5 at the working frequency.

The output susceptance of the amplifier can be combined with the X_{C1} of the matching network to produce an equivalent reactance (X_{CT}) and therefore it is only necessary to match 100Ω to 50Ω. The Q is associated with the 100Ω node and the desired equations can be used to determine the required elements of the matching network as shown below.

$$R_m = R_s/(1+Q_1^2) = 3.85\Omega$$

$$X_{L1} = \sqrt{R_m(R_s - R_m)} = 19.24\Omega$$

$$X_{CT} = \frac{R_m^2 + X_{L1}^2}{X_{L1}} = 20.0\Omega$$

$$X_{L2} = \sqrt{R_m(R_L - R_m)} = 13.32\Omega$$

$$X_{C2} = \frac{R_m^2 + X_{L2}^2}{X_{L2}} = 14.45\Omega$$

The required elements of the matching network are shown in Fig. 5.

The values of the elements of the series equivalent circuit of the parallel circuit consisting of a 100Ω resistance in parallel with X_{CT} is given by the intersection of the constant Q (=5) circle and constant conductance ($\bar{G}=0.5$) circle at point A. The required value of X_{CT} in parallel with the 100Ω resistance is found by moving diametrically opposite point A to point A', which gives the admittance values of the elements of the parallel network i.e. $\bar{G}=0.5$ and $\bar{B}=2.57$, from which $\bar{X}_{CT}= 1/2.57=0.39$ and hence $X_{CT}=19.5\Omega$.

The required normalized value of $\bar{X}_L$ is found by travelling from point A on the constant resistance circle (0.075) to the intersection of the constant con-

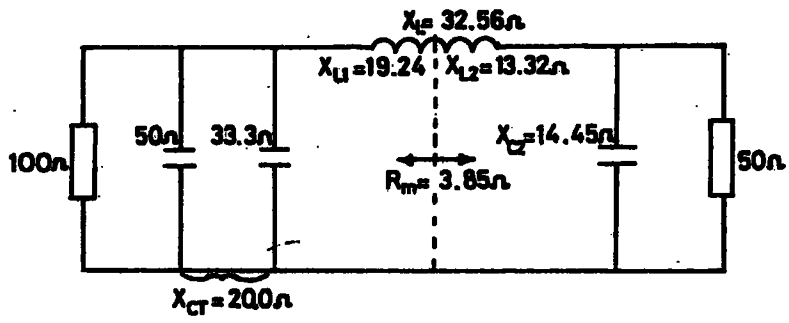

FIG. 5 Required elements of the π matching section.

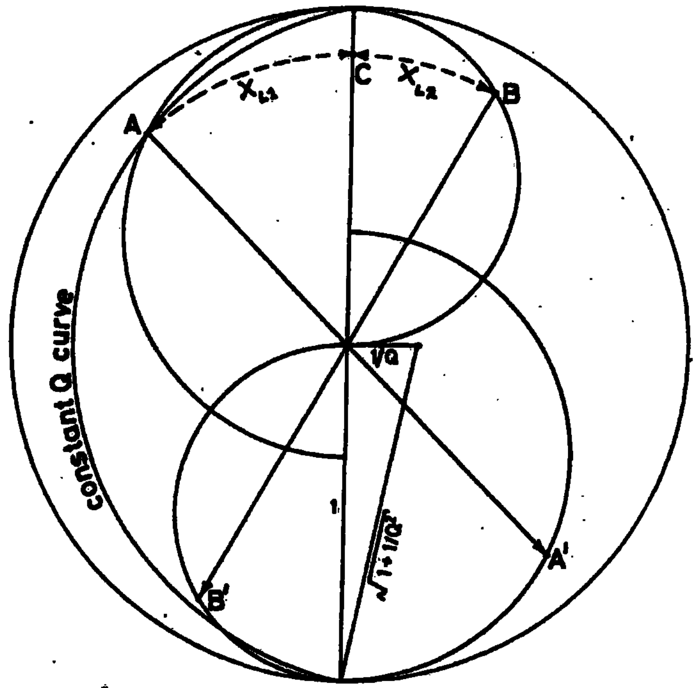

FIG. 6 : Design of the π matching section using a Smith chart.
Point A = 0.075 − j0.38, point A′ = 0.5 + j2.55,
point B = 0.075 + j0.256, point B′ = 1 − j3.7 and point C = 0.075 + j0.

ductance ($\bar{G} = 1$) circle at point B. The normalized value of X_{C2} is obtained in a similar manner to that already described for X_{CT}, from a point diametrically opposite to B i.e. B′.

Renormalizing the results determined from the Smith chart the values of the required elements of the π matching section are,

$R_m = 3.75\Omega$ (point C), $X_{CT} = 19.5\Omega$, $X_{L1} = 19.0\Omega$, $X_{L2} = 12.8\Omega$, $X_{C2} = 13.5\Omega$ As can be seen, the results obtained using the Smith chart are comparable with those given by the analytic method.

5 CONCLUSIONS

The aforegoing analysis has shown how parallel resonant circuits form the basis of π matching networks. The important point is to find the effective resistance R_m of the two back-to-back LC sections to give the desired bandwidth. If the source and load are complex the problem is reduced to matching resistive elements by combining the effective parallel susceptance with the capacitive shunt arms of the matching section. This concept may be used to explain how the first capacitive element of the matching network may be used as part of the tank circuit in an r.f. amplifier.

The same principles also apply to tee networks where the central element is divided in such a manner as to produce the required bandwidth. In this case the effective resistance R_m will exceed both R_s and R_L and the design equations follow directly from the theory of series resonant circuits.

In an identical manner it is also possible to design matching networks with the inductance and capacitance interchanged on either one or both of the basic half sections. The choice of the form of the matching network may often depend on the nature of the source and load impedance. For example, if the output capacitance of an amplifier exceeds the value of X_1 in a π matching network then clearly the first shunt element of the network must be inductive.

It is considered that the results presented in this article give a valuable insight into the many apparently diverse matching networks used in practice. The graphical solution is another indication of the versatility of the Smith chart.

6 REFERENCES

[1] Colussi, E. J., 'Internally matched R. F. power transistors', *Microwave Journal*, 21, No. 4, pp. 81–84.

[2] Przedpelski, A.B., 'Bandwidth of transmission line matching circuits', *Microwave Journal*, 21, No. 4, pp. 71–76.

[3] Gelnovatch, V. G., Burke, J. F., 'Computer aided design of wide-band integrated microwave transistor amplifiers on high dielectric substrates' *IEEE Journal of Solid-State Circuits* (June, 1968).

[4] Smith, P. H., *Electronic Applications of the Smith Chart*, McGraw-Hill, pp. 115–127 (1969).

APPENDIX

The relationship between normalized impedance $\bar{Z}$ and the voltage reflection coefficient p is given by,

$$p = U + jV = \frac{\bar{z}-1}{\bar{z}+1} \tag{A1}$$

Equation (A1) can also be expressed in the form shown below,

$$\bar{z} = \bar{r} + j\bar{x} = \frac{(1+U)+jV}{(1-U)-jV} \tag{A2}$$

Hence,

$$\bar{r} = \frac{1-U^2-V^2}{(1-U)^2+V^2} \tag{A3}$$

and,

$$\bar{x} = \frac{2V}{(1-U)^2+V^2} \tag{A4}$$

The Q of a circuit is defined as,

$$Q = \bar{x}/\bar{r}$$

and hence from equations (A3) and (A4) it can be shown that,

$$U^2+\left(V+\frac{1}{Q}\right)^2=1+\frac{1}{Q^2} \qquad \text{(A5)}$$

which is an equation of a circle of radius $\left[1+\frac{1}{Q^2}\right]^{\frac{1}{2}}$ and centre $U=0$ and $V=-1/Q$.

In a similar manner it may be shown that when dealing with admittance equation (A5) is modified to,

$$U^2+\left(V-\frac{1}{Q}\right)^2=1+\frac{1}{Q^2} \qquad \text{(A6)}$$

which is a circle centred on,

$$U=0 \text{ and } V=+\frac{1}{Q}$$

ABSTRACTS–ENGLISH, FRENCH, GERMAN, SPANISH

Application of resonant circuit theory to matching networks
A wide variety of matching networks are used in high frequency communication systems and this paper shows how such networks can be conveniently designed using the theory of resonant circuits. A graphical method is also included which provides a valuable insight into the properties of the Smith Chart.

Application de la théorie des circuits résonnants aux réseaux adaptateurs
Une grande variété de réseaux adaptateurs est utilisée dans les systèmes de communication à haute fréquence. Cet article montre comment de tels réseaux peuvent être calculés de façon commode par la théorie des circuits résonnants. Une méthode graphique utilisée donne en outre un précieux aperçu des propriétés de l'abaque de Smith.

Anwendung der Resonanzkreistheorie auf Anpassungsnetzwerke
Eine grosse Vielfalt von Anpassungsnetzwerken wird in Hochfrequenz-Fernmeldesystemen verwendet; diese Arbeit zeigt, wie derartige Netzwerke bequem bei Benutzung der Theorie von Resonanzkreisen entworfen werden können. Ferner wird eine graphische Methode angegeben, die einen wertvollen Einblick in die Eigenschaften des Smithschen Leitungsdiagramms gibt.

Aplicación de la teoría de circuitos resonantes para redes de acoplamiento
Una amplia variedad de redes de acoplamiento se utilizan en los sistemas de comunicación de alta frecuencia. En este artículo se muestra cómo tales redes pueden calcularse apropiadamente utilizando la teoría de circuitos resonantes. Se incluye un método gráfico que proporciona una valiosa profundización en las propiedades de la carta de Smith.

APPENDIX B

B1. Expansion of $T_n(\chi)$

$$\chi = a \cos \theta - b \cos (2\theta - \phi)$$

Appendix B1

Expansion of $T_n(\chi)$, $\chi = a \cos \theta - b \cos (2\theta - \phi)$.

The equation of the Chebyshev polynomial $T_n(\chi)$, where $\chi = a \cos \theta - b \cos (2\theta + \phi)$ is facilitated by the recurrence relationship[20].

$$T_0(\chi) = 1$$

$$T_1(\chi) = \chi$$

$$T_{n+1}(\chi) = 2 \; T_n(\chi) - T_{n-1}(\chi)$$

Thus

$$T_0(\chi) = 1$$

$$T_1(\chi) = a \cos \theta - b \cos (2\theta - \phi)$$

Fundamental component $= a \cos \theta$ (1)

Second harmonic $= - b \cos \phi \cos 2\theta - b \sin \phi \sin 2\theta$ (1a)

$$T_2(\chi) = 2 \left[a \cos \theta - b \cos (2\theta - \phi) \right] \left[a \cos \theta - b \cos (2\theta - \phi) \right] - 1$$

$$= a^2 + b^2 - 1$$

$$- 2ab (\cos \phi \cos \theta + \sin \phi \sin \theta)$$

$$+ a^2 \cos 2\theta$$

$$- 2ab (\cos \phi \cos 3\theta + \sin \phi \sin 3\theta)$$

$$+ b^2 (\cos 2 \phi \cos 4\theta + \sin 2 \phi \sin 4\theta)$$

Fundamental $= - 2ab (\cos \phi \cos \theta + \sin \phi \sin \theta)$

Second Harmonic $= a^2 \cos 2\theta$ (2a)

$$T_3(\chi) = 2\left[a\cos\theta - b\cos(2\theta - \phi)\right] X\, T_2(\chi) - \left[a\cos\theta - b\cos(2\theta - \phi)\right]$$

$$= -3\,a^2b\cos\phi$$

$$+ 3a\,(a^2 + 2b^2 - 1)\cos\theta$$

$$- 3b\,(b^2 + 2a^2 - 1)\cos(2\theta - \phi)$$

$$+ 3ab^2\cos(3\theta - 2\phi) + a^3\cos 3\theta$$

$$- 3a^2b\cos(4\theta - \phi)$$

$$+ 3ab^2\cos(5\theta - \phi)$$

$$- b^3\cos(6\theta - 3\phi)$$

Fundamental $= 3a\,(a^2 + 2b^2 - 1)\cos\theta$ (3)

Second harmonic $= -3b\,(b^2 + 2a^2 - 1)\ \cos\phi\cos 2\theta + \sin\phi\ \sin 2\theta$

(3a)

A device having a characteristic of the form

$$q = Q_0 + Q_1\,T_1(\chi) + Q_2\,T_2(\chi) + Q_3\,T_3(\chi) \qquad (4)$$

when stimulated by a drive of the form

$$\chi = a\cos\theta - b\cos(2\theta - \phi) \qquad (5)$$

has a fundamental component given by the weighted sum of equations (1), (2) and (3), i.e.

$$q_1 = Q_1\,a\cos\theta + Q_2\,(-2ab\left[\cos\phi\cos\theta + \sin\phi\sin\theta\right])$$

$$+ Q_3\left[3a\,(a^2 + 2b^2 - 1)\right]\cos\theta \qquad (6)$$

up to terms of third order.

APPENDIX C

C1. Determination of modified parameter r_m & V_1

Appendix C1

Determination of modified parameters r_m and V_1

The term $\ln (1 + \exp (\alpha (V - V_o)))$

$$= \alpha (V - V_o) + \ln (1 + \exp[- \alpha (V - V_o)])$$

$$\simeq \alpha (V - V_o) + \exp[- \alpha (V - V_o)]$$

if $\exp[- (\alpha (V - V_o))] << 1$

Furthermore if $\alpha (V - V_o) \geq 3$, i.e. if

$$V \geq V_o + 3/\alpha$$

then

$$\ln (1 + \exp[\alpha (V - V_o)]) \simeq \alpha (V - V_o)$$

For this condition the two term solution becomes

$$i + I_s = \frac{V - V_o}{r} - \frac{1}{r} \frac{(V - V_o)}{[1 + \alpha (V - V_o)]} \ln[\alpha (V - V_o)]$$

To linearise the equation about a point $V_p \geq V_o + 3/\alpha$ let

$$V = V_p + x, \qquad x \text{ small and then}$$

$$V - V_o = (V_p - V_o) + x$$

$$= \Delta V + x$$

where $\Delta V = V_p - V_o$

The following are then readily determined

$$\text{(i)}\quad \frac{V - V_o}{r} = \frac{\Delta V}{r} + \frac{x}{r}$$

$$\text{(ii)}\quad \frac{1}{1 + \alpha\,(V - V_o)} = \frac{1}{(1 + \alpha\Delta V)\ (1 + \frac{\alpha x}{1 + \alpha\Delta V})}$$

$$\approx \frac{1}{1 + \alpha\Delta V}\ (1 - \frac{\alpha V}{1 + \alpha\Delta V})$$

$$\text{(iii)}\quad \frac{1}{r}\ \frac{(V - V_o)}{1 + \alpha\,(V - V_o)} = \frac{\Delta V + x}{1 + \alpha\Delta V}\ (1 - \frac{\alpha x}{1 + \alpha\Delta V})$$

$$= \frac{1}{r}\,\frac{\Delta V}{1 + \alpha\Delta V}\ (1 + \frac{x}{\Delta V})\left[1 - \frac{\alpha x}{1 + \alpha\Delta V}\right]$$

$$\approx \frac{1}{r}\,\frac{\Delta V}{1 + \alpha\Delta V}\left[1 + x\,(\frac{1}{\Delta V} - \frac{\alpha}{1 + \alpha\Delta V})\right]$$

$$\text{(iv)}\quad \ln\left[\alpha\ (V - V_o)\right] = \ln\left[\alpha\ (\Delta V + x)\right]$$

$$\approx \ln \alpha\Delta V\quad \ln\,(1 + x/\Delta V)$$

$$\approx \ln\left[\alpha\Delta V\right] + x/\Delta V$$

The equation of the tangent to the $i - V$ curve at the point V_p may then be determined as

$$i + I_s = \frac{1}{r}\left[\Delta V - \frac{\Delta V\ \ln\,\alpha\Delta V}{1 + \alpha\Delta V}\right] + \frac{x}{r}\left[1 - \frac{1}{1 + \alpha\Delta V} - \frac{\ln\,\alpha\Delta V}{(1 + \alpha\Delta V)^2}\right]$$

The slope of the tangent is

$$\frac{1}{r_m} = \frac{1}{r}\left[1 - \frac{1}{1 + \alpha\Delta V} - \frac{\ln\,\alpha\Delta V}{(1 + \alpha\Delta V)^2}\right]$$

$$\approx \frac{1}{r}\left[1 - \frac{1}{1 + \alpha\Delta V}\right]$$

and therefore

$$r_m = r\ (1 + 1/\alpha\Delta V) = r\ (1 + \frac{1}{\alpha\ (V_p - V_o)})$$

The turn on voltage is given by $x = x_o$ when $i = 0$ i.e.

$$V - \frac{\Delta V \ln \alpha\Delta V}{1 + \alpha\Delta V} = - x_o \left[1 - \frac{1}{1 + \alpha\Delta V}\right]$$

and therefore

$$x_o = - \frac{(1 + \alpha\Delta V - \ln \alpha\Delta V)}{\alpha}$$

when $x = x_o$ let $V = V_1$ so that

$$V_1 = V_p + x_o$$

$$\therefore V_1 = V_p - \frac{1 + \alpha\Delta V - \ln \alpha\Delta V}{\alpha}$$

$$= V_p - \left\{\frac{1}{\alpha} + \frac{\alpha(V_p - V_o)}{\alpha} - \frac{\ln\left[\alpha\ (V_p - V_o)\right]}{\alpha}\right\}$$

$$= V_o + \frac{1}{\alpha}\ (\ln\left[\alpha\ (V_p - V_o)\right] - 1)$$

If V_p is taken as $2V_o$ then

$$r_m = r\ (1 + \frac{1}{\alpha V_o})$$

and $V_1 = V_o + \frac{1}{\alpha}\left[\ln(\alpha V_o) - 1\right]$

APPENDIX D

D1. Normal curve form of positive exponential cusp current

D2. Numerical comparison of exact and approximate positive cusp current

D3. Harmonic components of positive exponential cusp current

D4. Numerical comparison of exact and approximate negative exponential cusp current

D5. Harmonic components of negative exponential cusp current

Appendix D1

Normal curve form of positive exponential cusp current.

The positive exponential cusp current is given by

$$i_{c+} = \frac{\ln(2)}{\alpha r_m} \exp\left[\alpha\hat{V}\ (\cos\theta - \cos\theta_o)/\ln(4)\right]$$

which becomes

$$i_{c+} = \frac{\ln(2)}{\alpha r_m} \exp\left[-\alpha\hat{V}\ (\frac{\phi^2}{2}\cos\theta_o + \phi\sin\theta_o)/\ln(4)\right]$$

under the change of variable

$$\theta = \theta_o + \phi, \qquad \phi \geqslant 0$$

together with the approximations

$$\sin\phi \approx \phi \text{ and } \cos\phi \approx 1 - \phi^2/2$$

The argument of the exponential may be modified as follows:-

$$\alpha\hat{V}\ (\frac{\phi^2}{2}\cos\theta_o + \phi\sin\theta_o)/\ln(4)$$

$$= \frac{\alpha\hat{V}\cos\theta_o}{2}(\phi^2 + 2\tan\theta_o\ \phi)/\ln(4)$$

$$= \frac{\alpha\hat{V}\cos\theta_o}{2}\left[(\phi + \tan\theta_o)^2 - \tan^2\theta_o\right]/\ln(4)$$

The positive cusp current will then be

$$i_{c+} = \frac{\ln(2)}{\alpha r_m} \exp\left[\frac{\alpha\hat{V}\sin\theta_o\ \tan\theta_o}{2\ln(4)}\right] \exp\left[\frac{-\alpha\hat{V}\cos\theta_o\ (\phi + \tan\theta_o)^2}{2\ln(4)}\right]$$

$$= A\exp\left(\frac{-q^2}{2\sigma^2}\right)$$

where

$$A = \frac{\ln(2)}{\alpha r_m} \exp\left(\frac{\alpha\hat{V}\sin\theta_o \tan\theta_o}{2\ln(4)}\right)$$

$$q = (\phi + \tan\theta_o)$$

$$\sigma^2 = \ln(4)/\alpha\hat{V}\cos\theta_o$$

In terms of the dimensionless variables

$$\beta = \alpha V_2/\ln(4) \quad \text{(Bias coefficeint)}$$

$$\chi = \sqrt{\frac{\hat{V}^2 - V_2^{\,2}}{V_2^{\,2}}} \quad \text{(overdrive coefficient)}$$

the parameters of the gaussian curve become

$$A = \frac{\ln(2)}{\alpha r_m} \exp\left(\frac{\beta\chi}{2}\right)$$

$$2 = \ln(4)/\alpha\hat{V} \cos\theta_o$$

$$= \ln(4)/\alpha V_2 = 1/\beta$$

Furthermore the mean value of the gaussian curve

$$\tan\theta_o = \frac{\sin\theta_o}{\cos\theta_o} = \sqrt{\frac{\hat{V}^2 - V_2^{\,2}}{V_2^{\,2}}} = \surd\chi$$

Hence the positive cusp component of current may be expressed as

$$i_{c+} = \frac{\ln(2)}{\alpha r_m} \exp\left(\frac{\beta\chi}{2}\right) \exp\left[-\left(\frac{\phi + \surd\chi}{2/\beta}\right)^2\right]$$

Appendix D2

Numerical Comparison of exact and approximate values of positive cusp current i_{c+}

```
10 INPUTA,R,I1:PRINTA,R,I1
20 OPEN1,4:PRINT#1,A,R,I1:CLOSE1
30 V0=LOG(A*R*I1)/(-A):PRINTV0
40 V1=(A*V0+LOG(A*V0)-2)/(A*(1-1/(A*V0))):PRINTV1
50 OPEN1,4:PRINT#1,V0,V1:CLOSE1
60 PRINT"INPUT PEAK VOLTS":INPUTV2:PRINTV2
70 OPEN1,4:PRINT#1,V2
80 T=SQR(V2*V2-V1*V1):Q=ATN(T/V1):PRINTQ
90 PRINT#1,Q:CLOSE1
105 INPUT U
106 W=180*U/π
110 Y1=EXP((A*V2)*(COS(U)-COS(Q))/LOG(4))
120 T=TAN(Q):S=SIN(Q):C=COS(Q)
130 Z=A*V2*C*T*T/(2*LOG(4))
135 B=((U-Q)+T):B=B*B
140 Y=A*V2*C*B/(2*LOG(4))
150 Z=EXP(Z):Y=EXP(-Y):Y2=Z*Y
160 PRINTW,Y1,Y2
170 OPEN1,4:PRINT#1,W,Y1,Y2:CLOSE1
180 GOTO105
READY.
```

$\alpha = 40$, $r = 10$, $I_s = 10^{-8}$ $V_1 = .352$ $\hat{V} = 0.352V$

angle(degrees)	exact values	approximate values
2.52502501E-03	1	1
2.57831008E-03	1	.999999999
2.86478898E-03	.999999997	.999999997
3.43774677E-03	.999999992	.999999992
5.72957795E-03	.999999959	.999999959
.0572957795	.999994931	.999994931
.572957795	.999492233	.999492228
5.72957795	.950517501	.950477283
6.30253575	.940451511	.940393257
6.87549354	.929553102	.92947156
1.71887339	.99543959	.995439249
7.44845134	.917854858	.917743971
8.02140914	.905391428	.905244321
8.59436693	.892199349	.892008336
9.16732473	.878316853	.878073461
10.3132403	.848640961	.848264384
11.4591559	.816696456	.816144302
12.6050715	.782830836	.782056288
14.3239449	.729209653	.728007514
17.1887339	.63527258	.633104848
20.0535228	.540173752	.536767589
22.9183118	.443485634	.443677902
25.7831008	.363753523	.357536333
28.6478898	.288361183	.280894628
34.3774677	.169606082	.160658069
40.1070457	.0917414153	.0830128121
45.3366236	.0459171982	.0387499533
51.5662016	.0214128585	.0163410785
57.2957795	9.37504783E-03	6.22549261E-03
35.9436693	7.95088354E-05	1.0886565E-05

$\hat{V}$ = 0.38 volts

angle(degrees)	Exact values	Approximate Values
22.1097394	1	1
22.345354	.983088233	.983088186
22.9183118	.942472579	.942470741
23.4912696	.902622926	.902614095
24.0642274	.863589365	.863565294
24.6371852	.825417016	.825366967
25.210143	.788146081	.788057346
25.7831008	.751811911	.751670308
26.3560586	.716445089	.716235435
26.9290164	.682071557	.681778099
27.5019742	.648712732	.648319558
28.074932	.616385679	.615877071
28.6478898	.585103248	.584464023
29.7938054	.525703777	.524761277
30.939721	.470540254	.469246582
32.0856366	.419583907	.417903293
33.2315521	.372758134	.37066861
34.3774677	.329945536	.327439571
37.2422567	.239414551	.235925105
40.1070457	.169974509	.165724996
42.9718347	.118171801	.11349396
45.8366236	.080525849	.075775419
48.7014126	.0538349764	.0493236054
51.5662016	.0353458626	.0313005631
57.2957795	.0144932776	.0116804461
35.9436693	8.41753333E-05	1.84182317E-05

$\hat{V}$ = 0.6 volts

angle(degrees)	Exact values	Approximate Values
54.072509	1	1
53.8580328	1.05380315	1.05380329
54.4209906	.915843543	.915843023
55.0039484	.795143916	.795135906
55.5769062	.68966627	.689636959
56.149864	.597595335	.597528363
56.7228217	.517316842	.517196241
57.2957795	.447397443	.447209502
63.0253575	.0997194095	.0988106125
60.1605685	.21350692	.212898144
68.7549354	.0205489668	.0197233025
74.4845134	3.97721034E-03	3.55663385E-03
35.9436693	1.31885173E-04	8.52724259E-05

Appendix D3

Harmonic components of positive exponential cusp current.

The harmonic components of the positive cusp currents is given by

$$a_{n+} = \frac{2}{\pi} \int_{\theta_o}^{\pi} i_{c+} \cos n\theta \, d\theta$$

$$= \frac{2A}{\pi} \int_{o}^{\infty} \cos n(\theta_o + \phi) \exp\left[- \frac{(\phi + \tan \theta_o)^2}{2\sigma^2} \right] d\phi$$

where $\theta = \theta_o + \phi$, $\phi \geq 0$ and the upper limit $\phi = (\pi - \theta_o)$ has been replaced by ∞ in accordance with Laplaces method because of the dominance of the exponential for large values of ϕ.

Again in accordance with Laplaces method the term $\cos n(\theta_o + \phi)$ may be replaced by

$$(1 - \frac{n^2\phi^2}{2}) \cos n\theta_o - n\phi \sin n\theta_o$$

and therefore a_{n+} may be written as

$$a_{n+} = \frac{2A}{\pi} \int_{o}^{\infty} \cos n\theta_o \exp\left[- \frac{(\phi + \tan \theta_o)^2}{2\sigma^2} \right] d\phi$$

$$- \frac{2A}{\pi} \int_{o}^{\infty} n \sin(\theta_o) \phi \exp\left[- \frac{(\phi + \tan \theta_o)^2}{2\sigma^2} \right] d\phi$$

$$- \frac{2A}{\pi} \int_{o}^{\infty} \frac{n^2}{2} \cos(n\theta_o) \phi^2 \exp\left[- \frac{(\phi + \tan \theta_o)^2}{2\sigma^2} \right] d\phi$$

The first two integrals of this expression are dominant, the last term takes account of the curvature of cos $n\phi$. The first integral is easily expressed in terms of error functions and the remaining two integrals may be determined by integration by parts.

In terms of the normalised parameters β and χ the harmonic components are then given by

$$a_{n+} = \frac{\ln(2)}{\alpha r_m}\sqrt{\frac{2}{\pi\beta}}\exp\left(\frac{\chi\beta}{2}\right)\operatorname{erfc}\left[\sqrt{\frac{\chi\beta}{2}}\right]\cos n\theta_o$$

$$- \frac{\ln(2)}{\alpha r_m}\frac{2n\sin n\theta_o}{\pi\beta}$$

$$+ \frac{\ln(2)}{\alpha r_m}\sqrt{\frac{2\chi}{\pi\beta}}\exp\left(\frac{\chi\beta}{2}\right)\operatorname{erfc}\left[\sqrt{\frac{\chi\beta}{2}}\right]n\sin n\theta_o$$

$$+ \frac{\ln(2)}{\alpha r_m}\frac{\sqrt{\chi}}{\pi\beta}n^2\cos n\theta_o$$

$$- \frac{\ln(2)}{\alpha r_m}\sqrt{\frac{2}{\pi\beta}}\left(\frac{1}{\beta}+\chi\right)\exp\left(\frac{\chi\beta}{2}\right)\operatorname{erfc}\left[\sqrt{\frac{\chi\beta}{2}}\right]\frac{n^2}{2}\cos n\theta_o$$

The last two terms of this expression are due to the curvature of cos nϕ and is a second order correction. The limiting case when the overdrive coefficients is zero is given by

$$a_{n+}(\chi = 0) = \frac{\ln(2)}{\alpha r_m}\sqrt{\frac{2}{\pi\beta}}\exp(o)\operatorname{erfc}(o)\cos 0$$

$$- \frac{\ln(2)}{\alpha r_m}\sqrt{\frac{2}{\pi\beta}}\frac{n^2}{2\beta}\exp(o)\operatorname{erfc}(o)\cos 0$$

$$= \frac{\ln(2)}{\alpha r_m}\sqrt{\frac{2}{\pi\beta}}\left(1 - \frac{n^2}{2\beta}\right)$$

Numerical values of a_{n+} for $\chi = 0$ are given in table 4.1.

Appendix D4

Numerical Comparison of exact and approximate values of negative exponential cusp currents

```
READY.

10 INPUTA,R,I1:PRINTA,R,I1
20 OPEN1,4:PRINT#1,A,R,I1:CLOSE1
30 V0=LOG(A*R*I1)/(-A):PRINTV0
40 V1=(A*V0+LOG(A*V0)-2)/(A*(1-1/(A*V0))):PRINTV1
50 OPEN1,4:PRINT#1,V0,V1:CLOSE1
60 PRINT"INPUT PEAK VOLTS":INPUTV2:PRINTV2
70 OPEN1,4:PRINT#1,V2
80 T=SQR(V2*V2-V1*V1):Q=ATN(T/V1):PRINTQ
81 Q1=180*Q/π:PRINTQ1
90 PRINT#1,Q,Q1:CLOSE1
104 PRINT"INPUT ANGLE IN DEGREES"
105 INPUT W
106 U=W*π/180
110 Y1=EXP((A*V2)*(COS(U)-COS(Q))/LOG(4))
111 Y1=1/Y1
120 T=TAN(Q):S=SIN(Q):C=COS(Q)
130 Y2=1+A*V2*C*(Q-U)*(Q-U)/LOG(8)
135 Y2=Y2*EXP((-1)*(A*V2*S*(Q-U)/LOG(4)))
160 PRINTW,Y1,Y2
170 OPEN1,4:PRINT#1,W,Y1,Y2:CLOSE1
180 GOTO105
READY.
```

$\alpha = 40$, $r = 10$, $I_s = 10^{-8}$, $V_1 = .352$

$\hat{V} = .38$ volts

angle(degrees)	exact	approximate
0	.446517414	.408551226
4	.458604103	.454915465
8	.49679824	.512585387
12	.567408014	.584584006
16	.682814924	.693586207
18	.763656711	.769694098
19	.811463179	.815273538
20	.864989694	.866912144
21	.924945334	.925525428
22	.992145466	.992151624
22.1997	.99999716	.999997158

$\hat{V}$ = 0.5 volts

angle(degrees)	exact	approximate
0	.0139993417	1.6024109E-03
10	.0174299171	6.53314534E-03
20	.0334169039	.0253724974
30	.0967233806	.0969346311
40	.409229255	.413898772
35	.190203547	.194880174
41	.481932	.48576798
42	.569436442	.572224428
43	.675029998	.676677569
44	.802780306	.803401308
45	.957730327	.957759139
45.24	.99963191	.999631908

$\hat{V}$ = 0.8 volts

angle(degrees)	exact	approximate
0	2.43657978E-06	3.62659309E-10
20	9.80289584E-06	6.32026422E-07
40	5.39703369E-04	3.83936495E-04
50	9.2851537E-03	9.18271968E-03
55	.045879877	.0466251143
58	.125683944	.127169076
59	.177139224	.178807326
60	.250735947	.252310266
61	.356039522	.357367836
62	.507294634	.50815495
63	.725196903	.725483887
63.5	.868113735	.868181406
63.8	.967415252	.967419432
63.8916	.999997512	.999997519

Appendix D5

Harmonic Components of negative exponential cusp current

The harmonic components of the negative exponential cusp current is given by

$$a_{n-} = \frac{2}{\pi} \int_0^{\theta_o} i_{c+} \cos n\,\theta \;\; d\theta$$

With the change of variable

$$\theta = \theta_o - \phi, \qquad \phi \geq 0$$

the above equation becomes

$$a_{n-} = \frac{2}{\pi} \int_{\theta_o}^{o} \frac{\ln(2)}{\alpha r_m} \left(1 + \frac{\beta\phi^2}{2}\right) \exp\left(-\beta\sqrt{\chi}\phi\right) \cos\left(\theta_o - \phi\right) \left(-d\phi\right)$$

$$= \frac{2}{\pi} \frac{\ln(2)}{\alpha r_m} \int_o^{\theta_o} \left(\cos n\theta_o \cos n\phi + \sin n\theta_o \sin n\phi\right) \exp\left(-\beta\sqrt{\chi}\phi\right) d\phi$$

$$+ \frac{2}{\pi} \frac{\ln(2)}{\alpha r_m} \int_o^{\theta_o} \left(\cos n\theta_o \cos n\phi + \sin n\theta_o \sin n\phi\right) \frac{\beta\phi^2}{2} \exp\left(-\beta\sqrt{\chi}\phi\right) d\phi$$

The above are standard integrals[24] and reduce to

$$a_{n-} = \frac{2}{\pi} \frac{\ln(2)}{\alpha r_m} \; \frac{\beta\sqrt{\chi} \cos n\theta_o + n \sin n\theta_o - \beta\sqrt{\chi} \exp\left(-\beta\sqrt{\chi}\theta_o\right)}{n^2 + \beta^2\chi}$$

$$- \frac{2}{\pi} \frac{\ln(2)}{\alpha r_m} \frac{\beta \sin n\theta_o}{n\left(n^2 + \beta^2\chi\right)}$$

$$+ \frac{\beta}{2} \frac{\exp\left(-\beta\sqrt{\chi}\theta_o\right)}{\left(n^2 + \beta^2\chi\right)} \left(\beta\sqrt{\chi}\theta_o^{\;2} + \frac{2\left(\beta^2\chi - n^2\right)\theta_o}{\left(n^2 + \beta^2\chi\right)} + \frac{2\beta\sqrt{\chi}\left(\beta^2\chi - 3n^2\right)}{\left(n^2 + \beta^2\chi\right)^2}\right.$$

when $\theta_o = 0$, $\chi = 0$ and the contribution from this term is seen to be zero, as it should be. As the overdrive increases i.e., as $\chi \to \infty$, the exponential terms tend to zero and the expression is dominated by

$$\frac{2}{\pi}\frac{\ln(2)}{\alpha r_m}\frac{\beta\sqrt{\chi}\cos n\theta_o + n\sin n\theta_o - (\beta/n)\sin n\theta_o}{n^2 + \beta^2\chi}$$

$$\longrightarrow \frac{2}{\pi}\frac{\ln(2)}{\alpha r_m}\frac{\beta\sqrt{\chi}\cos n\theta_o}{\beta^2\chi} + \frac{n\sin n\theta_o}{\beta^2\chi} - \frac{\beta\sin n\theta_o}{n\,\beta^2\chi}$$

The most significant contribution is then seen to be given by

$$\frac{2}{\pi}\frac{\ln(2)}{\alpha r_m}\frac{\cos n\theta_o}{\beta\sqrt{\chi}}$$

which agrees with the expression obtained for the hard driven case as given by equation (4.32).

APPENDIX E

E1 Solution of

$$\varepsilon \frac{dy_o}{d\theta} = y_o \sin \theta - y_o^2$$

E2 Evaluation of

$$\frac{1}{\varepsilon} \int_o^{\theta} \exp \left[(\cos \theta_c - \cos \phi)/\varepsilon \right] d\phi$$

Appendix E1

Solution of

$$\frac{\varepsilon dy_o}{d\theta} = y_o \sin\theta - y_o^{\,2} \tag{1}$$

Put $y_o = uV$ (2)

then (1) becomes

$$\frac{\varepsilon u dV}{d\theta} + \frac{\varepsilon V du}{d\theta} = uV \sin\theta - u^2V^2 \tag{3}$$

Equate $\frac{\varepsilon u dV}{d\theta} = uV \sin\theta$ (4)

to give

$$\frac{dV}{V} = \frac{\sin\theta \; d\theta}{\varepsilon} \tag{5}$$

from which is obtained

$$V = \exp\,(-\cos\theta/\varepsilon) \tag{6}$$

Now equate

$$\frac{\varepsilon V du}{d\theta} = -u^2V^2 \tag{7}$$

which becomes

$$-\frac{du}{u^2} = \frac{1}{\varepsilon}\exp\,(-\cos\theta/\varepsilon) \tag{8}$$

on cancelling a common factor and using equation (6) and therefore

$$\frac{1}{u} = A + \frac{1}{\varepsilon}\int_0^\theta \exp\,(-\cos q/\varepsilon)\, dq \tag{9}$$

where q is a dummy variable. The required solution is therefore

$$y_o = uV = \frac{\exp\,(-\cos\theta/\varepsilon)}{A + \frac{1}{\varepsilon}\int_0^\theta \exp\,(-\cos q/\varepsilon)\, dq} \tag{10}$$

Appendix E2

Evaluation of $\frac{1}{\varepsilon} \int_0^{\theta} \exp\left[(\cos\theta_c - \cos\phi)/\varepsilon \right] d\phi$

Figure E1 shows a graph of the variation of the intergrand over the range 0 to 2π. The function achieves a local maximum at $\phi = \pi$, and the effect of the small parameter ε is to concentrate the majority of the area in the neighbourhood of $\phi = \pi$.

Range 1, θ close to θ_c

Let $\phi = \theta_c + q$ and therefore $d\phi = dq$

When $\phi = 0, \quad q = -\theta_c$

$\phi = \theta_c \quad q = 0$

$\phi = \theta \quad q = \theta - \theta_c$

Also $\cos\theta_c - \cos\theta \approx q \sin\theta_c$

Then

$$\frac{1}{\varepsilon}\int_0^{\theta} e^{(\cos\theta_c - \cos\phi)/\varepsilon}\, d\phi = \frac{1}{\varepsilon}\int_0^{\theta_c} e^{(\cos\theta_c - \cos\phi)/\varepsilon}\, d\phi$$

$$+ \frac{1}{\varepsilon}\int_{\theta_c}^{\theta} e^{(\cos\theta_c - \cos\theta)/\varepsilon}\, d\phi$$

$$= \int_{-\theta_c}^{0} \frac{e^{q\sin\theta_c/\varepsilon}}{\varepsilon}\, dq + \int_0^{\theta-\theta_c} \frac{e^{q\sin\theta_c/\varepsilon}\, dq}{\varepsilon}$$

$$= \left. \frac{e^{q\sin\theta_c/\varepsilon}}{\sin\theta_c} \right|_{-\theta_c}^{0} + \left. \frac{e^{q\sin\theta_c/\varepsilon}}{\sin\ \ c} \right|_{0}^{\theta-\theta_c}$$

$$= \frac{1}{\sin\theta_c}\left(1 - e^{-\theta_c \sin\theta_c/\varepsilon}\right) + \frac{1}{\sin\theta_c}\left(e^{(\theta-\theta_c)\sin\theta_c/\varepsilon} - 1\right)$$

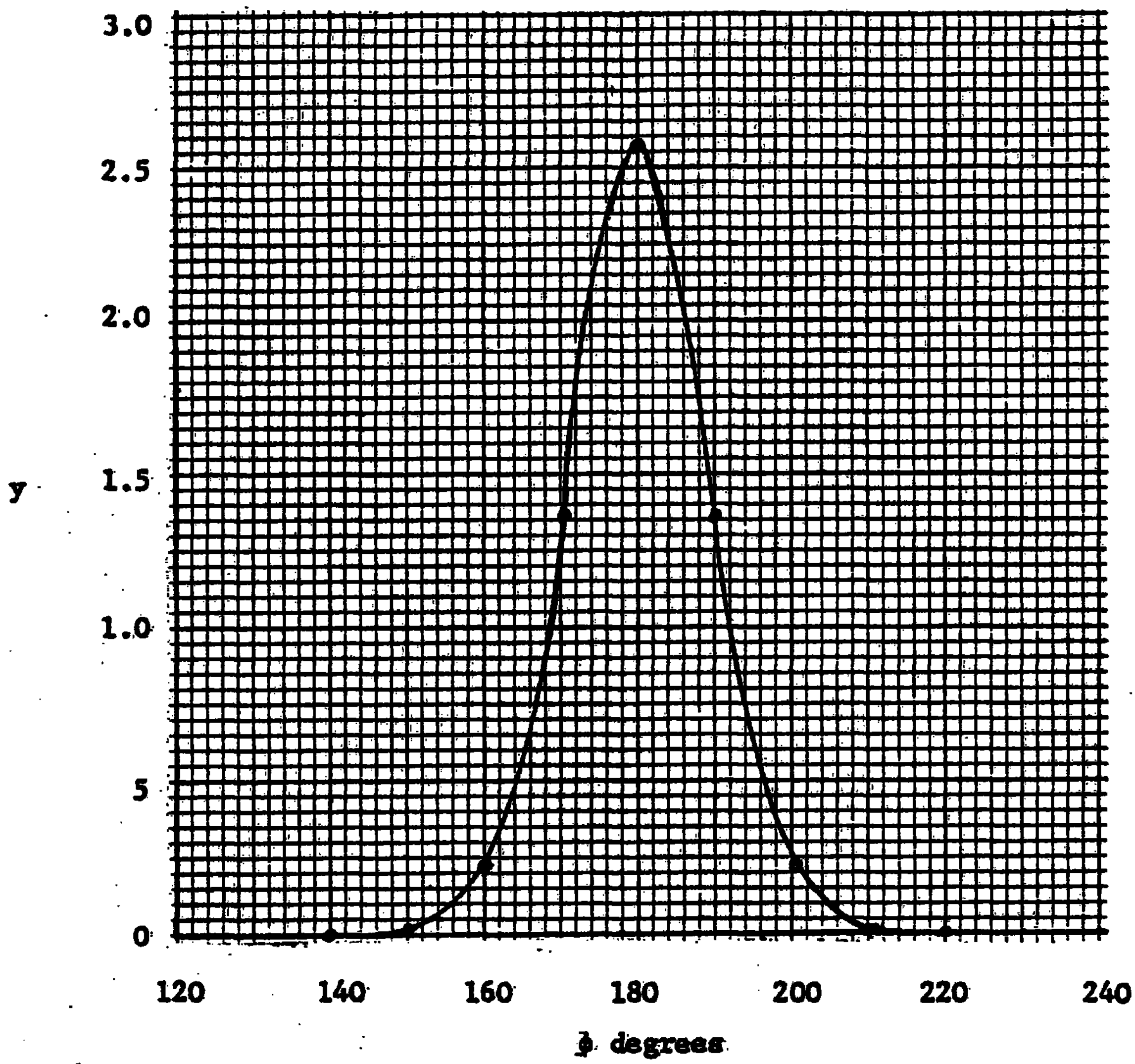

Figure E1

Graph of $y = \exp\left[(\cos\theta_c - \cos\phi)/\varepsilon\right]/10^{32}$

$\varepsilon = 0.025 \qquad \theta_c = 30^{\circ}$

Since ε is small the first term approximates to $1/\sin\theta_c$ and if θ is close to θ_c the second term approximates to $(\theta - \theta_c)/\varepsilon$. Thus when θ is close to θ_c the integral approximates to

$$1/\sin\theta_c + (\theta - \theta_c)/\varepsilon$$

<u>Range 2,</u> $\theta_c < \theta < \pi$

In this range the supremum of the integrand occurs at the upper limit of integration. The substitution $\theta = \phi + q$ transforms the integral into

$$\frac{1}{\varepsilon}\int_0^{\theta} e^{\frac{\cos\theta_c - \cos\theta}{\varepsilon}}\, e^{-q\sin\theta/\varepsilon}\, dq$$

which readily integrates to

$$\frac{\exp\left[(\cos\theta_c - \cos\theta)/\varepsilon\right]}{\sin\theta}$$

which is exponentially large since $\cos\theta_c > \cos\theta$

<u>Range 3,</u> $\pi < \theta \leq 2\pi$

In this range the integrand has a local maxima at $\theta = \pi$. The substitution

$$\pi + q = \phi$$

converts $-\cos\phi$ into

$$-\cos(\pi + q) = -\cos\pi\cos q + \sin\pi\sin q$$

$$\doteq +(1 - q^2/2)$$

hence the integral becomes

$$\frac{e^{\cos\theta_c/\varepsilon}}{\varepsilon}\, e^{+1/\varepsilon}\int_{-\infty}^{+\infty} e^{-q^2/2\varepsilon}\, dq$$

$$= \frac{e^{\cos\theta_c/\varepsilon}}{\varepsilon}\, e^{+1/\varepsilon}\sqrt{2\pi\varepsilon}$$

<u>Note</u>: this value is achieved for θ exceeding π by approximately $3/\varepsilon$, the value of the integral remains essentially constant for values of θ exceeding $\pi + 3/\varepsilon_o$

APPENDIX F

F1	Sampling Theorems
F2	Programme to transfer data to computer and evaluate harmonic content
F3	Error due to false periodic time
F4	Effect of quantising error

Appendix F1

Sampling Theorems

1. Definition

The spectral density function $F(\omega)$ of a time signal $f(t)$ is the Fourier Transform at $f(t)$ and is given by

$$F(\omega) = \int_{-\infty}^{+\infty} f(t) \exp(-j\omega t)\, dt$$

2. The Frequency Translation Theorem

If the spectral density of $f(t)$ is $F(\omega)$ then the spectral density of $f(t) \exp(jat)$ is $F(\omega - a)$

Proof

By definition 1 the spectral density of $f(t) \exp(at)$ is

$$\int_{-\infty}^{+\infty} f(t) \exp(jat) \exp(-j\omega t)\, dt$$

$$= \int_{-\infty}^{+\infty} f(t) \exp\left[-j(\omega - a)t\right] dt$$

$$= F(\omega - a)$$

3. The spectral density of the gate function $G_\varepsilon(t, T)$, defined as unity for $T - \varepsilon/2 \leq t \leq T + \varepsilon/2$

$$F(\omega) = \varepsilon \exp(-j\omega T)\, Sa(\omega\varepsilon/2)$$

where $Sa(\omega\varepsilon/2)$ is the sampling function defined by

$$Sa(\omega\varepsilon/2) = \frac{\sin(\omega\varepsilon/2)}{(\omega\varepsilon/2)}$$

<u>Proof</u>

$$F(\omega) = \int_{T-\varepsilon/2}^{T+\varepsilon/2} \exp(-j\omega t)\, dt$$

$$= \varepsilon . \exp(-j\omega T) \frac{\exp(j\omega\varepsilon/2) - \exp(-j\omega\varepsilon/2)}{2j\,(\omega\varepsilon/2)}$$

$$= \varepsilon . \exp(-j\omega T)\ Sa\ (\omega\varepsilon/2)$$

4. <u>Fourier Series of an Impulse Chain</u>

Let $I(t, T_s)$ be an infinite chain of unit impulses of periodic time T_s i.e.

$$I(t, T_s) = \sum_{-\infty}^{+\infty} \delta(t - kT_s) \qquad \text{where } \delta(t) \text{ is the dirac impulse function}$$

Then the complex Fourier coefficients $C_n(j\omega)$ are

$$C_n(j\omega) = 1/T_s \text{ for all } n,$$

and

$$I(t, T_s) = \frac{1}{T_s} \sum_{-\infty}^{+\infty} \exp(jn\ \omega_s t)$$

<u>Proof</u>

$$C_n(j\omega) = \frac{1}{T_s} \int_{-T_s/2}^{+T_s/2} \delta(t) \exp(-jn\ \omega_s t)\, dt$$

$$= 1/T_s$$

5. <u>The spectral density of an impulse sampled waveform</u>

Let $f(t)$ be a time signal having a spectral density $F(\omega)$. Then the impulse sampled waveform F_{IS} is given by

$$f_{IS} = \sum_{-\infty}^{+\infty} f(t)\ \delta(t - nT_s)$$

where T_s is the sampling interval

then

$$F_{IS}(\omega) = \sum_{-\infty}^{+\infty} \int_{-\infty}^{+\infty} \delta(t - nT_s) f(t) \exp(-j\omega t)\, dt$$

$$F_{IS}(\omega) = \sum_{\infty}^{\infty} f(nT_s) \exp(-jn\omega T_s)$$

Alternatively

$$f_{IS}(t) = f(t).\ I(t, T_s)$$

$$= f(t) \frac{1}{T_s} \sum_{\infty}^{\infty} \exp(jn\omega_s t) \qquad \text{from (4)}$$

$$\therefore\ F_{IS}(\omega) = \frac{1}{T_s} \sum_{-\infty}^{+\infty} \int_{-\infty}^{+\infty} f(t) \exp(jn\omega_s t) \exp(-n\omega t)\, dt$$

$$= \frac{1}{T_s} \sum_{-\infty}^{+\infty} F(\omega - n\omega_s) \qquad \text{by the Translation Theorem}$$

hence

$$F_{IS}(\omega) = \frac{1}{T_s} \sum_{-\infty}^{+\infty} F(\omega - n\omega_s) = \sum_{-\infty}^{+\infty} f(nT_s) \exp(-jn\omega T_s)$$

6. Return to Zero Sample and Hold (RZ)

Let $F(\omega)$ be the spectral density of $f(t)$ then the sampled-and-held waveform may be expressed as

$$f_{RZ}(t) = \sum_{\infty}^{\infty} f(nT_s)\, G_\varepsilon\, (nT_s + {}^{\varepsilon}/2)$$

where T_s is the sampling interval, ε is the sample width and $G_\varepsilon\, (nT_s + {}^{\varepsilon}/2)$ is the gate function of width ε centred on $t = (nT_s + {}^{\varepsilon}/2)$

Then

$$F_{RZ}(\omega) = \sum_{\infty}^{\infty} f(nT_s) \int_{\infty}^{\infty} G_\varepsilon\, (nT_s + {}^{\varepsilon}/2) \exp(-jn\omega t)\, dt$$

which by 3 becomes

$$\varepsilon \exp(-j\omega\varepsilon/2)\ Sa(\omega\varepsilon/2) \sum_{-\infty}^{+\infty} f(nT_s) \exp(-j\, n\omega T_s)$$

which by 5 is

$$F_{RZ} = \frac{\varepsilon}{T_s} \exp(-j\omega\varepsilon/2)\ Sa(\omega\varepsilon/2) \sum_{-\infty}^{+\infty} F(\omega - n\omega_s)$$

7. <u>Non Return to Zero Sampling (NRZ)</u>

In this form of sampling the sample width ε equals the sampling interval T_s. From (6) the spectral density will be

$$F_{NRZ}(\omega) = \exp(-j\omega T_s/2)\ Sa(\omega T_s/2) \sum_{-\infty}^{+\infty} F(\omega - n\omega_s)$$

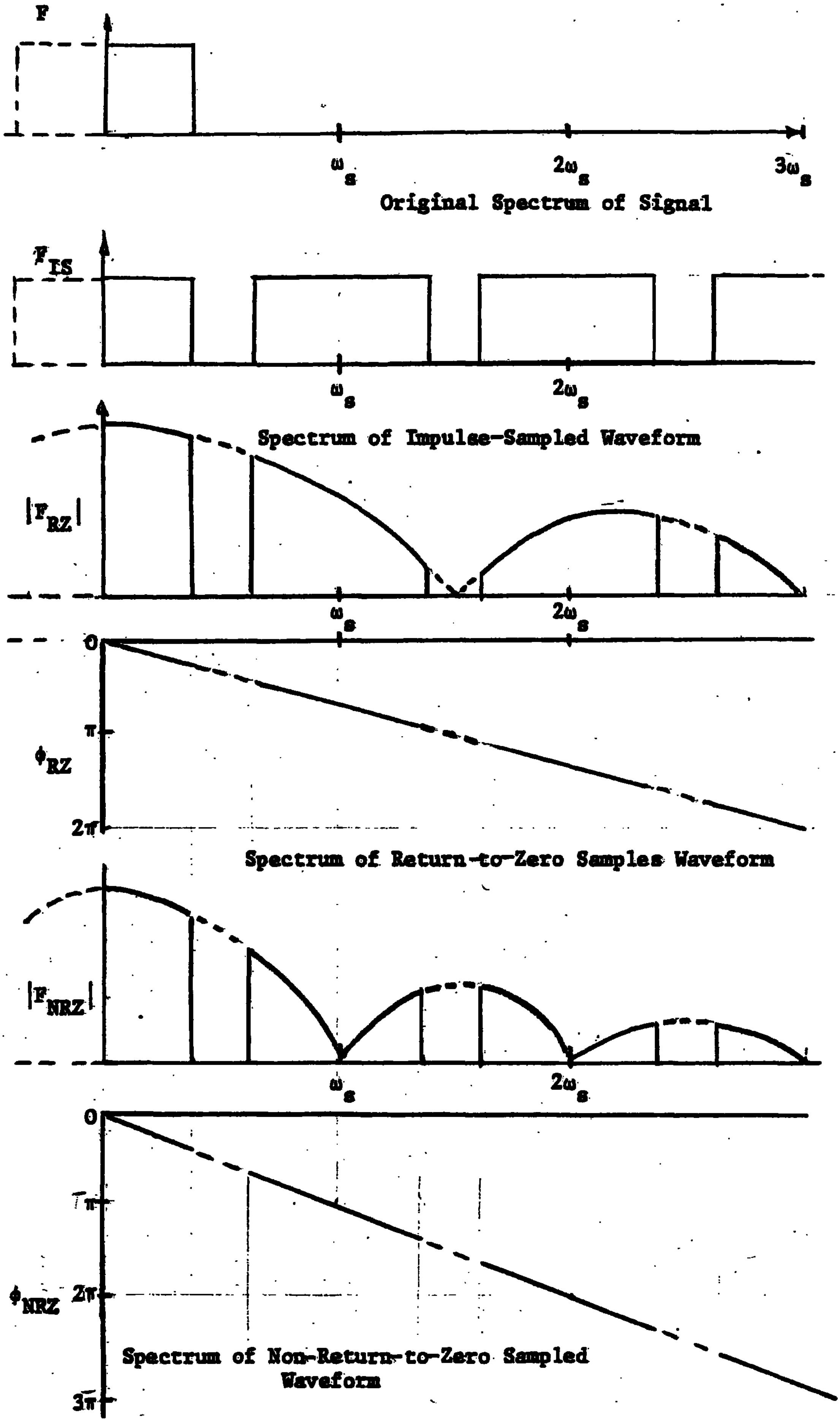

Figure F1

Effect of Sampling on Signal Spectrum

Appendix F2

Programme to transfer data to computer and evaluate harmonic content

```
READY.

0 OPEN1,4
1 REM DATA TRANSFER FROM 901 TO PET
2 PRINT"□"
3 PRINT"  THIS PROGRAM ENABLES THE 1024 WORD    STORED";
4 PRINT" IN THE 901 MEMORY TO BE READ OUT IN SEQUENCE TO THE PET.";
5 PRINT"THE NUMBER OF    WORDS OR SAMPLES TO BE STORED IN THE PET";
6 PRINT"IS GIVEN BY (N+1) WHERE N=N2-N1 N2>N1";
7 PRINT",  AND N1,N2 ARE TWO NUMBERS BETWEEN 0 AND  1023 INCLUSIVE."
8 PRINT"THE ARRAYS ALLOCATED FOR DATA STORAGE   ARE FROM X(0) TO X(N).";
9 PRINT"MAXIMUM ARRAY SIZE IS 255."
10 PRINT:PRINT:PRINT
11 A=59457:POKE 3999,PEEK (A)
12 B=59459 :POKE B,0
13 C=59468:POKE C,PEEK (C) OR 1
14 D=59467:POKE D,PEEK (D) AND 227 OR 1
15 E=59469 :L=0
16 INPUT "N1=";N1:PRINT#1,"N1=",N1
17 INPUT "N2=";N2:PRINT#1,"N2=",N2
18 IF N2>1023 OR N1<0 THEN 40
19 IF N2<N1 THEN 40
20 N=N2-N1
21 DIM X(N):INPUT"RESISTOR VALUE";RES
22 INPUT "VOLTS FULL SCALE=";F
23 PRINT:PRINT"DATA TRANSFER BEGINS.WATCH THE SCOPE"
24 FOR I=0 TO 1023
25 POKE C,PEEK (C) OR 224
26 POKE C,PEEK (C) AND 31 OR 192
27 WAIT E,2
28 IF N1=<I AND I<=N2 THEN 30
29 GOTO 32
30 K=I-N1
31 X(K)=PEEK (A)*F/(256*RES)
32 NEXT I
33 PRINT"END OF DATA TRANSFER"
34 PRINT"□"
35 FOR J=N1 TO N2
36 K=J-N1
37 PRINT J,X(K)
38 NEXT J
39 GOTO 80
40 PRINT"TRY AGAIN"
41 IF L=3 THEN 43
42 L=L+1:GOTO 15
```

```
46 GOTO 19
47 IF N<255  GOTO 80
48 PRINT"ERROR ARRAY CAN ONLY HANDLE 255 SAMPLES"
80 PRINT "HOW MANY HARMONICS REQUIRED"
81 INPUT H
82 DIM A(H+1),B(H+3)
83 IF H>0 GOTO 86
84 PRINT "ERROR"
85 GOTO 410
86 IF H<N/2 GOTO 89
87 PRINT "ERROR TOO MANY HARMONICS REQUESTED"
88 GOTO 410
89 COEFF=2.0/(N-1)
90 K1=π*COEFF
91 S1=SIN(K1)
100 C1=COS(K1)
110 C=1.0
120 S=0.0
121 PRINT"PLEASE DON'T WORRY! COMPUTATION TAKES        TIME"
130 J=1
140 FTTZ=X(1)
150 U2=0.0
160 U1=0.0
170 I=N
180 U0=X(I)+2.0*C*U1-U2
190 U2=U1
200 U1=U0
210 I=I-1
220 IF (I-1)>0 GOTO180
230 A(J)=COEF*(FTTZ+C*U1-U2)
240 B(J)=COEF*S*U1
250 IF (J-H-0)>0 GOTO 301
260 Q=C1*C-S1*S
270 S=C1*S+S1*C
280 C=Q
290 J=J+1
300 GOTO 150
301 PRINT#1,"RESISTOR VALUE=",RES
302 PRINT#1,"VOLTS FULL SCALE=",F
310 A(1)=A(1)*0.5
311 PRINT#1,"DC VALUE=",A(1)
312 PRINT#1,"COS TERM",           "SIN TERM"
320 FOR L=2 TO H+1:PRINT#1,A(L),B(L):NEXT L
330 PRINT "FOR MAGNITUDE & PHASE TYPE 1,OTHERWISE TYPE 0"
340 INPUT Y
350 IF Y=0 GOTO 410
360 DIM R(H+1),P(H+1)
365 PRINT#1,"MAGNITUDE              PHASE"
370 FOR L=2 TO H+1
380 R(L)=SQR(A(L)↑2+B(L)↑2)
390 P(L)=ATN(-B(L)/A(L))*180/π
400 PRINT#1,R(L),P(L):NEXT L
```

```
410 PRINT"FOR  CHEBYCHEV TYPE 1,OTHERWISE 0"
420 INPUT Y
430 IF Y=0 GOTO 630
440 DIM D(13)
450 FOR E=1 TO 13:READ D(E):NEXT E
460 DATA -1,-0.866,-0.66,-.5,-0.33,-0.167,0,0.167,0.33,0.5,0.66,0.866,1
461 DIMB1(H+3)
462 DIM A1(13)
470 FOR E=1TO 13
480 M=2*D(E)
500 B1(H+2)=0
510 B1(H+1)=0
520 FOR I=H+1TO2 STEP -1
530 B1(I)=A(I)+M*B1(I+1)-B1(I+2)
534 NEXT I
540 A1(E)=(A(1)-B1(3))+B1(2)*D(E)
541 NEXT E
549 V=H+2
560 DIMF1(13)
565 DIMT(V)
566 FOR E=1 TO 13
570 T(H+2)=0
580 T(H+1)=0
590 FOR I=H TO 2STEP-1
600 T(I)=B(I+1)+M*T(I+1)-T(I+2)
610 NEXT I
620 F1(E)=(B(2)-T(3))+T(2)*2*D(E)
621 F1(E)=SQR(1-D(E)↑2)*F1(E)
622 NEXT E
629 PRINT#1,"A(N)                    +/- B(N)"
631 FOR E=1 TO 13:PRINT#1,A1(E),F1(E):NEXT E
632 CLOSE1
650 END
EADY.
```

Appendix F3

Error due to false periodic time

Let $f_T(t)$ be the periodic wave under investigation, where T is the true periodic time. Then it may be represented as

$$f_T(t) = \sum_{n=-\infty}^{+\infty} C_n \exp(jn\omega_o t) \quad ; \quad \omega_o T = 2\pi \tag{1}$$

Let the measurement of the periodic time be $\overline{T}$, then the signal transferred for computation will be

$$f_{\overline{T}}(t) = \sum_{k=-\infty}^{+\infty} \overline{C}_k \exp(kj\overline{\omega}_o t) \quad ; \quad \overline{\omega}_o \overline{T} = 2\pi \tag{2}$$

To determine the modified coefficients $\overline{C}_k$, $f_{\overline{T}}(t)$ may be written as

$$f_{\overline{T}}(t) = \sum_n C_n \exp(jn\omega_o t) \tag{3}$$

with $0 \leq t \leq \overline{T}$

and then

$$\overline{C}_k = \frac{1}{\overline{T}} \int_0^{\overline{T}} (\sum_n C_n \exp(jn\omega_o t) \exp(-jk\overline{\omega}_o t) dt \tag{4}$$

which integrates to

$$\overline{C}_k = \sum_n C_n \exp\left[-j(n\omega_o - k\overline{\omega}_o)\overline{T}/2\right] Sa\left[(n\omega_o - k\overline{\omega}_o)\overline{T}/2\right] \tag{5}$$

where Sa is the sampling function

The arguments of the functions in (5) may be modified as follows

$$(n\omega_o - k\overline{\omega}_o)\overline{T}/2 = (n\omega_o/\overline{\omega}_o - k)\pi$$

$$= \left[n - k - n\varepsilon\right]\pi \tag{6}$$

where

$$\frac{\omega_o}{\overline{\omega}_o} = \frac{\overline{\omega}_o - \Delta\omega}{\overline{\omega}_o} = 1 - \varepsilon$$

$\Delta\omega$ is the error in angular frequency

and ε is the per unit error in ω_o

The modified coefficients are then given by

$$\overline{C}_k = \sum_n C_n \exp\left[-j\,(n-k-n\varepsilon)\pi\right] \mathrm{Sa}\left[(n-k-n\varepsilon)\pi\right] \tag{7}$$

Note that if $\varepsilon = 0$ then the sampling function is unity for $n = k$ and zero otherwise and

$$\overline{C}_k = C_k \tag{8}$$

as expected.

<u>Special Case</u>

Consider the case of a cosinusoidal wave

$$f_T(t) = C_o + a_1 \cos \omega_o t \tag{9}$$

$$= C_{-1} \exp\,(-j\omega_o t) + C_o + C_1 \exp\,(j\omega_o t)$$

where

$$C_{-1} = C_1 = a_1/2$$

Then equation (7) shows that

$$\overline{C}_o = C_o - \varepsilon a_1 \tag{10}$$

$$\overline{C}_1 = \frac{a_1}{2} \exp\,(j\varepsilon\pi) - \frac{\varepsilon a_1}{4} \exp\,(-j\varepsilon\pi) \tag{11}$$

$$\overline{C}_{-1} = \frac{a_1}{2} \exp\,(-j\varepsilon\pi) - \frac{\varepsilon a_1}{4} \exp\,(+j\varepsilon\pi) \tag{12}$$

resulting in

$$\overline{a}_1 = \overline{C}_1 + \overline{C}_{-1}$$

$$= a_1 - \varepsilon a_1/2 \tag{13}$$

and $\bar{b}_1 = - a_1 \varepsilon\pi - \varepsilon^2 a_1 /4$ (14)

where $\bar{b}_1$ is the magnitude of the sine component created by the false measurement of periodic time which creates a phase error of

$$\phi_\varepsilon \approx \tan^{-1}\left[\frac{-a_1\ \varepsilon\pi}{a_1}\right] \approx -\varepsilon\pi \qquad (15)$$

In a similar manner the second harmonic coefficient $\bar{C}_2$ of the modified wave may be expressed in terms of C_o and a_1 as

$$C_2 = \frac{-\varepsilon a_1}{3.2} \exp\ (-\ j\varepsilon\pi) + \frac{\varepsilon a_1}{2} \exp\ (j\varepsilon\pi) \qquad (16)$$

which shows that higher harmonics are present in the wave-form which is transferred to the computer than in the wave-form stored in the transient recorder.

<u>Appendix F4</u>

<u>Effect of Quantising Error</u>

Let one cycle of a waveform be sampled N times, where the samples are numbered from 0 to N-1. For convenience take N odd so that N-1 is divisible by powers of 2.

The coefficient of cos pθ, is given by

$$a_p = \frac{1}{\pi} \int_0^{2\pi} f(t) \cos p\theta \quad d\theta \tag{1}$$

which may be approximated by the sum

$$a_p = \frac{2}{N} \sum_{k=0}^{N-1} f\left(\frac{k2\pi}{N}\right) \cos \left(\frac{pk2\pi}{N}\right) \tag{2}$$

Now $\left|f(2\pi k/N) - \bar{f}(2\pi k/N\right| \leq 1/2M$ (3)

where $\bar{f}$ represented the quantised level and M is the number of levels available.

If $\bar{a}_p$ is the coefficient representing the quantised wave then

$$|a_p - \bar{a}_p| = \frac{2}{N} \left| \sum_{k=0}^{N-1} \left[f(2\pi k/N) - \bar{f}(2\pi k/N)\right] \cos (pk2\pi/N) \right| \tag{4}$$

$$\leq \frac{1}{NM} \sum_{0}^{N-1} |\cos(pk2\pi/N)|$$

$$= \frac{4}{NM} \sum_{0}^{(N-1)/4} |\cos pk2\pi/N| \tag{5}$$

Equation (5) is readily summed to give

$$|a_p - \bar{a}_p| \leq \frac{4p}{NM} \frac{\sin\left\{\left[\frac{(N-1)}{4} + p\right] \pi/N\right\} \cos \left(\frac{N-1}{N} \frac{\pi}{4}\right)}{\sin (p\pi/N)} \tag{6}$$

If the (max p)/N is small equation (6) simplifies to

$$\frac{2}{\pi M} \left(1 + \frac{p\pi}{N}\right) \tag{7}$$

Equation (7) gives the error per full scale; the absolute error is then given by multiplying equation (7) by the system scale factor. If N is even the effect of the extra term may be added separately. An identical argument shows that the quantising error produced in the coefficient of sin pθ is also given by equation (7).

APPENDIX G

G1	Measured diode waveforms
G2	Predicted diode waveforms
G3	Programme to transfer data to computer and print sample values
G4	Measured spectrum (20 kHz)
G5	Predicted spectral response (20 kHz)
G6	Predicted and measured spectrum (10 MHz)
G7	Harmonic contribution from positive exponential cusp by method of steepest descent.

Appendix G1

Measured diode Waveforms

DIODE TYPE HP 5082-2800

ALPHA= 37.54 IS= 3.4E-09 **RS = 22.65**

TEST FREQ= 40000
TEST VOLTS= .499142 SOURCE RES= 55
VOLTS FULL SCALE= .1 MONITOR RES= 45
NS= 151 NF= 277 SAMPLES= 127
RT= 122.65
V0= .294745568 V3= .45
V1= .315063016 RM= 143.694048

0	-3.48583878E-05
4	1.25490196E-03
8	1.08932462E-03
12	7.93028323E-04
16	4.53159042E-04
20	1.1328976E-04
24	8.71459695E-06
28	0
32	0
36	0
40	0
44	0
48	0
52	0
56	0
60	0
64	0
68	0
72	0
76	0
80	0
84	0
88	0
92	0
96	0
100	0
104	4.35729848E-05
108	2.70152505E-04
112	6.2745098E-04
116	9.32461874E-04
120	1.17647059E=03
124	1.28104575E-03

DIODE TYPE HP 5082-2800

ALPHA= 37.54 IS= 3.4E-09 RS = 22.65

TEST FREQ= 40000.

TEST VOLTS= .69286 SOURCE RES= 55

VOLTS FULL SCALE= .2 MONITOR RES= 45

NS= 152 NF= 276 SAMPLES= 125

RT= 122.65

V0= .294745568 V3= .6

V1= .333072616 RM= 133.353143

0	1.74291939E-05
3	2.63180828E-03
6	2.47494553E-03
9	2.23093682E-03
12	1.88235294E-03
15	1.44662309E-03
18	9.41176471E-04
21	4.18300654E-04
24	6.97167756E-05
27	1.74291939E-05
30	0
33	1.74291939E-05
36	0
39	1.74291939E-05
42	0
45	1.74291939E-05
48	0
51	1.74291939E-05
54	1.74291939E-05
57	1.74291939E-05
60	0
63	1.74291939E-05
66	1.74291939E-05
69	1.74291939E-05
72	1.74291939E-05
75	1.74291939E-05
78	1.74291939E-05
81	0
84	1.74291939E-05
87	1.74291939E-05
90	1.74291939E-05
93	1.74291939E-05
96	0
99	1.74291939E-05
102	1.56862745E-04
105	5.40305011E-04
108	1.04575163E-03
111	1.53376906E-03
114	1.96949891E-03
117	2.30065359E-03
120	2.52723312E-03
123	2.64923747E-03

DIODE TYPE HP 5082-2800
ALPHA= 37.54 IS= 3.4E-09 RS = 22.65

TEST FREQ= 40000
TEST VOLTS= .33936 SOURCE RES= 55
VOLTS FULL SCALE= .02 MONITOR RES= 45
NS= .158 NF= 282 SAMPLES= 125
RT= 122.65
V0= .294745568 V3= .4
V1= .304709135 RM= 153.690799

0	5.22875817E-06
3	3.10239651E-04
6	2.61437909E-04
9	1.84749455E-04
12	1.04575163E-04
15	4.53159042E-05
18	1.39433551E-05
21	3.48583878E-06
24	0
27	0
30	0
33	0
36	0
39	-1.74291939E-06
42	0
45	-1.74291939E-06
48	0
51	0
54	-1.74291939E-06
57	0
60	-1.74291939E-06
63	0
66	0
69	0
72	0
75	0
78	0
81	0
84	0
87	0
90	0
93	0
96	0
99	0
102	1.74291939E-06
105	8.71459695E-06
108	3.31154684E-05
111	8.71459695E-05
114	1.60348584E-04
117	2.37037037E-04
120	2.98039216E-04
123	3.24183007E-04

Appendix G2

Predicted Diode Waveforms
Diode Type HP5082-2800

Peak Test Voltage = 0.7 Volts

Sample Number	System Voltage (Volts)	Diode Current (amperes)
0	.69286	2.69801267E-03
3	.684870163	2.63809976E-03
6	.661084925	2.4597461E-03
9	.622052853	2.16708514E-03
12	.568674158	1.7669838E-03
15	.502179931	1.26953733E-03
18	.424103751	6.94401731E-04
21	.336246318	1.50857765E-04
24	.240633918	1.13294623E-05
27	.139471693	7.31978375E-07
30	.0350927836	4.33468573E-08
33	-.0700954835	2.51129995E-09
36	-.173667113	1.52002911E-10
39	-.273233398	1.02543893E-11
42	-.366498004	8.20499131E-13
45	-.451309938	8.25379149E-14
48	-.525713152	1.10062622E-14
51	-.587991659	2.0380647E-15
54	-.636709109	5.44853703E-16
57	-.670741912	2.16790168E-16
60	-.689305159	1.3113779E-16
63	-.691970719	1.22005591E-16

Peak Test Voltage = 0.5 volts

Sample Number	System Voltage (Volts)	Diode Current (amperes)
0	.499142	1.28192719E-03
4	.489245256	1.21332366E-03
8	.459947479	1.01082528E-03
12	.412410474	6.8666884E-04
16	.348519322	2.84761772E-04
20	.270807627	3.87641355E-05
24	.18235705	3.53356814E-06
28	.0866750989	2.64821222E-07
32	-.0124439553	1.80829923E-08
36	-.111069544	1.25138567E-09
40	-.205290667	9.75686856E-11
44	-.291370984	9.48350983E-12
48	-.365896977	1.2604091E-12
52	-.425913317	2.48138238E-13
56	-.469040053	7.71800078E-14
60	-.493566996	3.97244123E-14
64	-.498521527	3.47368214E-14

Peak Voltage = 0.34 Volts

Sample Number	System Voltage (Volts)	Diode Current (amperes)
0	.33936	2.72466566E-04
3	.33544661	2.52258921E-04
6	.323796698	1.95842792E-04
9	.304678948	1.20040643E-04
12	.278534281	5.91365305E-05
15	.24596568	2.44813385E-05
18	.207724286	8.69160544E-06
21	.164692074	2.71033375E-06
24	.117861511	7.62562265E-07
27	.0683126659	1.99324047E-07
30	.0171883022	4.99246815E-08
33	-.0343324817	1.23711149E-08
36	-.0850614433	3.13194803E-09
39	-.133828603	8.36164806E-10
42	-.179509226	2.42699122E-10
45	-.221049766	7.88013561E-11
48	-.257492156	2.93734922E-11
51	-.287995915	1.28593297E-11
54	-.311857523	6.73900239E-12
57	-.328526651	4.29101005E-12
60	-.337618853	3.35452738E-12
63	-.338924434	3.23800233E-12

Appendix G3

Programme to enable waveform samples to be transferred to computer and print sample values.

```
READY.

 1 REM DATA TRANSFER FROM 901 TO PET
 2 PRINT"J"
 3 PRINT"  THIS PROGRAM ENABLES THE 1024 WORD    STORED";
 4 PRINT" IN THE 901 MEMORY TO BE READ OUT IN SEQUENCE TO THE PET.";
 5 PRINT"THE NUMBER OF    WORDS OR SAMPLES TO BE'STORED IN THE PET";
 6 PRINT"IS GIVEN BY (N+1) WHERE N=N2-N1 N2>N1";
 7 PRINT",  AND N1,N2 ARE TWO NUMBERS BETWEEN 0 AND  1023 INCLUSIVE."
 8 PRINT"THE ARRAYS ALLOCATED FOR DATA STORAGE   ARE FROM X(0) TO X(N)."
 9 PRINT"MAXIMUM ARRAY SIZE IS 255."
 10 PRINT:PRINT:PRINT
 11 A=59457:POKE 3999,PEEK (A)
 12 B=59459 :POKE B,0
 13 C=59468:POKE C,PEEK (C) OR 1
 14 D=59467:POKE D,PEEK (D) AND 227 OR 1
 15 E=59469 :L=0
 16 INPUT "N1=";N1
 17 INPUT "N2=";N2
 18 IF N2>1023 OR N1<0 THEN 40
 19 IF N2<N1 THEN 40
 20 N=N2-N1
 21 DIM X(N)
 23 PRINT:PRINT"DATA TRANSFER BEGINS.WATCH THE SCOPE"
 24 FOR I=0 TO 1023
 25 POKE C,PEEK (C) OR 224
 26 POKE C,PEEK (C) AND 31 OR 192
 27 WAIT E,2
 28 IF N1=<I AND I<=N2 THEN 30
 29 GOTO 32
 30 K=I-N1
 31 X(K)=PEEK (A)
 32 NEXT I
 33 PRINT"END OF DATA TRANSFER"
 34 PRINT"J"
 35 FOR J=N1 TO N2
 36 K=J-N1
 37 PRINT J,X(K)
 38 NEXT J
 39 GOTO 50
 40 PRINT"TRY AGAIN"
 41 IF L=3 THEN 43
 42 L=L+1:GOTO 15
 43 PRINT:PRINT"POOR OLD CHAP! YOU CAN'T EVEN THINK OF TWO SIMPLE NUMBER
 45 PRINT"WELL TRY N1=0,N2=1023"
 46 GOTO 19
 47 IF N<255  GOTO 50
 48 PRINT"ERROR ARRAY CAN ONLY HANDLE 255 SAMPLES"
 50 PRINT
 51 INPUT"TYPE NUMBER";TYPE$:PRINTTYPE$
 55 INPUT"ALPHA IS RS";AA,IS,RS
 60 INPUT"TEST VOLTAGE";VT:VT=VT*1.414:PRINTVT
 61 INPUT"SOURCE RES";RG
 62 INPUT"TEST FREQUENCY";FT:PRINT FT
 83 INPUT"VOLTS FULL SCALE";F:PRINT F
 84 INPUT"RESISTOR VALUE";RES:PRINTRES
```

```
100 INPUT"NS&NF";NS,NF:PRINTNS,NF
102 SA=NF-NS+1:PRINTSA
104 TS=2*π/(NF-NS):PRINTTS
112 RT=RG+RES+RS:PRINTRT
114 V0=LOG(AA*RT*IS)/(-AA):PRINTV0
116 B=V0+(3/AA):PRINT"V3 MUST EXCEED",B
118 INPUT"V3=";V3:PRINT V3
120 V1=V0+(LOG(AA*(V3-V0))-1)/AA:PRINT V1
122 RM=RT*(1+1/(AA*(V3-V0))):PRINTRM
200 PRINT"DO YOU REQUIRE A PRINT OUT OF SAMPLE VALUES 1FOR YES 0 FOR NO"
201 INPUT PR:IF PR=0 GOTO228
202 PRINT"I WILL PRINT EVERY J,TH SAMPLE":INPUT"J=";J
203 SC=F/(255*RES):INPUT"ZERO REF=";M
204 M=M-N1:Z=X(M)
205 FOR K=0TO(N2-N1)
206 X(K)=SC*(X(K)-Z)
208 NEXTK:OPEN1,4
209 INPUT"HEADINGS";H:IFH=0GOTO220
210 PRINT#1,"DIODE TYPE",TYPE$
212 PRINT#1,"ALPHA=",AA,"IS=",IS,"RS=",RS
213 PRINT#1,"TEST FREQ=",FT
214 PRINT#1,"TEST VOLTS=",VT,"SOURCE RES=",RG
216 PRINT#1,"VOLTS FULL SCALE=",F,"MONITOR RES=",RES
217 PRINT#1,"NS=",NS,"NF=",NF,"SAMPLES=",SA
218 PRINT#1,"RT=",RT:PRINT#1,"V0=",V0,"V3=",V3
219 PRINT#1,"V1=",V1,"RM=",RM:PRINT#1
220 FOR K=0 TO (NF-NS)STEP J
222 PRINT#1,K,X(K)
224 NEXTK
226 CLOSE1
228 LOAD"WF"
230 END
READY.
```

Programme to evaluate predicted diode current from equations (3.50) and (3.51)

```
READY.

10 REM WF
12 OPEN1,4:PRINT#1:PRINT#1
14 EX=EXP(AA*V1/LOG(4))
16 KP=LOG(2)/(AA*RM*EX):KN=EX*EX*KP
18 PRINT"I WILL CALUATE EVERY J,TH SAMPLE"
20 INPUT"J=";J:K=0
22 V=VT*COS(K*TS):IFV>V1GOTO30
24 IP=KP*EXP(AA*V/LOG(4)):IN=0:IB=0
26 ID=IP+IN+IB
28 PRINT#1,K,V,ID:GOTO36
30 IP=0:IN=KN/EXP(AA*V/LOG(4)):IB=(V-V1)/RM
32 ID=IP+IN+IB
34 PRINT#1,K,V,ID
36 IF K>(NF-NS)/2GOTO40
38 K=K+J:GOTO22
40 CLOSE1
42 END
READY.
```

Appendix G4

Measured Spectrum

Diode Type HP5082-2800/1

Source Resistance = 50Ω, Monitor Resistance = 50Ω

Test 1 **Peak Volts = 0.848 (0.6 V rms)**

```
N1=                330

N2=                577
RESISTOR VALUE=              50
VOLTS FULL SCALE=            .2
DC VALUE=              1.09025715E-03
COS TERM              SIN TERM
 1.53366168E-03             -5.6304278E-05
 1.04697428E-03             -7.31053325E-05
 4.20959701E-04             -4.83787319E-05
 2.05269809E-05             -2.74587574E-06
-8.89518464E-05              1.76178647E-05
-2.66871537E-05              1.01515908E-05
 5.34900158E-05             -5.41300492E-06
 6.78694052E-05             -1.21106481E-05
 3.73585305E-05             -3.07974576E-06
 1.44803742E-05              5.59809897E-06


MAGNITUDE               PHASE
 1.53592791E-03             2.34165487
 1.04395847E-03             4.32083812
 4.23730541E-04             6.55594698
 2.07098233E-05             7.6191734
 9.0679767E-05             11.2030525
 2.85527401E-05             20.8264351
 5.37632069E-05             5.7784634
 6.89414531E-05             10.1173996
 3.74852588E-05             4.71266735
 1.55266826E-05            -21.1337935
```

Test 2 **Peak Volts 0.6 V (0.424 V rms)**

```
N1=             329
N2=             574
RESISTOR VALUE=          50
VOLTS FULL SCALE=         .1
DC VALUE=            4.46369261E-04
COS TERM           SIN TERM
 7.36452531E-04          -2.82619206E-05
 5.30624503E-04          -4.11337913E-05
 2.85300135E-04          -3.39139851E-05
 9.09527686E-05          -1.48889353E-05
-9.657026E-06            2.07439776E-06
-2.64322943E-05           7.29461299E-06
-2.64131763E-06           3.75835378E-06
 2.200851E-05            -2.93458906E-06
 2.89861163E-05          -4.94361955E-06
 2.20051043E-05          -3.11246956E-06
MAGNITUDE            PHASE
 7.36994616E-04           2.19769028
 5.32216452E-04           4.43258016
 2.87308763E-04           6.77901068
 9.21633686E-05           9.29633938
 9.87731123E-06           12.1233158
 2.74203859E-05           15.4280946
 4.59366758E-06           54.9009965
 2.22032954E-05           7.59435303
 2.94046648E-05           9.67874194
 2.22241329E-05           8.05068684
```

Test 3 Peak Volts 0.5 V (.354 V rms)

```
N1=             327
N2=             574
RESISTOR VALUE=          50
VOLTS FULL SCALE=         .1
DC VALUE=            4.45407959E-04
COS TERM             SIN TERM
 4.611933E-04           -1.10142048E-05
 3.45571718E-04            -1.59629379E-05
 2.03799057E-04            -1.42269209E-05
 8.24733221E-05            -8.93353743E-06
 9.36601491E-06            -2.63473176E-06
-1.46335531E-05             1.5845506E-06
-8.24680673E-06             2.36489601E-06
 6.90848645E-06             1.6137792E-08
 1.59362422E-05            -6.95292694E-07
 1.68481428E-05            -1.65722197E-06
MAGNITUDE             PHASE
 4.61324802E-04             1.36807607
 3.45940208E-04             2.64477453
 2.04295034E-04             3.99325818
 8.29557529E-05             6.18219375
 9.72954503E-06             15.7116994
 1.47190922E-05             6.18002388
 8.5791931E-06             16.3010415
 6.90850528E-06            -.133839112
 1.59514027E-05             2.49821055
 1.69294507E-05             5.61767352
```

Test 4 Peak Volts 0.4 (.283 V rms)

```
N1=                 324
N2=                 574
RESISTOR VALUE=              50
VOLTS FULL SCALE=              .05
DC VALUE=            3.06146316E-04
COS TERM            SIN TERM
 2.19622213E-04            3.34533219E-06
 1.72106109E-04            4.90251035E-06
 1.11663236E-04            3.94691099E-06
 5.62774548E-05            1.79420399E-06
 1.81903314E-05           -3.56615136E-07
-3.70092663E-07           -1.89934604E-06
-3.76958238E-06           -2.06981802E-06
-2.87143651E-08           -1.38218487E-06
 4.38797696E-06           -6.07366361E-07
 6.97503878E-06           -8.88715326E-08
MAGNITUDE             PHASE
 2.19647689E-04           -.872673995
 1.7217592E-04           -1.63165164
 1.11732969E-04           -2.02436577
 5.63060484E-05           -1.8260511
 1.81938267E-05            1.12312001
 1.93506691E-06           -78.9739229
 4.30045323E-06           -28.7704917
 1.3824831E-06           -88.3098732
 4.42981215E-06            7.88058104
 6.97560492E-06            .729987083
```

Appendix G5

Predicted Spectral Response

Bi-linear approximations fitted at V_3 volts

Effective turn voltage V_1 volts

Effective total resistance RM

```
DIODE TYPE          HP 5082-2800/1
ALPHA=              37.54            IS=           3.4E-09            RS= 22.65
SOURCE RES=               50
MONITOR RES=               50
TOTAL RES=             122.65
VO=                .294745568
PEAK VOLTS=              .848
V3=                .6
V1=                .333072616
RM=                133.353143
BIAS FACTOR=              9.0194019
OVERDRIVE FACTOR=                  2.34138249
ANGLE=             1.16714992           RADIANS
ANGLE=             66.8727644           DEGREES
NUMBER OF HARMONICS =              10
```

(a) bi-linear

```
 9.33555034E-04
 1.63134551E-03
 1.04953709E-03
 4.12231209E-04
-1.5610824E-05
-1.45585777E-04
-7.49987231E-05
 2.8606531E-05
 5.91449402E-05
 2.00449695E-05
-2.47797943E-05
```

(b) positive exponential cusp

```
 4.38963406E-06
 7.43080239E-07
-1.74585374E-05
-1.81035338E-05
 4.46353594E-06
 1.93913708E-05
 3.37503649E-06
-2.5973736E-06
 8.3055837E-06
 1.71891263E-05
-1.52543016E-05
```

(c) negative exponential cusp

```
 3.40352439E-06
 1.3537323E-06
-2.22946536E-06
-3.31041755E-06
-6.48961822E-07
 1.78762723E-06
 3.12650025E-06
-1.14312883E-07
-1.22212033E-06
-1.75115303E-06
 9.27122426E-07
```

(b) + (c)

```
 7.49915945E-06
 1.39681353E-06
-1.36300629E-05
-2.14140514E-05
 3.81462411E-06
 2.2178998E-05
 1.20815367E-05
-2.72138619E-06
 5.01943237E-06
 1.44279813E-05
-1.42671695E-05
```

(a) + (b) + (c)

```
 9.41054194E-04
 1.63324232E-03
 1.02985703E-03
 3.90817158E-04
-1.17961999E-05
-1.23406779E-04
-6.29171863E-05
 2.58851448E-05
 6.4154503E-05
 3.44324782E-05
-3.90469638E-05
```

```
IODE TYPE            HP 5082-2800/1
LPHA=             37.54             IS=              3.4E-09                  RS=22.65

OURCE RES=              50
ONITOR RES=              50
OTAL RES=              122.65
Q=              .294745568
EAK VOLTS=              .6
3=              .5
1=              .322500019
M=              138.567716
IAS FACTOR=              8.73310247
VERDRIVE FACTOR=              1.56886266
NGLE=              1.00332666              RADIANS
NGLE=              57.4063833              DEGREES
UMBER OF HARMONICS =              10
```

4.18965314E-04			
7.58157021E-04			
5.50983157E-04			
2.96153464E-04			
8.08223639E-05	(a)	9.94305152E-06	
-4.07951239E-05	bi-linear	5.60241108E-06	
-6.5962985E-05		-1.89824474E-05	
-3.27850978E-05		-3.48342592E-05	
9.23411662E-06		-1.30233783E-05	
2.76123995E-05		3.54875259E-05	
1.84101058E-05		6.15932658E-05	(b) + (c)
		2.74136253E-05	
5.903345549E-06		-4.60624754E-05	
3.39961751E-06		-8.36966896E-05	
-1.75781511E-05		-4.81382994E-05	
-3.09119382E-05	(b)		
-9.71825281E-06	positive	4.28908365E-04	
3.5438181E-05	exponential	7.63759433E-04	
5.80861112E-05	cusp	5.3200071E-04	
2.32126361E-05		2.61319205E-04	
-4.74385724E-05		6.77989856E-05	
-8.58896064E-05		-5.30759799E-06	
-4.32856123E-05		-4.36971919E-06	(a) + (b) + (c)
		-5.37147256E-06	
4.03959603E-06		-3.68283588E-05	
2.20279357E-06		-6.10842901E-05	
-1.40429633E-06		-2.97281936E-05	
-3.92232099E-06			
-3.3051255E-06	(c)		
4.93448669E-08	negative		
3.50715465E-06	exponential		
4.20098914E-06	cusp		
1.37609698E-06			
-2.80708318E-06			
-4.3526871E-06			

[illegible]
[illegible] TYPE HP5082-2[illegible]
[illegible]= [illegible]7.54 IS= [illegible].4E-0[illegible] **RS = 22.65**

SOURCE RES= 50
MONITOR RES= 50
TOTAL RES= 122.65
VO= .294745568
PEAK VOLTS= .5
[illegible]= .45
V1= .315063016
RM= 143.694048
BIAS FACTOR= 8.53171301
OVERDRIVE FACTOR= 1.23228185
ANGLE= .889080816 RADIANS
ANGLE= 50.9405784 DEGREES
NUMBER OF HARMONICS = 10

(a) bi-linear

2.39528594E-04
4.42808484E-04
3.45702498E-04
2.17836143E-04
3.55765702E-05
7.68833213E-06
-3.40405041E-05
-3.60188777E-05
-1.63941705E-05
5.08269684E-06
1.56735006E-05

(b) positive exponential cusp

7.18025706E-06
5.50518262E-06
-1.58516547E-05
-3.78525711E-05
-2.64743414E-05
2.71283971E-05
8.19030748E-05
7.47867716E-05
-1.40742713E-05
-1.22489774E-04
-1.45989682E-04

(c) negative exponential cusp

4.08721012E-06
2.62052255E-06
-4.32947848E-07
-3.251111E-06
-4.22968737E-06
-2.63034769E-06
7.56753707E-07
3.93673118E-06
4.807799E-06
2.53060472E-06
-1.70670115E-06

(b) + (c)

1.12674672E-05
8.12570517E-06
-1.62546026E-05
-4.11036821E-05
-3.07040288E-05
2.44980494E-05
8.26647611E-05
7.87235028E-05
-9.26647233E-06
-1.19959169E-04
-1.47696383E-04

(a) + (b) + (c)

2.50796061E-04
4.50934189E-04
3.29447895E-04
1.76732461E-04
6.48725414E-05
3.21863815E-05
4.86242571E-05
4.27046251E-05
-2.56606428E-05
-1.14876473E-04
-1.32022882E-04

DIODE TYPE HP 5082-2800/1

ALPHA= 37.54 IS= 3.4E-09 RS= 22.65

SOURCE RES= 50

MONITOR RES= 50

TOTAL RES= 122.65

VO= .294745568

PEAK VOLTS= .41

V3= .4

V1= .304709135

RM= 153.690799

BIAS FACTOR= 8.25133628

OVERDRIVE FACTOR= .900273647

ANGLE= .732966268 RADIANS

ANGLE= 41.9958737 DEGREES

NUMBER OF HARMONICS = 10

(a) bi-linear

1.05585148E-04
2.00156354E-04
1.69559968E-04
1.26015783E-04
7.84728659E-05
3.57553866E-05
4.33041959E-06
-1.30501869E-05
-1.74928229E-05
-1.29707579E-05
-4.64238355E-06

(b) positive exponential cusp

9.1693202E-06
8.68576096E-06
-1.09579963E-05
-4.11705528E-05
-4.81495303E-05
-4.21987328E-06
7.26856572E-05
1.18402219E-04
7.49113556E-05
-4.71752788E-05
-1.60328395E-04

(c) negative exponential cusp

3.75811779E-06
2.87200151E-06
1.04292679E-06
-1.21296552E-06
-3.19739784E-06
-4.15367424E-06
-3.52224366E-06
-1.26525493E-06
1.925801 75E-06
4.74291191E-06
5.7615203E-06

(b) + (c)

1.2927438E-05
1.15577616E-05
-9.91506948E-06
-4.23835183E-05
-5.13469281E-05
-8.37354751E-06
6.91634135E-05
1.17136964E-04
7.68371574E-05
-4.24323669E-05
-1.54566875E-04

(a) + (b) + (c)

1.18512586E-04
2.11714115E-04
1.59644898E-04
8.36322648E-05
2.71259379E-05
2.73818391E-05
7.34938331E-05
1.04086778E-04
5.93443345E-05
-5.54031247E-05
-1.59209259E-04

Appendix G6

Predicted and Measured Spectrum

Predicted Spectrum

```
DIODE TYPE            HP 5082-2835
ALPHA=            38.16          IS=          8.9E-09          RS=8.05

SOURCE RES=             50
MONITOR RES=             50
TOTAL RES=             108.05
VO=               .267631882
PEAK VOLTS=               .47
V3=               .45
V1=               .292266574
RM=               123.576283
BIAS FACTOR=             8.04511133
OVERDRIVE FACTOR=             1.25938595
ANGLE=            .899701486          RADIANS
ANGLE=            51.549098           DEGREES
NUMBER OF HARMONICS =          5
```

2.70779532E-04 4.99640669E-04 3.37651931E-04 2.41058971E-04 1.02350829E-04 4.50864371E-06	(a) bi-linear	1.59420262E-05 1.0629117E-05 -2.08926614E-05 -5.13828264E-05 -3.73094018E-05 3.07286886E-05	(b) + (c)
8.51192436E-06 6.3572513E-06 -1.94916042E-05 -4.51104281E-05 -2.98740071E-05 3.47319539E-05	(b) positive exponential cusp	2.86721558E-04 5.10269786E-04 3.66759319E-04 1.89676145E-04 6.50414267E-05 3.52373323E-05	(a) + (b) + (c)
7.43010182E-06 4.27186567E-06 -1.40105716E-06 -6.2723983E-06 -7.43539471E-06 -4.00326525E-06	(c) negative exponential cusp		

Predicted Spectrum

DIODE TYPE HP 5082-2835

ALPHA= 38.16 IS= 8.9E-09 RS=8.05
.05
SOURCE RES= 50
MONITOR RES= 50
TOTAL RES= 108.05
VO= .267631882
PEAK VOLTS= .4
V3= .4
V1= .283869287
RM= 129.441095
BIAS FACTOR= 7.8139624
OVERDRIVE FACTOR= .992754097
ANGLE= .781762054 RADIANS
ANGLE= 44.7916663 DEGREES
NUMBER OF HARMONICS = 5

1.47286328E-04
2.77166556E-04
2.29322673E-04 **(a)**
1.62744159E-04 **bi-linear**
9.27296709E-05
3.34956323E-05

1.05467195E-05
9.52823871E-06
-1.54205768E-05 **(b)**
-4.94138886E-05 **positive**
-4.98381363E-05 **exponential**
1.04704081E-05 **cusp**

9.1978461E-06
5.4178752E-06
5.72135284E-07 **(c)**
-4.5654426E-06 **negative**
-8.05876613E-06 **exponential**
-8.32706842E-06 **cusp**

1.87445656E-05
1.49461139E-05
-1.48484415E-05
-5.39793312E-05 **(b) + (c)**
-5.78969024E-05
2.1433397E-06

1.66030893E-04
2.92112669E-04
2.14474231E-04 **(a) + (b) + (c)**
1.08764828E-04
3.48327686E-05
3.5638972E-05

Measured Spectrum

Diode Type HP5082-2835

Peak Volts 0.47 V

Frequency 10 MHz

```
N1=             325
N2=             575
RESISTOR VALUE=             50
VOLTS FULL SCALE=            .1
DC VALUE=            6.34475435E-04
COS TERM            SIN TERM
 5.2063247E-04            -1.94308653E-05
 3.97284068E-04            -9.49837528E-06
 2.40875748E-04            -4.63403513E-06
 9.87959815E-05             3.27697944E-06
 1.14059892E-05             8.62619613E-06


MAGNITUDE            PHASE
 5.2099494E-04            2.13738128
 3.97397596E-04            1.36958213
 2.40920319E-04            1.10213631
 9.88503139E-05           -1.89975622
 1.43006241E-05           -37.099726
```

Measured Spectrum

Diode Type HP5082-2835

Peak Volts 0.41 V

Frequency 10 MHz

```
N1=             325
N2=             575
RESISTOR VALUE=             50
VOLTS FULL SCALE=            .05
DC VALUE=            2.50878598E-04
COS TERM            SIN TERM
 2.84874715E-04            -2.77894511E-05
 2.33445223E-04            -2.22034239E-05
 1.56948927E-04            -1.88503976E-05
 8.06362228E-05            -9.82502714E-06
 2.7033297E-05            -2.58416789E-07
MAGNITUDE            PHASE
 2.86226933E-04            5.57155946
 2.34498751E-04            5.43316775
 1.5807689E-04            6.8487208
 8.12325771E-05            6.94689524
 2.70345321E-05            .54768534
```

Appendix G7

Harmonic contribution from positive exponential cusp (using method of steepest descent).

Using the "normal" form of the positive exponential cusp current the harmonic contribution may be written as

$$a_{n+} = \frac{2A}{\pi} \int_0^\infty \cos\,(n\theta_o + nx)\, \exp\left[-\frac{\beta}{2}\,(x + \sqrt{\chi})^2\right] dx \qquad (1)$$

where

$$A = \frac{\ln(2)}{\alpha r_m} \exp\,(\frac{\beta\chi}{2}) \qquad (2)$$

$$\theta = \theta_o + x$$

The cosine function may be replaced by the complex exponential function $\exp\left[-j\,(n\theta_o + nx)\right]$ and therefore

$$a_{n+} = \mathrm{Re}\,\frac{2A}{\pi} \exp\,(-jn\,\theta_o) \int_o^\infty \exp\left[-\frac{\beta}{2}\,(x + \sqrt{\chi})^2 - jnx\right] dx \qquad (4)$$

where Re denotes the real part is to be taken

By completing the square in the exponential contained in the intergrand the integral may be written as

$$a_{n+} = B \int_o^\infty \exp\left[-\frac{\beta}{2}\,(x + Z_o)^2\right] dx \qquad (5)$$

where

$$B = \frac{2A}{\pi} \exp\,(-n^2/2\beta)\, \exp\left[jn(\sqrt{\chi} - \theta_o)\right] \qquad (6)$$

and $Z_o = \sqrt{\chi} + jn/\beta$ (7)

The integral in (5) may be written as an integral in the complex plane as follows:-

$$I = \int_o^\infty \exp\left[-\frac{\beta}{2}\,(x + Z_o)^2\right] dx = \int_{T_1} \exp\left[-\frac{\beta}{2}\,(Z + Z_o)^2\right] dz \qquad (8)$$

where the path of integration T_1 is the real line and $Z = x + jy$. The complex integral in (8) may be written concisely by means of the substitution

$$Z_1 = Z + Z_o \tag{9}$$

so that

$$I = \int_{T_2} \exp\left(-\frac{\beta}{2} Z_1^2\right) dz_1 \tag{10}$$

where T_2 is the line parallel to the real axis starting at Z_o, i.e.

$$y = j\, n/\beta, \qquad \sqrt{\chi} \leq x < \infty \tag{11}$$

Lines of constant magnitude and phase may be obtained by observing that

$$Z_1^2 = (x^2 - y^2) + j2xy \tag{12}$$

and therefore

$$\exp\left(-\frac{\beta}{2} Z_1^2\right) = \exp\left[-\frac{\beta}{2}(x^2 - y^2)\right] \exp\left[-j\beta xy\right] \tag{13}$$

Lines of constant magnitude and phase are shown in Figure G1. The origin, $Z_1 = 0$, is a saddle point. The initial limit of the integral, $Z_1 = \sqrt{\chi} + jn/\beta$, is dictated by the degree of overdrive $\sqrt{\chi}$, the harmonic number n, and the bias factor β. Since the function to be integrated is analytic, Cauchy's Theorem allows the path of integration to be distorted along a line of constant phase i.e. maximum descent, as shown in Figure G1.

For the case $\sqrt{\chi} = 0$, the lines of maximum descent consist of the axes $y = 0$ and $x = 0$.

Then

$$I = \int \exp\left[-\frac{\beta}{2} Z_1{}^2\right] dz_1$$

$$= \int_{\frac{n}{\beta}}^{o} \exp\left[\frac{\beta y^2}{2}\right] j\ dy + \int_{o}^{\infty} \exp\left[-\frac{\beta}{2} x^2\right] dx \qquad (15)$$

$$= jY + \sqrt{\frac{\pi}{2\beta}} \qquad (15)$$

where Y represents the value of the integral along the imaginary axis.

$$a_{n+} = \text{Re}\left\{\frac{2A}{\pi} \exp\ (-\ n^2/2\beta)\left[\ jY + \sqrt{\frac{\pi}{2\ \beta}}\ \right]\right\} \qquad (16)$$

$$= \frac{2\ln(2)}{\pi\alpha r_m} \exp\ (-\ n^2/2\beta)\ \sqrt{\frac{\pi}{2\beta}}$$

$$= \frac{\ln(2)}{\alpha r_m} \sqrt{\frac{2}{\pi\beta}} \exp\ (-\ n^2/2\beta) \qquad (17)$$

Equation (17) gives the harmonic contribution when the overdrive $\sqrt{\chi} = 0$ and is uniform for all harmonic numbers. For sufficiently large bias factor β, (17) may be approximated as

$$\frac{\ln(2)}{\alpha r_m} \sqrt{\frac{2}{\pi\beta}}\ (1 - n^2/2\beta) \qquad (18)$$

which is the limiting case of equation (4.41) used to compile Table (4.1). It will be observed that the non-zero integral along the y axis does not contribute to the harmonic content.

For $\sqrt{\chi} > 0$ the integral in (10) may be transformed by the conformal mapping.

$$\omega = u + jv = Z_1{}^2 = (x + jy)^2 \qquad (19)$$

into

$$I = \int_{T_{vo}} \exp\left[-\frac{\beta}{2} Z_1{}^2\right] dz_1 = \int_{T_{vo}} \frac{\exp\left[\ -\ \beta\omega/2\ \right] d\omega}{2\sqrt{\omega}}$$

where T_{vo} is a line of constant phase given by

$$V_o = 2\sqrt{\chi}\, n/\beta \tag{21}$$

and therefore

$$I = \int_{u_o}^{\infty} \frac{\exp\left[-\frac{\beta}{2}(u + jV_o)\right]}{2\sqrt{u + jV_o}}\, du$$

$$= \frac{1}{2}\exp\left(-\frac{j\beta V_o}{2}\right) \int_{u_o}^{\infty} \frac{\exp\left[-\frac{\beta u}{2}\right]}{\sqrt{u + jV_o}}\, du \tag{22}$$

where $u_o = \chi^2 - n^2/\beta^2$ (23)

For sufficiently large β and since $u \neq 0$ on T_{V_o} then the integral in (22) is dominated by values close to u_o.

The substitution

$$u = u_o + \delta \tag{24}$$

converts (22) into

$$I = \frac{1}{2}\exp\left(\frac{-j\beta V_o}{2}\right) \int_0^{\infty} \frac{\exp\left(\frac{-\beta u_o}{2}\right)\exp\left(-\frac{\beta\delta}{2}\right) d\delta}{\sqrt{u_o + jV_o + \delta}} \tag{25}$$

$$I = \frac{1}{2}\exp\left(\frac{-\beta Z_o^2}{2}\right) \int_0^{\infty} \frac{\exp(-\beta\delta/2)}{Z_o\sqrt{1 + \delta/Z_o^2}}\, d\delta \tag{26}$$

since $w_o = u_o + jV_o = Z_o^2$ (27)

Application of Watsons Lemma(23) now gives an asymptotic expansion for large β, i.e.

$$I = \frac{1}{2Z_o}\exp\left(\frac{-\beta Z_o^2}{2}\right) \int_0^{\infty} \exp\left(\frac{-\beta\delta}{2}\right)\left[1 - \frac{\delta}{2Z_o^2} + \frac{3}{8}\frac{\delta^2}{Z_o^4} - \cdots\right] \tag{28}$$

$$= \frac{1}{\beta Z_o}\exp\left[-\frac{\beta Z_o^2}{2}\right] + 0\,({}^1/\beta^2) \tag{29}$$

Substituting (29) into (5), combining the exponentials and selecting the real part we find that the contribution to the harmonic component from the first term of the asymptotic series (29) is given by

$$a_{n+} = \frac{2\ln(2)}{\pi\alpha r_m} \frac{\cos(n\theta_o + \psi)}{\sqrt{n^2 + \beta^2\chi}},$$

$$\text{where } \tan\psi = n/\beta\sqrt{\chi} \tag{30}$$

Equation (30) is uniform for all harmonic numbers n, and resembles the form of the denominator for the expansion of the negative cusp harmonic contribution, which were exactly integratable. Regretably (30) does not contain the case of zero overdrive as a limiting form. If $\sqrt{\chi} = 0$, but $n \neq 0$ then since the integral is dictated by values of the variable close to the supremum of the function the process would force the integral to be purely imaginary which as has been seen does not contribute to the Fourier coefficients. If both $\sqrt{\chi}$ and n are zero then $Z_o = 0$ and the expansion of the denominator of (26) is not possible.

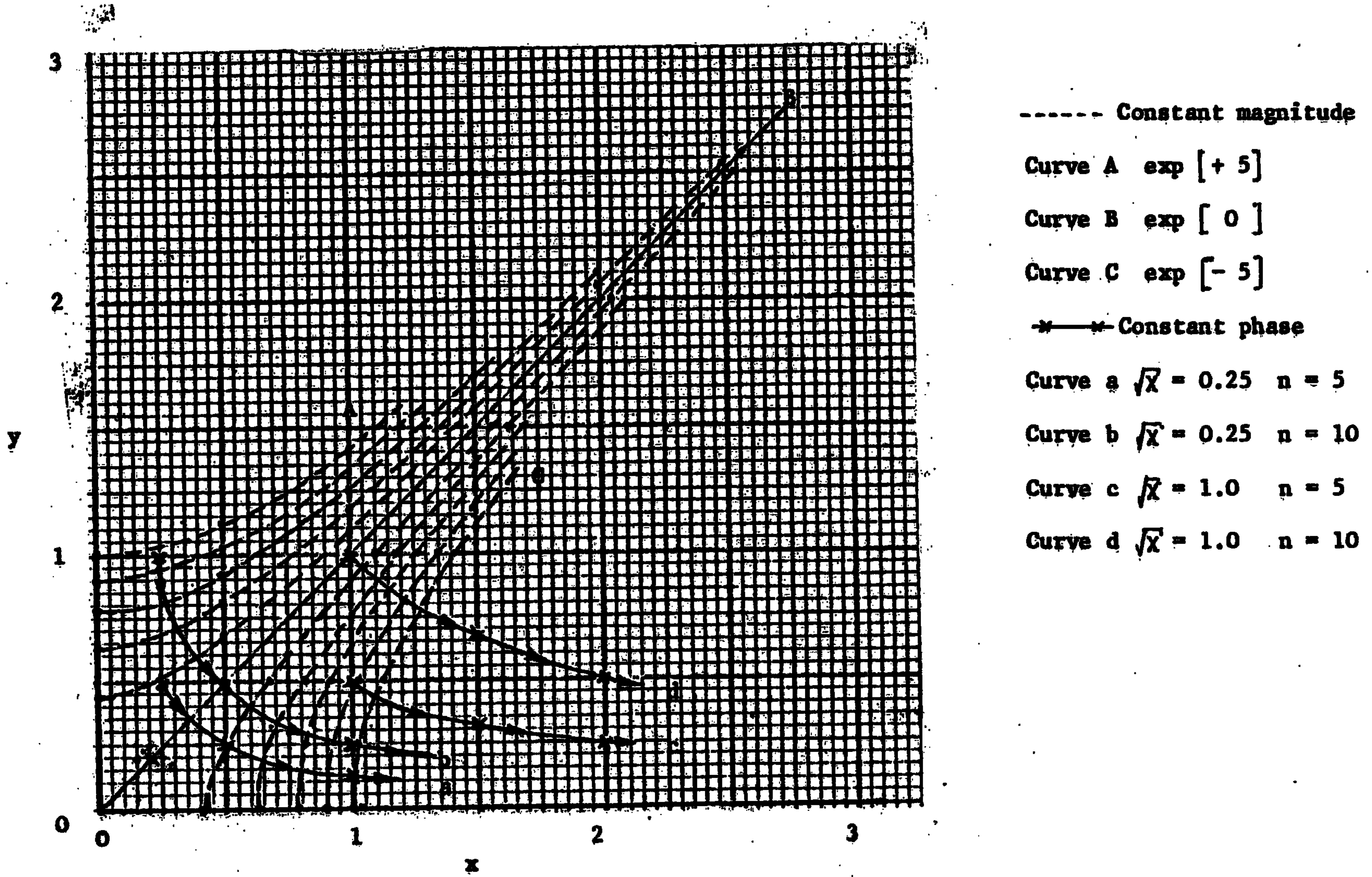

Figure G1

Constant magnitude and constant phase contours of $\exp\left[-\beta Z^2/2\right]$, $\beta = 10$